Petrology, Geochemistry, Sulphide and Platinum-Group Element Mineralization of the Geordie Lake Intrusion, Coldwell Complex, Ontario.

by

Thomas Mulja ©

A Thesis Submitted in Partial Fulfillment of the
Requirements for the Degree of
Master of Science

Lakehead University
Thunder Bay, Ontario
Canada

April, 1989

ISBN 0-315-51235-0

To my family who sent me to Canada for post-secondary education and never failed to provide all the necessities.

Petrology, Geochemistry, Sulphide and Platinum-Group Element Mineralization of the Geordie Lake Intrusion, Coldwell Complex, Ontario

Abstract

The Geordie Lake Intrusion (GLI) consists of alternating zones of layering-free troctolite and olivine gabbro outcropping in the north-central part of the Coldwell alkaline complex, northwestern Ontario. The troctolite exhibits harrisitic texture in which dendritic olivine (Fo_{44-56}), plagioclase (An_{48-57}), and skeletal magnetite are the main constituents. Small amounts of clinopyroxene ($Di_{36}Hd_{60}Ae_4$-$Di_{30}Hd_{66}Ae_4$) are present in the troctolite. The ophitic olivine gabbro consists of clinopyroxene ($Di_{41}Hd_{54}Ae_5$-$Di_{29}Hd_{66}Ae_5$), plagioclase (An_{46-54}), altered olivine, and skeletal magnetite. Some gabbros contain high-alumina clinopyroxenes (Ti-$Px_4CATS_{48}Ae_{48}$-Ti-$Px_8CATS_{42}Ae_{50}$). Mineral chemistry and whole-rock geochemistry indicate that the troctolite and gabbro are not related by differentiation and their parent magma is a relatively evolved low-alumina tholeiite. The GLI is characterized by high Sr, Rb, Ba, Th, Ta and light rare-earth element (LREE) content but low in Ni and Cr content. Europium anomalies are absent. Fe-Ti oxide geothermometry and geobarometry of the troctolite and olivine gabbro give an average equilibration temperature of 603° ± 35°C and oxygen fugacity of 10^{-17} bar.

Disseminated chalcopyrite is the dominant style of Cu-sulphide mineralization in the GLI. Massive chalcopyrite aggregates are rare. Bornite

exsolved from chalcopyrite. The other sulphides present are pyrite, millerite, siegenite with exsolved pentlandite, galena, and supergene chalcocite. The tellurides and PGM occur as small inclusions (5 - 10 μm) in, and as coarser sunhedral to anhedral grains on the margins of, the disseminated chalcopyrite. Small amounts of tellurides and PGM are also present in the massive chalcopyrite and silicate minerals. The tellurides are melonite, hessite, unnamed Ag_3Te_2, and altaite. The PGM are kotulskite, merenskyite, michenerite, sopchiete, palladium bismuthotelluride, paolovite, palladium arsenide, guanglinite, and palladium antimonide. Sperrylite is the only platinum mineral present in the GLI. Electrum forms small discrete and replacement minerals. Two probable new minerals are $Pd_{1.6}As_{1.5}Ni$ and $AgSb_4$. Textural evidence from the sulphides, tellurides, PGM, and host rock silicates favour a late stage magmatic origin. Cu-sulphide mineralization was induced by precipitation of magnetite and other Fe-bearing minerals, and subsequent mineralization resulted from cycles of sulphide and magnetite deposition. Conditions of deposition for the tellurides and PGM associated with the disseminated chalcopyrite have been estimated to be approximately from 550°C to between 450° and 400°C, and at log $P(Te_2)$ from -2.4 ± 0.13 bar to between -6.4 and -9.7 bar, and at log $P(S_2)$ from between -3.7 and -0.8 to between -4.2 and -2.3 bar. The predominance of palladium over platinum minerals reflects the relatively evolved nature of the GLI.

Acknowledgements

This thesis would not have been written without the efforts of the following individuals:

Professor Roger Mitchell initiated, supervised, and financed this thesis. His patience in reading and correcting (from English to thesis organization) the earlier versions of this thesis is gratefully acknowledged. Dr. Mitchell also introduced the neutron activation analysis method and taught predominance diagrams.

St Joe Canada Ltd., the then operator/owner of the Geordie Lake Property, permitted the use of its cores as thesis materials.

Professor Marcos Zentilli, of Dalhousie University (the writer's Alma Mater), whose lectures inspired the writer with an interest in economic geology. Dr. Zentilli is always a constant source of encouragement.

Professor Arthur Barabas, of California State University, who was the adviser for the writer's first year of graduate study in California.

Critical but constructive comments made by professors Stephen Kissin (Lakehead University) and James Crocket (McMaster University) are sincerely appreciated. The writer is, however, fully responsible for all the contents of this thesis.

The writer would like to thank the following individuals, in addition to

Dr. Mitchell, who made the thesis ready on time:

Al MacTavish, of St Joe Canada Inc. (now Bond Gold Inc.), provided geological maps, core logs, and helped us in collecting the samples.

Maureen Downey, the former NAA technician at Lakehead, patiently taught the writer how to perform NAA and helped in the sample preparation. Additional sample preparation was also done by Shelley Moogk.

Al MacKenzie, of Lakehead University Science Instrumentation Laboratory, taught the writer how to operate the scanning electron microscope (SEM) and X-ray microanalysis (EDS). Al also developed most of the microphotographs, even at short notices.

Reynolds Viitala and Ann Hammond: made more than two hundred good-quality thin sections in a very short time.

Bob McKay, of Dalhousie University, taught the writer how to use the electron microprobe and allowed long hours of using the probe.

Elenor Jensen, Keith Pringnitz and Henry Connor,of Lakehead University, performed the FeO analysis, and H_2O and CO_2 analyses, respectively.

The hospitality of many people made the writer's stay within and outside the University community a comfortable and memorable one. They are (in no particular order): Sandra Millar (Secretary of the Geology Department), all Geology faculty members, Gail Godemair (Landlady),

Drs. Tom Griffith and Steve Kinrade (Lakehead University), Darlene Kostamo (Registrar), Ain Raitsakas (Instrumentation Laboratory), Kris Delorey (Graduate Office), and all fellow graduate students.

The writer is especially grateful to Karen Knudsen who voluntarily spent days and nights drafting most of the figures and provided solace during the seemingly endless periods of writing and editing.

Major funding for this thesis was provided by the NSERC grant (No. 5049) of Dr. Mitchell. Additional funding came from a graduate scholarship awarded to the writer by the Centre for Northern Studies. The Graduate School is also thanked for awarding a University entrance scholarship.

TABLE OF CONTENTS

Page

Abstract i
Acknowlegements iii
List of Figures viii
List of Tables xi

CHAPTER 1 INTRODUCTION

1.1 General Statement 1
1.2 The Coldwell Alkaline Complex: A Brief Survey
1.2.1 Regional Geologic Setting 3
1.2.2 Geology of the Coldwell Complex 5
1.2.3 Current Petrologic Knowledge 10
1.3 The Present Study: The Geordie Lake Intrusion
1.3.1 Location and Access 15
1.3.2 Geology and Mineralization 15
1.3.3 Objectives and Methods 20

CHAPTER 2 PETROCHEMISTRY OF THE GEORDIE LAKE INTRUSION

2.1 Introduction 22
2.2 Petrography 22
2.2.1 Troctolite 22
2.2.2 Olivine Gabbro 26
2.2.3 Altered Gabbroic Rocks 34
2.2.4 Quartz Syenite of Center I 36
2.2.5 Comparisons to Other Basic Intrusions 39
2.2.6 Discussion 41
2.3 Mineral Chemistry
2.3.1 Olivine 45
2.3.2 Plagioclase 51
2.3.3 Alkali-feldspar 61
2.3.4 Clinopyroxene 64
2.3.5 Amphibole 71
2.3.6 Biotite 76
2.3.7 Magnetite and Ilmenite 77
2.3.8 Evaluation of the Mineral Chemistry 94

2.4 Whole-rock Chemistry
2.4.1 Introduction 95
2.4.2 Major Elements 95
2.4.3 Trace Elements 112
2.5 Discussion
2.5.1 Parent Magma 139
2.5.2 Conditions of Crystallization 143

CHAPTER 3 SULPHIDE AND PLATINUM-GROUP ELEMENT MINERALIZATION
3.1 Introduction 148
3.2 Style of Mineralization 148
3.3 Descriptive Mineralogy and Mineral Chemistry
3.3.1 Sulphides 151
3.3.2 Sulpharsenide and Arsenide 166
3.3.3 Tellurides 168
3.3.4 Platinum-Group Minerals (PGM) 179
3.3.5 Other Minerals 191
3.3.6 New Minerals ? 198
3.4 Paragenesis 200
3.5 Conditions of Deposition
3.5.1 Temperature 204
3.5.2 Tellurium and Sulphur Fugacities 206
3.6 Speculation on the Mechanism of Mineralization 214

CHAPTER 4 COMPARATIVE STUDIES, SUMMARY, AND RECOMMENDATIONS
4.1 Comparisons to Other Platinum Deposits 217
4.2 Summary 222
4.3 Recommendations 223

REFERENCES 226

APPENDICES
I Whole-Rock Analyses
II Analyses of Mineral Compositions
III Compositions of plagioclase, clinopyroxene, amphibole, and magnetite-ilmenite pairs of the GLI, and biotite of Center II.

LIST OF FIGURES

CHAPTER 1		Page
1.1	Location map of the study area	2
1.2	Tectonic map of Lake Superior region	4
1.3	Geological map of Coldwell complex	6
1.4	Gravity anomaly and infrastructure of Coldwell complex	8
1.5	Geological map of the Geordie Lake Intrusion	16
1.6	Cross section geology of the study area	18

CHAPTER 2		
2.1	Photomicrograph of dendritic olivine	24
2.2	Photomicrograph of magnetite-rich troctolite	24
2.3	Photomicrograph of skeletal magnetite and exsolved ilmenite	27
2.4	Discrete magnetite and ilmenite coexisting with chalcopyrite	27
2.5	Photomicrograph of ophitic olivine gabbro	28
2.6	Allotriomorphic gabbro	28
2.7	Back-scattered electron image of greenockite	33
2.8	Back-scattered electron image of a Y-Nb mineral	33
2.9	Weakly altered gabbroic rock	35
2.10	Photomicrograph of unaltered clinopyroxene in weakly altered gabbroic rock	35
2.11	Sericitized plagioclase in altered rock	37
2.12	Strongly altered rock	37
2.13	Recrystallization of Center I syenite at the GLI-Center I contact	38
2.14	Texture of a weakly recrystallized Center I syenite	38
2.15	Olivine compositions vs. height	47
2.16	Comparative olivine compositions	50
2.17	Ab-An-Or ternary plot for plagioclases of the GLI	53
2.18	Ab-An-Or ternary plot for zoned plagioclases of the GLI	55
2.19	Plagioclase compositions vs height	56
2.20	Ab-An-Or ternary plot for plagioclases of Center I and II	60
2.21	Comparative plagioclase compositions	62
2.22	Di-Hd-Es-Fs diagram of clinopyroxenes of the GLI	66

2.23 Clinopyroxene Mg/(Mg+Fe) ratios vs. height 67
2.24 Compositions of low-Al clinopyroxene in the system Ae-Di-Hd 69
2.25 CATS-Ae-TiPx ternary plot for the Al-high clinopyroxenes of the GLI 70
2.26 Comparative clinopyroxene compositions 72
2.27 The compositions of amphiboles of the GLI 75
2.28 Biotite compositions vs. height 79
2.29 Mg-Fe-Al plot for the biotites of the GLI and western gabbro 80
2.30 TiO2-FeO-Fe2O3 plot for the Fe-Ti oxides of the GLI and other basic intrusions 84
2.31 Fe-Ti oxide compositions vs height 87
2.32 Fe-Ti oxide re-equilibration temperature vs. height 92
2.33 T-fO_2 plot for the Fe-Ti oxides of the GLI and other basic intrusions 93
2.34 The AFM diagram of the GLI 98
2.35 The Di-Fo-Ab-Q diagram of the GLI 99
2.36 Variation diagrams of the GLI 102
2.37 The AFM diagram of Center I gabbroic rocks 108
2.38 Variation diagrams of Center I and II gabbroic rocks 109
2.39 REE distribution patterns of the GLI 130
2.40 REE distribution patterns of the eastern syenite 134
2.41/42 REE distribution patterns of Center I gabbroic rocks 137
2.43/44 REE distribution patterns of Center II gabbroic rocks 138
2.45 Comparison of REE distribution patterns 140
2.46 Al_2O_3 vs SiO_2 of clinopyroxenes 142
2.47 TiO_2 vs Al^{iv} of clinopyroxenes 142
2.48 Two-feldspar geothermometer diagram 145
2.49 Fo-Plag-Cpx diagram of the GLI 147

CHAPTER 3
3.1 Style of chalcopyrite mineralization 150
3.2A-D Textures of chalcopyrites 152
3.3 Exsolved bornite 156
3.4A-D Style of pyrite mineralization 156

3.5	Galena replacement of hessite and melonite	163
3.6A-B	Siegenite with exsolved pentlandite, millerite, and chalcopyrite	165
3.7A-B	Style of cobaltite mineralization	165
3.8A-B	Niccolite mineralization	167
3.9	Textures of hessite	171
3.10	Style of melonite mineralization	173
3.11	Pd-Ni-Te diagram of melonite	176
3.12	Altaite inclusion in chalcopyrite and replacement of melonite	177
3.13	The ternary system Pd-Bi-Te	181
3.14	Style of kotulskite mineralization	183
3.15	Textures of sopcheite	186
3.16	Paolovite mineralization	186
3.17A-C	Palladium arsenide style of mineralization	189
3.18A-D	Modes of occurrence of palladium antimonide	192
3.19	The ternary system Au-Ag-Te	195
3.20	Spectrum of naumannite	196
3.21	Spectrum of lead antimonide	197
3.22	Spectrum of clausthalite	197
3.23	Pd-Ni-As, the probable new PGM	199
3.24	Paragenetic sequence for the mineralization of the GLI	201
3.25	Predom of tellurides, PGM and sulphides at 550°C	208
3.26	Predom of tellurides, PGM and sulphides at 500°C	209
3.27	Predom of tellurides, PGM and sulphides at 450°C	210
3.28	Predom of tellurides, PGM and sulphides at 400°C	211
3.29A-D	Possible pathways of mineralization in the GLI	213

LIST OF TABLES

CHAPTER 1 Page

1.1 Radometric ages of Coldwell intrusions 9

CHAPTER 2

2.1 The compositions of olivines in the troctolite from the GLI 46
2.2 The compositions of olivines from western Coldwell gabbros 49
2.3 Representative compositions of plagioclases of the GLI 52
2.4A-B Plagioclase compositions from Center I and II gabbros 58
2.5 The compositions of alkali-feldspars of the GLI 63
2.6 Representative compositions of clinopyroxenes of the GLI 65
2.7 Representative compositions of amphiboles of the GLI 73
2.8 Amphibole silica vs. host rock silica contents 74
2.9 The compositions of biotites from the GLI 78
2.10 The compositions of biotites from Center I and II gabbros 81
2.11 Representative compositions of Fe-Ti oxides from the GLI 82
2.12 Summary of compositions of major elements in the Fe-Ti oxides 85
2.13 Comparative magnetite compositions 89
2.14 T-fO_2 of the Fe-Ti oxides of the GLI 90
2.15 Whole-rock analyses of the GLI 96
2.16 Whole-rock analyses of Center I gabbros 106
2.17 Whole-rock analyses of Center II gabbros 107
2.18 Comparison of whole-rock analyses 111
2.19 Whole-rock analyses of eastern syenite 113
2.20 Trace element concentrations (ppm) of the GLI 114
2.21 Summary of trace element concentrations of the GLI 116
2.22 Trace element abundances of the Center I gabbros 121
2.23 Trace element abundances of the Center II gabbros 124
2.24 Comparison of trace element data 126

2.25 REE concentrations (ppm) of the GLI 128
2.26 REE concentrations (ppm) of the Center I and II gabbros 135

CHAPTER III

3.1 Analyses of chalcopyrite 155
3.2 Analyses of bornite 158
3.3 Analyses of pyrite 162
3.4 Analyses of siegenite, millerite, sphalerite, and chalcocite 164
3.5 Analyses of cobaltite 169
3.6 Analyses of niccolite 169
3.7A Analyses of hessite 172
3.7B Analyses of unnamed Ag_3Te_2 172
3.8 Analyses of melonite 175
3.9 Analyses of altaite 178
3.10 Analyses of Pd-Bi-Te minerals 180
3.11 Analyses of sopcheite 187
3.12 Analyses of paolovite 188
3.13 Analysis of Palladium arsenide 190
3.14 Analyses of guanglinite 191
3.15 Analyses of palladium antimonide 193
3.16 Analyses of electrum 194

CHAPTER 1
INTRODUCTION

1.1 General Statement

In 1963 Ameranium Mines Ltd. discovered Cu-sulphide mineralization in gabbroic rocks adjacent to Geordie Lake in the Coldwell Alkaline Complex (Patterson *et al.*, 1986., Figure 1.1). However, it appears that there was no further exploration of this prospect until 1986 when a group of prospectors from Marathon rediscovered the Ameranium trench and reported the presence of platinum-group elements (PGE). In 1987, St. Joe Canada Inc., having obtained the prospect from Fleck Resources Ltd., conducted mapping and core-drilling in the mineralized area.

Preliminary studies have indicated that the gabbroic rocks are surrounded by a variety of syenitic rocks, and that the PGE-bearing Cu-sulphide mineralization occurs in the gabbros and at the eastern gabbro-syenite contact zone. Assay results on sulphide-mineralized gabbros have shown the presence of platinum, palladium, silver and copper.

This thesis is the first petrological and geochemical investigation of these gabbroic rocks and of the platinum-group element mineralization. Throughout this thesis the studied gabbros and related rocks are collectively referred to as the Geordie Lake Intrusion (GLI), named after the nearby lake.

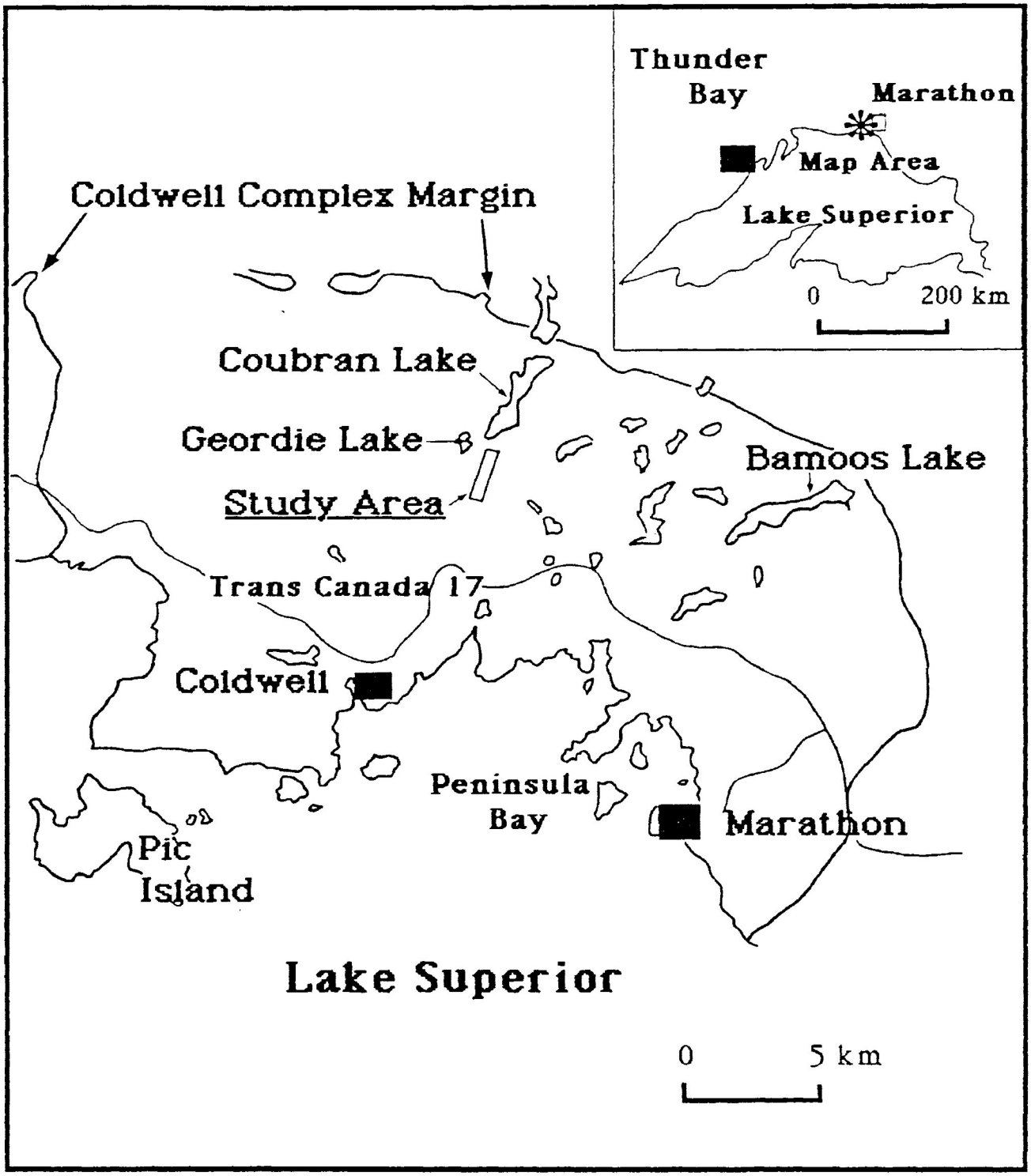

Figure 1.1 Location map of the Geordie Lake Intrusion in the Coldwell Complex

1.2 The Coldwell Alkaline Complex: A Brief Survey

1.2.1 Regional Geologic Setting

The Coldwell Alkaline Complex, which is the southernmost member of a north-south trending belt of alkaline intrusions (Chipman-Killala-Prairie-Coldwell., Figure 1.2), consists of multiple intrusions of gabbros, syenites and granites outcropping in the east-west trending Archean Schreiber-White River greenstone belt of the Canadian shield (Mitchell and Platt, 1978). These Archean rocks consist of three distinct units: mafic volcanic rocks, felsic volcanic rocks, and sedimentary rocks (Currie, 1980). The mafic volcanic rocks are made up of massive and pillows of basaltic lavas together with andesitic flows and tuffs. They outcrop west of the Coldwell complex and in an east-west belt near Heron Bay. The felsic volcanic rocks are composed primarily of rhyolite and dacite porphyry. These rocks occur mainly on the east side of the complex. The sedimentary rocks form a belt about 2 km wide which is intersected by the west side of the Coldwell intrusion near Middleton. These rocks are also exposed along Highway 17 at the east side of the complex.

The Archean rocks underwent greenschist to amphibolite facies regional metamorphism prior to the emplacement of the Coldwell rocks. Subsequent Coldwell intrusions produced a 2 km wide contact metamorphic aureole (Walker, 1967). Within this aureole rocks have been metamorphosed to pyroxene hornfels grade (McGill, 1980).

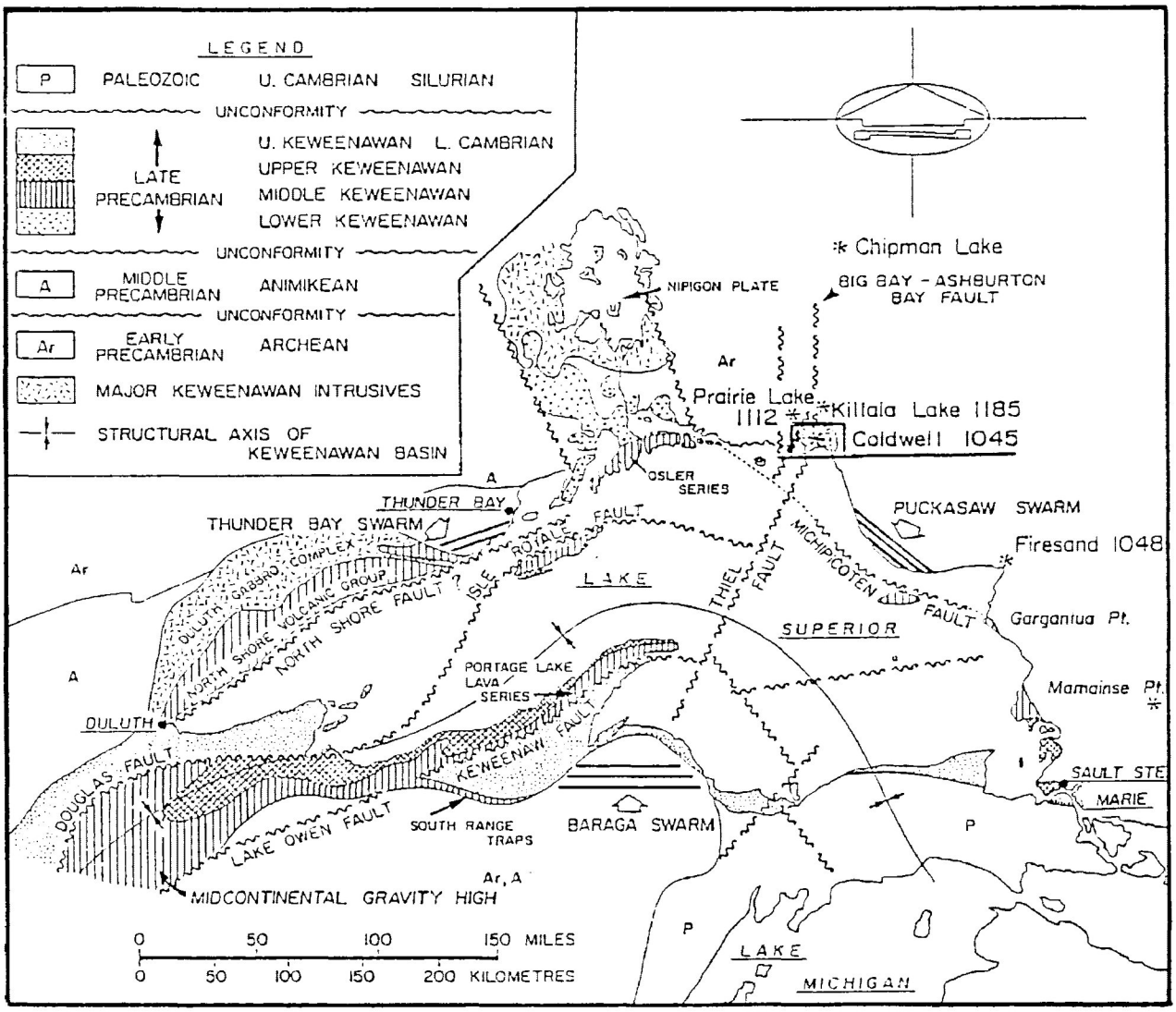

Figure 1.2 Regional tectonic setting of the Coldwell complex (Compiled by Mitchell and Platt, 1978). Alkaline complexes are designated * and their radiometric ages mostly K-Ar are given in Millions of years.

The relationship between the Coldwell complex and the tectonism in the Lake Superior basin has been discussed by several authors. Card *et al.*, (1972) and Halls (1978) stated that the complex is part of the widespread magmatism associated with the Keweenawan rift system. Mitchell *et al.*, (1983) proposed that during rifting the sources of upper mantle-derived basic magma migrated from the Duluth complex and the North Shore volcanics in the southwest, towards Coldwell in the northeast, and that the large basic intrusion underlying the Coldwell complex represents the final point of the migration of this activity.

Two hypotheses have been proposed to account for the tectonic setting of the Coldwell complex. Mitchell and Platt (1982) suggested that the Coldwell magmas were emplaced at a triple junction associated with a "failed arm" during the waning of a rifting episode. This deduction has been based on the petrological and tectonic similarities of the Coldwell complex to alkaline complexes located at triple junctions in younger rift systems. The other hypothesis is that of Klasner et al. (1982) who proposed that the complex was emplaced where a late fracture intersected the rift.

1.2.2 Geology of the Coldwell Complex

The Coldwell Complex (Figure 1.3) is a sub-circular body with a diameter of about 25 km and is the largest alkaline intrusion in North America (Mitchell and Platt, 1982). More than one third of the complex is covered by Lake Superior (Currie, 1980). On the basis of geological,

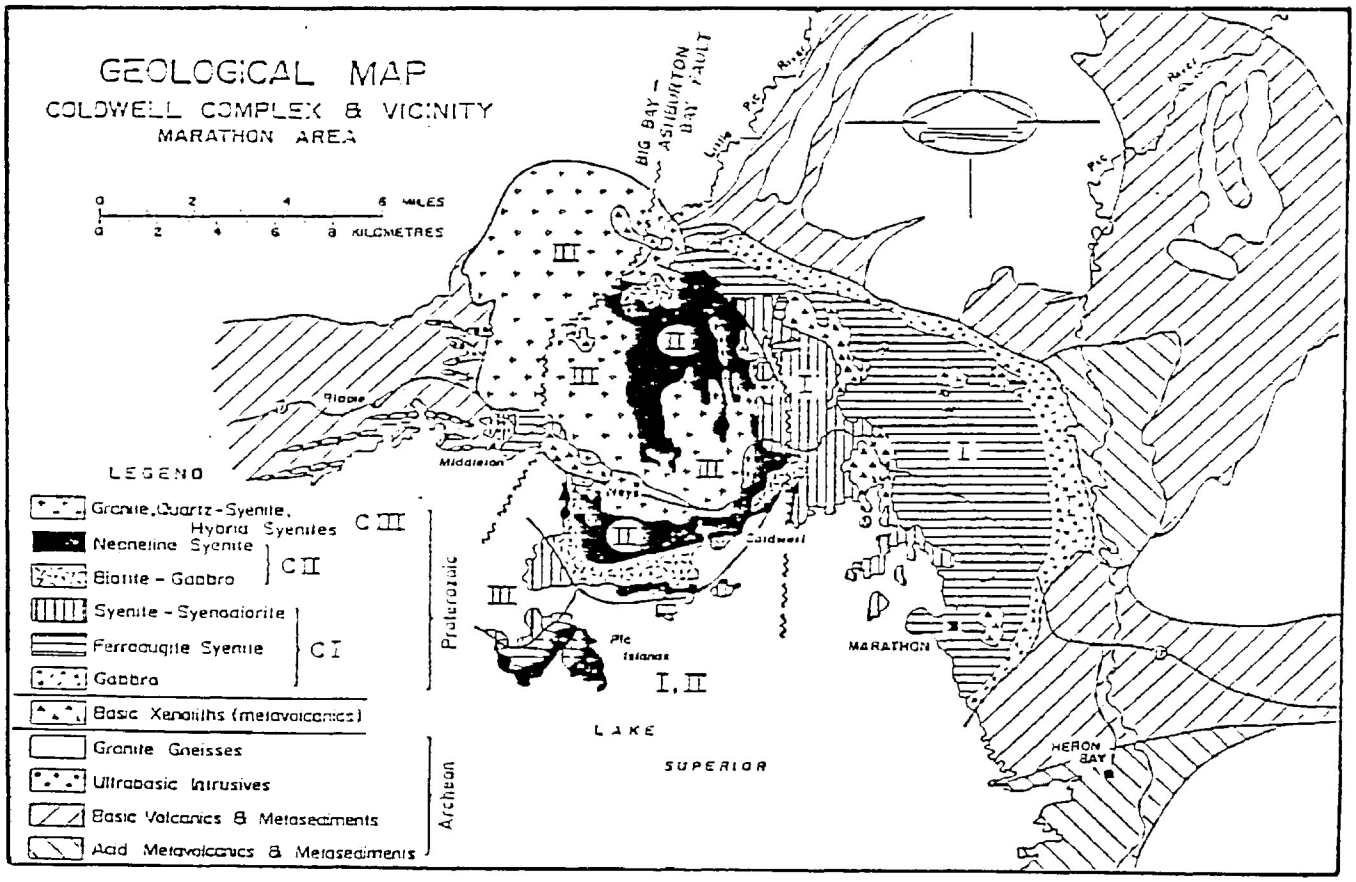

Figure 1.3 Geological map of the Coldwell complex showing the setting of the different centers and their rock types (After Mitchell and Platt, 1978). The Geordie Lake Intrusion is situated left of the upper end of the N-S trending fault, between Center II nepheline syenite and Center I. syenite-syenodiorite

petrological and geochemical evidence, Mitchell and Platt (1982) interpreted the Coldwell Complex to have developed by at least three major episodes of magmatism and a series of cauldron subsidences at three different centers migrating in a westerly direction. This style of magmatism is in contrast with a single funnel-shaped intrusion proposed by Lilley (1964) and a lopolith by Puskas (1967).

Mitchell et al. (1983) have deduced from a gravity survey the infrastructure of the Coldwell complex to be a series of layered basic and ultramafic intrusions with a convex base (Figure 1.4). This interpretation has raised a question whether or nor there is a differentiation relationship between the syenites and the mafic rocks occurring at depth. However, the co-existence of undersaturated and oversaturated syenites, which require several basic parents of differing degrees of silica activity, does not support such simple differentiation relationship. The possibility of generating oversaturated felsic magmas by partial fusion of upper crustal materials is not supported by the initial Sr isotopic composition of all the Coldwell magmas. An alternative hypothesis (Mitchell *et al.*, 1983), which is yet to be tested, is that the felsic magmas have been formed by differentiation and/or lower crustal fusion together with mixing of magmas from various sources.

Several authors have determined the K/Ar, Rb/Sr and U/Pb ages of the Coldwell intrusions. Table 1.1 lists the results of this geochronological study. Platt and Michell (1982) have questioned the validity of the data prior to theirs because the analytical methods and the samples used by the other authors are not reported. The age reported by Platt and Mitchell was

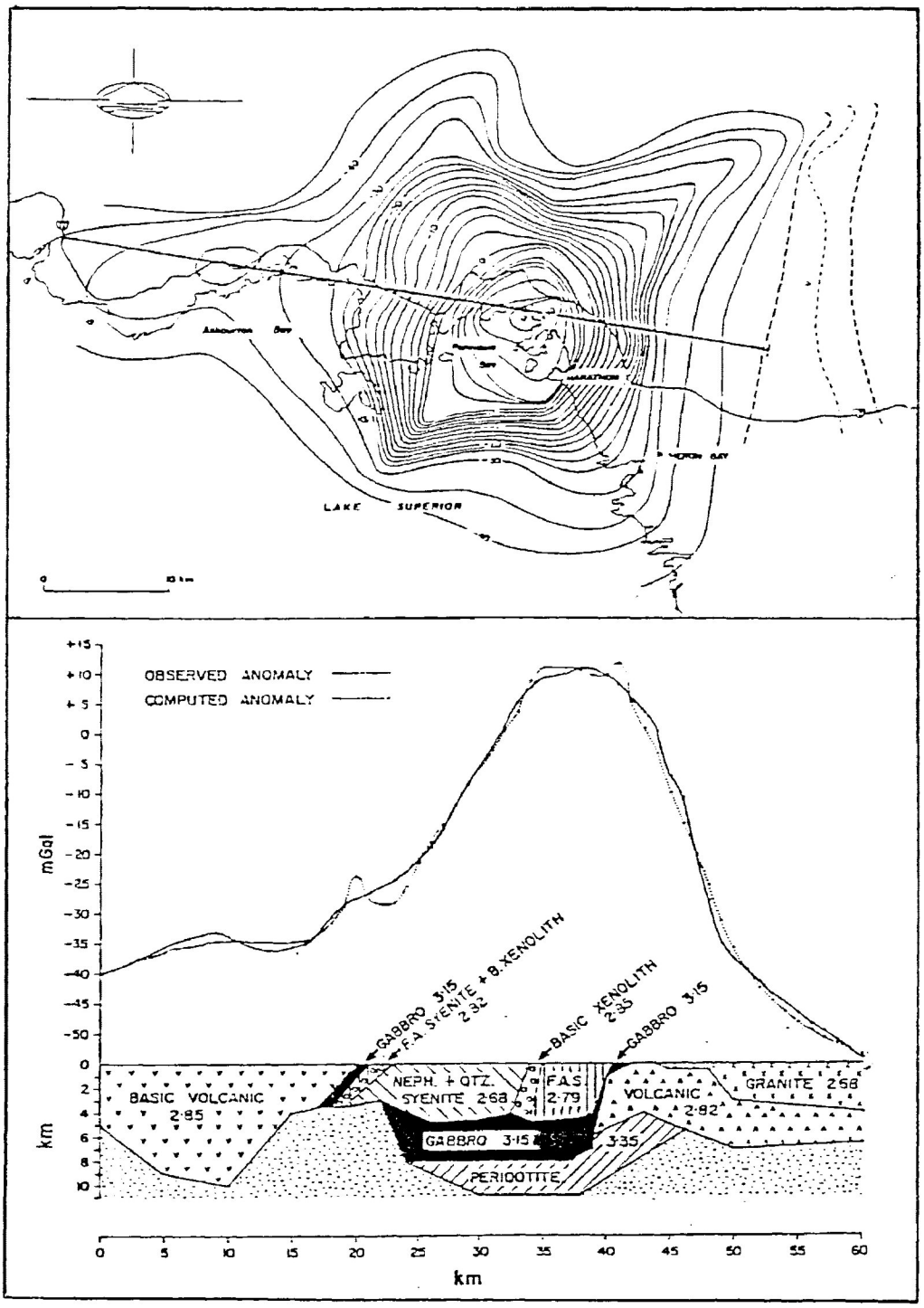

Figure 1.4 Bouguer anomaly map of the Coldwell complex (upper map), observed and computed gravity anomaly profiles and the interpreted infrastructure of the complex (Mitchell *et al.*, 1983). Solid straight line is the location of the gravity anomaly profile.

Table 1.1 Radiometric ages of Coldwell rocks (Compilation of data prior to 1982 is after Platt and Mitchell, 1982)

Age (Ma) 2σ	Method	M:Mineral R: Whole Rock Isochron	Number of Samples	Reference
1108 ± 1	U/Pb	M: Zircon/Baddeleyite	12	Heaman and Machado (1987)
1044 ± 6.2	Rb/Sr	R	17	Platt and Mitchell (1982)
1085± 15	Rb/Sr	R	11	Bell et al., (1979)
1070±15	Rb/Sr	R	11	Bell and Blenkinsop (1980)
1052±15	Rb/Sr	M/R	1	Chaudhuri et al., (1971)
1047±84	Rb/Sr	M: Biotite	1	Fairbairn (1959)
1071±43	Rb/Sr	M: Biotite	1	Fairbairn (1959)
1335±147	Rb/Sr	M: Alkali-feldspar	1	Fairbairn (1959)
1224±98	Rb/Sr	M: Alkali-feldspar	1	Fairbairn (1959)
1055±?	K/Ar	M: Biotite	1	Fairbairn (1959)
1065±32	K/Ar	M: Biotite	1	Fairbairn (1959)
1015±36	K/Ar	M: Biotite	1	Currie (1980)
1005±36	K/Ar	M: Biotite	1	Currie (1980)

based on 17 samples representing rocks from the 3 Centers and related dykes. The reported U/Pb ages by Heaman and Machado (1987) for the Center I gabbro and Center II syenite are greater than the Rb/Sr ages by Platt and Mitchell (1982). The U/Pb ages also suggest no significant age variation between the emplacement of Center I and Center II rocks. Heaman and Machado pointed out that a granitoid rock of Center III is approximately 10 Ma younger than Center I and II intrusions.

1.2.3 Current Petrologic Knowledge

The intrusions emplaced by the three magmatic episodes are collectively grouped as rocks of Center I, II, and III (Figure 1.3). The following are brief descriptions of these Centers.

Center I Intrusions The earliest intrusions in the Coldwell complex are the gabbros which form a small outcrop at the western margin of the Complex and an arcuate intrusion at the eastern contact, from southeast of Marathon to the north of Coubran Lake. The subsequent intrusions are the ferroaugite syenite and syenite-syenodiorite.

Aubut (1977), Jago (1980) and McGill (1980) studied the petrography of the layered section of the western margin gabbro. Jago reported that the layering is characterized by cross and convolute layering, together with scour and fill structures. The thickness of individual layers ranges from several centimeters to tens of centimeters. The leucocratic layers consist of

cumulus labradorite, augite, olivine and apatite, and intercumulus clinopyroxene and opaque minerals. The melanocratic layers are composed of labradorite, augite and opaque minerals with subordinate apatite, olivine and biotite.

Small portions of Center I gabbro in the eastern margin have been described by Wilkinson (1983) and Lum (1973). Wilkinson divided the gabbro north of Coubran Lake into 2 series: a massive series composed of fine-grained, heterogeneous and mottled gabbro, and a layered series consisting of banded gabbro and subsidiary dioritic units. The gabbros from both series consist primarily of clinopyroxene and plagioclase. Olivine, biotite, amphibole, apatite and magnetite are minor phases. Lum (1973) divided the gabbro that is exposed along Highway 17 into chilled, massive and layered. The chilled gabbro is fine-grained and contains, in decreasing abundance, plagioclase, diopside or augite, enstatite, olivine, and opaque minerals (Ti-magnetite and sulphide). The massive gabbro exhibits ophitic texture and has mineralogy similar to that of the chilled gabbro. The layered gabbro consists of alternating melanocratic and leucocratic layers. However, Lum did not elaborate on the mineralogy of these layers except in stating that olivine, plagioclase and pyroxene form the cumulus phases.

The ferroaugite syenites which are exposed in the southwestern margin of the Coldwell Complex are divided into a lower and upper series (Mitchell and Platt, 1978). The lower series exhibits well developed layering which is defined by layers (1-5 cm) of mafic cumulus minerals olivine (Fa_{83-93}), ferroaugite ($Di_{50}Hd_{45}Ac_5$-$Di_5Hd_{90}Ac_5$) and ilmeno-

magnetite, and by layers of felsic bands (10-30 cm) consisting of even-grained alkali feldspar-rich cumulates. Hastingsitic hornblende is the main intercumulus phase for both layers. The upper series is a poorly-layered syenite consisting of cumulus alkali feldspar, olivine (Fa_{93}), and acmite-hedenbergite ($Di_5Hd_{50}Ac_5$-$Ac_{50}Hd_{50}$) and of intercumulus aenigmatite, and amphiboles. The amphibole compositions range from ferrorichteritic katophorite to ferrorichterite. This syenite also contains patchy peralkaline pegmatites composed of ferrorichterite, ferroactinolite, alkali feldspar, aenigmatite, quartz and zircon. Extreme differentiation of the ferroaugite syenitic magma is believed to have generated these iron-rich, oversaturated and peralkaline residual patches.

The syenite-syenodiorite of Center I remains unknown in terms of its field relations and petrology. Currie (1980), based on samples taken from road cuts, designated this intrusive body as fenite. Syenite which borders the gabbro in the study area (Figure 1.5) is considered to be a part of these syenite-syenodiorite intrusions. The petrology of this syenite is described in Chapter 2.

Center II Intrusions In Center II, intrusion of biotite-bearing alkaline gabbro was followed by several intrusions of nepheline syenite (Mitchell and Platt, 1982). The gabbro occurs in an arcuate outcrop on the Coldwell Peninsula. It consists of biotite, olivine, plagioclase, nepheline and amphibole. The nepheline syenites consist primarily of amphiboles (magnesian hastingsitic hornblende to ferroedenitic hornblende), nepheline

($Ne_{78}Ks_{18}Qtz_4$ to $Ne_{74}Ks_{17}Qtz_9$), alkali feldspar ($Or_{28}Ab_{68}An_4$ to $Or_{45}Ab_{53}An_1$, and $Or_{56}Ab_{42}An_2$ to $Or_{82}Ab_{18}$), and titanomagnetite and ilmenite. Minor phases include corroded diopside and diopsidic hedenbergite, biotite, and olivine.

Alkaline lamprophyric and analcite tinguaite dykes that are coeval and comagmatic with the Center II activity have been studied by Laderoute (1988). The 5 types of lamprophyres are ocellar camptonites, sannaites, quartz-bearing camptonites, amphibole camptonites, and monchiquites. The lamprophyres consist of clinopyroxene and brown amphibole phenocrysts set in a groundmass of Fe-Na-clinopyroxene, brown amphibole, biotite, plagioclase, alkali feldspar (for monchiquites, an isotropic glassy material is in place of feldspar), nepheline, calcite and opaque minerals. Tinguaites contain phenocrysts of alkali feldspar, nepheline, analcite and minor riebeckite in a groundmass of alkali feldspar, nepheline and analcite plus aegerine.

Geochemical studies indicate that all the dyke rocks, except the quartz camptonites, are co-magmatic and may have been produced by fractional crystallization of alkaline olivine basaltic magma. The quartz camptonites may result from silica contamination or are related to a tholeiitic magma associated with the Center I activity.

Center III Intrusions Center III syenites and granites occupies almost half of the Coldwell complex. Knowledge of these intrusions was scant until recent investigations by Jago (1980) and Lukosius-Sanders

(1988). Jago studied a small portion of these intrusions in the western contact zone. On the basis of field relations and petrographic studies, he determined that the earliest intrusion is a porphyritic quartz syenite, which contains numerous xenoliths of volcanic rocks. This syenite is medium- and coarse-grained, consisting mainly of subhedral perthitic alkali-feldspar (>85 %) and coarse strained quartz. Minor phases include plagioclase, amphibole, and biotite. The syenite is intruded by a quartz syenite, which is medium- to coarse-grained and contains alkali feldspar (>85 %) and quartz. This intrusion is also believed to metasomatise the volcanic xenoliths in the porphyritic quartz syenite. These xenoliths contain alkali-feldspar porphyroblasts.

Lukosius-Sanders (1988) recognized four major types of Center III syenites in her study area; in relative chronological order, these are synneuritic magnesio-hornblende syenite, perthitic ferro-edenite syenite, contaminated ferro-edenite syenite and quartz syenite. The evolutionary compositional trend of amphiboles in these syenites ranges from magnesian hastingsite in the magnesio hornblende syenite to riebeckite in the quartz syenite. Pyroxenes evolved from Ti-Al rich in the earliest syenites to Na-Fe rich members in the youngest syenites. Geochemically, the syenites are miaskitic and metaluminous with an increasing normative quartz content from the earliest to the latest type. The syenites are enriched in U, Th, rare-earth, and zirconium as a consequence of the presence of zircon, chevkinite, and REE-bearing minerals. Rare-earth element distribution patterns show pronounced negative Eu anomalies and significant heavy REE

enrichment.

These geochemical characteristics indicate that the syenites have petrological affinities with A-type granites and are likely to have formed by partial melting of the lower crust in response to the emplacement of basic intrusions at depth.

1.3 The Present Study: The Geordie Lake Intrusion

1.3.1 Location and Access

The PGE-bearing Geordie Lake intrusion (GLI) is located in the north central region of the Coldwell complex (Figure 1.1), about 15 km northwest of the town of Marathon, through which the Trans Canada Highway passes. Except in winter, the area is accessible by four-wheel drive vehicles via gravel roads. The topography within the Coldwell Complex is very rugged; hills with steep slopes and deep gorges are characteristic. The best bedrock exposures are limited to road cuts and coast lines along Lake Superior (Mitchell and Platt, 1978). Pine trees cover most of the area. In the Geordie Lake area, only small scattered outcrops are exposed.

1.3.2 Geology and Mineralization

The geology of the Geordie Lake area (Figure 1.5) was unknown until it was mapped by geologists from St. Joe Canada Inc. in 1987. The GLI

Figure 1.5 Geological map of the Geordie Lake area (modified from the geological map of the Geordie Lake prospect, St. Joe Canada, 1987).

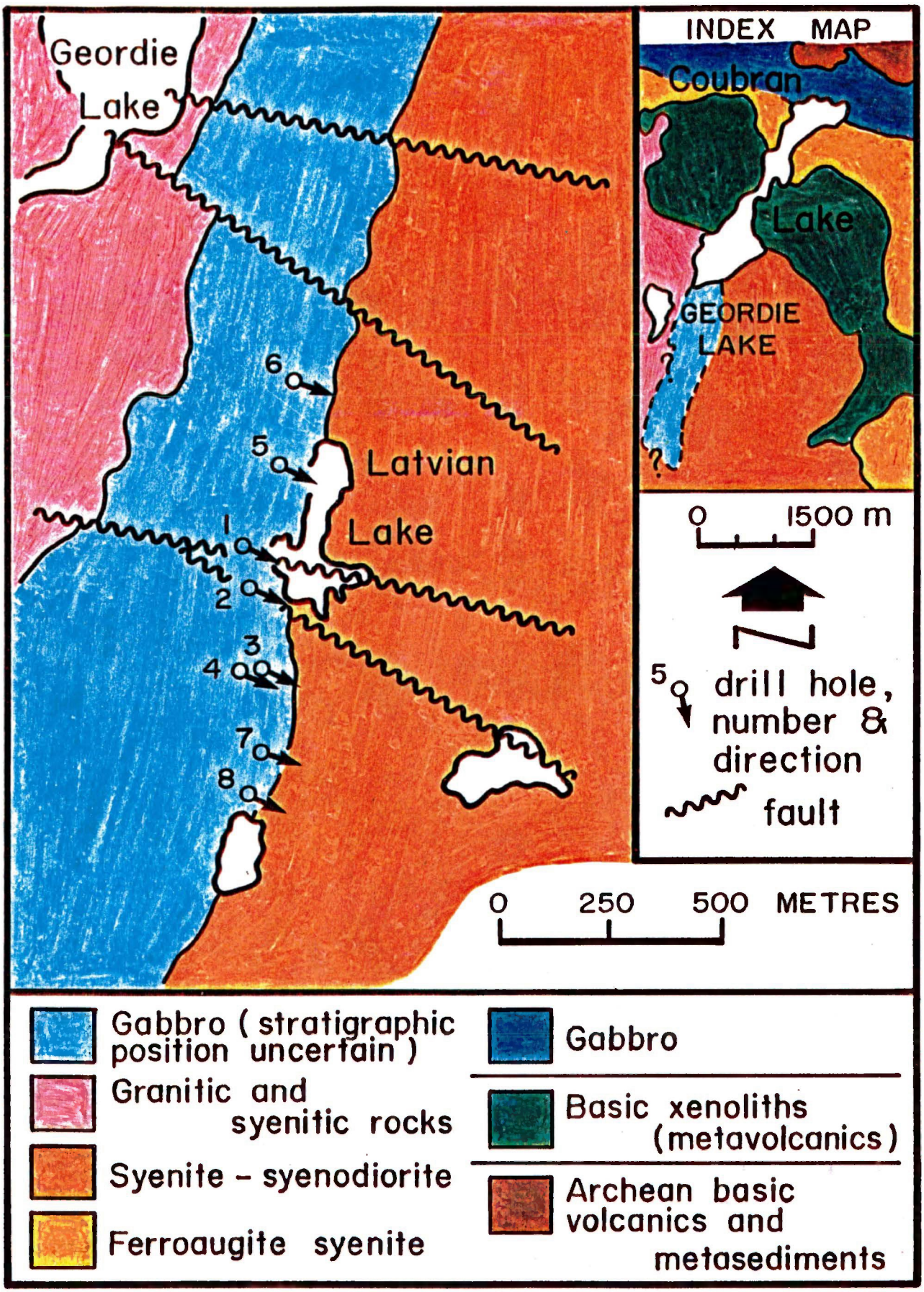
Geordie Lake
Latvian Lake
1
2
3
4
5
6
7
8
INDEX MAP
Coubran Lake
GEORDIE LAKE
0 1500 m
N
5 drill hole, number & direction
fault
0 250 500 METRES
Gabbro (stratigraphic position uncertain)
Granitic and syenitic rocks
Syenite - syenodiorite
Ferroaugite syenite
Gabbro
Basic xenoliths (metavolcanics)
Archean basic volcanics and metasediments

is shaped like a parallelogram oriented NNE-SSW that narrows towards Coubran Lake. The dimensions are about 400 to 500 m wide and 2000 m long.

The GLI is bounded to the east and south by the syenites of Center I, and to the west by porphyritic syenite. Both syenites are as yet insufficiently characterized. The porphyritic syenite has not been assigned to one of the magmatic episodes. An irregular contact zone between the GLI and Center I syenite is exposed on the western edge of Latvian Lake. This contact zone is characterized by fine-grained gabbroic rocks which contain numerous irregularly-shaped inclusions of pegmatitic rocks. The mafic minerals in some inclusions are attached perpendicularly to the contact with the gabbro, which itself exhibits a fine-grained chill margin. The nature of these inclusions has not been studied. The contact with the porphyritic syenite is not exposed.

In 1987 St. Joe Canada Inc., drilled eight inclined core holes penetrating the contact between the GLI and Center I syenite. Drill hole information and surface geology suggest that the GLI dips westerly, ranging from 30° in drill-hole 8 to 56° in drill-hole 5. The western contact between the GLI and syenitic rocks is undefined yet. This thesis is based on the petrology and geochemistry of materials obtained from drill cores 1, 2, 3 and 6.

Figure 1.6 is a fence diagram showing the lithological variations within the drill cores studied. On the basis of the modal mineralogy, augmented by the anorthite contents of plagioclase (Chapter 2), the major lithologies were

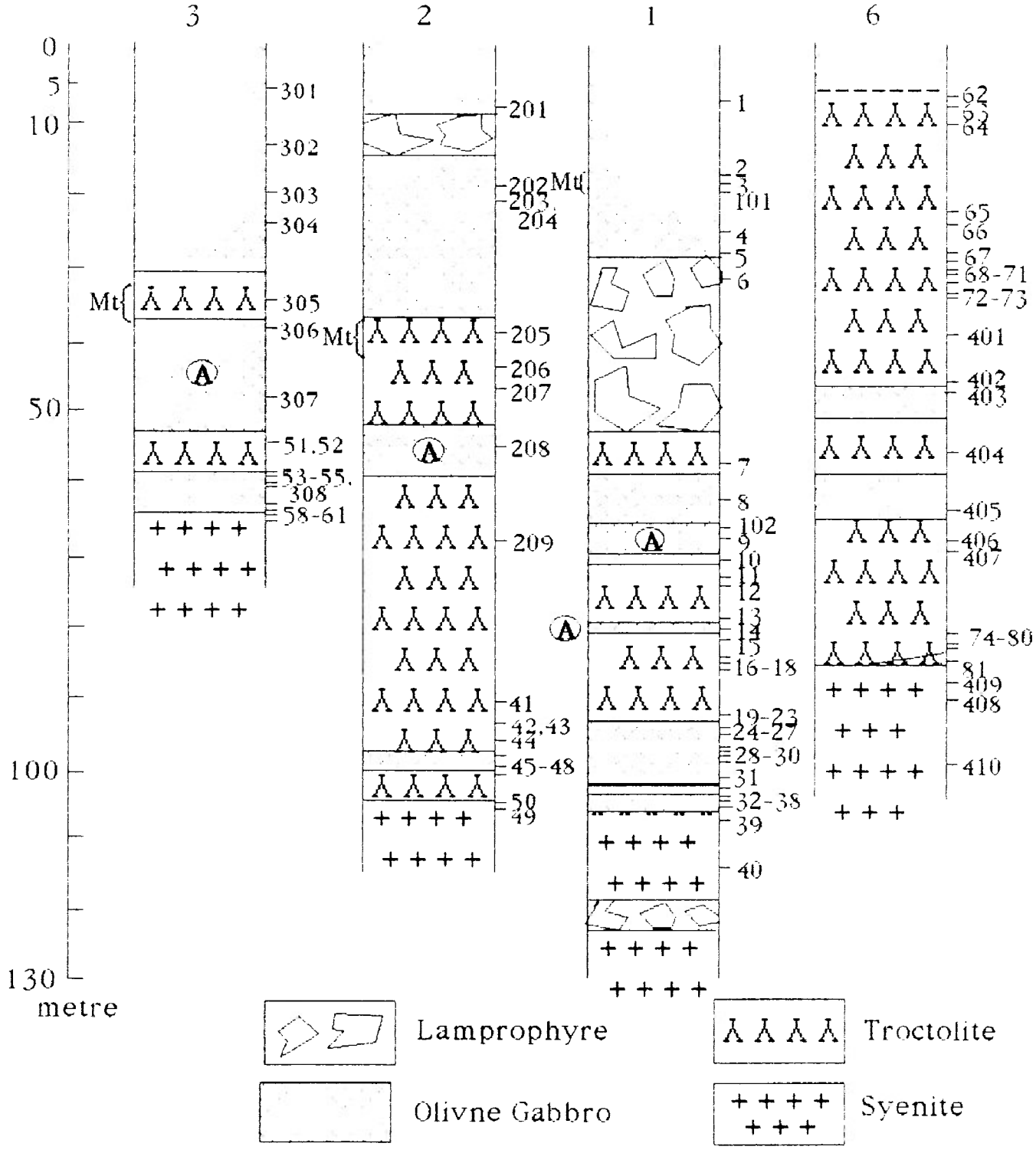

Figure 1.6 Fence diagram showing the lithologies of the studied cores. A: allotriomorphic gabbro, Mt: magnetite-rich layer, -101: sample location and number.

found to consist primarily of troctolite and gabbro which vary in thickness of the individual units and in the number of repetitions. The troctolite forms the basal units in cores 2 and 6. It is also the predominant rock type in lower section of cores 1 and 2, and in upper section of core 6. The gabbro, averaging 30 m thick, overlies the troctolite and extends up to the present surface in cores 1, 2 and 3. It exhibits ophitic and allotriomorphic textures. The contact between troctolite and gabbro is gradational, producing a rock with a characteristic of both rocks. The two rock types have undergone some degree of alteration which is characterized by red-brown pigmentation of the feldspar minerals. The extent of this alteration varies from core to core; its thickness ranges from few centimetres to over 25 cm. Approximately 10 % of rocks in core 1, 2 and 3 have been altered. However, about 30 % of the rocks in core 6 has been altered. The troctolite and gabbro were intruded by porphyritic olivine lamprophyre.

Disseminated and massive sulphide mineralization occurs in the troctolite and gabbro. The main sulphide minerals, chalcopyrite and bornite, are readily identifiable in hand specimens. The mineralization tends to become concentrated towards the gabbro-syenite contacts, and extends to a small portion of the syenite. Assay results show that palladium is the main platinum-group element present, and that silver and copper are the other principal metals. Detailed descriptions of the mineralization are given in Chapter 3.

1.3.3 Objectives and Methods

Objectives The three main objectives of this thesis are:

1. to determine the petrology and geochemistry of the Geordie Lake intrusion and its relationship to other gabbroic rocks in the Coldwell complex,

2. to characterize the mineralization in terms of modes of occurrence of the platinum-group minerals and associated tellurides, oxides, sulphides, and lesser sulpharsenide and arsenide, and

3. to combine objectives (1) and (2) in order to estimate the most likely conditions of mineralization in terms of temperature, and partial pressures of Te_2 and S_2.

Methods 109 core samples were collected from drill cores 1, 2, 3 and 6. Sample locations are shown in Figure 1.6. Both unmineralized and mineralized specimens were studied. Various analytical methods, described in Appendix I, were used to obtain the data. The following are brief descriptions of the methods used.

The composition of the silicate minerals, with the exception of olivine, was determined by the electron microprobe. Olivine compositions, tellurides, and platinum-group elements were analysed using an X-ray energy dispersive analyser attached to a scanning electron microscope. Sulfide, sulfarsenide and arsenide minerals were analysed using the electron microscope and energy dispersive analyser.

Thirty seven samples (24 from GLI and 13 from Center I and II rocks) were analysed by X-ray fuorescence and neutron activation analysis (NAA) methods for major and trace elements. The latter include Ni, Cu, Zn, Pb, Zr, Y, Sr, Ba, Rb, Ce, Cr, Ta, Sc, Co, Th, La, Ce, Nd, Sm, Eu, Tb, Yb, and Lu. The NAA was performed by the writer.

CHAPTER 2

PETROCHEMISTRY OF THE GEORDIE LAKE INTRUSION

2.1 Introduction

This chapter describes in detail the petrography, mineral chemistry, and whole rock geochemistry of the Geordie Lake intrusion (GLI). Each section includes a comparison with rocks that are relatively similar from other localities, and concludes with a discussion of the data. This chapter ends with an integration of the information gathered from all sections in order to define the nature of the GLI.

2.2 Petrography

Examination of more than 100 thin sections revealed that the GLI consists essentially of troctolite and olivine gabbro. The petrography of the troctolite is described first, followed by the gabbro and other subordinate lithologies, including the eastern syenite which borders the GLI. Criteria for the grain size are as follows: fine (<1 mm), medium (1 - 4 mm), and coarse (>4 mm). Visual estimation of the modal composition of rocks is based on the diagrams of Williams *et al.*, (1982). The rock classification and nomenclature used in this thesis are based on the IUGS system (Streckeisen, 1976).

2.2.1 Troctolite

The majority of the troctolite exhibits harrisitic texture, i.e. olivine occurs as branching/dendritic crystals (Figure 2.1). The other textural variety of troctolite is allotriomorphic, consisting of medium-grained subhedral to anhedral olivine and plagioclase. A magnetite-rich troctolite layer (Figure 2.2) occurs in the upper section of cores 1, 2 and 3. The order of crystallization of primary phases in the troctolite is apatite/magnetite, olivine, plagioclase, clinopyroxene, primary amphibole and biotite.

Olivine dendrites developed both non-crystallographic and crystallographic branching styles but they did not occur together. The first style is characterized by secondary bladed branches which have no fixed orientation with respect to the main crystal. In the crystallographic-branching olivine, the branches are inclined to between 50°-60° to the main branch. Dendritic olivines may reach 6 cm in length and 5 mm in width with numerous tiny branches and feather-like sub-branches. Medium-grained subhedral olivine is a minor feature in the troctolites. The olivines are generally enclosed by plagioclase oikocrysts. In sample G-87-7, numerous olivine and magnetite crystals are enclosed in plagioclase and clinopyroxene oikocrysts.

Unaltered olivine is colourless and has a narrow corona. Altered olivines are pseudomorphed by colourless to green serpentine minerals. The fractures and margins of altered olivine crystals are replaced by magnetite. The coronas of altered dendritic olivine range from less than 0.1 mm to 0.75 mm in width (generally about 0.2 mm in width). The corona of a

Figure 2.1 Photomicrograph of a dendritic olivine showing its branches and coronas. The olivine is reddish brown due to alteration. The opaque mineral along the cracks and rims is secondary magnetite. The plagioclase at left corner is unaltered despite the advancing coronas. Sample G-12.

Figure 2.2 Photomicrograph of a magnetite-rich (euhedral opaque) troctolite. The olivine (right) has been altered to aggregated serpentine mineral. The clinopyroxene (blue) is unaltered. Sample G-7.

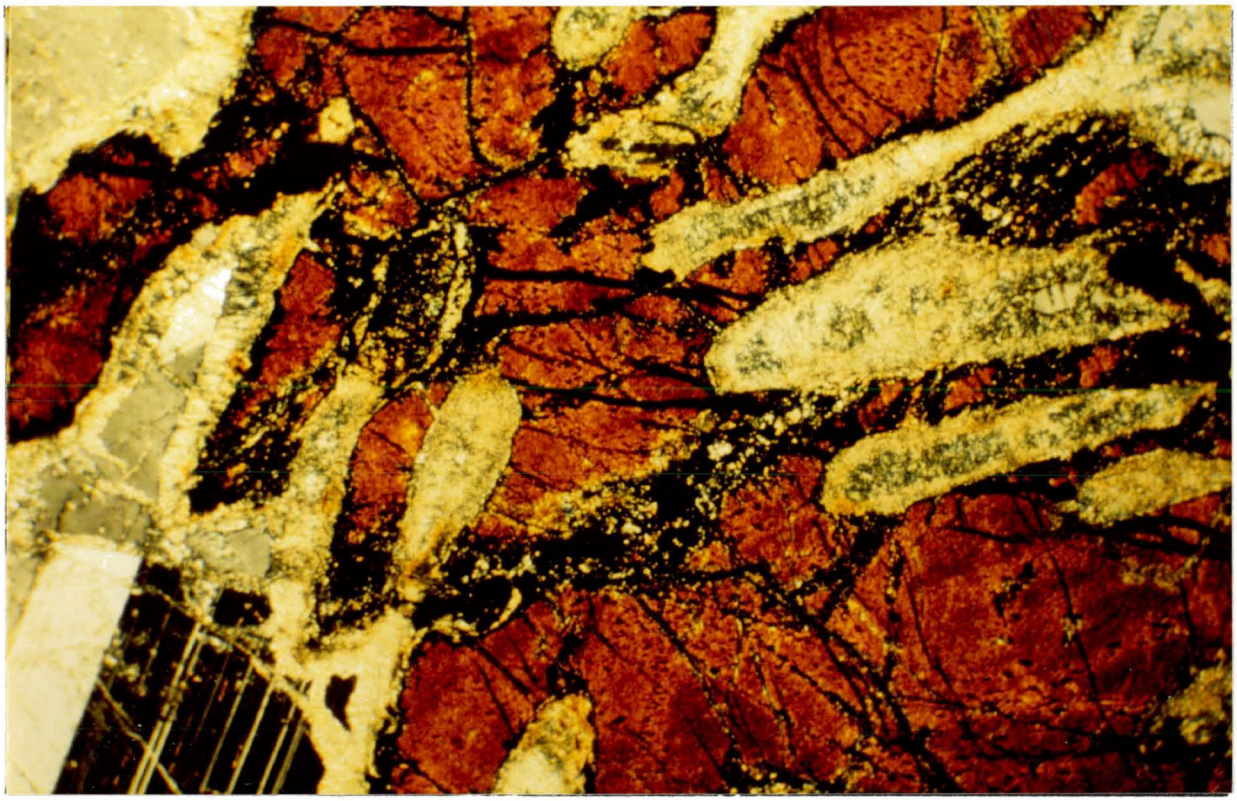

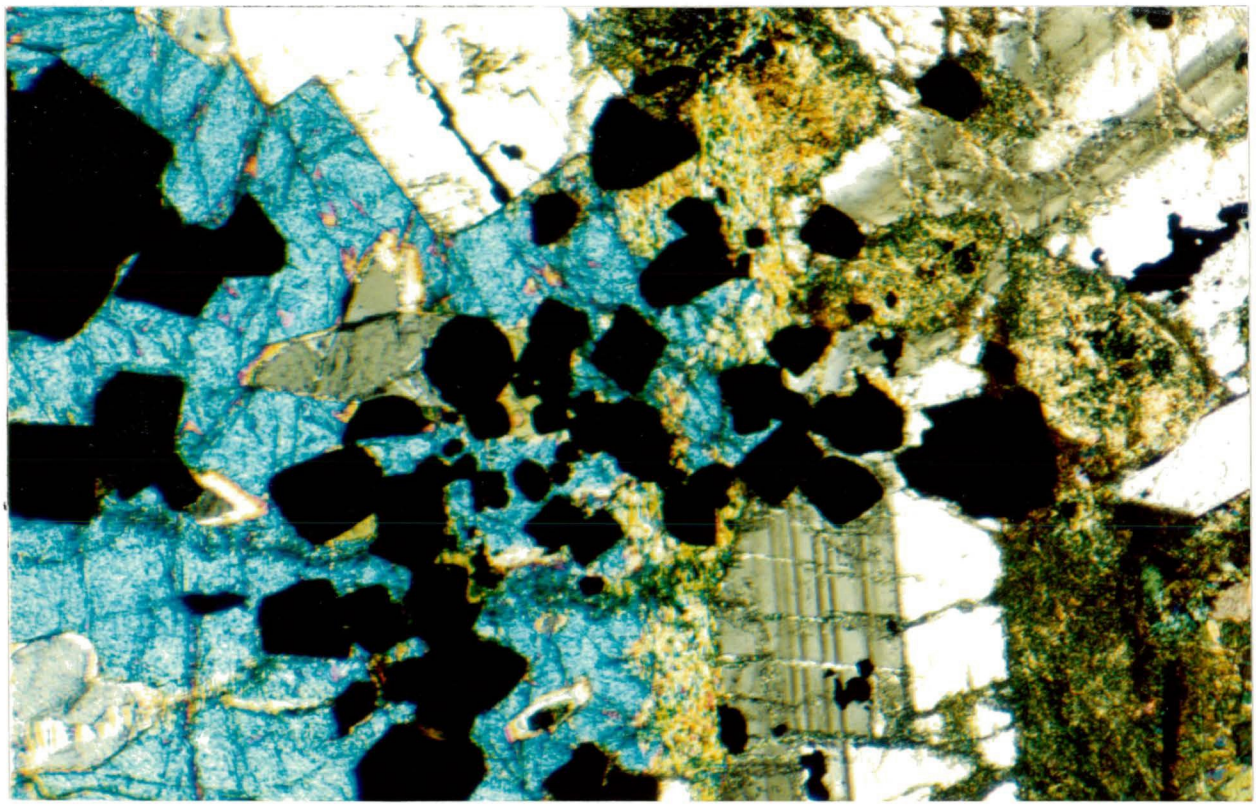

0 2mm

completely altered olivine can consist of at least 6 sub-shells; from inner to outer shells, they are 1) fine magnetite grains, 2) aggregated low birefringence minerals with yellow cores, 3) elongated and sinuous rods of magnetite, 4) elongated pyroxene fibres parallel to the olivine crystal edge, 5) massive tiny fibres, and 6) acicular pyroxene perpendicular to the olivine crystal edge. The contact between the outermost shell and the plagioclase is ragged. The width of this multiple corona is about 0. 75 mm.

Plagioclase (An_{49-57}) is medium- to coarse-grained. Twinning is common. In samples where olivine crystals have been extensively altered and have developed wide coronas, coarse-grained plagioclase remains unaltered. In these samples, finer plagioclase crystals are enclosed by the olivine coronas. The corona minerals also fill in cracks of the plagioclase.

Clinopyroxene is represented by augite and constitutes a minor phase in the troctolite. When present, it occurs as subhedral grains ranging from 2 mm to 5 mm. The abundance rarely exceeds 3 modal percent, especially in the coarse-grained troctolite. Uralitization along crystal edges is common in moderately and extensively altered troctolites.

Amphibole of primary origin is scarce and is not always present, especially in relatively-unaltered troctolites. Both brown and green amphiboles occur independently in the troctolites. Subsolidus amphiboles replacing clinopyroxenes are common in altered troctolites. Extensive amphibolization commonly leaves "islands" of unaltered clinopyroxene. Complete amphibole pseudomorphs after clinopyroxene resemble primary amphiboles and the amphibole is generally actinolite. Aggregated acicular actinolites also replaced clinopyroxene.

Magnetite occurs as euhedral and skeletal grains (1 to 5 mm in length) constituting approximately 3 % of the modal mineralogy, with the exception of the uppermost troctolite unit in core 1, 2 and 3 (Samples G-87-7, -205 and -305, respectively) which contains approximately 10 % magnetite. All primary magnetite grains have exsolved ilmenite lamellae (Figure 2.3). In the extensively-altered troctolite, some magnetite grains are corroded. Discrete grains of ilmeno-magnetite and ilmenite occur in sample 31 (Figure 2.4).

Biotite occurs as discrete grains dispersed in other silicate phases and as fringes to magnetite and serpentinized olivine. Clusters of biotite flakes are also commonly intergrown with subsolidus actinolites. Subsolidus biotites rim clinopyroxenes.

Apatite occurs as fine- to medium-grained euhedral crystals (0.1 to 0.5 mm across) dispersed randomly throughout the rock, and as tiny inclusions in the harrisitic olivines and skeletal magnetites. Apatite abundance varies from <1 to 3 modal percent. The grain boundary between apatite and any other phase is normally sharp, even though some apatites are surrounded by secondary actinolites. Apatite inclusions are resorbed, and have subrounded grain boundaries.

2.2.2 Olivine Gabbro

The olivine gabbro, hereafter referred as gabbro, is texturally divisible into ophitic and allotriomorphic varieties (Figures 2.5-2.6). The former type predominates (50 % of the GLI) and occurs in all cores, whereas

Figure 2.3 Photomicrograph of a skeletal magnetite showing exsolved ilmenite lamellae. Sample G-21.
Full scale bar in µm.

Figure 2.4 Photomicrograph of discrete magnetite (MT) and ilmenite (IL) co-existing with chalcopyrite (CC). Sample G-31.
Full scale bar in µm.

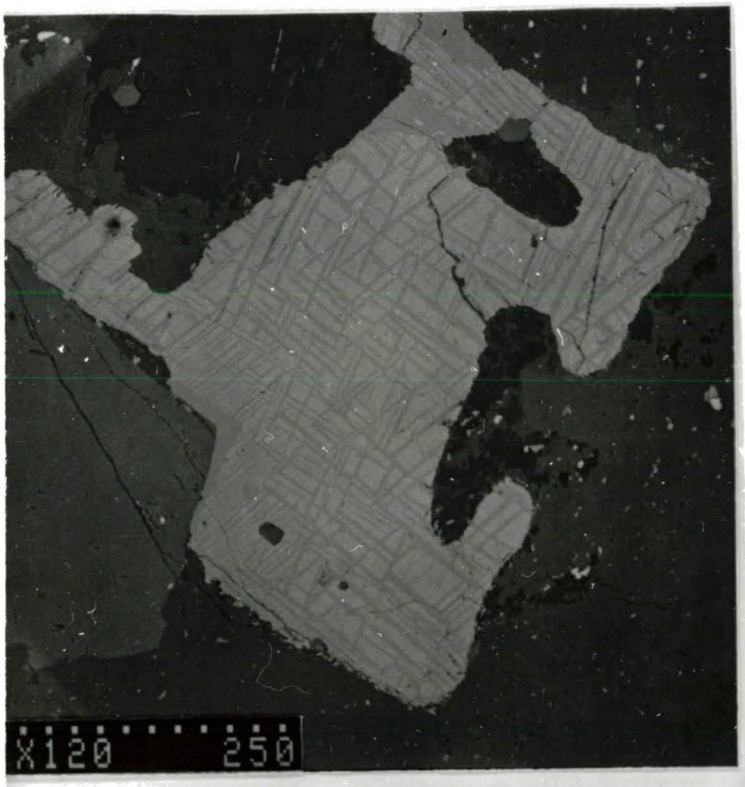
X120 250

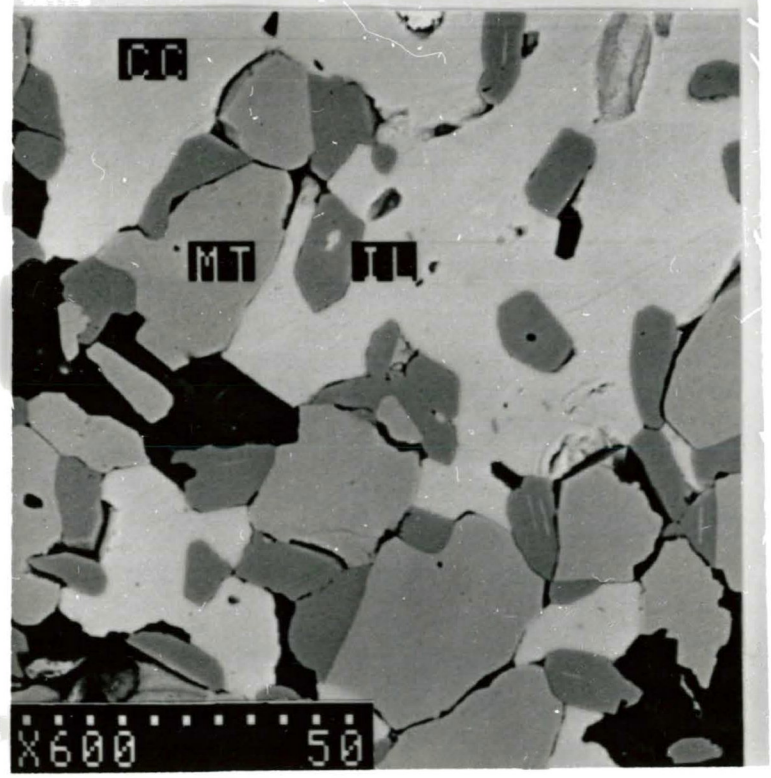
CC
MT
IL
X600 50

Figure 2.5 Photomicrograph of an ophitic olivine gabbro showing the clinopyroxene enclosing plagioclase laths. Sample G-1.

Figure 2.6 Photomicrograph of allotriomorphic gabbro. Clinopyroxene (high birefringence), plagioclase (white) and anhedral amphibole (green) are relatively unaltered. Olivine crystals (right top and bottom corners) have been completely pseudomorphed by magnetite and serpentine minerals. Sample G-9.

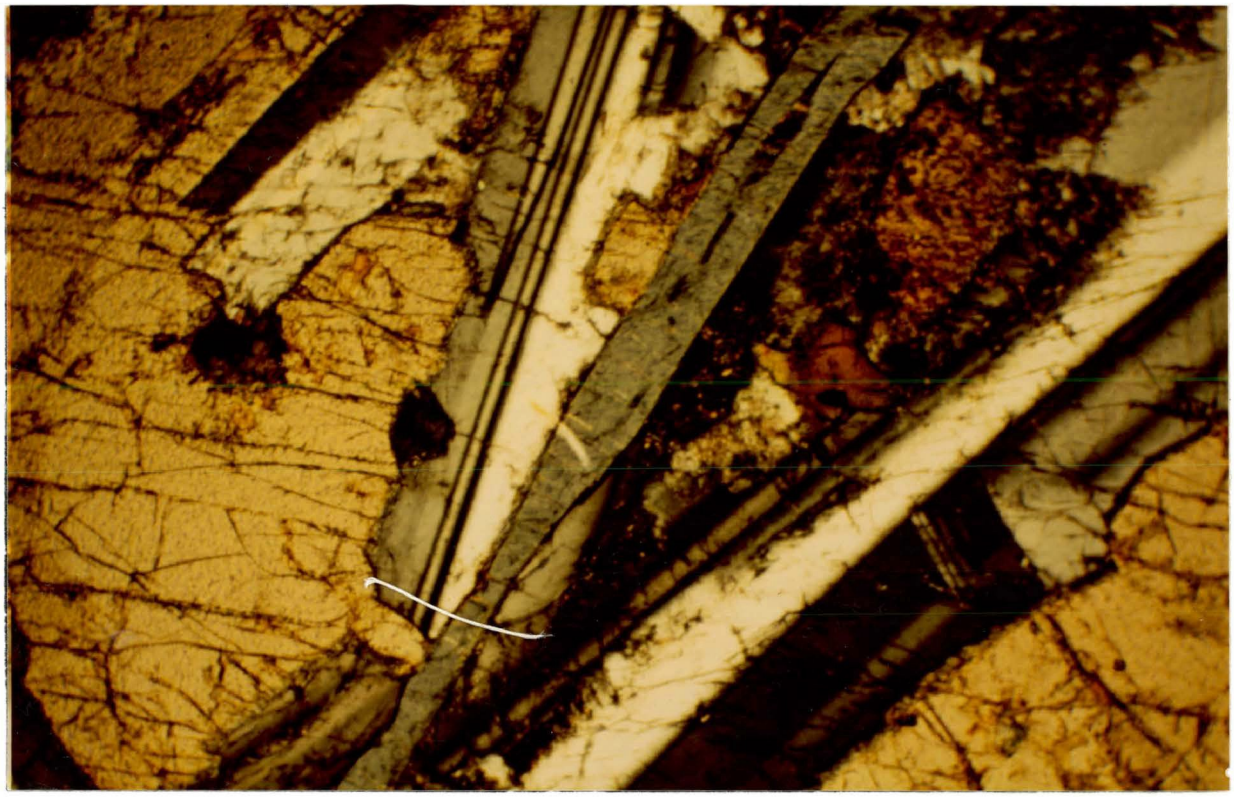

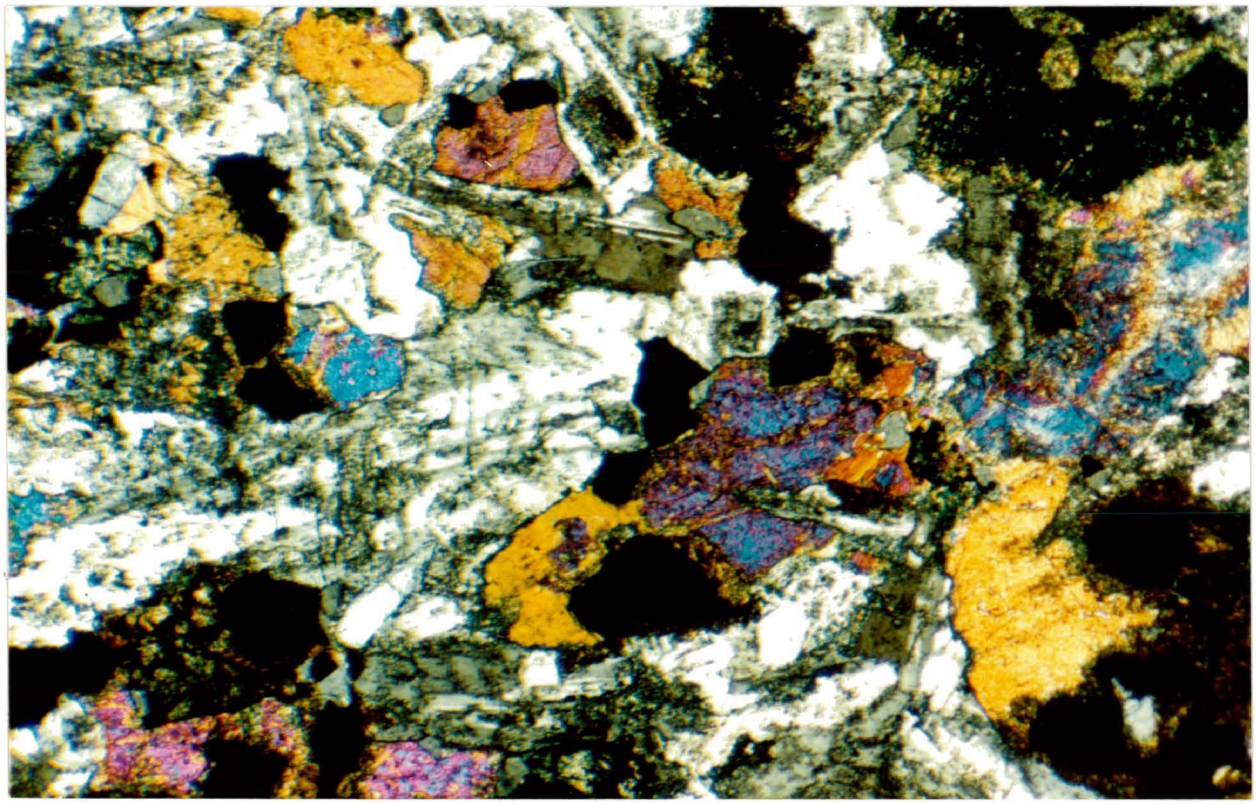

0 2mm

the latter constitutes about 25 % of the lithologies in drill core 3, and about 5 % in drill core 1 and 2. Sample G-15, which exhibits equigranular texture, only represents a small portion (less than 5 m in thickness) of core 1. The mineralogical character of this equigranular gabbro is similar to that of the ophitic gabbro.

Ophitic Gabbro is a medium- to coarse-grained rock, consisting primarily of subhedral clinopyroxene intergrown ophitically with plagioclase laths. Olivine and magnetite are minor phases. Accessory minerals are apatite, amphibole, biotite, zircon and sphene. Secondary minerals include actinolite, very fine-grained magnetite and serpentine. The texture and mineralogy of this gabbro remain relatively constant throughout the cores. A small portion of ophitic gabbro contains approximately 7 percent fine-grained magnetite. Representative samples of the magnetite-rich gabbro are G-87-2, -3, -4, and -205. The order of crystallization for the ophitic gabbro is apatite, magnetite/olivine, plagioclase, clinopyroxene, amphibole and biotite, and for the magnetite-rich gabbro is magnetite, apatite, olivine, plagioclase, clinopyroxene, amphibole/biotite.

Plagioclase generally occurs as subhedral to euhedral laths ranging from 2 mm to 5 mm in length. Albite and Carlsbad-albite twinning is common. Unaltered plagioclase has a narrow range of An-content (48 - 52). Many plagioclase crystals are mantled by a dusty feldspars, some of which have been determined by analysis to be albite and some alkali-feldspar (sections 2.3.2 and 2.3.3). The mantles, however, cannot be distinguished from one to another by petrographic observation.

Clinopyroxene is predominantly augite and rarely salite. Both types

are unzoned, colorless, and occur as medium- to coarse-grained subhedral grains. Many clinopyroxene crystals poikilitically enclose apatite and magnetite grains. Uralitization along crystal margins and cracks is common, whereas completely pseudomorphed clinopyroxenes by amphiboles occur in the more altered rocks.

Olivine in the ophitic gabbro is completely altered to aggregates of fine-grained magnetite and fibrous actinolite or serpentine. Its relicts consist of medium-grained anhedral to subhedral grains embedded in the plagioclase and clinopyroxene. Some olivine grains have developed both single- and multiple-shelled coronas. A single-shelled corona generally consists of massive, very fine yellowish green mineral aggregates. Some of these aggregates coarsen outwardly, forming perpendicular fibres to a plagioclase lath. The characteristics of the multiple-shelled corona are similar to those of troctolite.

Magnetite is common and occurs as small euhedral (< 1 mm across) to large skeletal grains (> 5 mm). It constitutes between 3 and 4 % of the modal mineralogy. A small portion portion of ophitic gabbro in core 1 contains about 10 % fine- to medium-magnetites which exhibit both euhedral and skeletal textures. All early crystallized magnetites host exsolved ilmenite lamellae (similar to Figure 2.3). Secondary magnetite (0.1 to <1 mm across) occurs as aggregated grains filling the irregular fractures of the partially and completely-altered olivine crystals.

Primary amphibole, when present, occurs as small subhedral individual grains constituting approximately 5 % of the modal mineralogy. Most amphiboles are green, although brown amphiboles are present in

samples G-11, 26 and 407. Both brown and green primary amphiboles have been observed to co-exist in sample 26. Subsolidus amphibole, mantling augite is common, particularly in rocks showing moderate and strong alteration. Subsolidus amphiboles are actinolite and actinolitic hornblende (microprobe analyses, Figure 2.27). Acicular amphibole aggregates completely replace clinopyroxene (?).

Biotite is not present in all samples. It occurs as tiny subhedral flakes exhibiting either brown or reddish-brown pleochroism, as discrete grains, as clustering flakes intergrown with acicular actinolites, and as tiny flakes fringing the skeletal magnetites. Some biotites also partially replace amphibole.

Feldspar occurs as anhedral grains in the more altered rocks. In handspecimens, it appears pink and mantles plagioclases (Figure 2.10). The optical character of this feldspar is obscured because it contains abundant fine yellowish-brown particles which cause the feldspar to appear dusty. Electron microprobe analyses of dusty feldspars show that some are albite and others are orthoclase (Section 3.3.2). However, they cannot be distinguished petrographically.

Apatite is present in all samples (1 to 3 % of the modal mineralogy). It is fine- to medium-grained ranging from <1 to 3 mm in length. Apatite is intergrown with magnetite grains in the magnetite-rich gabbro. Some apatite grains are entirely enclosed within magnetite grains. Only a few apatites show resorbed grain boundaries.

Rare minerals include zircon, sphene, monazite, thorite, uraninite, allanite, cerium niobate ($CeNbO_4$), greenockite (CdS, Figure 2.7) and

unidentified minerals containing Y, Nb, and Ca (Figure 2.8).

Allotriomorphic Gabbro is fine- to medium-grained, consisting of anhedral plagioclase, clinopyroxene and altered olivine (Figure 2.6). The former two minerals make up about 75 % of the modal mineralogy. The minor phases are biotite, amphibole, magnetite, and very fine-grained apatite. A narrow shear zone cuts this gabbro and has resulted in a weak parallel alignment of the plagioclase, clinopyroxene and amphibole grains. Representative samples of allotriomorphic gabbro are G-9, 208, 306, and 307.

Plagioclase occurs as fine subhedral laths (averaging 1 mm in length) with sutured grain boundaries. Most of the plagioclase crystals are mantled by clear albite and dusty feldspar.

Clinopyroxene is subhedral to euhedral and averages less than 1 mm in length. It is colourless and unzoned. In slightly-altered samples, the clinopyroxene is usually mantled by green actinolite.

Olivine in allotriomorphic gabbro has been completely altered and replaced by aggregates of serpentine or green actinolite. Magnetite replaces olivine margins and fills in cracks. The olivine relicts indicate that the original grains were fine-grained.

Biotite constitutes about 8 % of the modal mineralogy. It always occurs as individual or aggregates of fine-grained euhedra or subhedra. Some biotite flakes fringe magnetite and olivine. Altered biotites are mantled by light green amphibole.

Amphibole occurs as subhedral grains (5 modal %), approximately

Figure 2.7 Back-scattered electron image of a euhedral greenockite enclosed in massive chalcopyrite. Euhedral and subhedral grey crystals (lower photograph) are magnetite. Sample CW-1.

Figure 2.8 Back-scattered electron image of an unknow Y-Nb mineral in chalcopyrite. Sample G-55A.

Full scale bar in μm

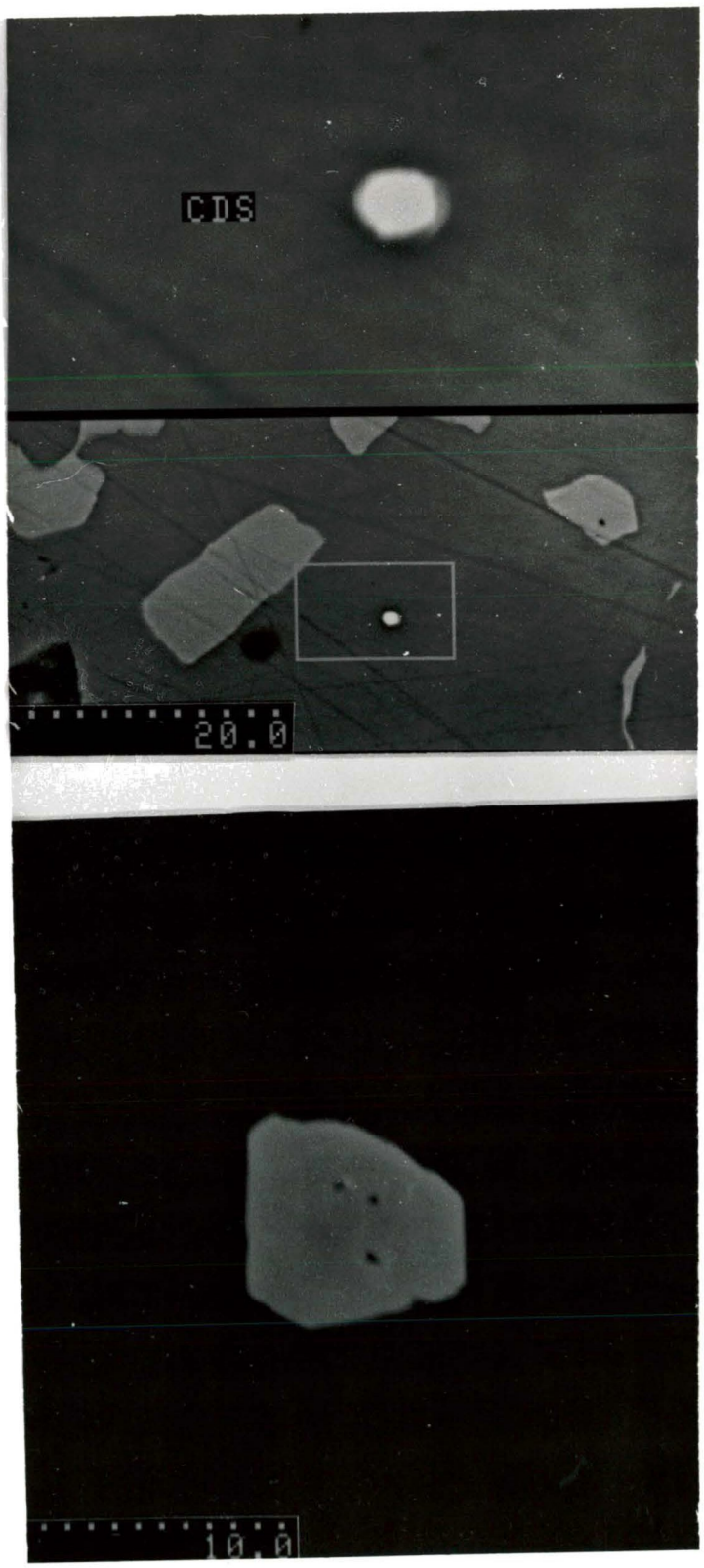
CDS
20.0
10.0

0.5 mm in average length. Subsolidus amphibole replaces clinopyroxenes in altered samples.

Magnetite, the only primary opaque mineral found in the allotriomorphic gabbro, is present as fine-grained subhedral to skeletal forms (3 or 4 modal %). Magnetite grains host crystallographically-controlled exsolution lamellae.

2.2.3 Altered Gabbroic Rocks

There are portions of troctolite and gabbro in which alteration is conspicuous in handspecimens. These rocks are called the altered gabbroic rocks. The term alteration in this section refers to mineralogical and textural changes due to fluids of unspecified origins. The relative intensity of alteration can be determined by the degree of preservation of the original texture and mineralogy. For the purpose of this thesis, the alteration intensity is divided into a weak and strong alteration.

Weak alteration, which is characterized, in handspecimen, by a pink pigmentation of the plagioclase crystals (Figure 2.9), occurs extensively in core number 6. In coarse-grained altered gabbros, this pink plagioclase commonly mantles white plagioclase. The clinopyroxene remains dark green or black. The gabbro, therefore, appears to be pink, white, and dark green. In fine-grained gabbros, the pink feldspar is the groundmass of the other phases.

In thin section, the clinopyroxene is slightly altered (Figure 2.10) and the feldspar is sericitized (Figure 2.11) and albitized. The tiny brown

Figure 2.9 Photograph of a portion of a weakly altered coarse-grained gabbroic rock showing albite (pink) mantles on plagioclase (white translucent). The black minerals are clinopyroxene. Sample G-402.

Figure 2.10 Photomicrograph of a relatively unaltered clinopyroxene in a weakly altered rock. This twinned clinopyroxene shows incipient uralitization along its margin. The opaque minerals are magnetite. Apatite occurs at center left. The greenish brown phase between the clinopyroxene and apatite is altered plagioclase. Cross-polars. Sample G-303.

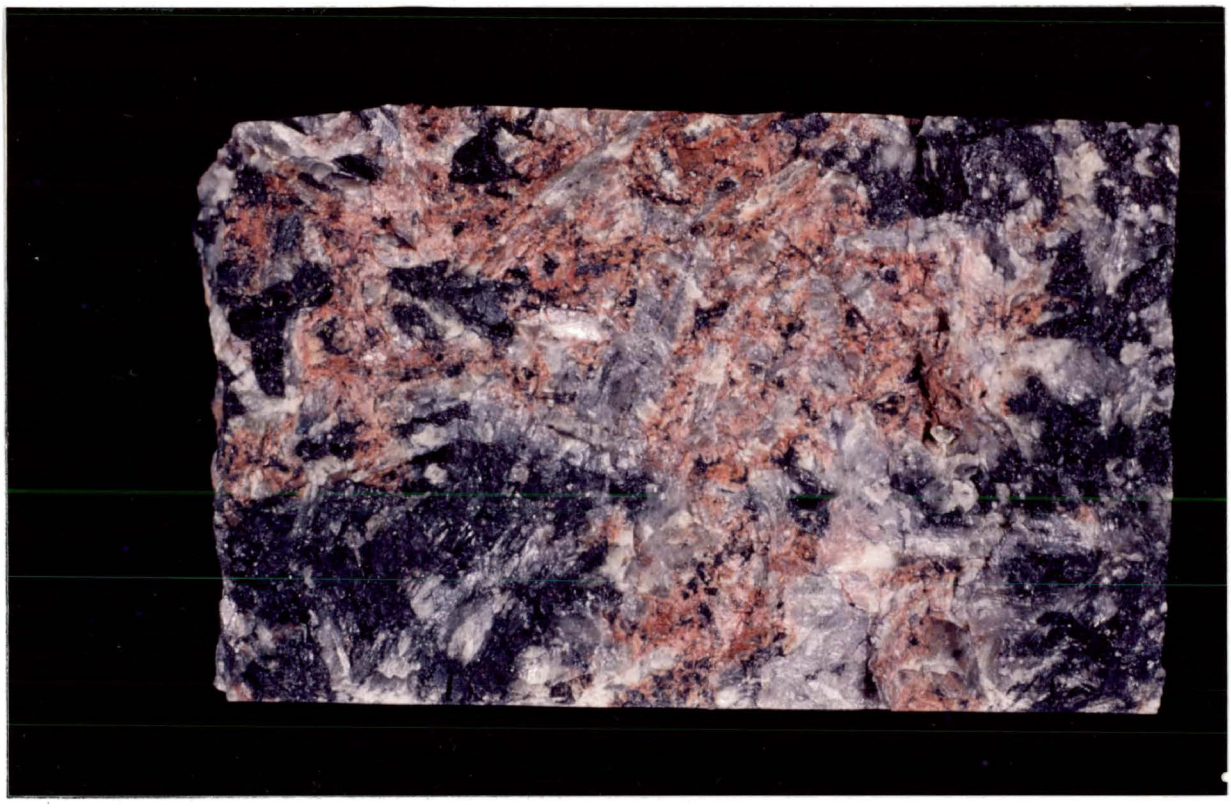

0 1cm

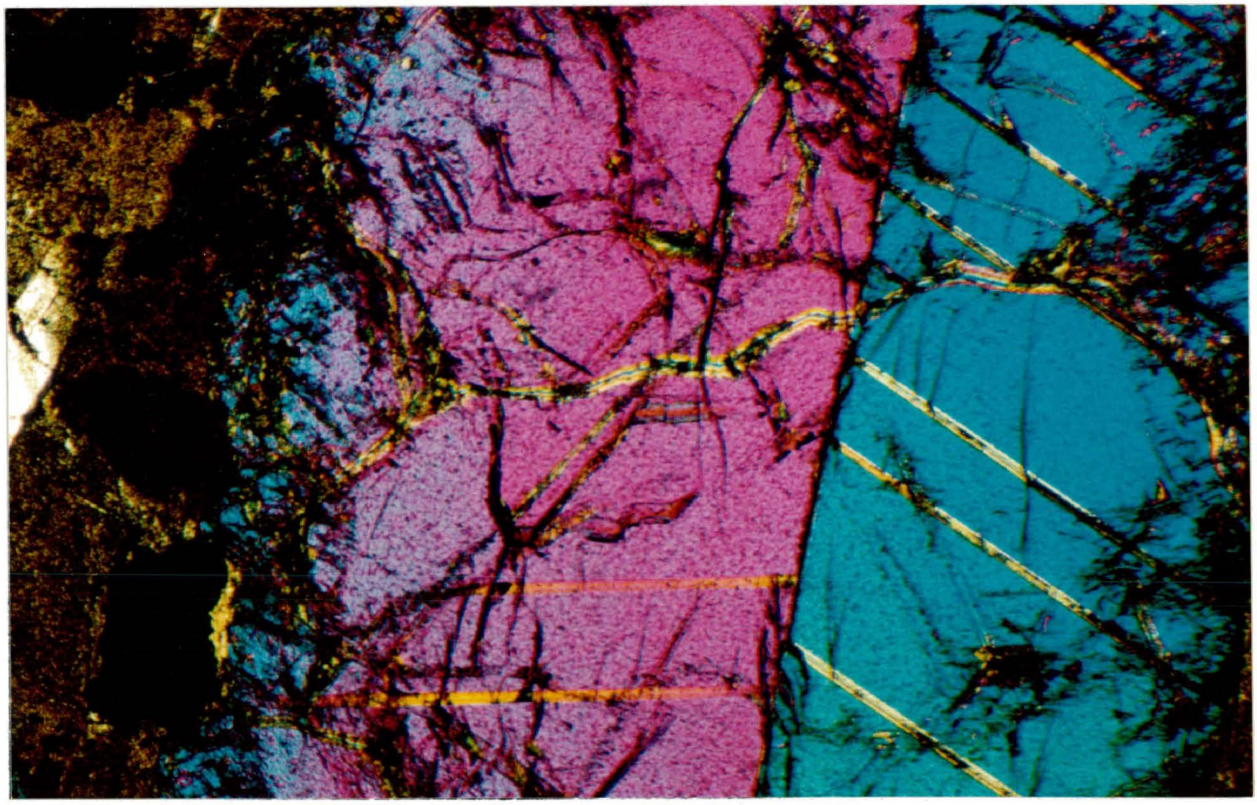

0 0.6mm

amphibole and biotite are subhedral and appear unaltered. Some apatite crystals are resorbed. Most skeletal magnetites are unaltered; some crystals have corroded edges. The olivine relicts are still present.

The strongly altered gabbroic rocks (samples G-30 and 44) appear pinkish white in handspecimen (Figure 2.12). In thin section, the rocks are allotriomorphic medium-grained and consist primarily of subhedral to anhedral plagioclase and K-feldspar (65 modal %) and subhedral clinopyroxene. Extensive albitization of plagioclase, including the development of dusty mantles, is common. Clinopyroxenes have been partially uralitized, corroded, and recrystallized into tiny aggregates. Amphibole is fine-grained and exhibits faint green pleochroism. It is also intergrown with some clinopyroxene crystals. Magnetite and actinolite aggregates replaced olivine and pyroxene. Small euhedral apatite crystals remained unaltered. Fine-grained magnetite is anhedral and shows corroded edges. Fine-grained quartz occurs interstitial to feldspars. The olivine relicts and abundant clinopyroxene demonstrate that the precursor to this strongly altered rock was gabbro.

2.2.4 Quartz Syenite of Center I

The Center I quartz syenite, referred to as syenite, bordering the GLI has been recrystallized (Figure 2.13). The feldspars have developed subgrains and anhedral grain boundaries, and the mafic minerals display mosaic aggregates typically intergrown with magnetite and chalcopyrite. A sample collected about 10 metres away from the contact exhibits less severe

Figure 2.11 Photomicrograph of sericitized plagioclase lath in the altered gabbroic rock. The anhedral and high relief grains are resorbed apatite. Sample G-303.

Figure 2.12 A strongly altered gabbroic rock which resembles a syenitic rock. This altered rock is rare and occurs in a zone less than 10 cm wide in core 2. Sample G-44.

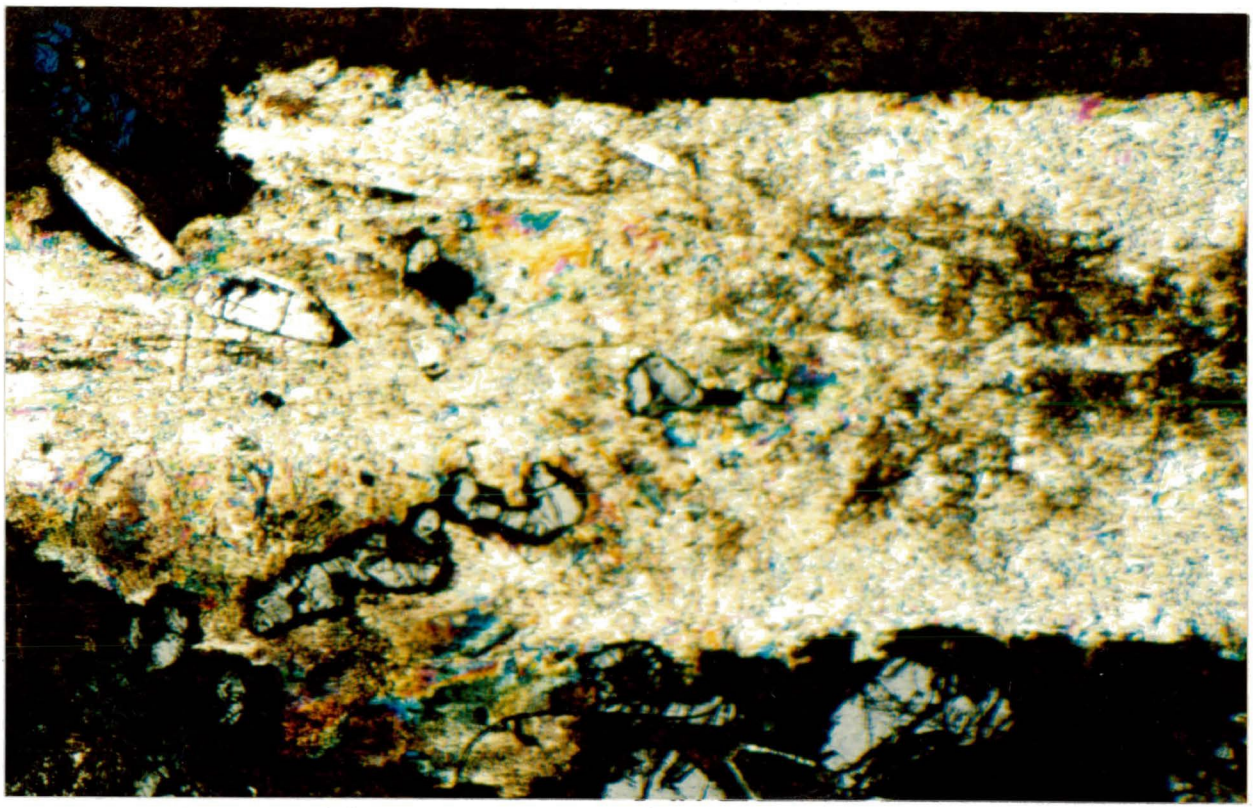

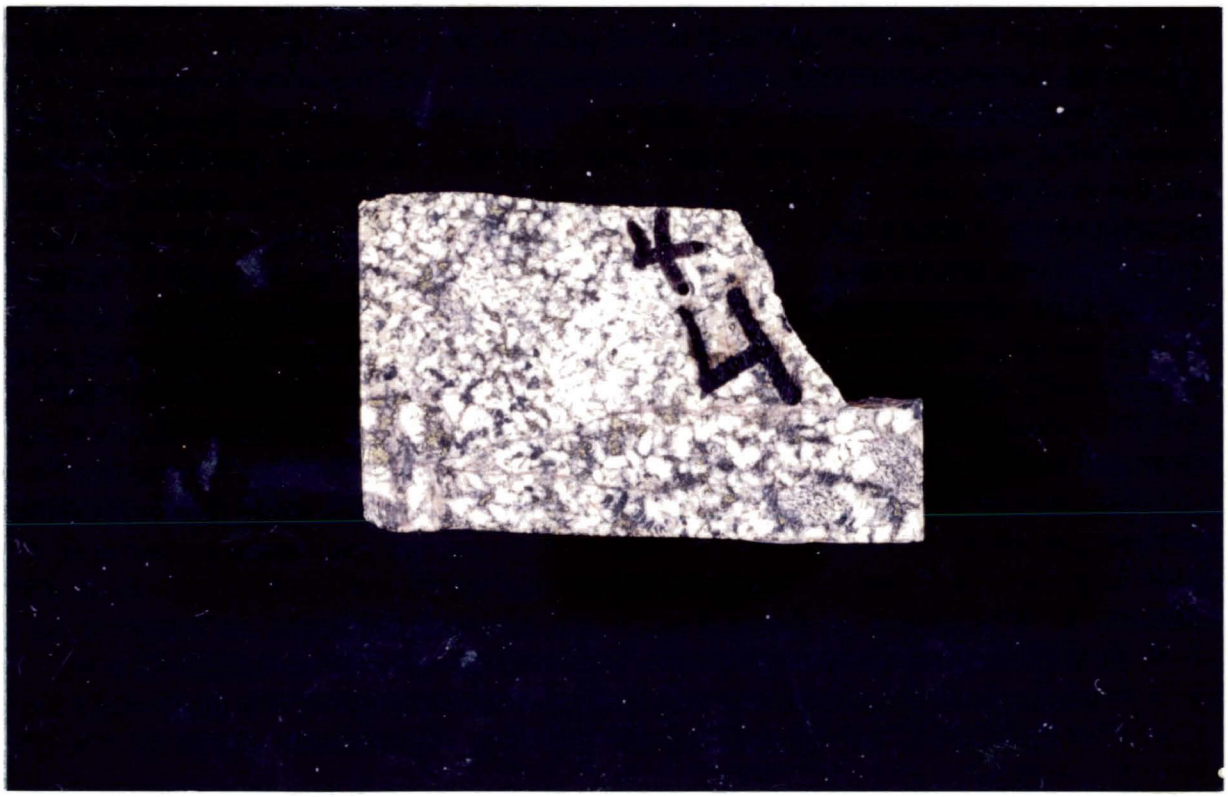

37 b

Figure 2.13 Photomicrograph of a recrystallized Center I syenite at the contact zone. The mafic minerals have been transformed into aggregates of crystals. Some of the feldspars have developed polygonalization (white, below). Sample G-61.

Figure 2.14 A less-severely recrystallized syenite, 10 metres away from the contact. The polygonalization of the feldspars is still apparent (right). However, the other feldspars (light green) and some clinopyroxene (light yellow, below) are not severely recrystallized. Sample G-410.

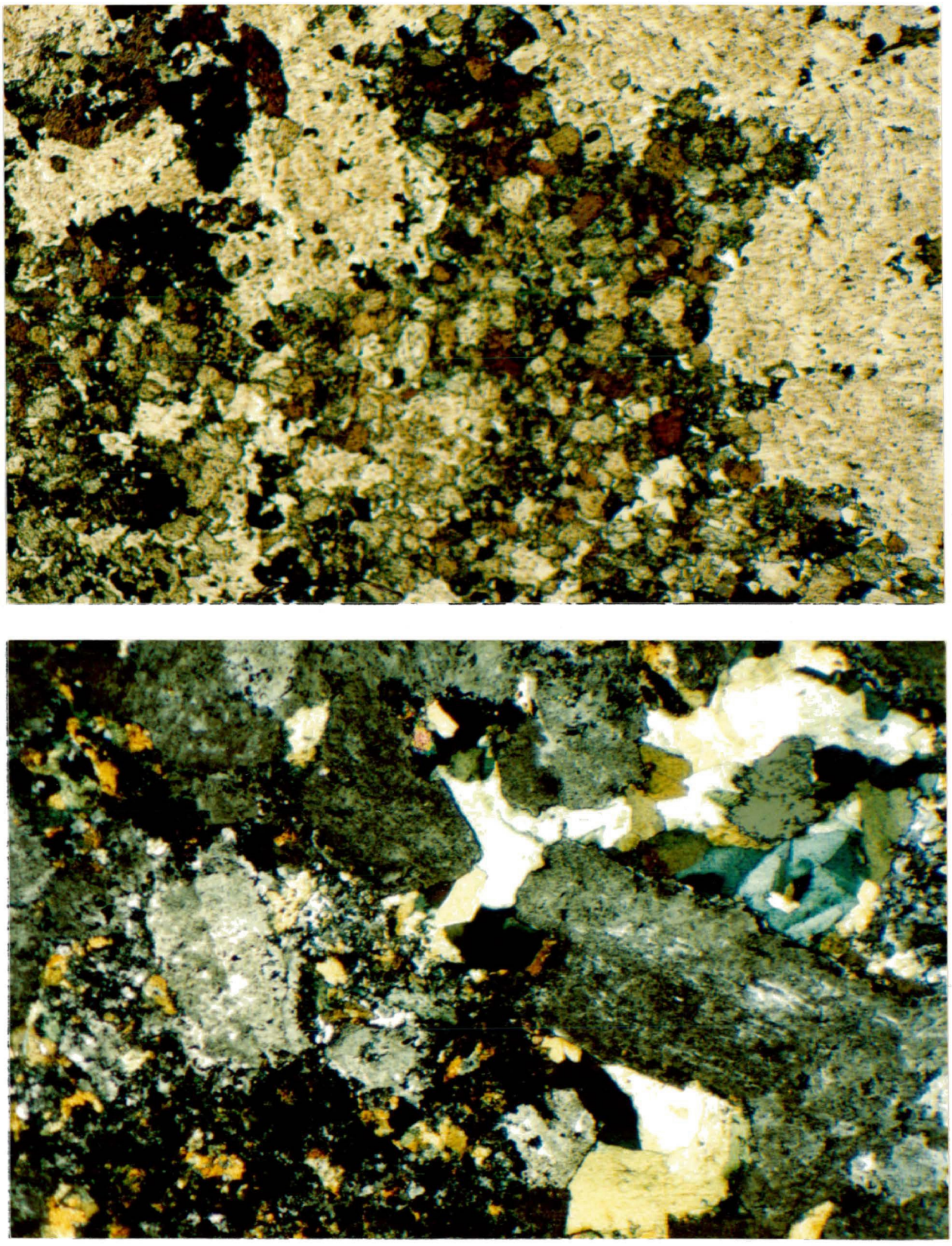
0
1mm

recrystallization (Figure 2.14) than at the contact zone. The GLI at the contact zone shows no evidence of deformation or recrystallization, illustrating that the GLI has possibly intruded the syenite.

The medium-grained syenite, consists primarily of anhedral alkali-feldspar containing small hematite particles, and plagioclase with albite mantles and amphibole. The alkali-feldspar also shows a perthitic texture in which trails of green epidote are aligned with the exsolved albite. Quartz and alkali-feldspar form a granophyric texture. Green amphibole occurs as tiny aggregates, most of which, together with epidote, form trails along the feldspar interstices. Magnetite and apatite are fine-grained and ubiquitous.

2.2.5 Comparisons to other Basic Intrusions

This section compares the petrography of the GLI to Center I and II gabbroic rocks of the Coldwell complex.

Aubut (1977) studied the Center I gabbro which is exposed in the western margin of the Complex. Much of this gabbro has undergone recrystallization as indicated by the polygonized plagioclase crystals. Examination of samples containing non-recrystallized plagioclases showed that the average length of these plagioclases is 2 mm (maximum 6 mm), and that the clinopyroxene is anhedral, averaging 2.5 mm in length. The original texture of the gabbro is most likely equigranular or subophitic. In contrast, the texture of the Geordie Lake gabbro is ophitic and allotriomorphic. Euhedral and skeletal magnetites in Center I gabbro average 1 mm in length.

In the GLI, the magnetite ranges from tiny euhedral to coarse skeletal grains.

Wilkinson (1983) divided the Center I gabbros just north of Coubran Lake (Figure 1.5) into two series: massive and layered. The former consists of:

1. fine-grained, subhedral-granular to porphyritic gabbro,
2. massive and subophitic heterogeneous gabbro, and
3. poikilitic to pegmatitic mottled gabbro.

The layered series consists of subophitic to poikilitic banded gabbro and its subsidiary dioritic units. Both series are considered to be mafic cumulus rocks. These gabbros are texturally different from the GLI, which is not layered or banded. Wilkinson described the olivine texture in the banded gabbro to be chain-like and aligned with the banding. This may be branching/dendritic olivine. However, the abundance of clinopyroxene and the interstitial habit of plagioclase in the banded gabbro make it distinct from the Geordie Lake troctolite. Furthermore, Wilkinson stated that the magnetite is subrounded and averages 2 mm in diameter. No skeletal magnetite is reported.

Lum (1973) studied Center I gabbros exposed at the road cut along Highway 17, and at a locality near Bamoos Lake (Figure 1.1), approximately 5 km north of the road cut. He defined 2 major types of gabbro: layered and massive. The layered gabbro is absent from the GLI. Lum made contradictory and ambiguous statements regarding the mineralogy of the massive gabbro; in one sentence he indicated that orthopyroxene is present, but in another, orthopyroxene is said to be virtually absent. In addition, he did not indicate whether the quartz in the massive gabbro is primary or secondary. The GLI is free of orthopyroxene and quartz. Nevertheless, the

massive gabbro and the Geordie Lake gabbro have similar ophitic textures.

Of the ten samples from Center II lithologies examined, only sample C-311 from Redsucker Cove can be compared with the GLI because the others are metasomatised and their original textures are obliterated. Sample C-311 is a medium- to coarse-grained gabbro containing subhedral ophitic clinopyroxene (>5 mm), slightly uralitized along its margins, and fine-grained plagioclase crystals (average 2 mm) with polysynthetic twinning. Many plagioclase laths are mantled by albite and contain hematite. Biotite is present as discrete and aggregated flakes and as replacement of magnetite. Euhedral apatite (2 mm in diameter) is ubiquitous. Skeletal magnetite is medium- to coarse-grained, some of which is enclosed in clinopyroxene or apatite crystals.

Most of the well-known basic intrusions such as the Muskox intrusion in Northwest Territories, Canada, the Bushveld complex of South Africa, and the Skaergaard Intrusion of Greenland are layered. The McIntosh (Mathison and Hamlyn, 1987) and Somerset Dam (Mathison, 1987) basic intrusions of Australia resemble the GLI in that they too consist of troctolite-olivine gabbro units. However, both intrusions are layered and contain cyclic units.

2.2.6 Discussion

An important aspect of petrography is that textures of an igneous rock or mineral can be used to infer the crystallization condition(s) of its parental magma (for example,Williams *et al.*, 1982). The Geordie lake intrusions feature mineral morphologies that indicate the relative cooling

rate of the parental magma.

The dendritic texture of olivine in the troctolite suggests that the rock crystallized rapidly. This inference is based on a study by Donaldson (1976) who examined experimentally the relationships between olivine morphology and crystallization conditions. His data show that there is a systematic change, with increase in cooling rate, from complete (euhedral) to progressively less complete (anhedral) crystals and from equant habit to elongated bladed habit to tabular habit. Ten categories of olivine morphology, ranging from slowest (1) to most rapid (10) cooling, were proposed with the dendritic/branching texture being the seventh.

According to Robins (1972) dendritic olivines are produced when the rate of crystal growth greatly exceeds the rate of spontaneous nucleation. Wager and Brown (1960) who studied the layered series of Rhum interpreted the dendritic olivine as the result of upward growth of cumulus crystals of olivine as they lay at the bottom of the magma, forming the temporary floor.

For the ophitic gabbro in which the olivine crystals have lost their original texture, crystallization conditions are inferred from the skeletal magnetites. The skeletal habit of a crystal has been interpreted as a result of growth and not of resorption (Donaldson, 1976). He also stated that an originally skeletal crystal will retain its skeletal shape during resorption, whereas, an originally polyhedral crystal becomes rounded, but not skeletal. The skeletal habit of the magnetites in the GLI is, therefore, a primary texture. Skeletal crystals in a basalt indicate that the basalt cooled rapidly (Craig and Vaughan, 1981). These observations suggest that the GLI

crystallized rapidly.

Another feature of petrological significance is the corona around olivine. Corona structures are believed to preserve evidence of changes in the environmental conditions experienced by the rock during its history (Griffin and Heier, 1973). Magmatic, metasomatic, deuteric, subsolidus, and metamorphic origins for corona development have been put forward by different researchers. It is beyond the scope of this thesis to elaborate upon these hypotheses. Instead, evidence against and for these hypotheses on the formation of corona in the studied rocks are presented below.

The metasomatic origin has been ruled out by Griffin and Heier (1973) as being unsatisfactory and unnecessary. The metamorphic origin is not applicable to the studied rocks because there is no evidence to show that the GLI had undergone metamorphism. Magmatic coronas are the mineral assemblage that was crystallized from the intercumulus liquid trapped between the olivine and plagioclase (Joesten, 1986). When in contact with a plagioclase, the typical mineral assemblage of the corona sequence consists of plagioclase: pargasite + spinel: orthopyroxene + spinel: orthopyroxene: olivine. In the coronas of the GLI, orthopyroxene is absent, and biotite (analysed by electron probe), instead of pargasite, borders the plagioclase.

The deuteric hypothesis suggests that the coronas were formed by an interaction between the olivine and deuteric fluid during the cooling of the rocks (e.g Williams *et al.*, 1982). The subsolidus hypothesis states that coronas represent the metastable products of early subsolidus reactions that occurred during cooling, as the rocks left the olivine-plagioclase stability field (Grant, 1988). The preceding descriptions have stated that coronas

developed around altered olivines and are in contact with the adjacent plagioclase and clinopyroxene which remain unaltered, and that coronas are also spatially related with secondary actinolites. These textural evidence do not allow a distinction to be made on whether the coronas are of deuteric or subsolidus origin.

The red pigmentation of the feldspars in the altered gabbro can be a result of potassic alteration and of iron staining. Boone (1969) suggested that decomposition and oxidation of biotite release the iron to form hematite that colours the feldspar. The present writer believes that in the GLI the altered olivine could have supplied the iron to colour the feldspars, since the biotite is unaltered and is not always present. Magnetite is unlikely to be the source of iron because it too is unaltered.

In summary, petrographic studies characterize the Geordie Lake intrusion as follows: (i) harrisitic troctolite and ophitic olivine gabbro are the major rock types, (ii) both rocks show a consistent mineralogy and texture throughout the succession, i.e., neither rock type is rhythmically layered, (iii) the absence of modal feldspathoids and alkali pyroxene and amphibole indicates that the GLI is mineralogically not alkaline, (iv) skeletal magnetites and dendritic olivines suggest that both rock types crystallized relatively rapidly, (v) recrystallization of the syenite at the contact zone appears to indicate that the Geordie Lake rocks intruded the syenite, and (vi) the GLI has no counterparts in the Center I and II gabbros of the Coldwell complex.

2.3 Mineral Chemistry

2.3.1 Olivine

Olivine compositions and their structural formulae from nine troctolite samples are listed in Table 2.1. Seven of these are from drill core 6, the other two from drill core 1. The olivines in other troctolites and in the gabbros could not be analyzed because they are completely altered.

The major elements in the olivines (Table 2.1) have a narrow range of composition: SiO_2 (35.02 to 36.22 wt. %), FeO (36.54 to 39.37 wt. %), and MgO (24.47 to 26.62 wt. %). MnO, the only minor oxide that can be accurately analyzed by the energy dispersive analysis method, varies from 0.55 to 0.99 wt. %. There is no significant difference in the major element composition between the core and rim. The MnO contents in the rims are slightly higher than in the cores. Simkin and Smith (1970) have shown that there is a positive correlation between Mn and Fe content in igneous olivines, however, such a relationship is not evident in the olivines of the GLI. Based on Brown's (1982) classification and nomenclature, olivines from drill core 6 are hyalosiderite and those from drill core 1 are hortonolite.

The olivine compositions represent solid solution mainly between forsterite (Fo: Mg_2SiO_4) and fayalite (Fa: Fe_2SiO_4). Olivine compositions from core 1 are Fo_{44} and Fo_{49}, whereas those from core 6 vary from $Fo_{56\text{-}51.5}$ (Figure 2.15), thereby recording a slight Fe-enrichment over a 45-metre interval.

Compositions of six olivines from Center I and II gabbros are given in

Table 2.1 EDS analyses of olivine from the Geordie Lake Troctolite.
Samples 11 and 13 are from core 1, the others from core 6. C:Core
*Fo: Mg2SiO4, Fa:Fe2SiO4, Tp:Mn2SiO4

Sample	11(C)	RIM	13(C)	RIM	68(C)	RIM	70(C)	RIM
SiO2	34.20	34.12	35.00	34.48	36.07	34.22	35.02	35.48
FeO	44.10	46.76	41.15	39.68	38.27	38.66	39.28	36.58
MnO	0.84	1.18	0.99	0.92	0.55	0.78	0.74	0.87
MgO	20.03	18.96	22.96	24.16	25.46	24.33	24.55	26.92
TOTAL	99.17	101.02	100.10	99.24	100.35	97.99	99.59	99.85
Structural Formulae based on 4 Oxygens								
Si	1.0051	0.9972	1.0019	0.9909	1.0075	0.9916	0.9957	0.9947
Fe2+	1.0846	1.1436	0.9857	0.9542	0.8945	0.9375	0.9346	0.8582
Mn	0.0209	0.0292	0.0240	0.0224	0.0130	0.0192	0.0178	0.0207
Mg	0.8782	0.8266	0.9805	1.0357	1.0609	1.0518	1.0413	1.1259
Fo	44.27	41.34	49.27	51.47	53.90	52.37	52.23	56.16
Fa	54.68	57.20	49.53	47.42	45.44	46.68	46.88	42.81
Tp	1.05	1.46	1.20	1.11	0.66	0.96	0.89	1.03

Sample	71(C)	RIM	72(C)	RIM	73(C)	74(C)	RIM	78(C)	RIM
SiO2	35.37	35.28	35.43	35.39	36.22	35.14	35.54	35.66	36.17
FeO	38.59	37.10	39.37	38.93	39.02	38.03	38.35	36.54	34.48
MnO	0.93	0.93	0.87	1.20	0.79	0.87	0.96	0.89	1.19
MgO	25.51	25.21	24.47	23.91	25.45	24.72	24.82	26.62	27.65
TOTAL	100.40	98.52	100.14	99.43	101.48	98.76	99.67	99.71	99.49
Structural Formulae based on 4 Oxygens									
Si	0.9958	1.0057	0.9961	1.0054	1.0060	1.0039	1.0050	0.9966	1.0071
Fe2+	0.9091	0.8850	0.9262	0.9254	0.9069	0.9092	0.9075	0.8546	0.8034
Mn	0.0222	0.0225	0.0207	0.0289	0.0186	0.0211	0.0230	0.0211	0.0281
Mg	1.0714	1.0720	1.0263	1.0133	1.0544	1.0536	1.0470	1.1098	1.1485
Fo	53.50	54.16	52.01	51.50	53.26	53.11	52.95	55.90	58.01
Fa	45.39	44.70	46.94	47.03	45.81	45.83	45.89	43.03	40.58
Tp	1.11	1.14	1.05	1.47	0.94	1.06	1.16	1.06	1.42

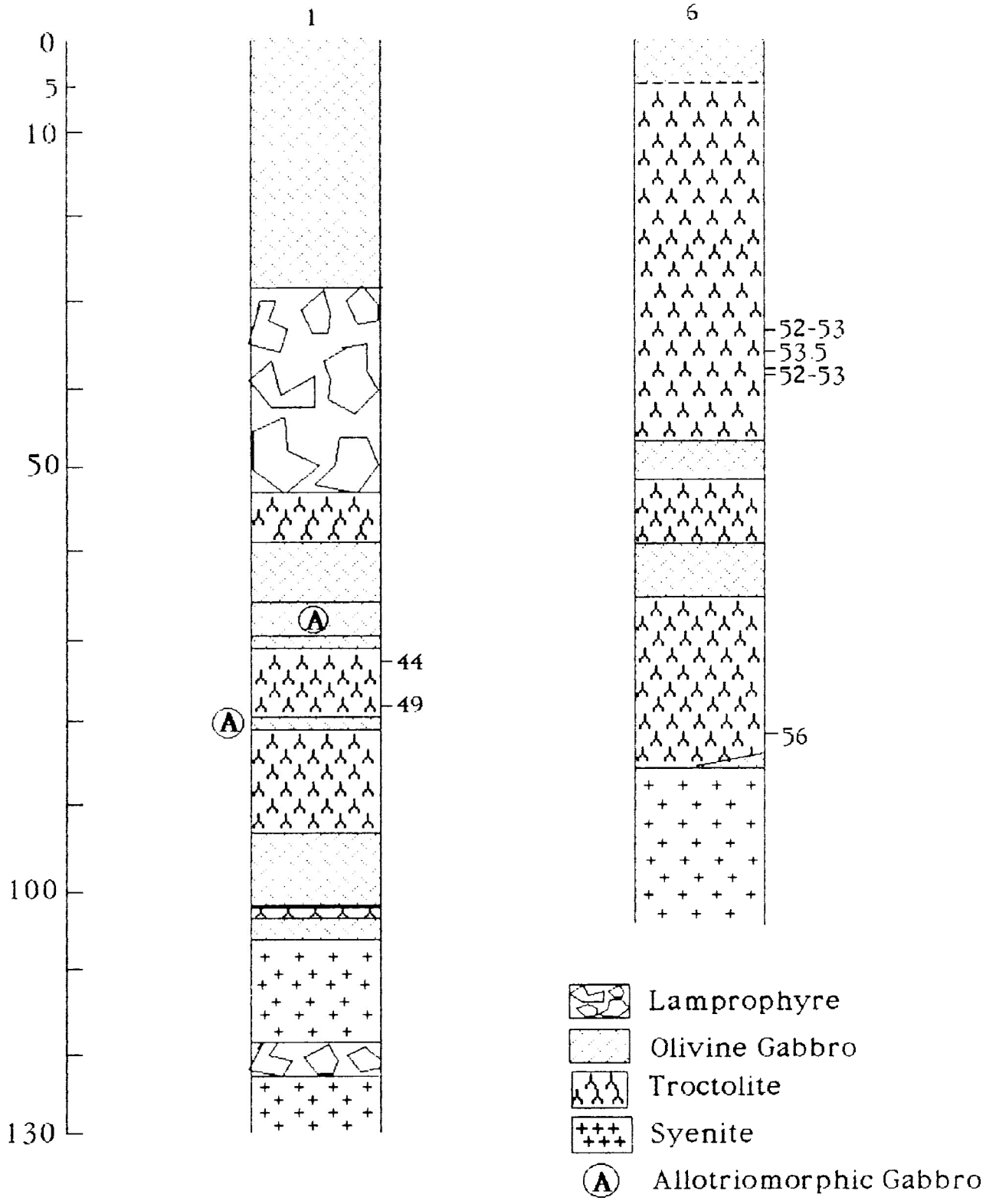

Figure 2.15 Olivine compositions (Fo) versus stratigraphic height in cores 1 and 6.

Table 2.2. With the exception of samples 138 and 420, the samples are metasomatized gabbroic rocks which occur as xenoliths in the the Center II syenite. The composition of the olivines from the metasomatized rocks range from Fo_{55-80}. It is not known if the metasomatism has affected the olivine compositions. Petrographically, the olivines are rimmed by magnetite but do not show extensive internal alteration. The compositions of the two olivines from Center I gabbro are Fo_{47} and $Fo_{45.5}$ which are lower in Mg than those of olivines from core 6 but are fairly close to olivine compositions in core 1. Lum (1973) reported olivine compositions (Fo_{43-67}) from Center I gabbros near Bamoos Lake (Figure 1.1) and olivine compositions (Fo46-55) from the eastern gabbros exposed on Highway 17. The olivines of northern gabbroic rocks, adjacent to Coubran Lake, have a composition ranging from Fo_{64-67} Wilkinson (1983). In the Coldwell complex, the olivine compositions of the troctolites of the GLI are, therefore, comparable to those of western and eastern gabbros of Center I, within the compositional range to those of northeastern gabbros, and more evolved than those of gabbroic rocks near Coubran Lake.

The olivines in the studied troctolite have a narrower range of Fo contents and are more evolved than those in the mid-ocean (Cayman) troctolites, the Pt-Pd bearing J-M Reef troctolite and anorthosite of the Stillwater complex, the Bushveld complex, the MacIntosh and Somerset Dam troctolite-olivine gabbro intrusions, the Keweenawan olivine basalts, and the basal zone of the Duluth complex (Figure 2.16). The maximum Fo content in the olivines of the GLI is less than those of the upper zone of Duluth. The cited gabbroic rocks from the Bushveld complex overlay the platiniferous

Table 2.2 EDS analyses of olivine compositions from the western gabbro, Coldwell complex. C: Core
*Fo:Mg2Si04, Fa:Fe2Si04, Tp:Mn2Si04

Sample	117(C)	RIM	592(C)	RIM	608(C)	RIM
Si02	36.58	36.48	36.31	36.21	35.41	35.30
FeO	33.08	32.83	30.44	31.63	36.44	37.66
MnO	0.98	1.29	0.90	0.68	1.29	1.04
MgO	29.79	30.12	30.96	30.40	25.97	25.65
TOTAL	100.43	100.72	98.61	98.92	99.11	99.65
Structural Formulae based on 4 Oxygens						
Si	0.9990	0.9949	0.9984	0.9980	1.0009	0.9981
Fe2+	0.7560	0.7493	0.7004	0.7295	0.8619	0.8911
Mn	0.0227	0.0298	0.0210	0.0159	0.0309	0.0249
Mg	1.2136	1.2254	1.2699	1.2500	1.0951	1.0819
End Members*						
Fo	60.91	61.13	63.77	62.64	55.09	54.15
Fa	37.95	37.78	35.17	36.56	43.36	44.60
Tp	1.14	1.49	1.05	0.80	1.55	1.25

Sample	1501(C)	RIM	138	420
Si02	39.89	39.44	34.64	35.27
FeO	17.96	17.95	42.72	44.08
MnO	0.30	0.44	1.19	0.94
MgO	42.63	42.04	21.77	21.07
TOTAL	101.36	100.69	100.48	101.59
Structural Formulae based on 4 Oxygens				
Si	1.0016	1.0026	0.9988	1.0087
Fe2+	0.3774	0.3818	1.0308	1.0549
Mn	0.0064	0.0095	0.0291	0.0228
Mg	1.5967	1.5943	0.9364	0.8989
End Members*				
Fo	80.62	80.29	46.91	45.48
Fa	19.06	19.23	51.64	53.37
Tp	0.32	0.48	1.46	1.15

Figure 2.16 Olivine Fo contents of the GLI and other intrusions

Source of data

1. Cayman Rise troctolite (Elthon, 1987)
2. The J-M Reef troctolite-anorthosite I, Stillwater complex (Todd *et al.*, 1982)
3. Upper zone gabbroic rocks, Bushveld complex (van der Merve, 1976)
4. The East Kimberley troctolite-olivine gabbro, Australia (Mathison and Hamlyn, 1987)
5. The Somerset Dam troctolite-olivine gabbro, Australia (Mathison, 1987)
6. Keweenawan olivine tholeiitic basalt (Basaltic Volcanism Study Project, 1981)
7/8. The Patridge River Troctolite, Duluth complex (Tyson and Chang, 1984)
9. Center I gabbroic rocks, Bamoos Lake (Lum, 1973)
10. Geordie Lake Intrusion (This study)
11. Center I gabbroic rocks, Coubran Lake (Wilkinson, 1983) and East Coldwell on Highway 17 (Lum, 1973)
12. Center I gabbroic rocks, western Coldwell (This study)

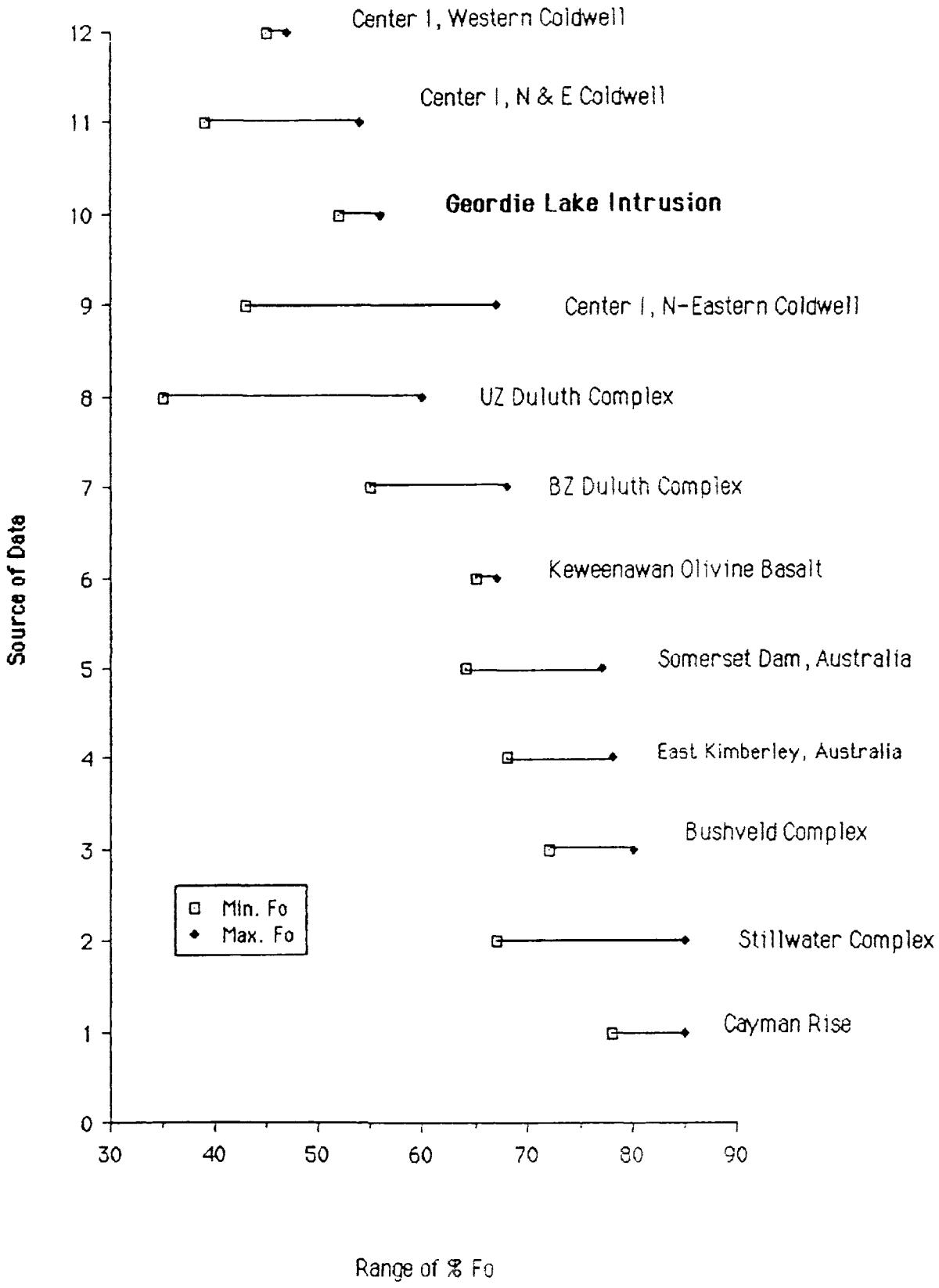
Center 1, Western Coldwell
Center 1, N & E Coldwell
Geordie Lake Intrusion
Center 1, N-Eastern Coldwell
UZ Duluth Complex
BZ Duluth Complex
Keweenawan Olivine Basalt
Somerset Dam, Australia
East Kimberley, Australia
Bushveld Complex
Stillwater Complex
Cayman Rise
Min. Fo
Max. Fo
Source of Data
Range of % Fo
0
1
2
3
4
5
6
7
8
9
10
11
12
30
40
50
60
70
80
90

basal mafic rocks of the Main Zone. Olivine compositions of the Bushveld gabbroic rocks, however, vary from one stratigraphic position to another. Although a troctolite layer has been listed in the stratigraphy of the Upper Zone of the Rustenburg Layered Suite in the eastern Bushveld (von Gruenewaldt *et al*, 1985), data on the olivine compositions have not been reported.

2.3.2 Plagioclase

Representative plagioclase compositions from the troctolite, gabbro and altered gabbro are given in Table 2.3. The plagioclase compositions are recast into three end members, i.e. anorthite (An), albite (Ab) and orthoclase (Or). Plagioclases in the range An_{57-50} have on average $Or_{1.17}$ (21 samples), and An_{49-40} have $Or_{1.6}$ (14 samples). The core compositions are plotted in the ternary system Ab-An-Or (Figure 2.17). Most plagioclases from the troctolite are labradorite, ranging from An_{49-57}: the majority of the troctolite plagioclases vary from An_{49-51}. The plagioclases with An_{56-57} occur only in core 6, hence, representing the least fractionated plagioclase in the GLI. Plagioclase from the ophitic gabbro ranges from calcic andesine to labradorite (An_{45-52}). Plagioclase in the fine-grained gabbro varies from calcic to sodic andesine (An_{47-24}).

Based on the IUGS classification scheme, basic plutonic rocks consisting of feldspars with An_{49} or less are called diorite. The mineralogy of these calcic andesine-bearing rocks, however, is characteristic of gabbro; olivine and clinopyroxene are the major mafic phases, although the former has

Table 2.3 Electron microprobe analyses of representative plagioclase from the GLI and Center I syenite (SN).

Rock type G: gabbro, TR;Troctolite, AG: Allotriomorphic gabbro, DR: Dioritic rock, W/SAG: Weakly/Strongly altered rocks C: Core, R: Rim, M: Mantle, D: Dusty *from PGM-bearing rock

Rock type	G		G	TR		TR		AG
Sample No.	1(C)	1(R)	407	18*(C)	18(R)	77(C)	77(R)	208
SiO2	54.97	57.78	55.43	54.77	66.66	53.15	59.54	56.16
Al2O3	27.96	26.57	28.40	28.19	21.16	29.17	24.70	27.50
FeO	0.67	0.52	0.39	0.39	0.10	0.68	0.59	0.59
CaO	10.89	8.74	10.64	10.42	1.77	11.60	6.26	9.83
Na2O	5.56	6.79	5.52	5.52	10.83	4.66	7.86	6.00
K2O	0.05	0.25	0.00	0.04	0.00	0.25	0.11	0.04
TOTAL	100.10	100.65	100.38	99.33	100.52	99.51	99.06	100.12
Structural Formula based on Thirty-two Oxygens								
Si	9.908	10.293	9.928	9.917	11.623	9.646	10.681	10.070
Al	5.943	5.581	5.998	6.019	4.351	6.243	5.225	5.815
Fe	0.100	0.078	0.059	0.059	0.015	0.103	0.089	0.089
Ca	2.106	1.671	2.045	2.024	0.331	2.257	1.205	1.891
Na	1.945	2.348	1.919	1.940	3.666	1.642	2.737	2.092
K	0.012	0.057	0.000	0.009	0.000	0.058	0.025	0.009
Mol. Percent End Members								
Anorthite	51.83	40.99	51.58	50.94	8.28	57.04	30.37	47.37
Albite	47.89	57.62	48.42	48.83	91.72	41.50	69.00	52.40
Orthoclase	0.28	1.40	0.00	0.23	0.00	1.46	0.64	0.23

Rock Type	AG	DR				WAG	SAG	SN
Sample No.	307(C)	26*(C)	26(R)	26(M)	26(D)	62	30	410
SiO2	57.26	55.77	59.64	63.83	62.82	54.84	60.94	69.18
Al2O3	27.10	26.83	25.17	22.55	22.67	27.63	24.25	20.16
FeO	0.60	0.63	0.57	0.30	0.13	0.47	0.50	0.12
CaO	8.77	9.22	6.88	3.40	3.67	10.41	5.55	0.28
Na2O	6.46	5.78	7.58	9.49	9.34	5.60	8.10	10.90
K2O	0.40	0.77	0.00	0.09	0.00	0.03	0.96	0.07
TOTAL	100.59	99.00	99.84	99.66	98.63	98.98	100.30	100.71
Structural Formula based on Thirty-two Oxygens								
Si	10.209	10.124	10.631	11.286	11.218	9.977	10.820	11.937
Al	5.698	5.743	5.291	4.702	4.774	5.928	5.077	4.102
Fe	0.090	0.096	0.085	0.044	0.019	0.072	0.074	0.017
Ca	1.678	1.796	1.316	0.645	0.703	2.032	1.057	0.052
Na	2.236	2.037	2.623	3.257	3.269	1.978	2.792	3.651
K	0.091	0.179	0.000	0.020	0.000	0.003	0.218	0.015
Mol. Percent End Members								
Anorthite	41.89	44.77	33.40	16.44	17.70	50.58	25.99	1.39
Albite	55.84	50.78	66.60	83.04	82.30	49.24	68.65	98.19
Orthoclase	2.27	4.45	0.00	0.52	0.00	0.17	5.35	0.41

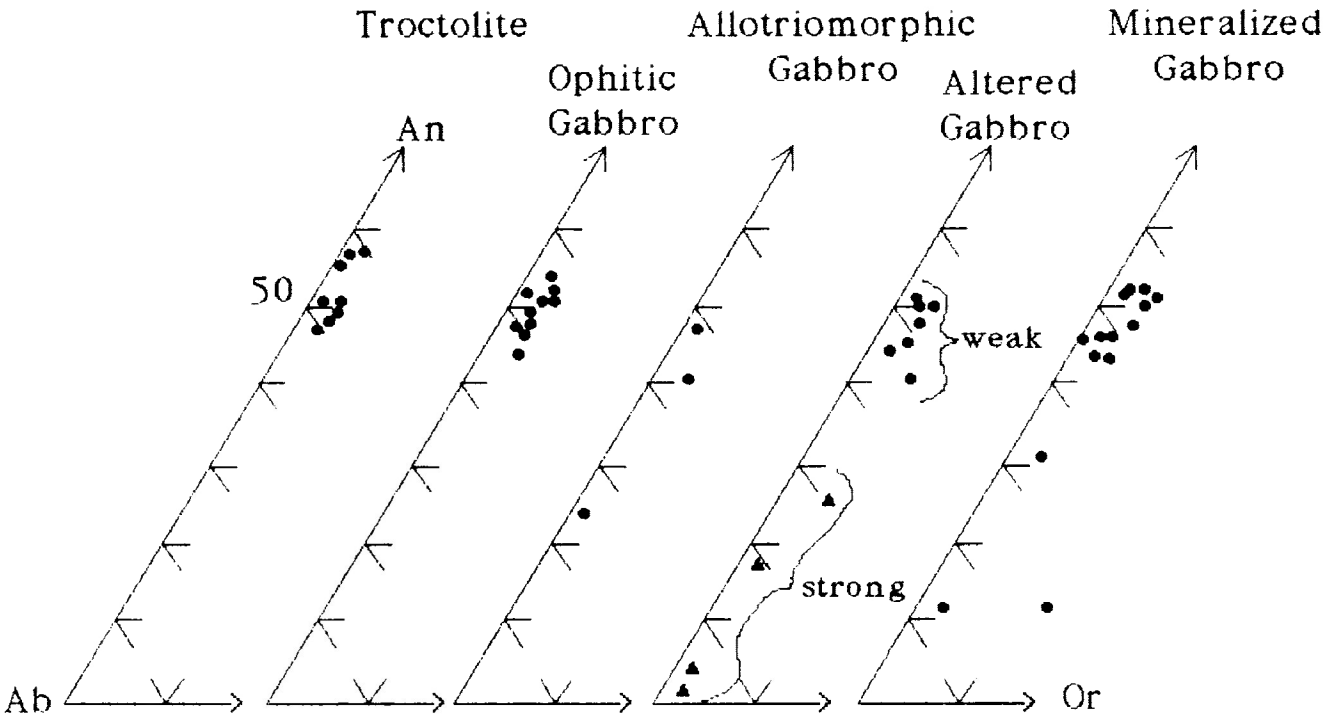

Figure 2.17: Ternary plots of plagioclase compositions in terms of Anorthite (An), Albite (Ab) and Orthoclase (Or) for the various rock types of the GLI. Each plot represents a complete analysis of six major oxides, SiO_2, Al_2O_3, FeO CaO, Na_2O, and K_2O.

been completely altered and the latter is partially uralitized. Furthermore, these "dioritic" rocks occur most frequently as narrow zones between the gabbro and troctolite, and there is no lithological contact between the gabbro and "diorite". The dioritic rocks with calcic andesine are, therefore, altered gabbroic rocks.

The compositions of the plagioclase cores in the weakly altered gabbroic rocks range from An_{41-50} (calcic andesine-labradorite), whereas, in the strongly altered gabbroic rocks plagioclase compositions vary from An_{26}/Ab_{68} (andesine) to An_{2}/Ab_{98} (nearly pure albite). The majority of the plagioclase in the rocks that host the platinum-group minerals and tellurides have similar compositions to those of the troctolite and gabbro. The significance of this observation is discussed in Chapter 3.

The compositional variations in zoned plagioclases are plotted on the Ab-An-Or ternaries (Figure 2.18). Individually, plagioclase compositions become more albitic in the rims, and even more albitic in the mantle. The variation in the degree of albitization is generally related to the degree of alteration in the rock: plagioclase rims in more altered rocks are more albitic than those in less altered rocks. Some of the feldspar mantles, which appear dusty and pink in thin sections, are also albite.

The core plagioclase compositions of the troctolite and gabbro are essentially constant with stratigraphic height (Figure 2.19). The plagioclase compositions in the rocks adjacent to the GLI-syenite contact remain within the overall compositional range. This constancy indicates that the plagioclase does not record any differentiation effects throughout the succession.

The compositions of the plagioclases from Center I gabbros of western

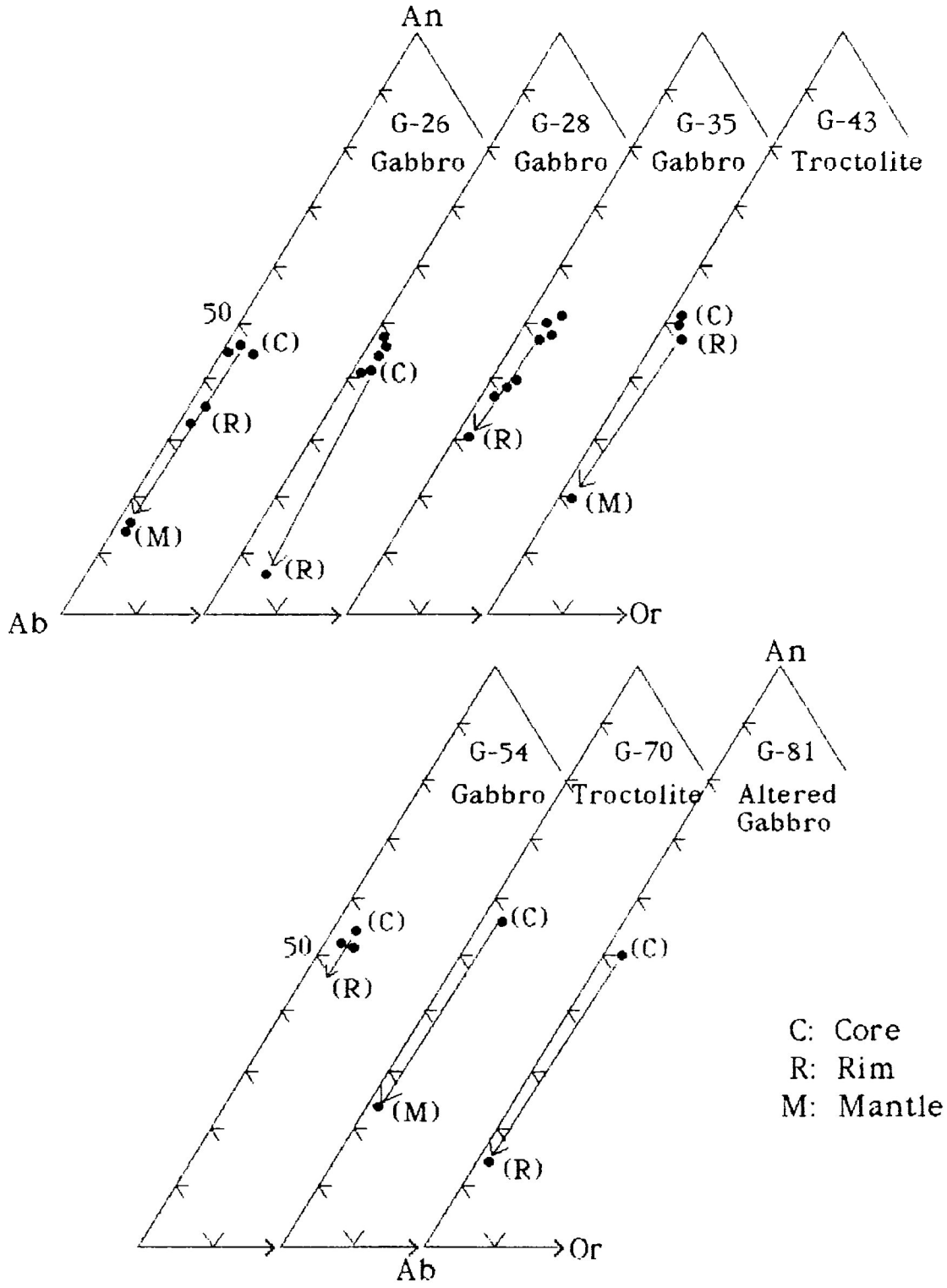

Figure 2.18: Compositions of zoned plagioclases of the GLI plot in the ternary system An-Ab-Or.

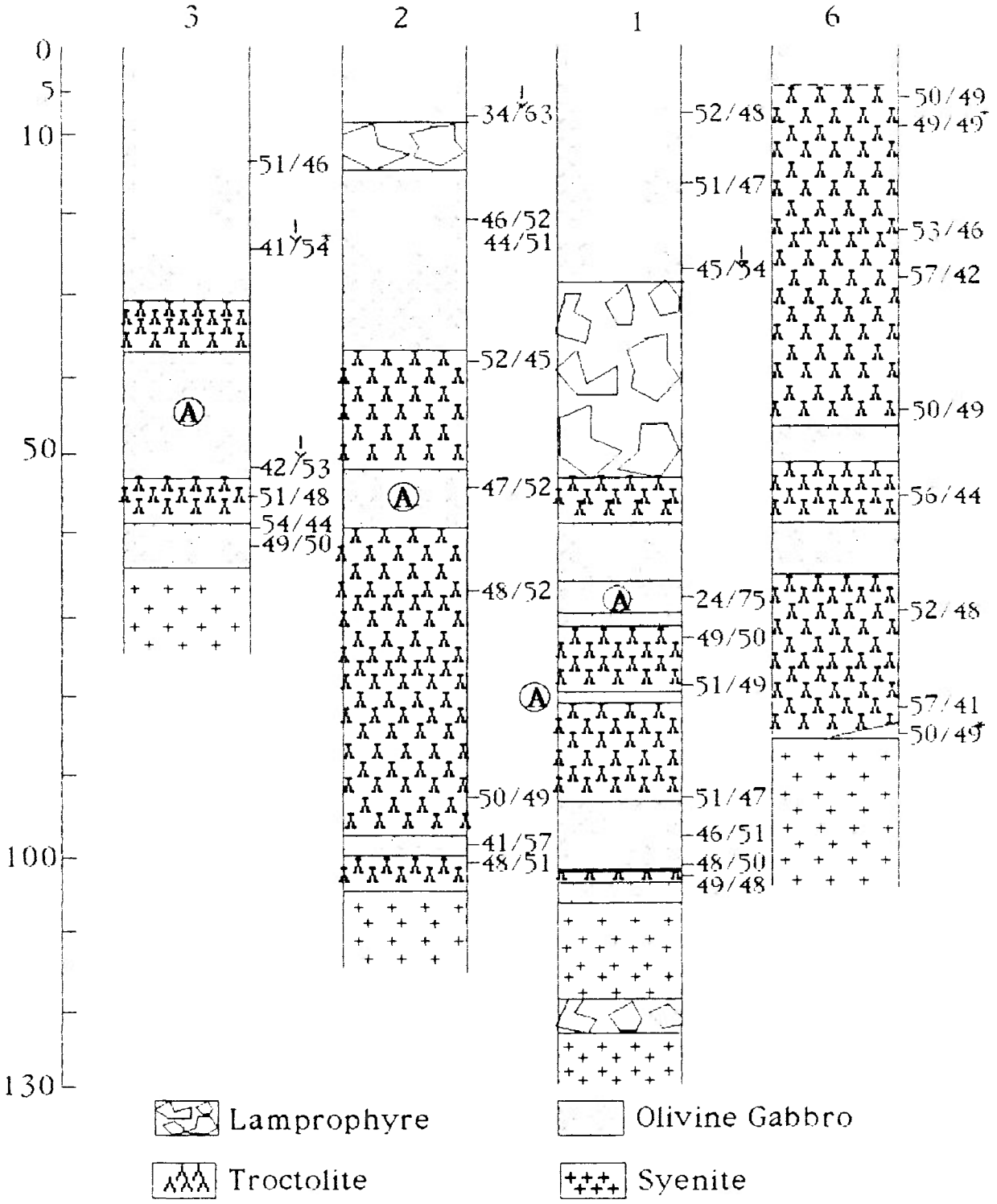

Figure 2.19 An/Ab contents in the plagioclases correlated with stratigraphic height. A: allotriomorphic gabbro. *: altered rock, ı altered mineral.

Coldwell and from Center II metasomatized gabbroic rocks of south-central Coldwell are given in Tables 2.4A and B, respectively, and plot in the ternary system An-Ab-Or (Figure 2.20). The core compositions of the Center I plagioclases, most of which have been recrystallized (showing polygonalization), vary from labradorite (An_{52}) to calcic andesine (An_{41}). The low-An content plagioclases are present in the slightly altered sample 907. Core compositions of some of the recrystallized grains are also of calcic andesine (An_{41-43}). The rim compositions show a decrease of the An content by 3 to 5 mole % and an increase in the albite content by that percentage. An alkali-feldspar rim,($An_{12}Ab_{55}Or_{33}$), is present in sample 907.

The Center II metasomatized gabbroic rocks (Table 2.4B) from the eastern Neys peninsula (samples C-1496, 1498, 1500 and 1503) are characterized by high SiO_2 and Na_2O and Low CaO contents. Only the rims of samples in C-1496 contains small amounts of K_2O. The An contents of these plagioclases are low, ranging from andesine (An_{41}) to albite ($An_{17}Ab_{83}$). These plagioclases have been recrystallized and metasomatized as they form polygonal crystals with sutured grain boundaries. Center II gabbro xenoliths (samples C-117, 308, 138 and 593) in Center II syenites show a wide compositional range (An_{40-75}). These samples show have lower SiO_2 and Na_2O and higher CaO contents than the Neys gabbros. Sample 117 shows an extensive metasomatism and its composition is approximately An_{49}. The composition of the plagioclase of sample 138, a medium-grained recrystallized gabbro, is approximately An_{50} in the core and An_{48} in the rim. Sample 593 has been recrystallized into fine-grained gabbro, in which the plagioclase composition is about An_{40}. Sample 308, which represents

Table 2.4A Electron microprobe analyses of plagioclase from the Center I gabbroic rocks

Sample No	414 CORE	RIM	414 CORE	RIM	420 CORE	RIM	420 POLY-C	POLY-R
SiO2	54.48	55.06	53.94	54.58	56.43	56.52	56.74	56.49
Al2O3	28.43	27.86	28.92	28.44	26.96	26.56	26.35	27.11
FeO	0.23	0.28	0.31	0.27	0.29	0.25	0.30	0.27
CaO	10.47	9.92	10.69	10.43	9.34	8.98	8.89	9.14
Na2O	5.41	5.89	5.25	5.37	6.12	6.39	6.20	6.14
K2O	0.46	0.40	0.23	0.27	0.53	0.80	0.90	0.79
TOTAL	99.48	99.41	99.34	99.36	99.67	99.50	99.38	99.94
Structural Formulae based on Thirty-two Oxygens								
Si	9.868	9.973	9.785	9.889	10.175	10.218	10.268	10.170
Al	6.072	5.951	6.186	6.077	5.732	5.662	5.623	5.755
Fe3+	0.035	0.424	0.047	0.041	0.044	0.038	0.045	0.041
Ca	2.035	1.928	2.081	2.028	1.807	1.742	1.726	1.766
Na	1.902	2.071	1.849	1.888	2.142	2.243	2.178	2.146
K	0.106	0.093	0.053	0.063	0.122	0.185	0.208	0.182
Mol. Percent End Member								
Anorthite	50.32	47.12	52.24	50.96	44.38	41.78	41.79	43.13
Albite	47.05	50.62	46.42	47.47	52.62	53.79	52.97	52.43
Orthoclase	2.63	2.26	1.34	1.57	3.00	4.43	5.06	4.44

Sample No	420 FINE	607	907 CORE	RIM	907 DUSTY	907 DUSTY	1084	1084
SiO2	56.11	61.53	58.33	57.64	56.72	58.69	54.70	55.82
Al2O3	26.97	24.90	26.97	28.12	27.65	26.94	28.12	27.23
FeO	0.27	0.10	0.08	0.55	0.15	0.06	0.13	0.09
CaO	9.26	6.23	8.42	2.14	9.17	7.73	10.40	9.35
Na2O	6.04	7.98	6.81	5.24	6.58	7.22	5.73	6.41
K2O	0.63	0.19	0.00	4.79	0.00	0.38	0.00	0.00
TOTAL	99.28	100.93	100.61	98.48	100.27	101.02	99.08	98.90
Structural Formulae based on Thirty-two Oxygens								
Si	10.158	10.842	10.340	10.438	10.130	10.380	9.926	10.120
Al	5.757	5.161	2.638	6.005	5.823	2.619	6.017	5.821
Fe3+	0.041	0.015	0.012	0.083	0.022	0.009	0.020	0.014
Ca	1.799	1.175	1.601	0.416	1.757	1.467	2.025	1.819
Na	2.123	2.723	2.343	1.842	2.281	2.479	2.018	2.256
K	0.146	0.025	0.000	1.107	0.000	0.086	0.000	0.000
Mol. Percent End Member								
Anorthite	44.22	29.81	40.59	12.35	43.51	36.38	50.08	44.63
Albite	52.20	69.10	29.41	54.73	56.49	61.49	49.92	55.37
Orthoclase	3.58	1.08	0.00	32.92	0.00	2.13	0.00	0.00

Table 2.4B Electron microprobe analyses of plagioclase from Center II gabbroic rocks
+ metasomatised, * gabbroic xenoliths

Sample No	1496+ CORE	RIM	1496 DUSTY	1498+	1498 FINE	1500+	1503+	1503
SiO2	60.86	65.05	62.82	65.75	57.40	64.75	58.12	56.96
Al2O3	23.93	21.61	23.06	21.92	27.50	22.09	25.63	26.38
FeO	0.11	0.05	0.14	0.10	0.22	0.05	0.12	0.00
CaO	5.57	2.40	3.93	2.64	9.49	3.11	7.50	8.60
Na2O	8.69	10.04	9.47	10.02	6.31	10.11	7.43	6.69
K2O	0.00	0.11	0.00	0.00	0.00	0.00	0.00	0.00
TOTAL	99.16	99.26	99.42	100.43	100.92	100.11	98.80	98.63
Structural Formulae based on Thirty-two Oxygens								
Si	10.880	11.499	11.151	11.466	10.183	11.370	10.486	10.311
Al	5.045	4.505	4.827	4.508	5.753	4.574	5.453	5.631
Fe3+	0.017	0.007	0.021	0.015	0.033	0.007	0.002	0.000
Ca	1.068	0.455	0.749	0.494	1.806	0.586	1.452	1.670
Na	3.016	3.445	3.263	3.392	2.173	3.446	2.602	2.351
K	0.000	0.025	0.000	0.000	0.000	0.000	0.000	0.000
Mol. Percent End Member								
Anorthite	26.16	11.59	18.66	12.71	45.39	14.53	35.81	41.53
Albite	73.84	87.77	81.34	87.29	54.61	85.47	64.19	58.47
Orthoclase	0.00	0.63	0.00	0.00	0.00	0.00	0.00	0.00
Sample No	117+* CORE	RIM	308*	138* POLYG.	138* CORE	RIM	593* CORE	RIM
SiO2	54.90	54.52	49.13	55.34	54.62	55.79	57.81	57.18
Al2O3	27.49	28.00	32.12	27.91	27.78	28.18	26.75	27.17
FeO	0.27	0.36	0.23	0.75	1.27	0.19	0.20	0.18
CaO	10.15	10.71	15.02	10.24	10.13	10.08	8.68	8.89
Na2O	5.57	5.32	2.80	5.85	5.57	6.03	7.07	6.57
K2O	0.45	0.34	0.05	0.06	0.15	0.05	0.06	0.00
TOTAL	98.83	99.25	99.35	100.15	99.52	100.32	100.57	99.99
Structural Formulae based on Thirty-two Oxygens								
Si	9.994	9.901	9.013	9.965	9.916	9.994	10.296	10.236
Al	5.901	5.996	6.951	5.927	5.947	5.953	5.618	5.736
Fe3+	0.041	0.055	0.035	0.113	0.193	0.029	0.030	0.027
Ca	1.983	2.087	2.956	1.979	1.973	1.937	1.659	1.708
Na	1.968	1.875	0.100	2.045	1.963	2.097	2.444	2.283
K	0.105	0.079	0.007	0.008	0.025	0.007	0.001	0.000
Mol. Percent End Member								
Anorthite	48.88	51.64	74.78	49.17	50.13	48.02	40.42	42.78
Albite	48.54	46.41	25.22	50.83	49.87	51.98	59.58	57.22
Orthoclase	2.58	1.95	0.00	0.00	0.00	0.00	0.00	0.00

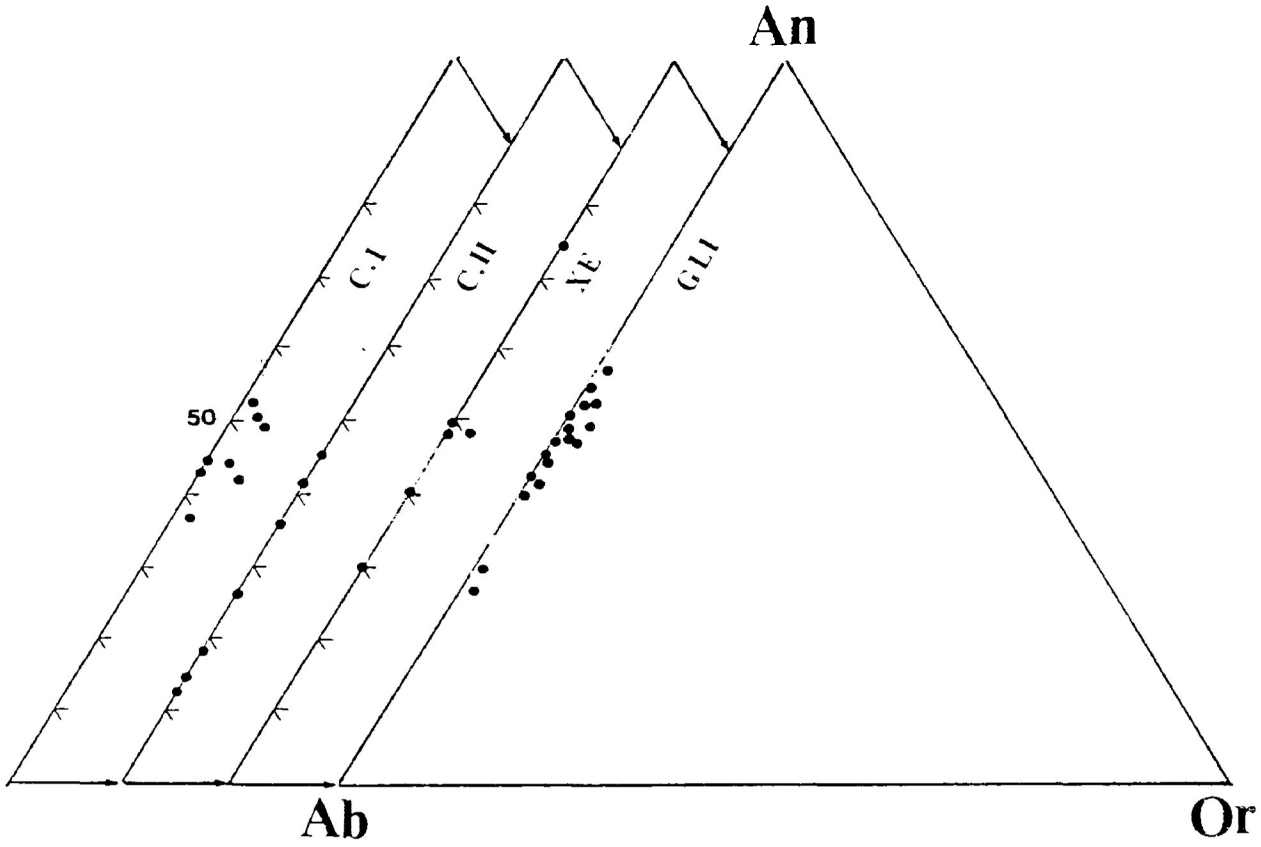

Figure 2.20 Ternary plots of plagioclase compositions in terms of An, Ab, and Or for gabbroic rocks from Center I and II. XE: Center II gabbroic xenoliths. The plagioclase compositions from the GLI are plotted for comparison.

the least altered and undeformed gabbro xenolith, has the least evolved plagioclase composition, An_{75}, and contains no alkali-feldspar.

From the above data, the range of plagioclase compositions of the GLI overlaps those of western Center I gabbros and of Center II gabbroic xenoliths, with the exception of sample C-308 (Figure 2.20). The plagioclases of the troctolite of the GLI, however, are more calcic than those of Center I and II gabbros. The plagioclases of the Neys gabbros (Center II) are low in An content perhaps due to metasomatism. The compositional range of the GLI plagioclases is within that of the eastern Center I gabbros (Figure 2.21). The GLI plagioclases are less calcic than those in the Stillwater complex, the McIntosh layered troctolite-olivine gabbro, the Cayman Rise, the Somerset Dam troctolite-olivine gabbro, and the Duluth complex. In addition, the plagioclases of these various intrusions, with the exception of the Cayman Rise and Somerset Dam, have a narrow range of An content.

2.3.3 Alkali-Feldspar

Table 2.5 lists seven analyses of alkali-feldspars (four rims and three fine-grained crystals) from the GLI and one from the eastern syenite. Some of the rim alkali-feldspars appear pink in handspecimen. The compositions of these feldspars vary from $Or_{11}Ab_{85}An_4$ to $Or_{95}Ab_4An_1$. The anhedral to subhedral alkali-feldspars in the slightly altered gabbro range from $Or_{19}Ab_{77}An_4$ to $Or_{98.7}Ab_{0.9}An_{0.3}$. The alkali-feldspar of the eastern syenite has the composition $Or_{86}Ab_{13.7}Ab_{0.3}$.

Figure 2.21 Comparisons of the An contents of plagioclase from the GLI and other intrusions.

1. The J-M Reef troctolite-anorthosite I, Stillwater complex (Todd *et al.*, 1982)
2. The East Kimberley troctolite-olivine gabbro, Australia (Mathison and Hamlyn, 1987)
3. The Somerset Dam troctolite-olivine gabbro, Australia (Mathison, 1987)
4. Cayman Rise troctolite (Elthon, 1987)
5/6. The Patridge River Troctolite, Duluth complex (Tyson and Chang, 1984)
7. Center I gabbroic rocks, Coubran Lake (Wilkinson, 1983) and East Coldwell on Highway 17 (Lum, 1973)
8. Geordie Lake Intrusion (This study)
9. Center I gabbroic rocks, western Coldwell (This study)

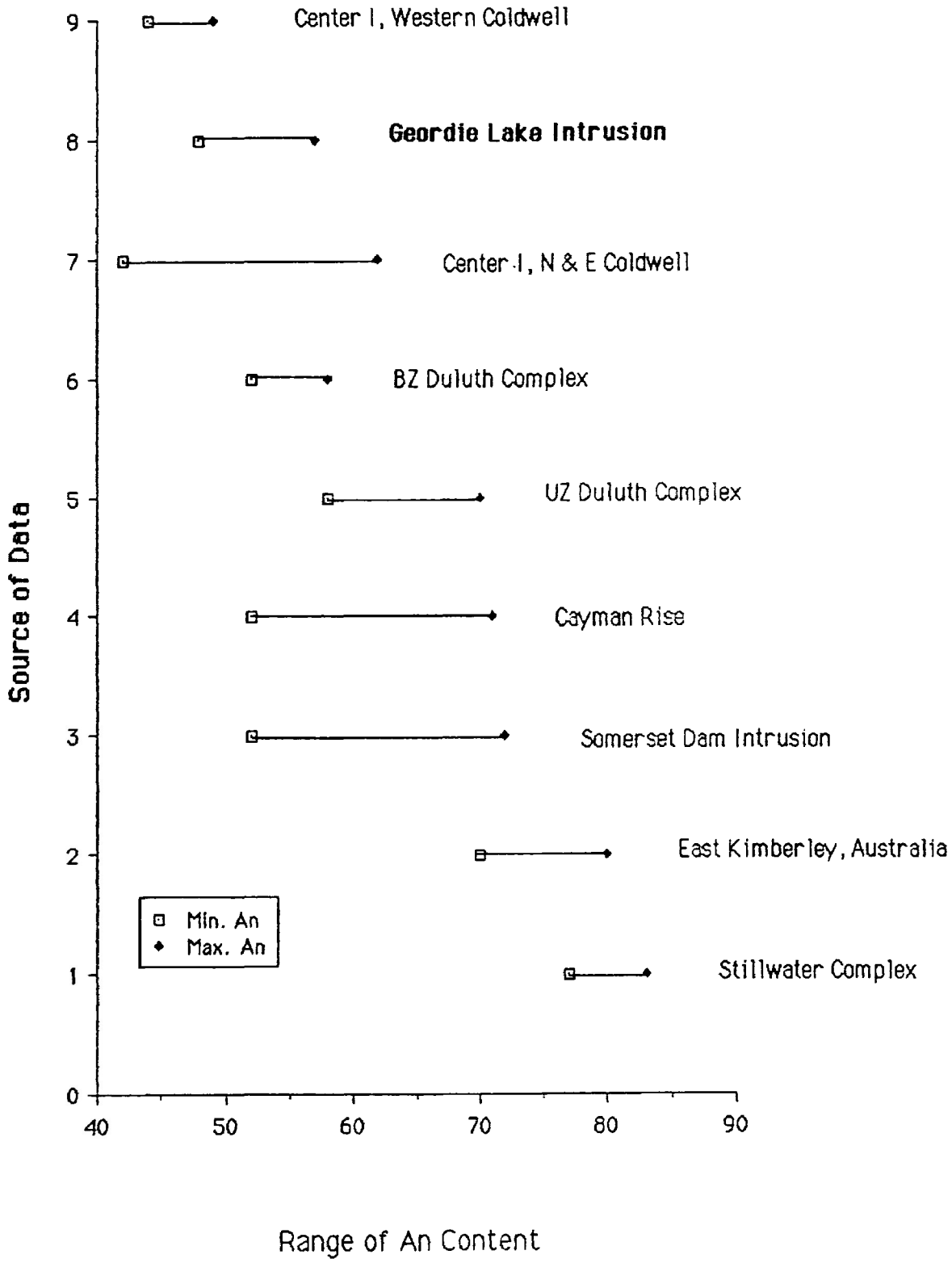
Center I, Western Coldwell
Geordie Lake Intrusion
Center I, N & E Coldwell
BZ Duluth Complex
UZ Duluth Complex
Cayman Rise
Somerset Dam Intrusion
East Kimberley, Australia
Stillwater Complex
Min. An
Max. An
Source of Data
Range of An Content
0
1
2
3
4
5
6
7
8
9
40
50
60
70
80
90

Table 2.5 Electron microprobe analyses of alkali-feldspar from the GLI.
Rock Type G: Gabbro, Tr: Troctolite, AG: Allotriomorphic Gabbro,
DR: Dioritic Rock, WAG: Weakly Altered Gabbro,
SAG: Strongly Altered Gabbro, SN: Syenite; M: Mantle

Rock Type	TR	G	AG	AG	SAG	SAG	SAG	SN
Sample No.	70(M)	29(M)	9(M)	307(M)	64	44	303	410
SiO2	61.26	61.97	61.19	65.63	66.48	63.61	65.22	65.07
Al2O3	19.51	20.73	25.51	18.83	19.95	20.58	18.34	18.74
FeO	4.11	0.75	0.33	0.27	0.21	0.18	0.09	0.23
CaO	0.74	1.49	1.27	0.15	0.76	0.14	0.07	0.06
Na2O	9.78	3.55	6.93	0.40	8.32	1.70	0.10	1.56
K2O	1.94	10.17	4.08	14.66	3.05	13.35	16.77	14.79
TOTAL	97.34	98.66	99.31	99.94	98.77	99.56	100.59	100.45
Structural Formula based on Thirty-two Oxygens								
Si	11.103	11.430	10.940	11.970	11.825	11.635	11.972	11.894
Al	4.170	4.509	5.378	4.050	4.185	4.439	3.970	4.039
Fe3+	0.623	0.116	0.049	0.041	0.031	0.028	0.014	0.035
Ca	0.144	0.295	0.244	0.029	0.145	0.028	0.014	0.012
Na	3.441	1.271	2.405	0.142	2.873	0.604	0.036	0.554
K	0.449	2.395	0.931	3.414	0.693	3.117	3.930	3.452
Mol. Percent End Members								
Anorthite	3.57	7.44	6.80	0.82	3.91	0.73	0.35	0.29
Albite	85.30	32.08	67.17	3.95	77.42	16.10	0.90	13.78
Orthoclase	11.13	60.48	26.02	95.23	18.67	83.17	98.76	85.93

2.3.4 Clinopyroxene

Table 2.6 lists the compositions, structural formulae, and end members of representative clinopyroxenes. All clinopyroxenes are free of zonation. Within single samples, compositional variations never exceed 2 molecular weight per cent wollastonite (Wo). The majority of the clinopyroxene in the GLI is Ca-rich augite (Figure 2.22). The augite from the troctolite, gabbro and the weakly altered gabbroic rocks plot in the same compositional field. The compositions extend from the middle of, and along the augite-salite boundary to near the augite-ferroaugite boundary. Restricted compositional variation is observed in the clinopyroxenes of the four drill cores studied. Ca-rich and Ca-poor augites have been found to co-exist in some samples (Figure 2.22). This association is particularly characteristic of rocks with tholeiitic affinities (Deer *et al*, 1978). Pigeonite is absent, suggesting that Ca content did not decrease to a minimum where an inverted ferropigeonite normally occurs. All salite compositions plot near the salite-augite boundary. Altered clinopyroxenes in the strongly altered rocks, which exhibit sieve-like texture and lower birefringence in comparison to fresh pyroxene, plots just above the salite-wollastonite boundary. Ferroaugite occurs only in the slightly altered gabbroic rocks and in the ophitic gabbro situated at a high stratigraphic level in core 1.

The Mg/(Mg+Fe) ratio of all clinopyroxenes is correlated with stratigraphic height (Figure 2.23) and ranges from 0.67 to 0.40. These ratios

Table 2.6 Electron microprobe analyses of representative clinopyroxene from the GLI
Rock Type. G:Gabbro, TR: Troctolite, AG: Allotriomorphic Gabbro
DR: Dioritic Rock, W/SAG: Weakly/Strongly Altered Gabbro
* from PGM-bearing rock

Rock Type	G	G	TR	TR	AG	DR	WAG	SAG
Sample No.	1	54	18*	77	208	26*	81	30*
SiO2	49.53	50.43	52.98	49.54	50.55	49.84	50.92	52.01
TiO2	0.21	1.05	0.25	1.12	0.78	0.79	0.93	0.11
Al2O3	4.03	2.66	2.26	2.77	1.74	2.11	2.34	0.29
FeO	23.52	12.25	18.04	12.32	13.78	11.88	11.29	12.42
MnO	0.57	0.41	0.51	0.41	0.41	0.29	0.36	0.81
MgO	8.83	12.42	12.82	11.97	11.71	12.26	12.96	10.50
CaO	11.94	21.02	12.01	21.24	21.33	21.34	21.00	24.24
Na2O	0.89	0.31	0.56	0.42	0.52	0.48	0.47	0.28
TOTAL	99.85	100.76	99.46	99.97	100.94	98.98	100.50	100.81
Structural Formula based on Six Oxygens								
Si	1.919	1.893	1.996	1.879	1.909	1.904	1.906	1.971
Al(iv)	0.081	0.107	0.004	0.121	0.078	0.095	0.094	0.013
Al(vi)	0.104	0.011	0.097	0.003			0.009	
Ti	0.006	0.030	0.041	0.032	0.022	0.023	0.026	0.003
Fe3(iv)					0.013			0.016
Fe3(vi)	0.067	0.023	0.041	0.031	0.025	0.034	0.034	0.004
Fe2+	0.696	0.362	0.528	0.360	0.397	0.344	0.320	0.373
Mn	0.019	0.013	0.016	0.013	0.013	0.001	0.011	0.026
Mg	0.511	0.696	0.721	0.677	0.660	0.699	0.724	0.594
Ca	0.497	0.847	0.486	0.865	0.864	0.875	0.843	0.986
Na	0.067	0.023	0.041	0.031	0.038	0.036	0.034	0.021
Mol. Percent End Members (Plotting Parameters)								
Wo.	25.92	43.25	27.92	44.43	44.34	44.96	43.65	50.40
Fs	42.73	19.44	30.47	19.29	20.92	18.16	17.26	19.15
En.	31.35	37.32	41.60	36.28	34.74	36.87	39.09	30.45
Ae	13.69	2.73	7.81	3.59	4.33	4.01	4.05	2.09
Di	49.78	33.31	38.98	33.47	35.96	31.68	29.39	37.80
Hd	36.52	63.96	53.21	62.94	59.71	64.31	66.56	60.11

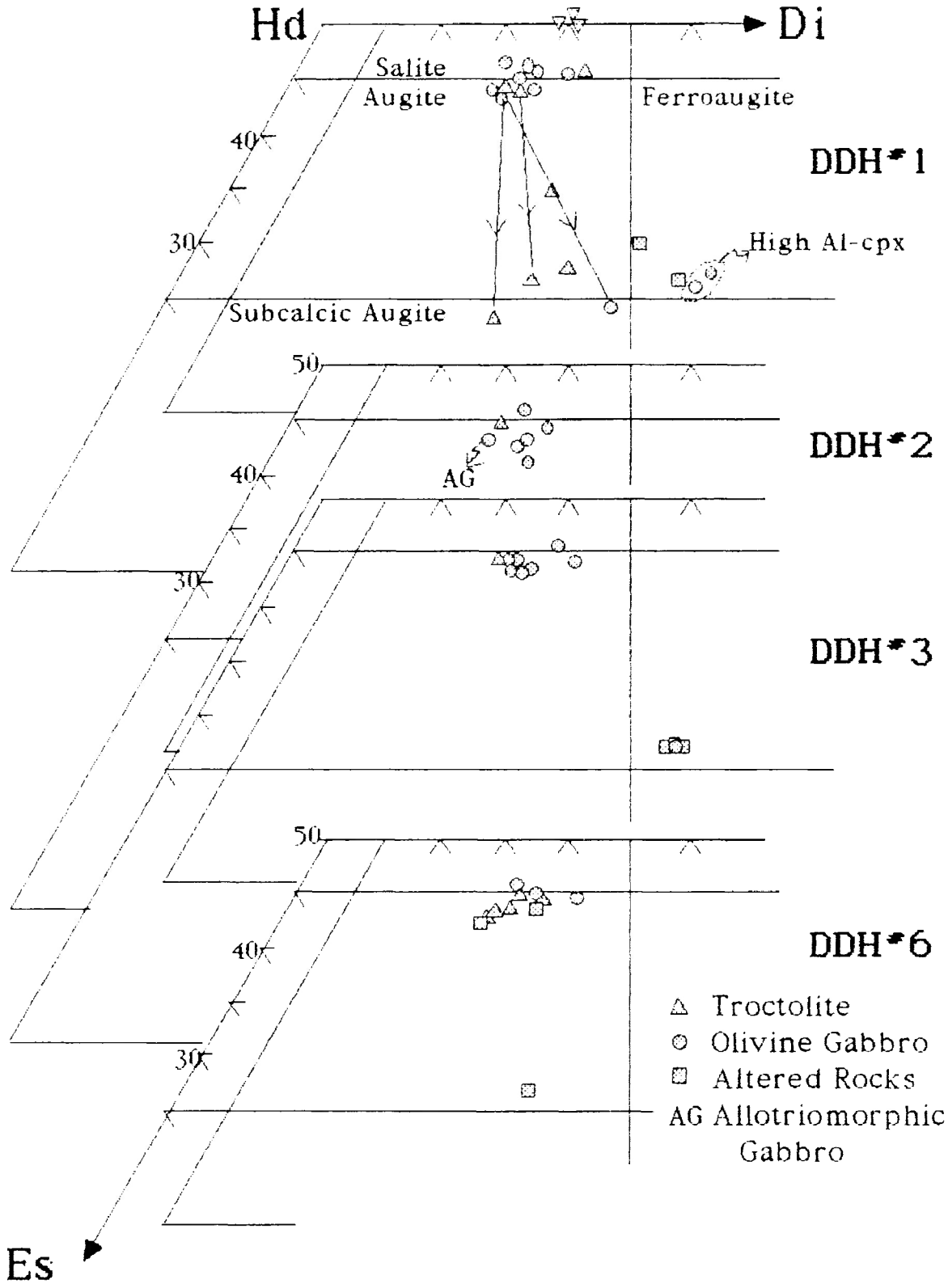

Figure 2.22: Compositions of clinopyroxenes of the GLI plotted in terms of hedenbergite (Hd), diopside (Di), enstatite (Es) and ferrosilite (Fs)-not shown. Core-rim compositional variations are indicated by the arrows. DDH: diamond drill hole (core).

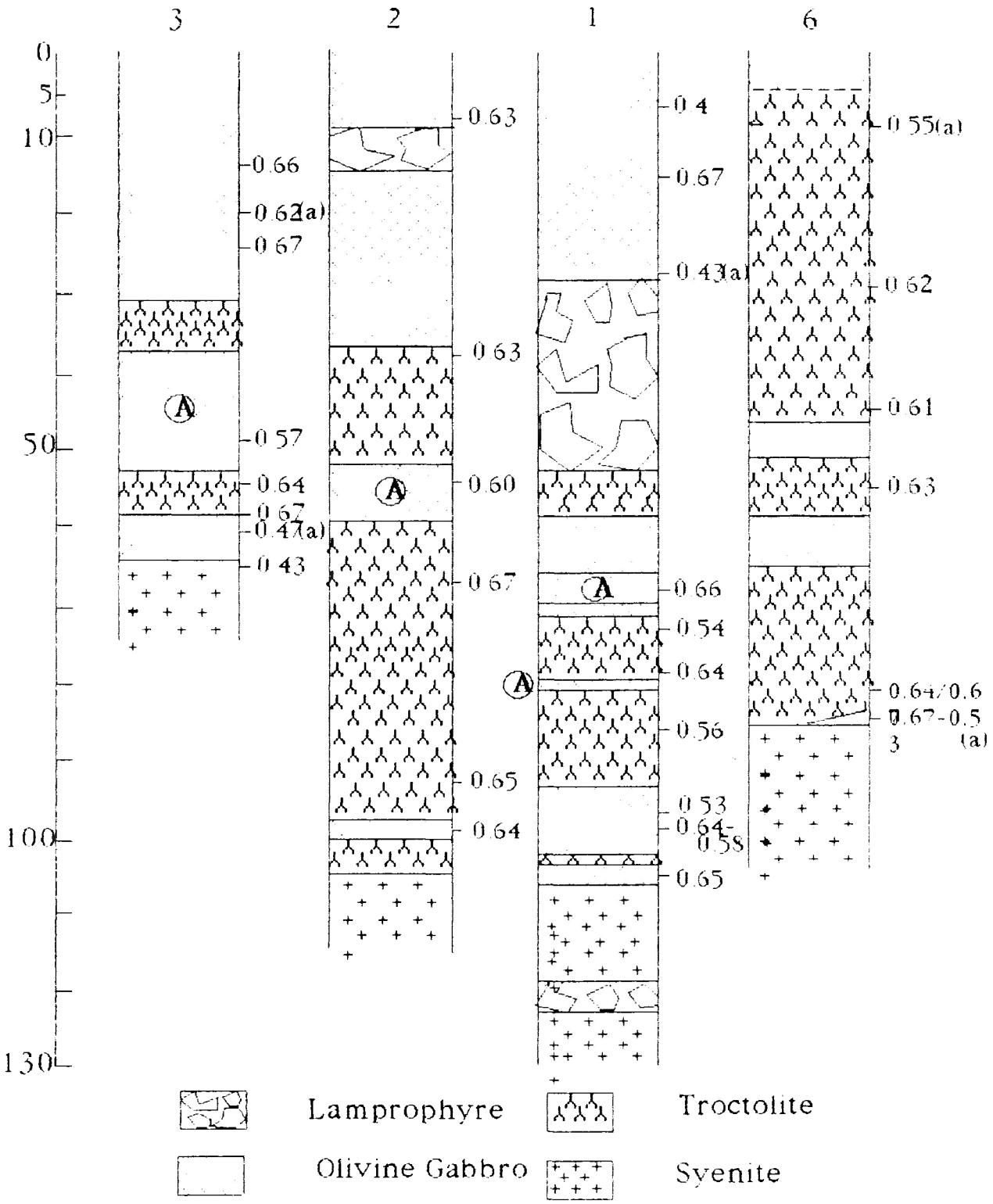

Figure 2.23 Mg/(Mg+Fe) ratios of clinopyroxene from the GLI plot against stratigraphic height. A: allotriomorphic gabbro, (a) altered rock/mineral

are lower than those of the McIntosh (Mathison and Hamlyn, 1987) and Somerset (Mathison, 1987) intrusions. The compositions of clinopyroxene in the troctolite of core 6 show a slight Fe enrichment from the basal to the upper sections. Compositions of clinopyroxene in the troctolite and gabbro from the other cores, however, do not show such a trend. Clinopyroxenes in the altered rocks are considerably less magnesian in comparison to those in unaltered samples.

Clinopyroxene compositions with low TiO_2 and Al_2O_3 contents have been recalculated in terms of aegirine (Ae: $NaFe^{3+}Si_2O_6$., formerly known as acmite., Morimoto *et al*, 1988), diopside (Di: $CaMgSi_2O_6$) and hedenbergite (Hd: $CaFeSi_2O_6$). Ferric iron was calculated from the total iron content by assuming that all the sodium in the pyroxene is combined with Fe^{3+} as aegirine (Mitchell and Platt, 1982). Clinopyroxenes having more than 5 per cent $CaAl_2SiO_6$ and/or $CaTiAl_2O_6$ are expressed as Ti-Px ($CaTiAl_2O_6$), CATS (Ca-Tschermack, i.e. $CaAl_2SiO_6$) and aegirine. Figure 2.24 plots the overall trend of low-Al clinopyroxene compositions on the ternary system Ae, Di and Hd. The majority of the clinopyroxenes from all rock types define a narrow compositional trend from Hd_{53-67}. A few clinopyroxenes from the weakly altered gabbroic rocks, gabbro and troctolite have compositions varying from Hd_{38-48}. They therefore are less evolved in terms of Mg and Fe contents but more evolved in terms of Na and Fe than the majority of the clinopyroxenes. There is a gap in the clinopyroxene composition from Hd_{48-53}. The high alumina clinopyroxenes plot in the CATS-Aegirine-TiPx ternary (Figure 2.25). The two compositional fields are defined primarily by the content of $CaAlSiAlO_6$. In field 1, $CaAlSiAlO_6$ is between 4 and 6 mole

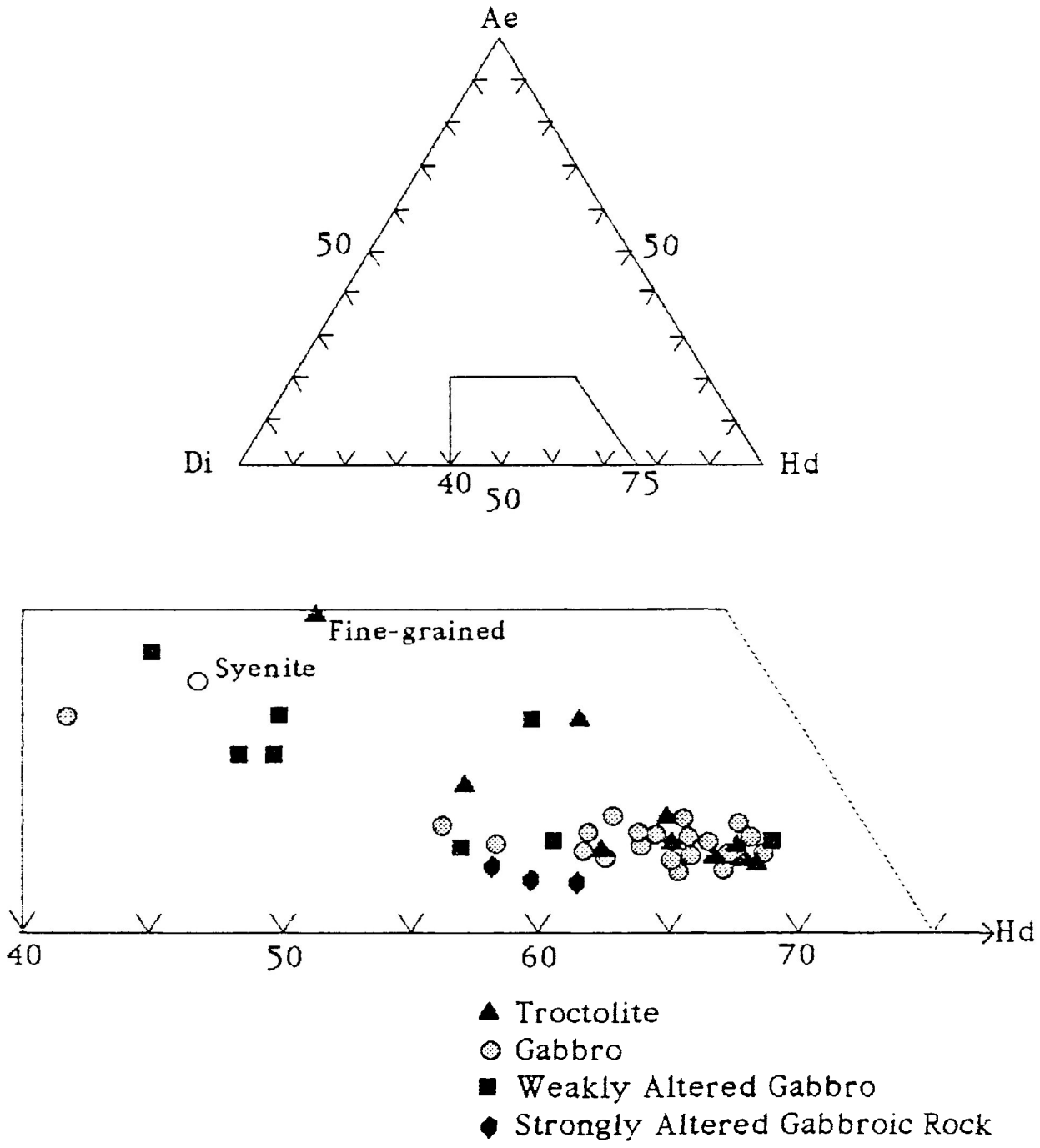

Figure 2.24 Plot of low-alumina clinopyroxene compositions in terms of aegerine (Ae), diopside (Di), and hendebergite (Hd).

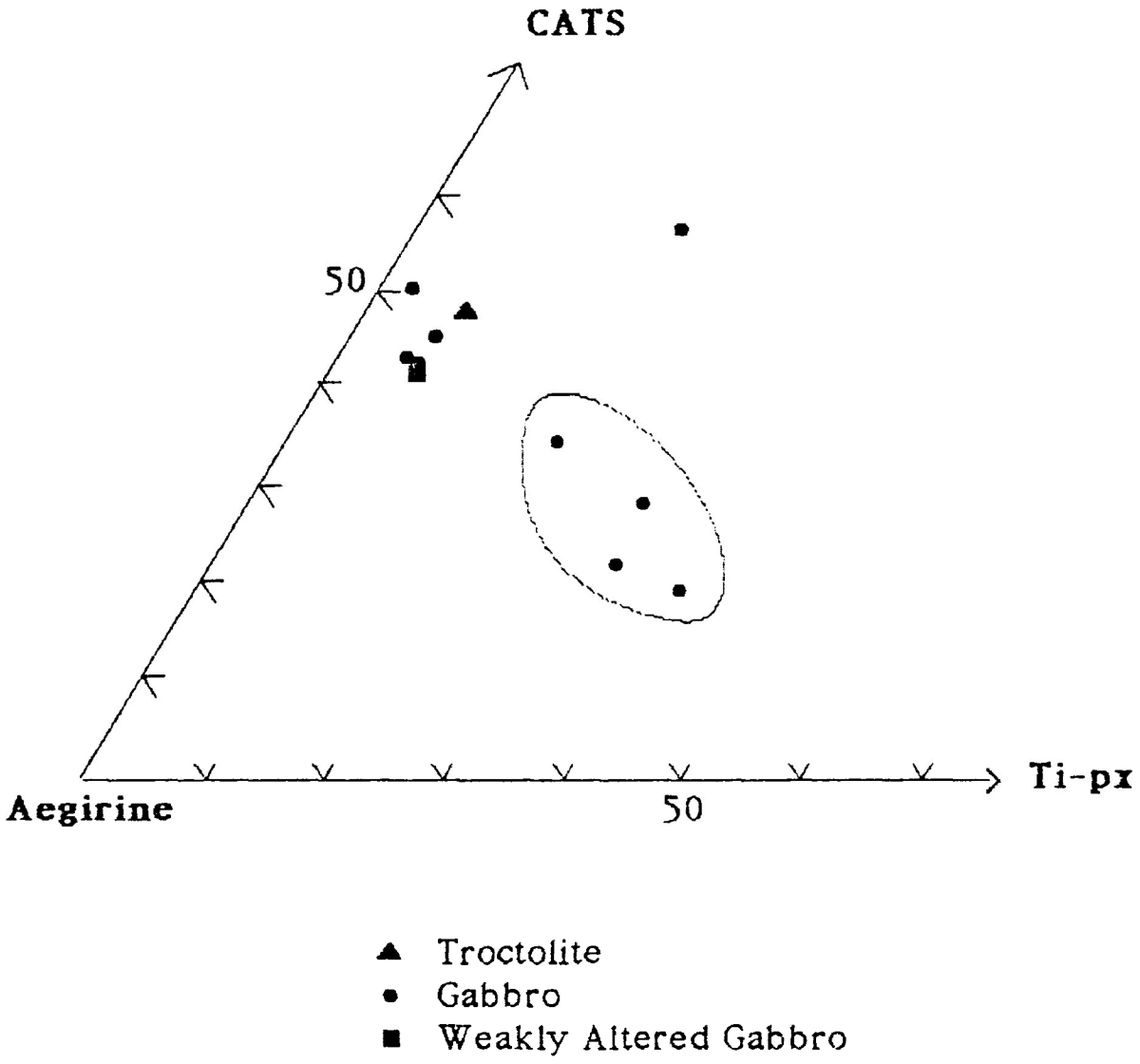

Figure 2.25 CATS-Ti-px-Aegirine Ternary for clinopyroxenes containing more than 5 mole % $CaSiAl_2O_6$, and $CaTiAl_2O_6$ and $CaSi_2AlO_6$ combined (circle).

per cent, whereas in field 2 it is more than 5 mole per cent of $CaAlSiAlO_6$ and $CaTiAl_2O_6$ combined. Sample 201 from the upper zone of core 2 has 9.8 mole per cent of $CaAlSiAlO_6$.

Figure 2.26 compares the overall clinopyroxene composition of the GLI to those of other gabbroic rocks from Coldwell and other localities. The Ca-rich clinopyroxenes of the GLI are more Fe-rich (i.e. more evolved) in comparison to the initial clinopyroxene composition of other rocks, with the exception of those studied by Lum (1973). The most evolved clinopyroxenes from the Center I gabbro north of Coubran Lake (Wilkinson, 1983) are comparable to the clinopyroxenes of the GLI. The Duluth clinopyroxene are less calcic than those of the GLI. There are insufficient data to delineate the compositional trend of the clinopyroxenes of all the Coldwell rocks, including the GLI, in order to make a comparison with the trends shown by pyroxenes of the Bushveld and Skaergaard intrusions.

2.3.5 Amphibole

A total of nineteen primary amphiboles were analysed from troctolite and gabbro. In addition, twelve analyses of discrete fine-grained amphiboles which replaced clinopyroxenes and a score of subsolidus actinolites rimming clinopyroxenes were also obtained. Representative amphibole compositions are given in Table 2.7.

In general, primary amphiboles contain less SiO_2 and MgO, but more Al_2O_3 and TiO_2 than subsolidus amphiboles. These chemical variations are similar to the amphiboles of gabbroic rocks in the Pliny Range, New

Figure 2.26 Comparison of clinopyroxene compositions from the GLI and other basic intrusions.

Sources of Data (from top to bottom)

Eastern border gabbro, Center I, Coldwell complex (Lum, 1973)

North-central gabbro, near Coubran Lake, Center I, Coldwell complex (Wilkinson, 1983)

Bushveld complex (Atkins, 1969)

Skaergaard intrusion (Deer *et al.*, 1978)

Duluth complex (Weiblen and Morey, 1980)

Geordie Lake intrusion (this study)

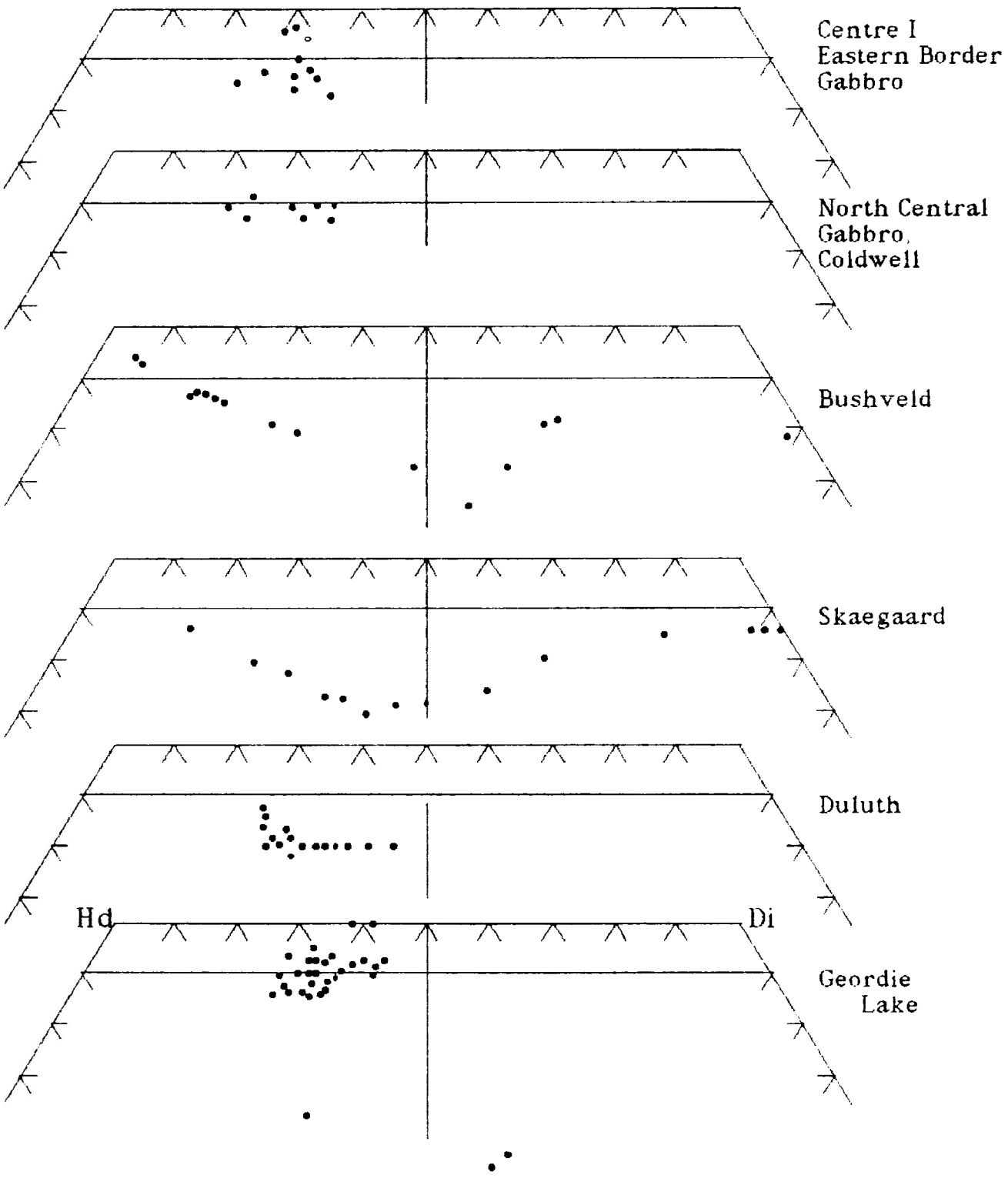
Centre I
Eastern Border
Gabbro
North Central
Gabbro,
Coldwell
Bushveld
Skaegaard
Duluth
Hd
Di
Geordie
Lake

Table 2.7 Electron microprobe analyses of amphibole from the GLI
TR:Troctolite, G: Gabbro, AG: Allotriomorphic Gabbro,
W/SAG: Weakly/Strongly altered gabbro
R: Replacement amphibole * from PGM-bearing rock

Rock Type	TR	TR	G	G	AG	WAG	SAG	G
Sample No.	43	407	2	22(R)*	9	5	30 (R)*	35
SiO2	42.63	45.16	42.49	47.04	42.06	41.87	45.50	39.69
TiO2	2.45	2.99	1.96	0.41	2.46	2.75	0.34	4.72
Al2O3	8.55	8.54	7.66	7.08	9.68	9.50	6.64	14.60
Fe2O3	1.91	1.63	3.02	11.86	0.42	0.68	5.22	3.17
FeO	14.84	10.12	13.10	5.63	16.76	16.58	19.33	7.75
MnO	0.37	0.24	0.27	0.69	0.26	0.29	0.75	0.14
MgO	11.40	14.24	12.81	12.98	10.54	10.49	7.57	12.73
CaO	10.97	11.48	11.22	10.29	11.39	11.32	11.64	10.28
Na2O	3.17	2.12	3.28	1.71	2.73	2.69	1.11	2.77
K2O	1.36	1.52	1.55	0.00	1.90	1.82	1.04	2.00
TOTAL	97.64	98.03	97.36	97.69	98.20	97.99	99.14	97.86
Structural Formulae based on Twenty-three Oxygens								
Si	6.467	6.554	6.457	6.850	6.389	6.374	6.910	5.836
Al(iv)	1.529	1.446	1.372	1.150	1.611	1.626	1.090	2.164
Al(vi)	0.000	0.048	0.000	0.066	0.122	0.078	0.100	0.366
Ti	0.279	0.337	0.224	0.045	0.281	0.315	0.039	0.522
Fe3+	0.218	0.182	0.346	1.300	0.048	0.078	0.597	0.351
Fe2+	1.882	1.256	1.664	0.686	2.129	2.111	2.455	0.953
Mn	0.048	0.030	0.347	0.085	0.033	0.037	0.096	0.017
Mg	2.578	3.151	2.902	2.818	2.387	2.381	1.714	2.790
Ca	1.783	1.825	1.827	1.605	1.854	1.846	1.894	1.619
Na	0.932	0.610	0.966	0.483	0.804	0.794	0.327	0.790
K	0.263	0.288	0.300	0.000	0.368	0.353	0.201	0.375
(Ca+Na)B	2.000	2.000	2.000	2.000	2.000	2.000	2.000	2.000
(Na+K)A	0.978	0.723	1.093	0.088	1.026	0.994	0.422	0.776
Na^B	0.217	0.175	0.173	0.395	0.146	0.154	0.106	0.388
Na^A	0.715	0.435	0.793	0.088	0.657	0.640	0.220	0.401
Mg/Mg+Fe2	0.580	0.715	0.636	0.804	0.529	0.530	0.410	0.750
A*	0.401	0.330	0.410	0.231	0.387	0.383	0.218	0.242

A*:Na+k/Ca+Na+k

Hampshire (Czamanke *et al*, 1977). According to the International Mineralogical Association classification (1978), all amphiboles are considered calcic. The primary amphiboles vary from magnesian-hastingsitic to edenitic hornblendes, and from ferro-edenitic to ferroan-pargasitic hornblendes (Figures 2.27A -B). The amphibole in Sample 35 is kaersutite (Table 2.7).

There is a positive correlation between Si and Mg/(Mg+Fe) contents (Figure 2.27A) in the hornblendes of the troctolite. Table 2.8 shows that SiO_2 contents of the hornblendes are lower than those of the host rock.

Table 2.8 SiO_2 Contents (weight per cent) in Amphiboles vs Host Rocks. The number of comparisons is small because amphibole is not present in all samples.

Sample No.	Amphibole	Host rock
9	41.99	46.80
28	42.79	43.20
30	43.71	45.50
44	41.87	47.38

Hornblendes are typically less siliceous than their hosts and fractionation of the amphibole should result in silica enrichment of the liquid (Wones and Gilbert, 1981). Accordingly, the trend of amphibole compositions in the troctolite is from magnesian-hastingsitic hornblende towards edenitic hornblende and not towards ferro-edenitic hornblende. However, Sample G-407, which is a brown amphibole, is stratigraphically lower than Sample

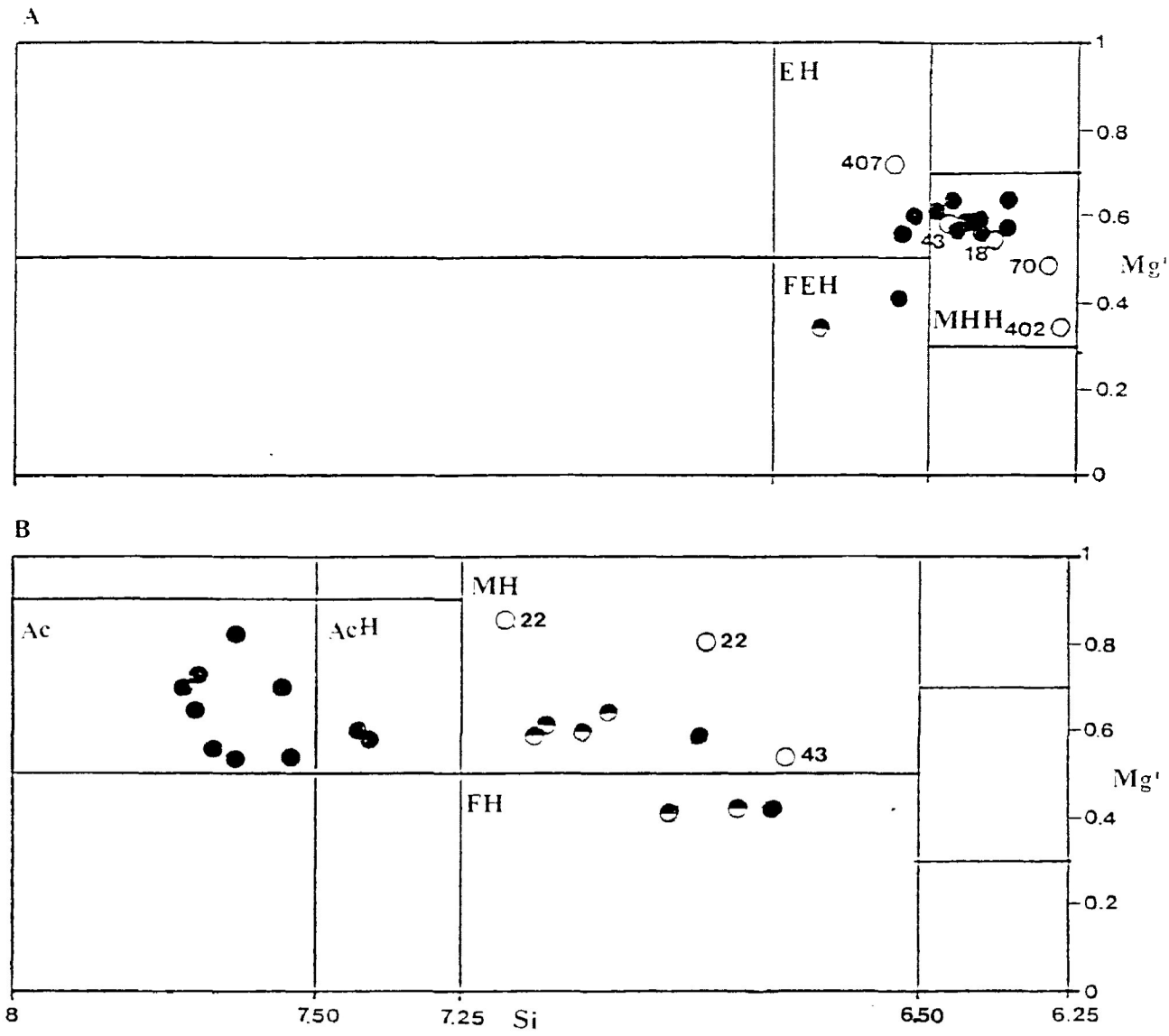

Figure 2.27A-B Classifications of amphiboles from the GLI based on Mg' ($Mg/(Mg+Fe^{2+})$ vs. Si cations. Sample numbers are given to troctolite and some gabbro amphiboles.

Symbols

○ : Troctolite, ● : Olivine Gabbro, ◓ : Altered Rock

Abbreviations

EH: Edenitic hornblende, FEH: Ferro-edenitic hornblende, MHH: Magnesian hastingsitic hornblende

Ac: Actinolite, AcH: Actinolitic hornblende, MH: Magnesio-hornblende, FH: Ferro hornblende

402, a green amphibole. Furthermore, there is a gabbro unit in between the two samples (Figure 1.6, Sample location map). The predicted trend is, thus, unlikely to exist in the studied amphiboles. Other calcic amphiboles are magnesio- and ferro-hornblendes, and actinolites (Figure 2.27B). Unlike the actinolites, which clearly display replacement texture, i.e. rimming clinopyroxenes, these hornblendes are discrete and fine-grained. The relatively coarser crystals exhibit a ragged subhedral habit and occur in altered and "dioritic" rocks. The SiO_2 and MgO contents of these hornblendes are higher than those of primary amphiboles. These observations suggest that the hornblendes are of secondary origin.

Compositions of amphiboles have been reported for some basic intrusions. McGill (1980) has indicated that the western border-group gabbro of Coldwell contains between one and five modal per cent brown amphibole. The amphiboles reported by Mathison (1987) and Mathison and Hamlyn (1987) for the Somerset Dam and McIntosh troctolite-olivine gabbro, respectively, are mostly brown hornblendes. The Somerset Dam rocks also contain kaersutite and titanian ferroan pargasitic amphibole. Currie *et al.* (1986) show that the amphiboles of the Sunrise suite of the Mont Saint Hilaire complex are kaersutitic. The composition of the sole brown amphibole from the GLI is fairly similar to those of the aforementioned basic intrusions, with the exception that it is slightly less siliceous.

2.3.6 Biotite

Biotite is not a major mafic phase of the GLI. All biotite data

obtained are presented in Table 2.9. The FeO and MgO contents show some variations, ranging from 13.3-26.3 wt. % and 8.8-18.7 wt. %, respectively. The Fe/(Fe+Mg) ratios increase against the stratigraphic height but this trend is not observed in the coexisting clinopyroxene (Figure 2.28). Petrographically, most biotites are spatially associated with late magmatic fine-grained amphiboles and actinolites, and fringe the early skeletal magnetites. These observations suggest that the biotite is a late magmatic phase. Biotite compositions in terms of Mg-Fe-Al are plotted in Figure 2.29. For comparison, the biotite compositions of the western gabbro (Table 2.10) are also plotted. The trend of biotites from the GLI shows small variations in the Al content ranging from 2.3 to 2 atoms per formula unit. The biotites of the western gabbros show a similar compositional trend, but their Al contents are higher and narrower in range than those of the GLI (Figure 2.29). The Fe contents of the biotites in the metasomatized host rocks are less than the recrystallized western gabbros.

One analysis of biotite is reported for the Somerset troctolite (Mathison, 1987) and shows greater Ti and Al but less Mn and K contents than biotite of the GLI.

2.3.7 Magnetite and Ilmenite

Sixty magnetite-ilmenite pairs (Fe-Ti oxides) from forty samples were analysed with the electron microprobe, and ten representative compositions are given in Table 2.11. The compositions of the Fe-Ti oxides from the GLI and other basic intrusions are plotted in the ternary system TiO_2-FeO-Fe_2O_3

Table 2.9 Electron microprobe analyses of biotite from the GLI
G: Gabbro, TR: Troctolite

Rock type	G		G	TR	TR	G	G	G	TR	G	TR
Sample No.	1	1	2	11	13	201	201	201	209	304	407
SiO2	37.18	35.88	37.71	39.61	39.46	37.46	36.19	37.03	39.39	37.38	41.32
TiO2	2.27	2.28	3.65	2.87	2.66	3.28	2.98	3.03	3.81	4.35	1.52
Al2O3	12.21	12.10	12.73	11.67	13.08	12.14	12.67	12.33	12.20	12.97	12.92
FeO	26.33	25.81	22.81	14.48	13.96	24.00	25.18	23.24	16.61	21.39	13.31
MnO	0.33	0.34	0.18	0.10	0.12	0.26	0.30	0.31	0.13	0.19	0.12
MgO	8.99	8.78	10.55	17.84	17.77	9.63	10.34	10.16	15.88	11.04	18.76
Na2O	0.12	0.13	0.45	0.51	1.36	0.28	0.25	0.25	0.63	0.78	0.51
K2O	10.47	9.07	9.66	10.26	8.79	9.50	8.84	9.74	8.82	8.68	8.19
TOTAL	97.9	94.39	97.74	97.34	97.2	96.55	96.75	96.09	97.47	96.78	96.65
Structural Formula based on 22 oxygen											
Si	5.752	5.723	5.707	5.798	5.727	5.773	5.595	5.730	5.761	5.651	5.934
Ti	0.264	0.274	0.416	0.316	0.290	0.380	0.347	0.353	0.419	0.495	0.164
Al	2.228	2.276	2.272	2.014	2.239	2.206	2.310	2.250	2.104	2.312	2.187
Fe	3.409	3.445	2.889	1.774	1.695	3.097	3.257	3.009	2.033	2.706	1.599
Mn	0.043	0.046	0.023	0.012	0.015	0.034	0.039	0.041	0.016	0.024	0.015
Mg	2.075	2.089	2.382	3.895	3.847	2.214	2.385	2.345	3.465	2.490	4.017
Na	0.036	0.040	0.132	0.145	0.383	0.084	0.075	0.075	0.179	0.229	0.142
K	2.068	1.847	1.867	1.917	1.629	1.869	1.745	1.924	1.647	1.675	1.501
Annite	61.69	61.75	54.58	31.23	30.52	57.95	57.35	55.79	36.88	51.85	28.40
Phlogopite	37.53	37.43	44.98	68.56	69.22	41.42	41.96	43.46	62.83	47.69	71.34
Mn-phyl*	0.78	0.82	0.44	0.22	0.27	0.64	0.69	0.75	0.29	0.47	0.26
Al	28.89	29.14	30.12	26.22	28.77	29.35	29.05	29.59	27.68	30.80	28.03
Fe	44.20	44.11	38.30	23.08	21.79	41.19	40.96	39.57	26.74	36.04	20.49
Mg	26.91	26.75	31.59	50.70	49.44	29.45	29.99	30.84	45.58	33.16	51.48
Fe/Fe+Mg	0.622	0.623	0.548	0.313	0.306	0.583	0.577	0.562	0.370	0.521	0.285

*Manganophyllite

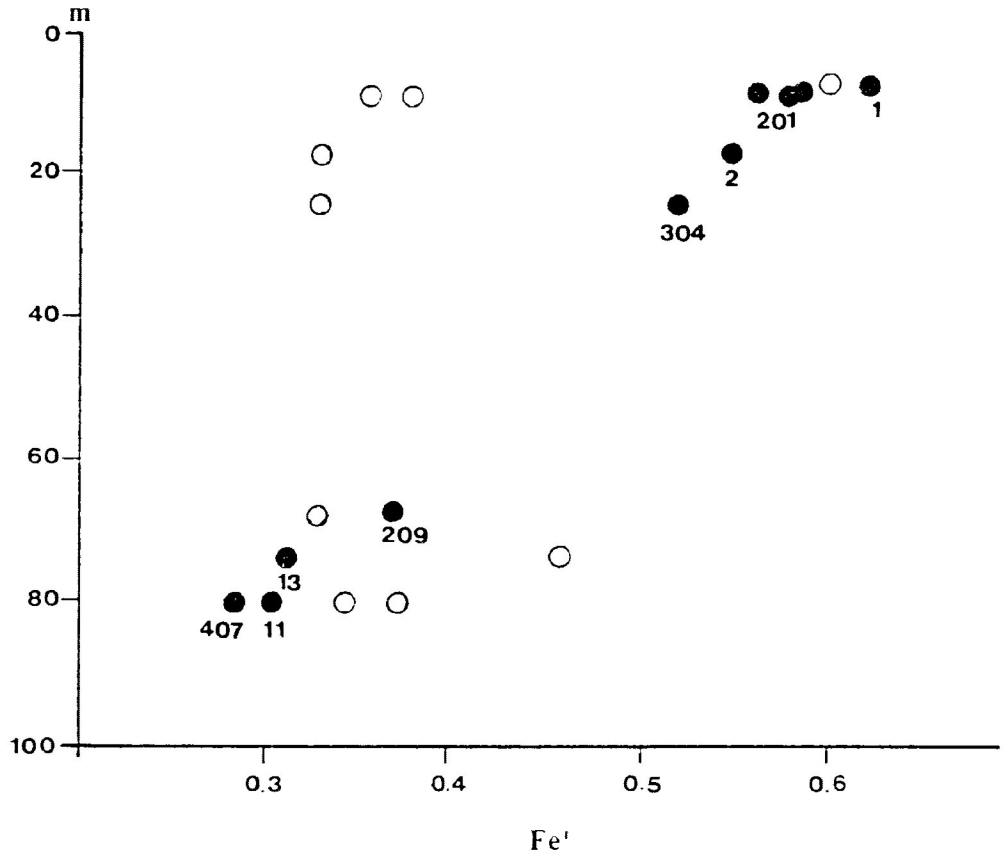

Figure 2.28 Plot of Fe/(Fe+Mg) ratio vs. height of the biotites and of the coexisting clinopyroxenes from the GLI. Samples numbers are given next to the biotite plots. Samples 1, 2,11 and 13 are from core 1, samples 201 and 209 from core 2, sample 304 from core 3, and sample 407 from core 6.

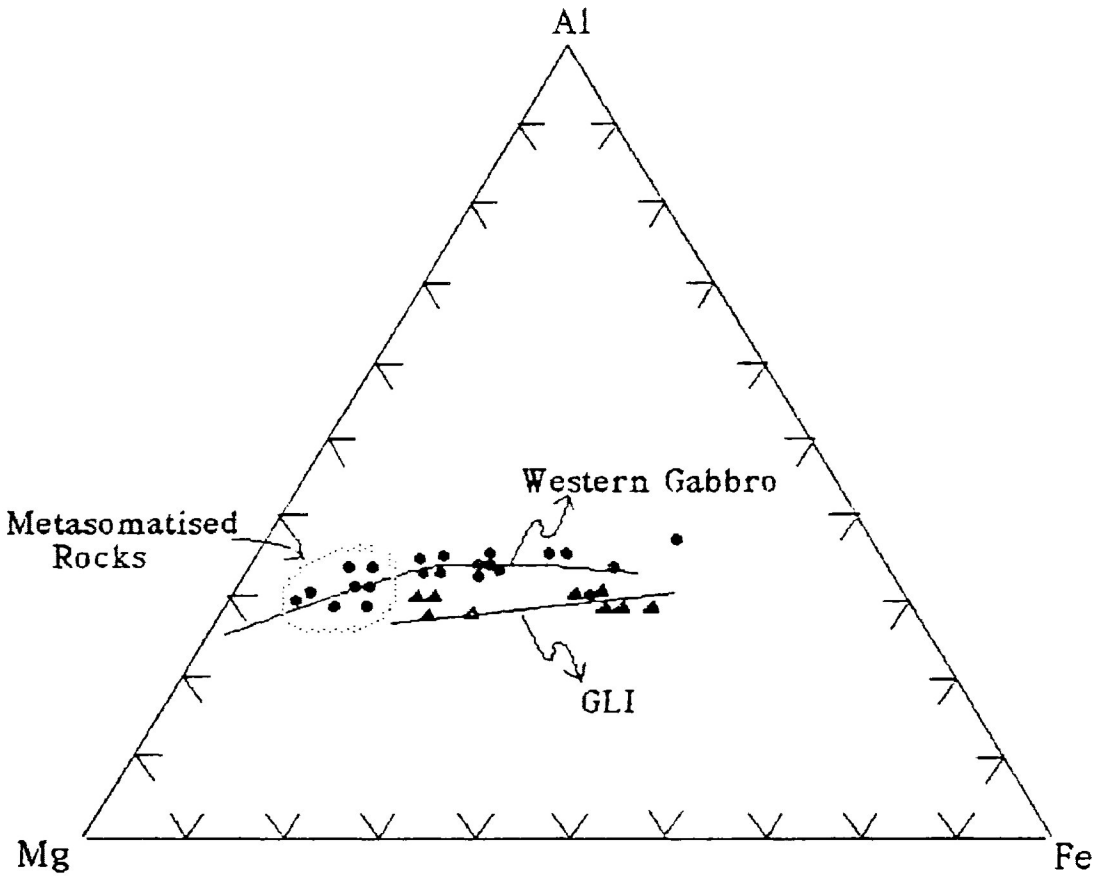

Figure 2.29 Biotite compositions plot in the system Al-Mg-Fe. The metasomatised rocks are from Center II gabbros (See Table 2.10).

Table 2.10 Electron Microscope analyses of representative biotites from Center I and II gabbros
*Metasomatised and Recrystallized, medium-grained size
**Mainly recrystallised, fine grains
+ Metasomatised, coarse grains

	Center I -->				Center II -->				
Sample No.	138	308	414	420	590*	593**	608	907*	1498+
SiO2	37.28	35.04	36.31	35.47	36.87	34.94	38.22	34.80	37.95
TiO2	2.57	1.98	3.39	5.41	0.74	4.23	2.34	2.45	5.47
Al2O3	15.62	15.93	14.85	14.46	16.89	15.38	15.73	13.73	13.21
FeO	13.10	16.50	17.47	16.16	12.02	19.27	12.09	23.49	9.46
MnO	0.12	0.16	0.15	0.12	0.15	0.24	0.10	0.33	0.08
MgO	17.05	14.42	13.94	13.01	18.79	12.00	18.20	11.74	18.95
Na2O	0.96	0.39	0.22	0.21	0.45	0.68	0.56	0.52	1.08
K2O	8.54	10.24	9.99	9.36	10.71	9.49	9.74	7.06	8.86
TOTAL	95.24	94.66	96.32	94.20	96.62	96.23	96.98	94.12	95.06
Structural Formulae based on 22 oxygens									
Si	5.4941	5.3460	5.4420	5.4089	5.3847	5.2888	5.5134	5.4527	5.5116
Ti	0.2849	0.2272	0.3821	0.6205	0.0813	0.4816	0.2539	0.2887	0.5975
Al	2.7145	2.8660	2.6245	2.6002	2.9088	2.7452	2.6758	2.5368	2.2624
Fe	1.6155	2.1066	2.1910	2.0621	1.4690	2.4408	1.4594	3.0799	1.1497
Mn	0.0150	0.0207	0.0191	0.0155	0.0186	0.0308	0.0122	0.0438	0.0098
Mg	3.7484	3.2819	3.1167	2.9595	4.0937	2.7097	3.9165	2.7441	4.1056
Na	0.2746	0.1155	0.0640	0.0622	0.1276	0.1998	0.1568	0.1582	0.3045
K	1.6068	1.9946	1.9115	1.8222	1.9969	1.8339	1.7938	1.4123	1.6428
Mol. PerCent End Members									
Annite	30.04	38.95	41.14	40.95	26.33	47.12	27.09	52.5	21.84
Phlogopite	69.68	60.66	58.5	58.74	73.34	52.29	72.68	46.76	77.97
Manganophyllite	0.28	0.38	0.36	0.31	0.33	0.59	0.23	0.75	0.19
Plotting Parameters									
Al	33.60	34.72	33.09	34.12	34.34	34.77	33.23	30.34	30.09
Fe	20.00	25.52	27.62	27.06	17.34	30.91	18.13	36.84	15.29
Mg	46.40	39.76	39.29	38.83	48.32	34.32	48.64	32.82	54.61

Table 2.11 Electron microprobe analyses of representative Fe-Ti oxides from the GLI
TR: Troctolite, G: Gabbro, a:altered

Host Rock	TR		TR		TR		aTR	
Sample No.	11		13		404		64	
	Mt	Il	Mt	Il	Mt	Il	Mt	Il
TiO2	1.70	50.70	2.30	50.70	1.85	50.21	1.24	48.73
Al2O3	1.04	0.09	2.96	0.09	0.32	0.09	0.13	0.06
Cr2O3	0.33	0.16	0.38	0.16	0.18	0.17	0.26	0.24
Fe2O3	63.71	4.51	61.06	4.51	65.13	4.67	67.37	7.02
FeO	31.88	43.25	32.67	43.25	32.16	39.84	32.14	38.18
MnO	0.33	1.52	0.34	1.52	0.43	4.84	0.37	5.28
MgO	0.14	0.39	0.41	0.39	0.10	0.15	0.00	0.03
TOTAL	99.13	100.62	100.12	100.62	100.17	99.97	101.51	99.53
Ti	0.049	0.955	0.065	0.955	0.053	0.953	0.035	0.930
Al	0.047	0.003	0.131	0.003	0.014	0.003	0.006	0.002
Cr	0.010	0.003	0.011	0.003	0.005	0.003	0.008	0.005
Fe3+	1.844	0.085	1.727	0.085	1.874	0.089	1.916	0.134
Fe2+	1.026	0.906	1.027	0.906	1.028	0.841	1.016	0.810
Mn	0.011	0.032	0.011	0.032	0.014	0.103	0.012	0.114
Mg	0.008	0.015	0.023	0.015	0.006	0.006	0.000	0.001

Rock type	G		AG		aG		aG	
	MR-5		9		5		303	
	Mt	Il	Mt	Il	Mt	Il	Mt	Il
TiO2	0.87	43.47	1.82	49.80	9.06	49.20	6.08	49.70
Al2O3	0.13	0.03	0.13	0.06	0.10	0.09	0.59	0.22
Cr2O3	0.16	0.14	0.20	0.19	0.21	0.16	0.21	0.21
Fe2O3	67.93	13.33	65.47	5.73	50.97	5.12	57.43	5.59
FeO	32.08	34.51	32.28	40.58	38.01	40.02	36.47	42.09
MnO	0.31	4.29	0.34	3.80	1.00	3.87	0.43	2.20
MgO	0.00	0.08	0.10	0.10	0.10	0.11	0.10	0.14
TOTAL	101.48	95.85	100.34	100.26	99.45	98.57	101.31	100.15
Ti	0.028	0.865	0.052	0.943	0.261	0.948	0.172	0.942
Al	0.006	0.001	0.006	0.002	0.005	0.003	0.026	0.007
Cr	0.005	0.003	0.006	0.004	0.006	0.003	0.006	0.004
Fe3+	1.934	0.266	1.883	0.109	1.468	0.099	1.624	0.106
Fe2+	1.015	0.764	1.032	0.854	1.217	0.857	1.146	0.887
Mn	0.010	0.096	0.011	0.081	0.032	0.084	0.014	0.047
Mg	0.000	0.003	0.006	0.004	0.006	0.004	0.006	0.005

(Figure 2.30). The magnetite compositions plot tightly at the Fe_3O_4 end-member and along the magnetite-ulvospinel tie-line. The magnetites from the altered samples 5 and 303 show the greatest TiO_2 and FeO content. The ilmenite compositions plot near the ilmenite end-member and slightly above the ilmenite-hematite tie-line. The deviation from the ilmenite-hematite tie line is due to their high MnO contents. The Fe-Ti oxide compositions of the troctolite and gabbro plot in the same field, indicating that the major element contents of the minerals of these two rock types are relatively similar. The Fe-Ti oxide compositions of the western gabbro display a similar trend in the ternary diagram. The TiO_2 contents in the magnetites of the Somerset Dam intrusions (Mathison, 1975) are greater than those of the GLI or western gabbro of Coldwell. However, the Somerset Dam ilmenites have lower TiO_2 contents than the Coldwell rocks.

A summary of the compositions of Fe-Ti oxides from the troctolite and gabbro of the GLI is given in Table 2.12. In general, the analysed magnetites have low concentrations of aluminum (average <1 wt. %). The high TiO_2 contents in the exsolved ilmenites, averaging 49 and 48 wt. % in the troctolite and gabbro, respectively, and the occurrence of exsolved ilmenites in all primary magnetites, suggest that the magnetites were originally Ti-rich. The data show that the two rock types contain magnetites of relatively similar Fe_2O_3, FeO, and MgO contents, although the calculated ferrous iron content of the troctolite has a narrower range. The average content of TiO_2 is slightly higher in the gabbro than in the troctolite due to high TiO_2 contents (6 and 9 wt. %) in two of the altered rocks. The majority of the TiO_2 contents of the magnetites of the two rock types are fairly

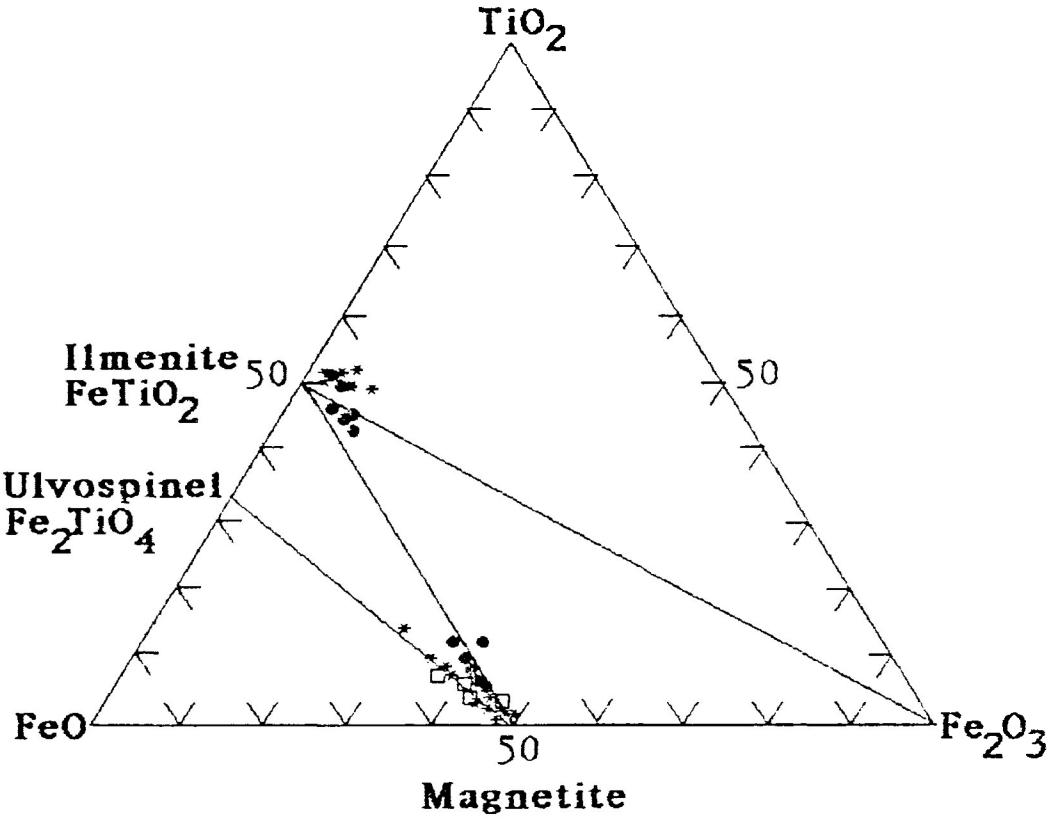

* Geordie Lake Intrusion
□ Western Gabbro, Coldwell
• Somerset Dam Intrusion

Figure 2.30 Compositional variations of the Fe-Ti oxides plot in the ternary system TiO_2-FeO-Fe_2O_3. Sources of data: western gabbro (this study) and Somerset Dam Intrusion (Mathison, 1987).

Table 2.12 Summary of the compositions of the Fe-Ti oxides from the GLI

Composition of Fe-Ti oxides in Troctolite

	Magnetite			Ilmenite		
	Min.	Max.	Mean	Min.	Max.	Mean
TiO2	0.7	2.3	1.5	46.7	50.7	49.2
Al2O3	0.1	3.9	0.1			
Cr2O3	0.1	0.4	0.3	0.1	0.2	0.2
Fe2O3	61.1	68.3	65.4	3.9	8.4	5.9
FeO	31.4	32.7	32.2	38.2	43.2	40.5
MnO	0.3	0.4	0.3	1.5	5.3	2.7
MgO	0	0.4	0.1	0	1.1	0.4

Composition of Fe-Ti oxides in Gabbro

	Magnetite			Ilmenite		
	Min.	Max.	Mean	Min.	Max.	Mean
TiO2	0.5	9.1	1.8	43.47	50	48.2
Al2O3	0.1	1.1	0.4			
Cr2O3	0.1	0.3	0.2	0.1	0.2	0.2
Fe2O3	51	69.3	66	5	21.6	7.4
FeO	30.7	38	32.6	33.2	42.1	39
MnO	0.2	1	0.4	1.8	6	3.8
MgO	0	0.1	0.1	0	0.4	0.2

similar. The manganese content is higher in the gabbro than in the troctolite.

The average contents of TiO_2 and FeO in the ilmenites of the troctolite and gabbro differ little. The MnO content is slightly higher in the ilmenite of gabbro than in that of troctolite. The Cr_2O_3 and MgO contents in the ilmenites of the two rock types are negligible. The major elements of the Fe-Ti oxides in the troctolite, therefore do not differ significantly from those in the gabbro.

Most minor elements demonstrate a consistent preference for either magnetite or ilmenite. Al and Cr are preferentially concentrated in the magnetite, whereas Mn and Mg indicate a preference for ilmenite. These patterns of element partitioning are attributed to Al and Cr substitutions for Fe^{3+} in the magnetite and to the higher degree of Mg and Mn ionic bonding in ilmenite compared to magnetite (Lister, 1966).

The compositional variations in the major elements of the Fe-Ti oxides with respect to stratigraphic height are best represented by the troctolite of core 6 and gabbro of core 3 (Figures 2.31). In between the basal and upper units of the troctolite, there is a gabbro unit (approximately 20-m thick). The magnetites of the basal troctolite do not show any relationship to those of the upper unit. The TiO_2 contents in the magnetites of the upper unit troctolite show a decreasing trend with height, from about 1.85 to 1.1 wt. % TiO_2. The Fe_2O_3 contents decrease slightly from 65 to 63 wt. % then increase to 68 wt. %. FeO concentrations do not show any significant variations with height. The contents of ilmenites in the upper unit troctolite show an abrupt decrease in TiO_2 and FeO, and a sudden increase in the Fe_2O_3.

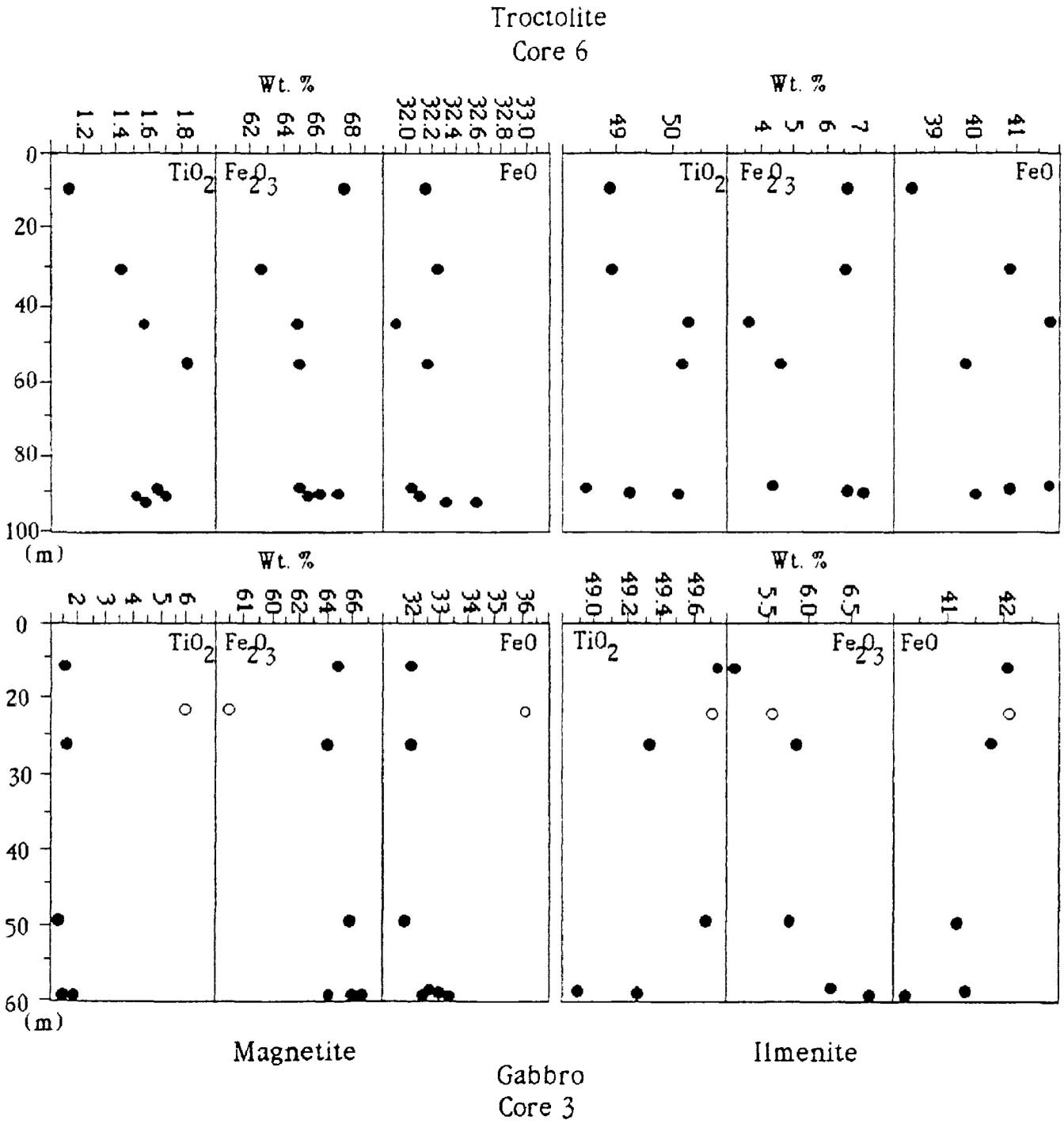

Figure 2.31 Compositional variations of the Fe-Ti pairs vs. height from the troctolite of core 6 and gabbro of core 3. The open circle is magnetite analysis from an altered rock.

The compositions of the magnetites in the ophitic gabbro of core 3 (Figure 2.31) vary little throughout the succession, even though two separate units of gabbros, between the 50-60 m interval and 30-50 m interval, are found. The composition of the ilmenite, however, does show some variation. There is a general increase in the TiO_2 and FeO contents, and a decrease in the Fe_2O_3 content, of the ilmenite from the basal to the upper unit. The amount of the variations is about 1 wt. % TiO_2, 1.5 wt. % Fe_2O_3 and 2 wt. % FeO.

Four magnetite grains lacking ilmenite exsolution were analysed for comparative studies (Table 2.13). These magnetites are characterized by lower Ti, Al, and Cr contents, but higher ferrous iron than their coexisting (samples 11 and 208) primary magnetites and the average composition of primary magnetites. These comparisons suggest that subsequent magnetites precipitated from fluids depleted in Ti, Al, and Cr, which were already partitioned into the primary magnetites.

The compositions of coexisting Fe-Ti oxides can be used to determine the temperature and oxygen fugacity of the oxides during the equilibration processes which led to ilmenite exsolution (Buddington and Lindsley,1964). Sixty magnetite-ilmenite pairs were used for geothermometry and fO_2 determinations. The calculations were performed using the "Oxtemp" computer program of Stormer (1983) and the results are given in Table 2.14. The temperatures obtained for the GLI Ti-Fe oxides range from 543-704°C (average 605°C $\pm$ 36) and fO_2 from -log14.97 to -log 21.38 (average -log18.5 $\pm$ 0.8) bar. The temperatures obtained are too low for magmatic conditions. They are, therefore, the subsolidus temperatures at which the ilmenite

Table 2.13 Comparisons of magnetite compositions of different paragenesis
Analysis 1: Magnetite replacing olivine
3: Fine-grained magnetite
5: Granular magnetite in Mt-Il-Chalcopyrite aggregate
6: Euhedral magnetite in massive chalcopyrite
2, 4: Magnetite compositions from Mt-Il Pairs
7: Average magnetite (n=60)

Analysis	1	2	3	4
Sample No.	11	11	208	208
TiO2	0.14	1.70	0.46	0.77
Al2O3	0.16	1.04	0.14	0.16
Cr2O3	0.20	0.33	0.21	0.21
Fe2O3	67.93	63.71	68.35	66.94
FeO	30.25	31.88	31.03	31.03
MnO	0.35	0.33	0.28	0.35
MgO	0.15	0.14	0.11	0.09
TOTAL	99.18	99.13	100.58	99.55

Analysis	5	6	7
Sample No.	34	55B	
TiO2	0.07	0.65	1.70
Al2O3	0.27	0.19	0.60
Cr2O3	0.20	0.17	0.24
Fe2O3	68.46	68.23	65.80
FeO	30.62	31.33	32.50
MnO	0.30	0.41	0.40
MgO	0.09	0.11	0.10
TOTAL	100.01	101.09	

Table 2.14 T-FO2 of equilibration of the Fe-Ti oxides from the GLI
* considered to be out of range by the Stormer's calculation method

Sample	T°C	+/-	f O2	+/-	Sample	T°C	+/-	f O2	+/-
1	633	37	-19.07	0.98	205	598	36	-19.50	0.95
2	588	38	-19.31	0.88	208	562	45	-20.03	0.95
5	659	40	-18.39	0.93	209	543	50	-21.09	1.13
9	600	35	-19.12	0.88	43	601	36	-18.42	0.74
11	575	40	-20.75	1.18	45	597	38	-18.24	0.70
13	604	35	-19.50	0.98	45A	597	38	-18.21	0.69
18	590	37	-19.82	1.00	302	585	38	-20.01	1.03
22	613	34	-17.85	0.66	303	647	35	-18.43	0.88
25	610	34	-18.20	0.69	304	601	35	-19.05	0.86
26	622	33	-17.09	0.56	307	590	37	-19.28	0.88
27A	603	36	-17.99	0.67	51	560	43	-21.38	1.29
27B	609	34	-18.13	0.71	53A	605	35	-18.43	0.75
27C	624	31	-17.65	0.66	53B	603	35	-19.00	0.86
28A	622	32	-17.96	0.71	54A	608	34	-18.60	0.79
28B	602	36	-18.21	0.70	54B	612	34	-17.90	0.67
28C	619	33	-17.27	0.58	64A	604	36	-18.11	0.69
29A	652	28	-16.26	0.49	64B	588	39	-18.79	0.77
29B	610	34	-18.24	0.73	70A	601	35	-18.64	0.78
29C	633	31	-16.93	0.56	70B	618	32	-18.00	0.70
30A	620	33	-17.50	0.62	402	560	43	-21.63	1.36
30B	626	32	-17.03	0.56	404	584	38	-20.25	1.08
30C	612	34	-17.91	0.67	407	573	40	-20.83	1.19
31	568	43	-20.00	0.97	77A	612	33	-18.34	0.75
35A	605	35	-18.13	0.70	77B	609	34	-18.28	0.73
35B	601	35	-18.98	0.85	78A	615	33	-17.94	0.69
35C	596	37	-18.46	0.73	78B	610	36	-17.35	0.58
37A	597	39	-17.93	0.64	81A*	704	25	-13.05	0.21
37B*	585	51	-17.42	0.54	81B	620	33	-17.41	0.61
38*	583	52	-17.52	0.55	MR5A	596	40	-17.84	0.63
201	591	37	-19.70	0.98	MR5B	650	33	-14.97	0.33

exsolved from the titaniferous magnetite.

The plot of subsolidus temperatures obtained for the GLI against height is shown in Figure 2.32. The temperatures remain constant (within a narrow range of ± 100°C.) throughout the succession. There is no difference in the range of temperature between the Fe-Ti oxides of the troctolite and gabbro. Multiple analyses of Fe-Ti oxides from the same samples indicate that all, except sample 81, show quite close results. The high temperature obtained in Sample 81 (704°C) suggests that disequilibrium had occurred during the oxidation-exsolution of the magnetites in that sample.

The temperatures and fO_2 during oxidation-exsolution of the Fe-Ti oxides of the GLI, Somerset Dam and Skaergaard are plotted in Figure 2.33. The majority of the Fe-Ti oxides from the GLI plot above the FMQ buffer curve (1.5 Kbar) and few T-fO_2 points plot just below the curve. The plots suggest that the oxides equilibrated under more oxidizing conditions than the FMQ. The data show that cores 1 and 6 have a wider range of T-fO_2 values than cores 2 and 4. The T-fO_2 data from the western gabbro plot below the FMQ buffer curve, indicating that they equilibrated under more reducing conditions then the FMQ. The equilibration conditions of the GLI are lower than those of group 1 of the Somerset Dam troctolite-olivine gabbro cyclic units and of the Skaergaard intrusions. There is an overlap in the T-fO_2 data between the GLI and group 2 of the Somerset Dam rocks.

A notable point is the deviation of the Fe-Ti oxide trend of the GLI from the FMQ curve with increasing T and fO_2. At T = 650°C the fO_2 of the GLI Fe-Ti oxides is higher than that of group 2 of the Somerset Dam intrusion. Mathison (1975), when comparing the fO_2 values of Somerset

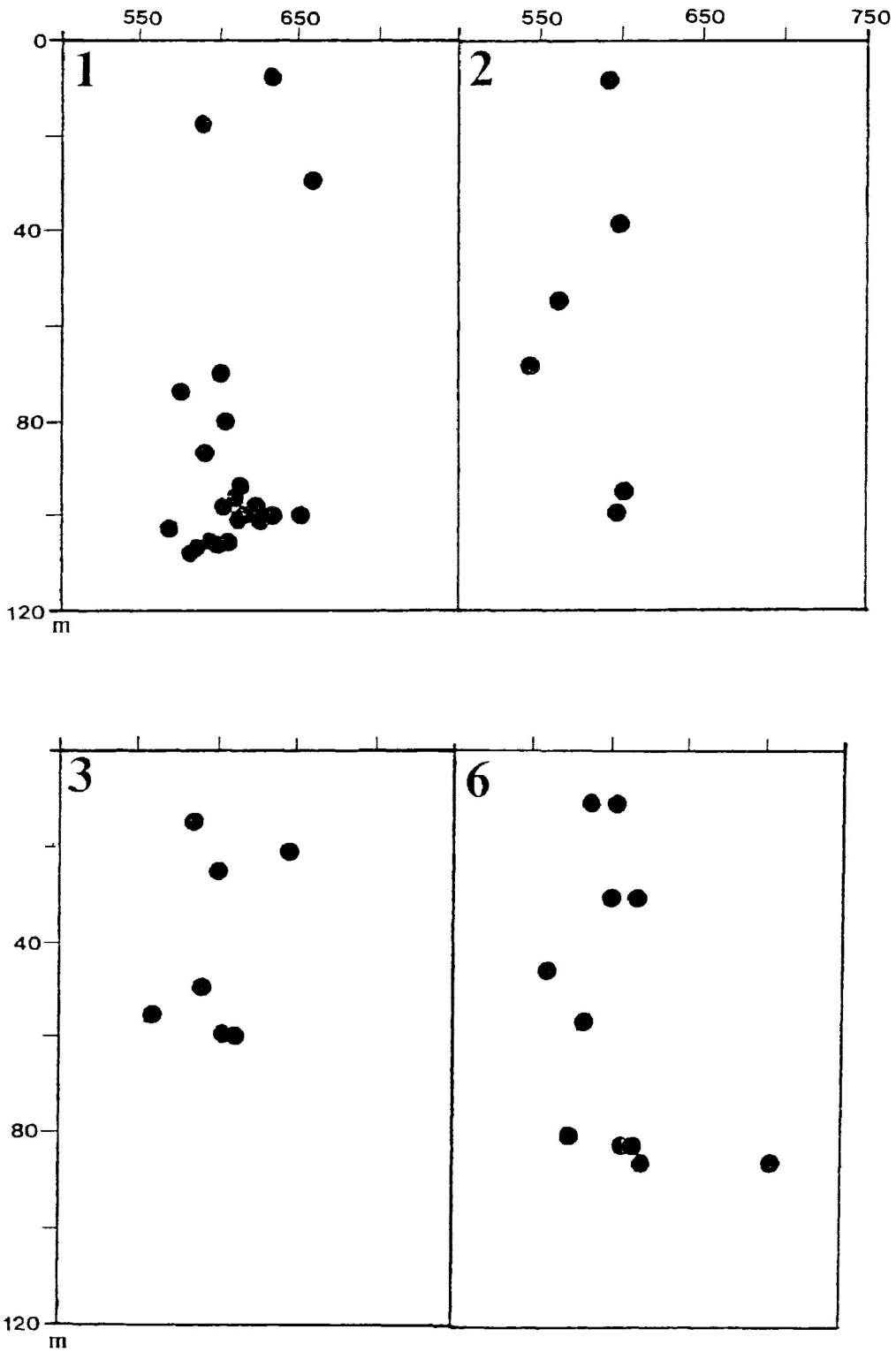

Figure 2.32 Subsolidus temperatures of the Fe-Ti pairs against height in all cores studied.

Figure 2.33 Temperature vs. fO_2 for the GLI, western gabbro (this study), skaergaard (Buddington and Lindsley, 1964), and Somerset Dam (Mathison, 1975). FMQ is the fayalite-magnetite-quartz buffer curve at 1.5 Kbar (Chou, 1978) and MH is the magnetite-hematite buffer curve (Haggerty,1976).

Symbols

GLI

Open circle: Core 1

Square: Core 2

Triangle: Core 3

Big solid circle: Core 6

Other Intrusions

Small solid circle: Somerset Dam (Groups 1 and 2)

Star: Western gabbro, Coldwell complex

Asterisk: Skaergaard intrusion

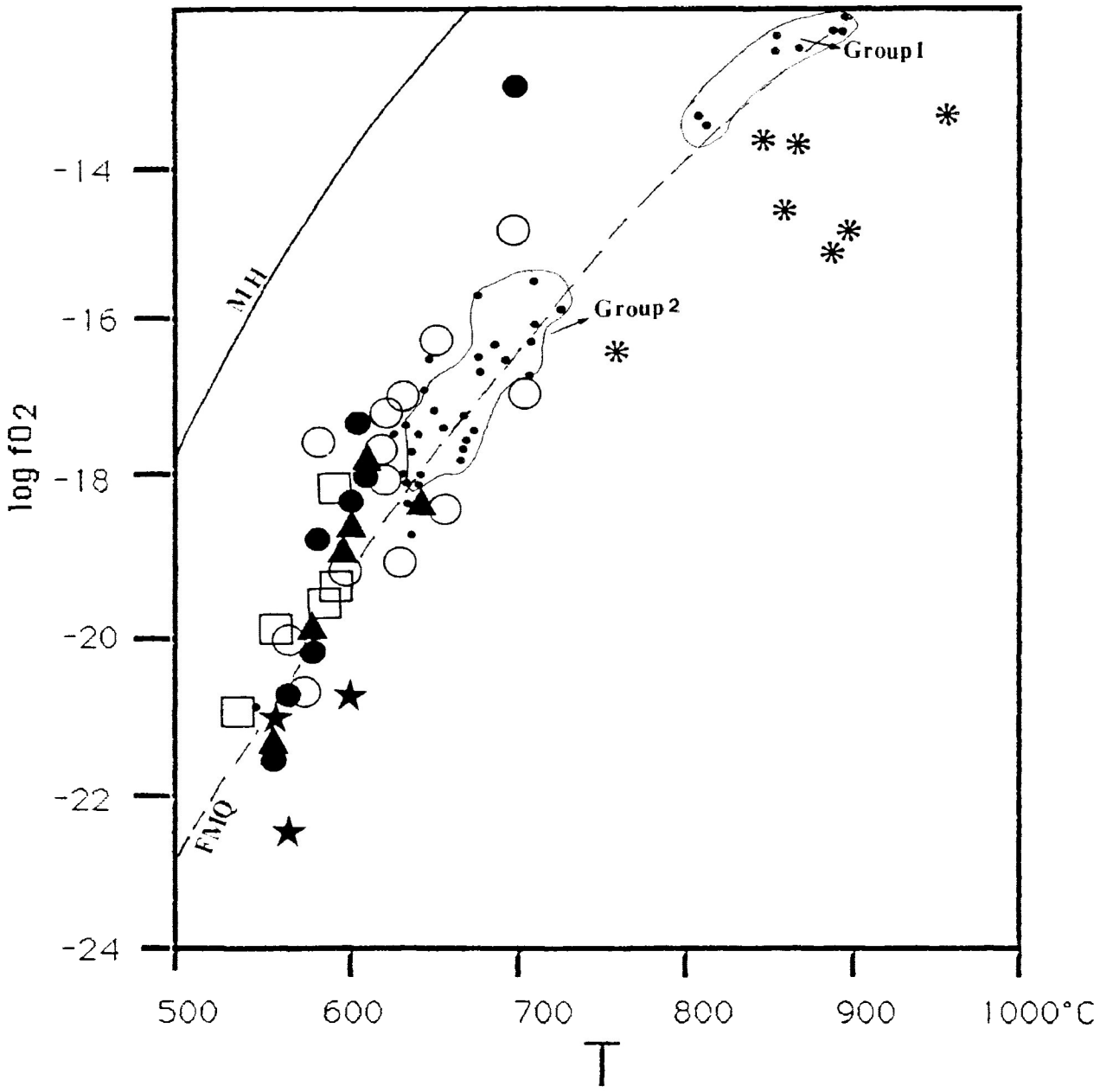
Group 1
Group 2
MH
FMQ
-14
-16
-18
-20
-22
-24
log fO2
500
600
700
800
900
1000°C
T

Dam to those of Skaergaard, stated that the higher H_2O content of the Somerset Dam magma had been partly responsible for the the higher fO_2. Petrographic examination of the GLI samples with high fO_2 values (samples 29 and 81) in the Fe-Ti oxides demonstrated that the samples contain secondary amphiboles and late stage biotite. The total H_2O content in these samples is 1.4 wt. % (section 2.4), which is higher than the other samples.

2.3.8 Evaluation of the Mineral Chemistry

The compositions of the major minerals of the troctolite are similar to those of olivine gabbro, suggesting that the two rock types are the products of fractionated magmas of quite similar composition. Each rock, however, represents a different situation in terms of conditions of crystallization. This conclusion is strongly supported by field relationships and petrography.

The plagioclase of the troctolite in core 6, with the composition An_{57}, represents the least evolved plagioclase in the GLI. There are local Fe-enrichments of the olivines (section 2.3.1) and clinopyroxenes (section 2.3.2) in core 6 with respect to height. This trend, however, is not accompanied by feldspar evolution, with the exception of the abrupt drop in the An-content of the plagioclase in the upper portion of the core. The present data indicate that *in situ* differentiation of the upper troctolite unit, approximately 40-m thick, has not occurred. Amphiboles become more abundant and the biotite evolves to Fe-rich compositions in rocks showing some degree of alteration. This evolutionary trend is, however, not evident

in the compositions of the major minerals. These observations demonstrate that relative water enrichment took place at the later stage of crystallization of the GLI. The "dioritic" rocks, whose clinopyroxene compositions are similar to those of troctolite and gabbro, are most likely altered olivine gabbro. Equilibration temperatures and oxygen fugacity calculated using magnetite- ilmenite pairs record subsolidus conditions. Further evaluation of the mineral chemistry is given in section 2.5.1.

2.4 Whole-Rock Geochemistry

2.4.1 Introduction

Twenty two samples representing all rock types of the GLI, thirteen samples from Center I and II gabbros of western Coldwell and three samples from the syenite east of the GLI were analysed for major and trace elements. The latter included Ba, Cr, Ni, Pb, Rb, Sr, Ta, Hf, Sc, Co, Th, Y, Cu, Zn, Zr, La, Ce, Nd, Sm, Eu, Tb, Yb, and Lu.

2.4.2 Major Elements

Geordie Lake Intrusion The composition (in weight percent) and the CIPW normative mineralogy of the GLI are presented in Table 2.15. Based on the ternary system AFM (Figure 2.34) and the quaternary system Di-Fo-Ab-Q (Figure 2.35) the GLI has tholeiitic affinities. The ternary plot also shows that altered rocks are proportionally higher in their alkali

Table 2.15 Whole rock analyses and CIPW norms of the GLI
Rock Type: TR:Troctolite, G: Ophitic Olivine Gabbro
Analyses by XRFmethods, except S by Alphamatic Titrator, CO2 and H20 by CHN elemental analyzer.

	TR	TR	TR	TR	G/TR	G	G	G	G	G	G
Sample	66	69	78	7	77	3	4	8	35	45	53
wt %											
SiO2	44.13	43.52	43.72	35.04	42.80	41.00	43.70	45.96	40.90	42.34	42.30
TiO2	1.79	1.60	1.20	3.75	1.95	3.12	2.39	1.70	2.43	2.25	2.10
Al2O3	12.79	11.13	11.14	7.83	13.00	11.20	13.80	14.06	10.81	12.08	12.90
Fe2O3	10.90	11.14	10.35	17.02	9.70	9.30	7.73	7.09	11.47	11.76	7.62
FeO	7.10	10.00	9.90	14.20	9.90	14.40	12.30	8.20	8.60	7.10	10.60
MnO	0.30	0.34	0.33	0.39	0.30	0.35	0.28	0.24	0.44	0.39	0.26
MgO	6.61	9.51	10.70	10.09	6.89	5.84	5.52	4.80	6.66	4.22	6.22
CaO	8.37	6.33	7.06	6.23	9.03	7.88	7.18	9.07	11.38	9.37	11.10
Na2O	3.04	2.59	2.07	1.29	2.34	2.18	2.91	3.39	2.06	2.47	2.18
K2O	1.29	1.03	1.11	0.95	0.93	1.20	1.22	1.57	0.88	1.85	0.97
P2O5	1.00	0.65	0.54	0.97	1.02	1.30	0.71	1.43	1.24	1.96	2.03
S	0.07	0.19	0.09	0.02	0.01	0.17	0.04	0.05	0.52	0.52	0.05
H2O(t)	1.26	0.81	1.26	0.90	1.17	0.99	0.81	0.72	0.63	0.63	0.09
CO2	1.90	0.37	0.00	0.00	0.00	0.04	0.07	0.00	0.07	1.83	0.37
TOTAL	100.54	99.21	99.46	98.69	99.04	98.97	98.66	98.28	98.09	98.76	98.78
CIPW Normative minerals											
Q	2.26								0.54	6.53	
Or	7.68	6.20	6.69	5.74	5.62	7.25	7.37	9.52	5.36	11.19	5.81
Ab	25.93	22.32	17.85	11.17	20.23	18.86	25.18	29.34	17.98	21.39	18.70
An	17.58	15.99	18.17	13.06	22.71	17.62	21.46	19.03	18.21	16.79	22.86
Di	4.39	7.42	11.14	9.63	13.12	11.09	8.06	14.25	24.61	4.55	14.00
Hy	16.04	22.08	19.77	19.97	14.84	17.44	11.33	6.07	7.66	8.65	14.01
Ol	0.00	3.86	7.39	5.59	2.90	4.54	8.62	4.48	0.00	0.00	3.70
Mt	15.93	16.45	15.29	25.24	14.37	13.79	11.46	10.54	17.16	16.12	11.20
Il	3.43	3.09	2.32	7.29	3.78	6.06	4.64	3.31	4.76	4.37	4.04
Ap	2.39	1.57	1.30	2.35	2.47	3.15	1.72	3.47	3.03	4.75	4.88
Cc	4.36	0.86	0.00	0.00	0.00	0.09	0.16	0.00	0.16	4.26	0.85
Pr	0.13	0.36	0.17	0.04	0.02	0.33	0.80	0.10	1.00	1.00	0.09
AFM Plotting parameters											
A	16	11	10	5	11	11	14	20	10	16	12
F	61	60	58	71	65	71	67	60	66	67	65
M	24	29	32	24	24	18	19	20	23	16	23
Di-Fo-Ab-Q Plotting parameters											
Di	7	10	15	16	18	16	11	19	36	11	19
Fo	19	29	30	35	19	25	23	13	8	11	19
Ab	65	53	48	41	58	52	62	66	52	67	57
Q	9	8	7	8	5	6	4	2	4	1	5

Table 2.15 (Cont.)

Rock Type: AG: Allotriomorphic Gabbro, DR: Dioritic Rock, WAG: Weakly Altered Rock, SAG: Strongly Altered Rock

* Cu and Ba

	G	AG	DR	DR	DR	WAG	WAG	WAG	SAG	SAG	SAG
Sample	54	9	27	28	29	5	67	81	30	44	64
SiO2	42.00	46.80	42.94	43.20	43.20	47.38	47.18	44.33	45.50	50.36	47.10
TiO2	2.48	2.10	2.17	2.16	2.01	1.92	1.88	2.04	1.39	0.59	1.70
Al2O3	12.50	13.01	12.58	11.00	12.10	13.48	13.44	11.25	12.90	14.26	13.91
Fe2O3	9.14	7.95	9.98	7.05	7.01	7.76	7.48	11.24	7.06	10.18	9.59
FeO	10.40	8.80	6.80	10.30	9.80	7.80	8.20	7.90	12.00	5.00	5.60
MnO	0.31	0.28	0.28	0.33	0.28	0.28	0.27	0.33	0.22	0.14	0.28
MgO	5.57	4.31	5.45	5.58	4.69	3.59	3.77	9.85	1.65	1.08	4.05
CaO	10.40	8.15	11.27	12.40	12.00	8.12	8.38	6.18	4.88	3.42	8.56
Na2O	2.25	3.55	3.18	2.49	2.78	4.53	4.17	3.51	4.35	4.37	3.90
K2O	1.28	2.28	0.71	1.15	0.99	1.18	2.16	0.28	2.22	3.97	1.90
P2O5	1.47	1.18	2.12	2.13	2.26	1.19	1.20	1.50	0.52	0.22	1.09
S	0.02	0.02	0.27	0.04	0.00	0.17	0.04	0.15	1.37	2.11	0.03
H2O(t)	0.45	0.90	0.18	0.90	1.44	0.99	0.18	1.44	1.08	0.99	1.35
CO2	0.18	0.07	0.00	0.04	0.26	0.37	0.26	0.11	0.07	0.51	0.43
TOTAL	98.45	99.41	97.94	98.77	98.81	98.75	98.61	100.11	95.22	97.20	99.49
										2.03*	
CIPW Normative minerals											
Q			0.36							4.08	0.86
Or	7.72	13.68	4.30	6.95	6.01	7.14	12.97	1.68	14.14	24.93	11.44
Ab	19.43	30.50	27.60	21.54	24.16	39.28	33.17	30.07	39.68	39.30	33.64
An	20.65	13.03	18.42	15.78	18.09	13.28	11.77	14.37	9.83	8.04	15.12
Di	17.12	16.09	19.35	26.71	21.53	14.32	17.03	4.80	10.38	3.92	14.12
Hy	9.78	3.21	5.54	3.24	6.62	5.76	0.00	24.21	1.16	1.04	3.75
Ol	3.05	4.77	0.00	5.96	3.26	1.07	5.49	0.45	7.80	0.00	0.00
Mt	13.53	11.70	14.84	10.45	10.44	11.57	11.02	16.54	11.04	7.69	14.17
Il	4.81	4.05	4.23	4.19	3.92	3.74	3.63	3.93	2.85	1.19	3.29
Ap	3.55	2.84	5.15	5.16	5.50	2.89	2.89	3.61	1.33	0.55	2.63
Cc	0.42	0.16	0.00	0.09	0.61	0.86	0.60	0.25	0.17	1.23	1.00
Pr	0.04	0.04	0.52	0.08	0.00	0.33	0.08	0.28	2.76	4.20	0.06
Ne							1.46			5.51	
AFM Plotting parameters											
A	13	22	15	14	15	24	25	12	25	35	24
F	67	61	63	64	66	61	60	57	69	60	59
M	20	17	22	22	19	15	15	31	6	5	17
Di-Fo-Ab-Q Plotting parameters											
Di	24	24	27	36	29		25	7	15		21
Fo	15	11	6	11	11		8	25	13		4
Ab	57	64	65	51	57		67	60	71		72
Q	3	1	2	1	2		0	8	4		3

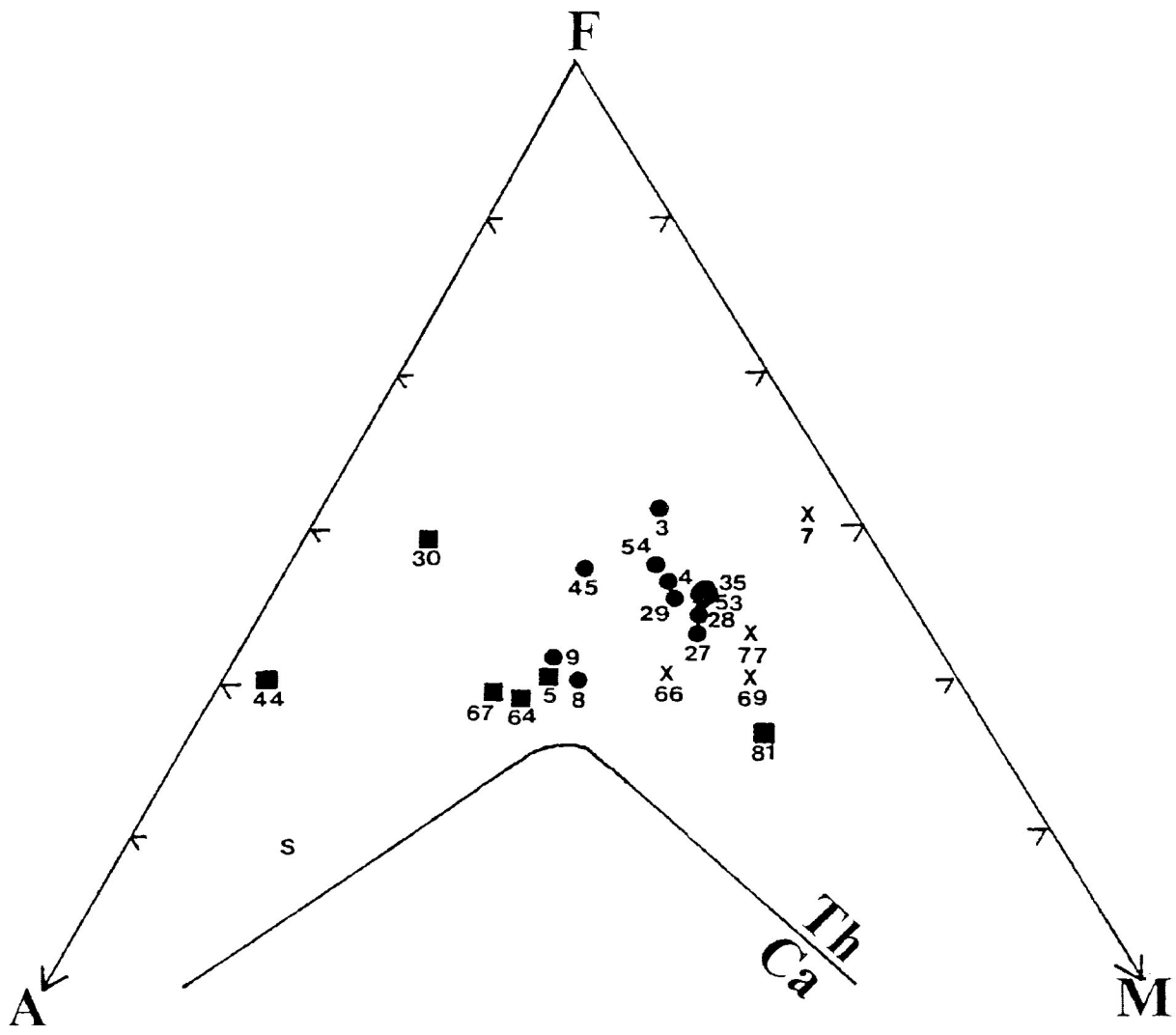

Figure 2.34 Compositions of the GLI plot in the ternary system AFM.

Plotting parameters: A: $Na_2O + K_2O$, F: $(FeO + 0.8998*Fe_2O_3)$

M: MgO

X: troctolite, filled circle: olivine gabbro, square: altered rocks, and S: eastern syenite (Center I).

The boundary line for the Ca: calc-alkaline and Th: tholeiitic fields is after Irvine and Baragar (1971)

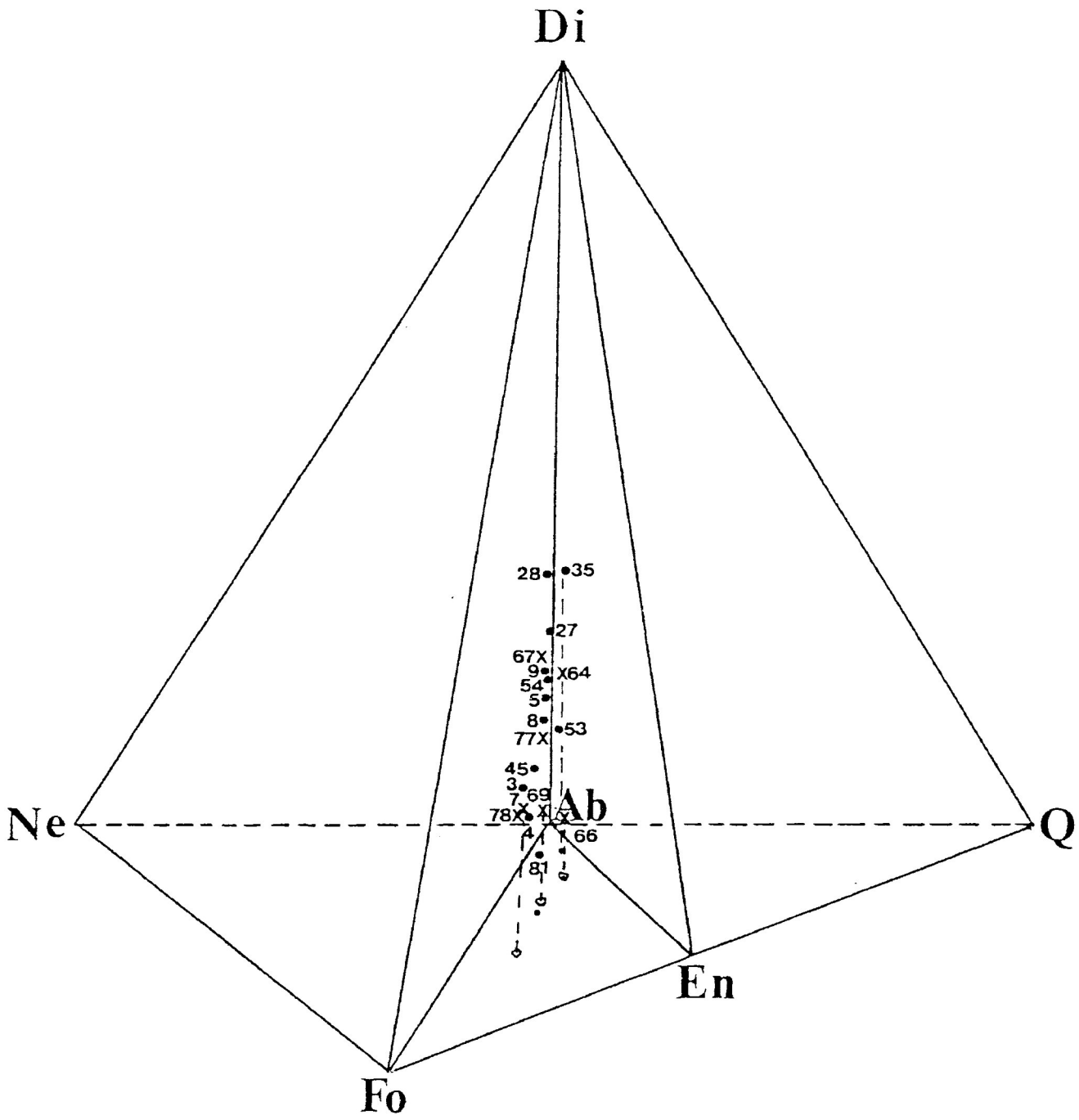

Figure 2.35 Normative percentage plots of the GLI in terms of the basalt tetrahedron system Di-Ne-Fo-Q. Alkali basalts occupy the sub-tetrahedron Ne-Fe-Di-Ab, olivine-tholeiites occupy Fo-Di-Ab-En, and quartz-tholeiites occupy Di-Ab-En-Q. All the GLI data plot in the olivine-tholeiite field, shown by the projection of the plot into the base.X: troctolite, filled circle: olivine gabbro. Sample 64 is an altered troctolite, samples 5 and 81 are altered gabbros.

contents but lower in MgO content than the less altered rocks. The whole rock $Na_2O + K_2O$ vs. SiO_2 plot is not applicable to the determination of the affinity of the GLI because of late stage alkali addition.

The major element compositions show that the magnetite-rich troctolite has the lowest SiO_2 content (35%). In general, the range of the SiO_2 content for the GLI is narrow: 42.7-44.2% in the troctolite and diorite and 41-43.7% in the olivine gabbro. Allotriomorphic gabbros (samples 8 and 9) which contain 46% and 46.8% SiO_2, respectively, are outside of this range. The SiO_2 content in the altered rocks varies from 44 to 50%. With the exception of the magnetite-rich gabbro, which has the lowest Al_2O_3 content (7.8 %) and the highest TiO_2 content (3.7 %), the concentration of Al_2O_3 varies little among the rock types but is generally higher in the altered rocks; 11.1-13 % in the troctolite, 10.8-14.1 % in the gabbro, 11-12.6 % in the "dioritic rocks", 11.2-13.5 % in the weakly altered rocks, and 12.9-14.3 % in the strongly altered rocks. The TiO_2 contents range from 1.62 to 1.95 % in the troctolite, 1.7-3.12 % in the gabbro, 2.01-2.17 % in the dioritic rocks, 1.88-2.04 in the weakly altered rocks, 0.59-1.7 %. in the strongly altered rocks. There is a gradational decrease in the MgO contents from the troctolite (10.7 %) to the altered gabbro (1.08%), which reflects the presence of abundant dendritic olivine in the troctolite and the decomposition of the mafic minerals in the altered rocks. The effect of alteration is also apparent in the troctolite that contains serpentinized olivines (Sample 66, analysis 1). The wide range in the FeO content in the GLI from 7-14 % is due to the presence of secondary magnetite which replaces the altered olivines in some samples. The altered rocks are low in FeO, with the exception of sample 30

(12 wt. % FeO), which hosts disseminated sulfides. The Fe_2O_3 contents of the troctolite vary little (9.7-11.1 %), whereas those of other rock types range from 7-11.7 %. The Na_2O and K_2O contents increase by 1 to 2 % from the troctolites through the altered rocks. This increase is attributed to the presence of abundant albite and some alkali-feldspar in the altered rocks.

Some of the CIPW norms do not agree with the modal mineralogy of the rocks, in which secondary minerals such as actinolites, serpentines and K-feldspars are present. For example, there is no modal hypersthene or nepheline in any of the samples analyzed, and samples containing serpentinized olivines have quartz in the norm. Only sample 44, which is a strongly altered gabbroic rock, containing small amounts of secondary quartz is quartz normative. The normative olivine contents of the troctolites are generally low. This may be attributed to alteration of the olivine dendrites.

Variation diagrams for the major elements of the GLI, excluding the magnetite-rich troctolite and altered rocks, are shown in Figures 2.36. The similarity in composition between the troctolite, "dioritic" rocks and some of the gabbros suggests that they were derived from magmas of similar composition. The comparatively silica-rich gabbros are represented by only two separate rock units in the middle of core 1, and may represent batches of magma of slightly different composition. In the olivine gabbro, the SiO_2 and Al_2O_3 contents are positively correlated with the Na_2O and K_2O contents. The increase in sodium and potassium contents is reflected in the presence of albite, alkali-feldspar, secondary biotite and amphibole in some samples. The erratic variation displayed by other oxides is the result of selective alteration of the phases. All rocks have undergone some degree of

Figure 2.36 Variation diagrams of the major element compositions of the GLI. Sample numbers are given in the Al_2O_3 vs SiO_2 plot. Samples 8 and 9 are allotriomorphic gabbro, the other gabbros are ophitic. Sample 3 is a magnetite-rich gabbro.

Symbols: Solid circle: Olivine Gabbro

X: Troctolite

Open circle: "Dioritic" Rock

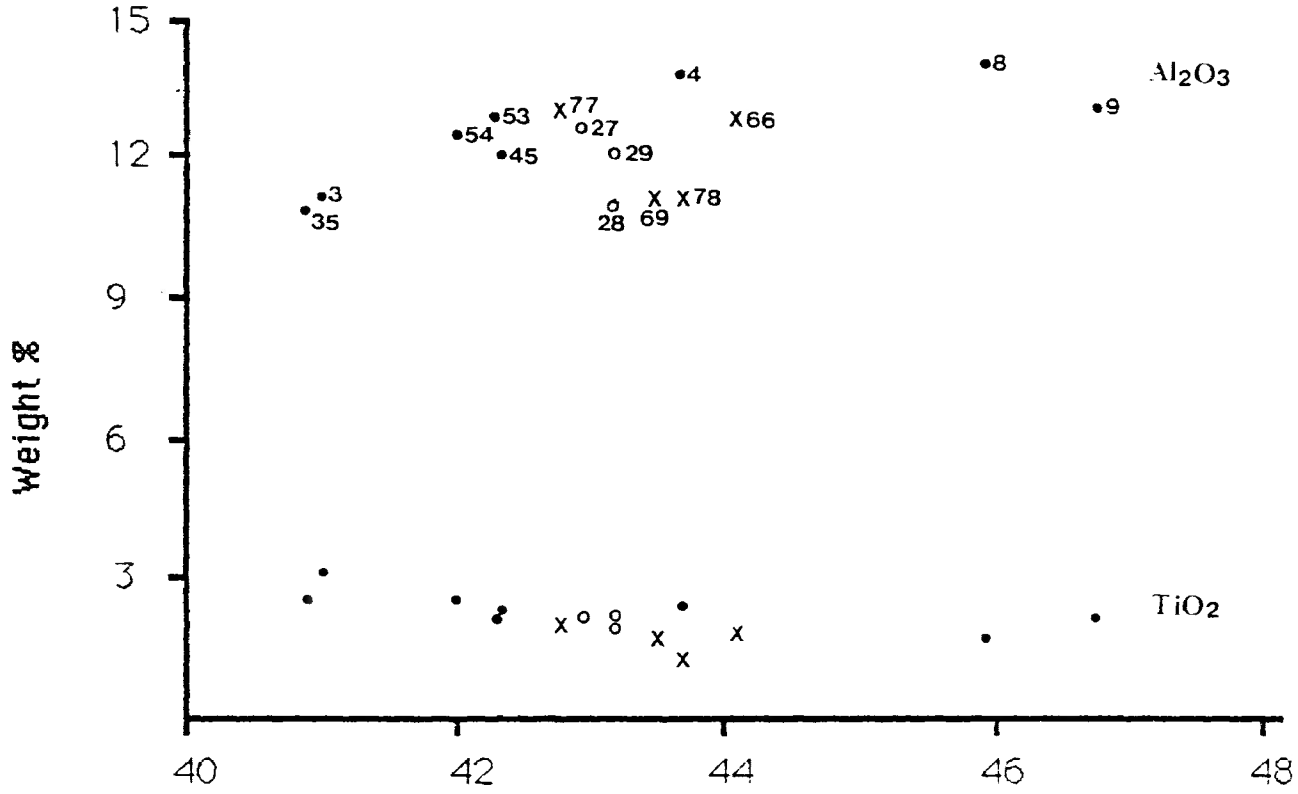
15
12
9
6
3
Weight %
40
42
44
46
48
Al2O3
TiO2
•8
•4
•9
•53
X77
X66
•54
o27
•45
o29
•3
X
X78
•35
28
69

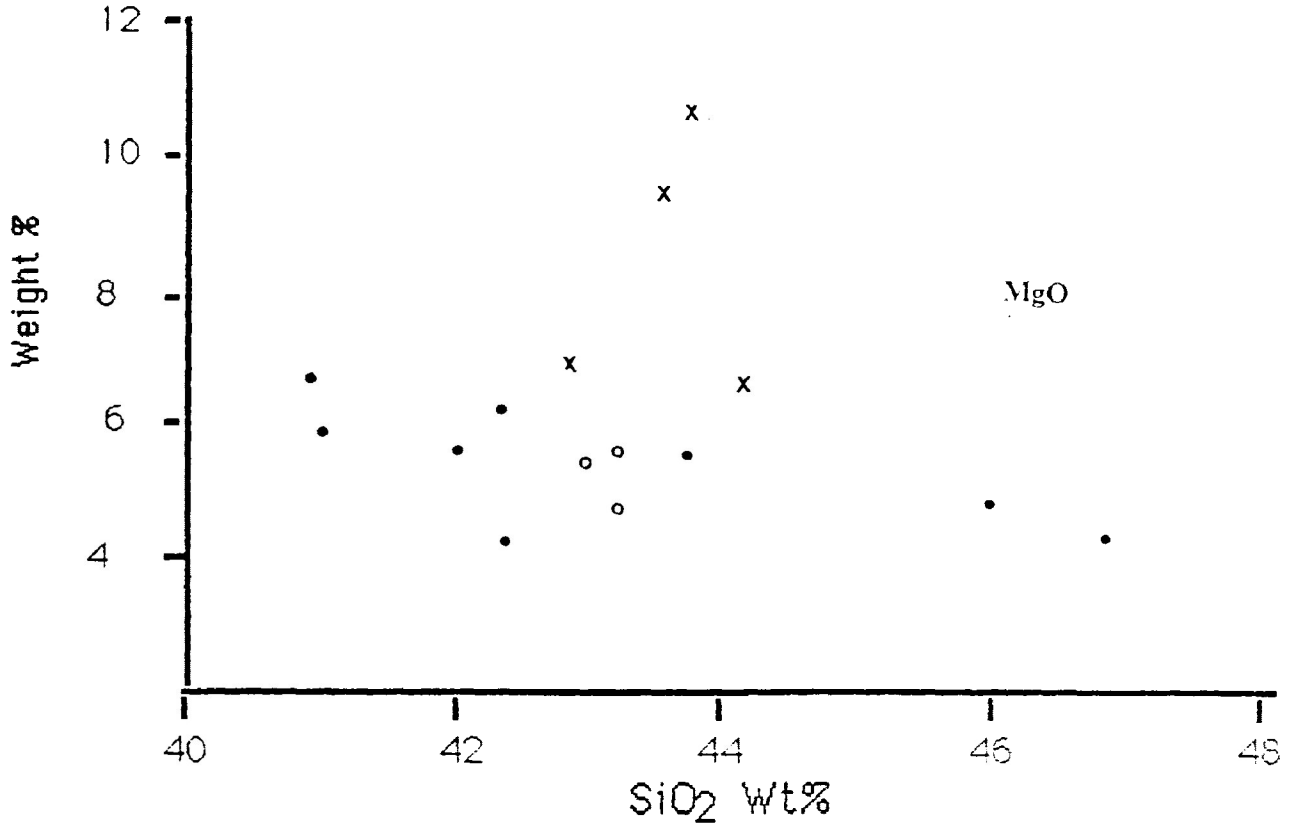
12
10
8
6
4
Weight %
40
42
44
46
48
MgO
SiO2 Wt%

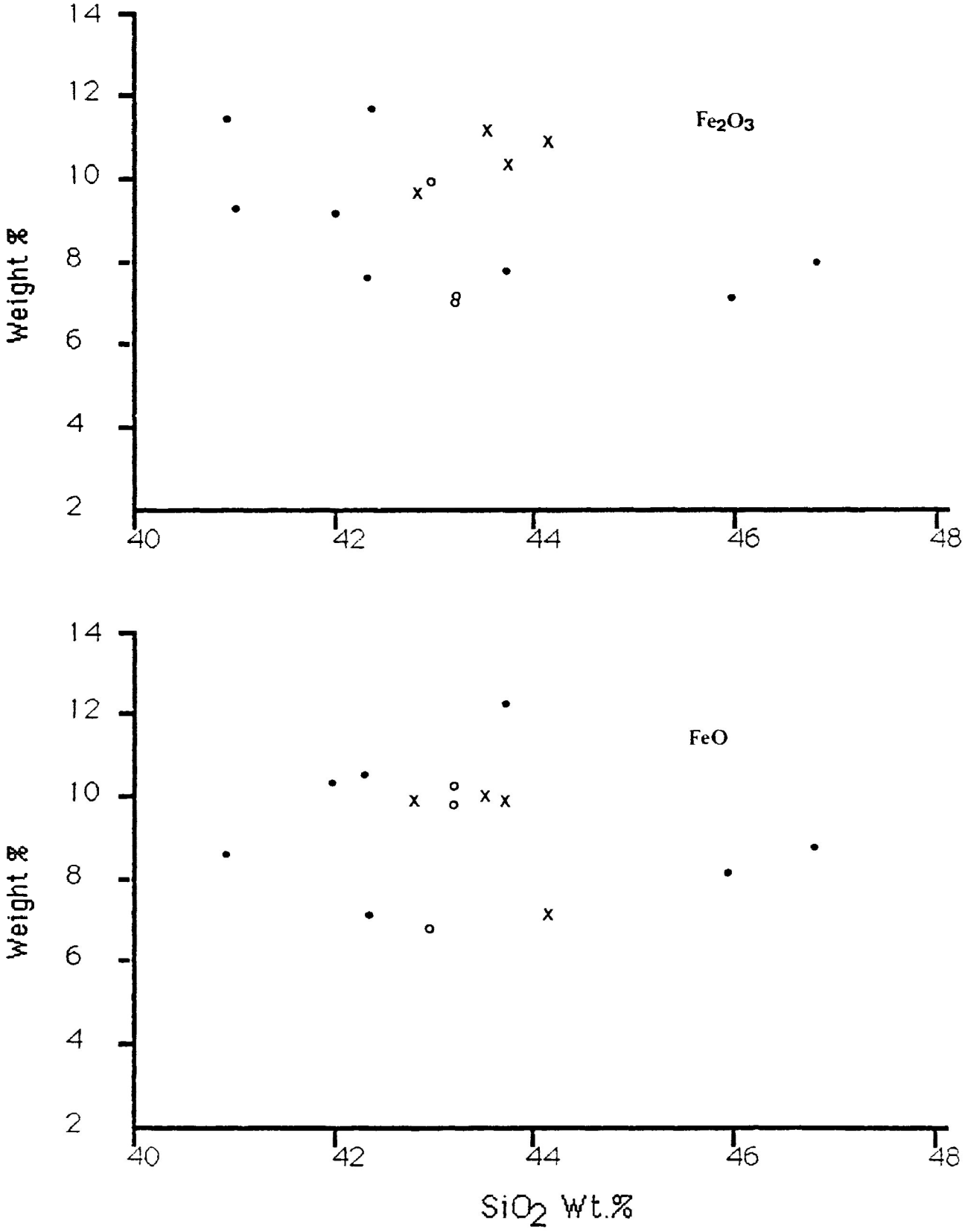
Fe2O3
FeO
Weight %
SiO2 Wt.%
14
12
10
8
6
4
2
40
42
44
46
48

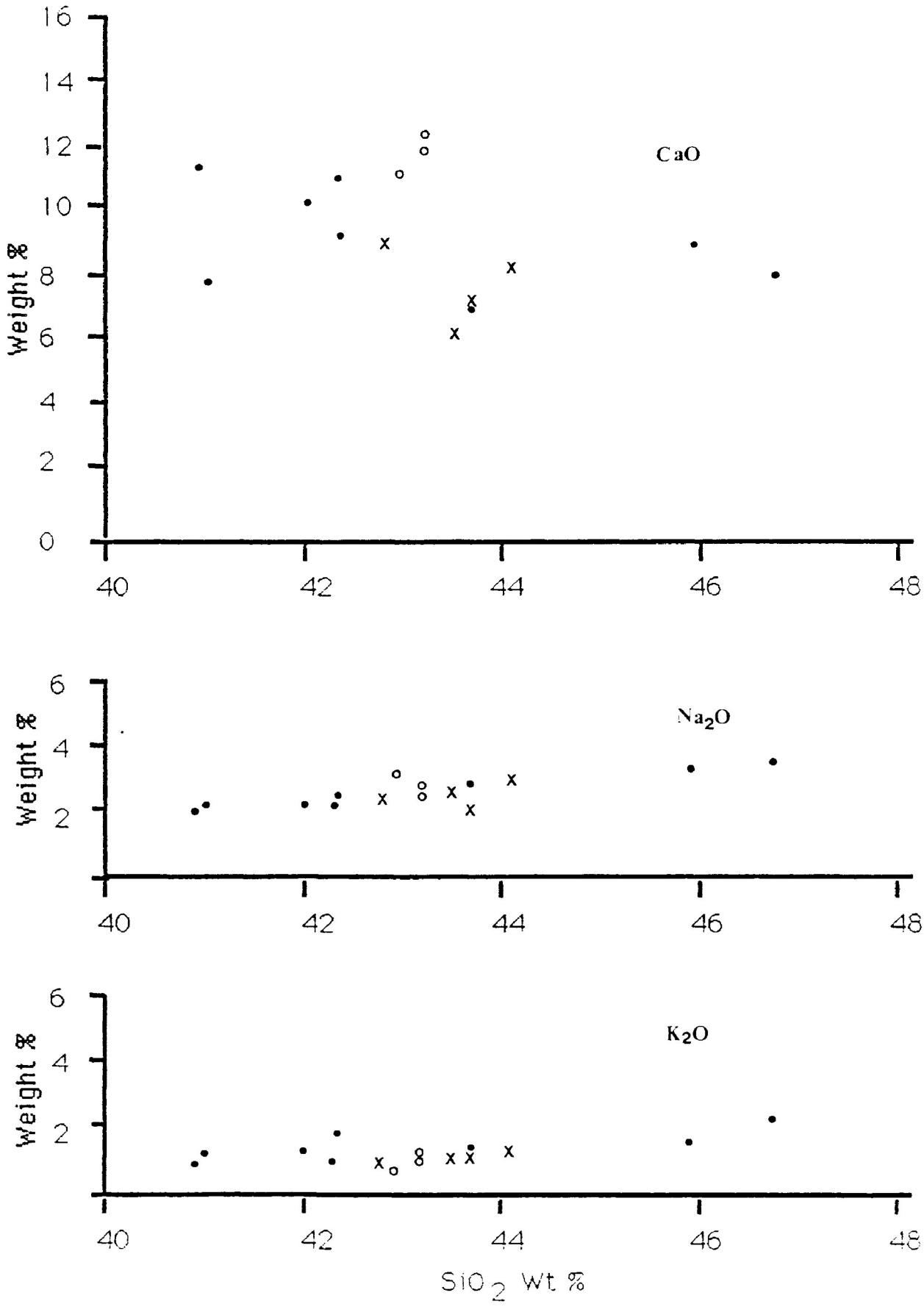
CaO
Weight %
16
14
12
10
8
6
4
2
0
40
42
44
46
48
Na_2O
Weight %
6
4
2
K_2O
Weight %
6
4
2
SiO_2 Wt. %

alteration (Section 2.2). The removal of some elements, for example magnesium from olivines during serpentinization, results in a proportional increase in other elements.

Center I and II Gabbros, Western Coldwell Compositions and CIPW norms of nine Center I gabbros and four Center II gabbros are given respectively in Tables 2.16 and 2.17. Sample C-408 from Center I and all Center II samples are metasomatised. In the ternary system AFM (Figure 2.37) Center I sample C-406, whose outcrop is very close to the contact between western gabbro and country rock, plots in the tholeiitic field. The compositions of other samples are proportionally higher in alkali contents, corresponding to a decrease in clinopyroxene, olivine, and magnetite and an increase in feldspar and biotite. The metasomatised sample C-408 and feldspar-rich sample C-420 plot just below the tholeiitic-calc alkaline boundary line. These observations show that metasomatism has changed the alkali, magnesium and iron contents of the rocks.

Samples 907 and 408 of Center I and samples 117, 308, and 608 of Center II show normative nepheline, suggesting that the rocks are alkaline. However, modal nepheline is not observed in thin section. The high alkalinity in the samples may be due to metasomatism.

The variation diagrams for the major elements in Center I and II gabbros are given in Figures 2.38. Apart from the five metasomatised gabbros, the western gabbros show a wide range of composition which is related to the modal mineralogy of the rocks and not to differentiation. The SiO_2 content increases from 34 wt.% at the Coldwell-country rock contact

Table 2.16 Whole rock analyses and CIPW norms of Center I gabbroic rocks
*Metasomatised + showing some alteration
Analyses by XRF methods, except S by Alphamatic Tritrator, CO2 and H2O by CHN elemental analyzer

Sample No	406	408*	411	414	420	423	465	321	907+
SiO2	33.92	46.58	44.40	43.77	47.10	36.38	42.81	40.88	45.21
TiO2	2.46	0.90	1.71	1.74	1.21	4.07	1.87	1.39	2.55
Al2O3	4.04	13.07	17.95	18.52	20.48	10.86	17.86	17.57	17.63
Fe2O3	11.02	5.05	6.71	6.86	4.12	8.45	7.22	10.64	5.17
FeO	10.76	5.42	4.62	3.64	3.30	13.94	4.64	5.14	6.50
MnO	0.31	0.20	0.18	0.15	0.11	0.37	0.16	0.16	0.23
MgO	9.56	7.75	3.48	3.14	2.49	6.28	3.91	4.34	3.01
CaO	15.99	12.11	10.63	12.19	11.34	11.66	11.52	10.31	8.84
Na2O	0.68	2.92	3.37	3.33	4.09	2.09	3.18	2.72	4.02
K2O	0.44	1.32	1.36	0.70	0.94	0.48	0.65	0.74	1.98
P2O5	4.78	0.65	2.38	2.44	2.15	2.51	2.39	1.87	0.58
S	0.45	0.05	0.10	0.11	0.07	0.32	0.10	2.76	0.08
H2O	1.89	1.62	0.90	1.08	0.54	0.36	1.35	2.07	1.62
CO2	3.08	0.48	0.26	0.77	0.15	0.18	0.51	0.15	0.48
TOTAL	99.37	98.13	98.04	98.44	98.09	97.94	98.17	100.72	97.91
CIPW Norms									
Q	4.01		0.28	1.23			0.69	0.30	
Or	2.60	7.80	8.04	4.14	5.56	2.84	3.84	4.37	11.70
Ab	5.75	21.91	28.52	28.18	34.61	17.69	26.91	23.02	26.77
An	6.67	18.66	29.84	33.52	34.75	18.83	32.54	33.55	24.21
Ne	0.00	1.51	0.00	0.00	0.00	0.00	0.00	0.00	3.92
Di	17.47	27.11	4.45	4.80	5.12	17.56	4.51	3.46	10.33
Hy	20.77	0.00	6.60	5.60	2.15	0.68	7.65	9.21	0.00
Ol	0.00	7.50	0.00	0.00	1.46	12.41	0.00	0.00	4.07
Mt	17.73	8.21	10.16	6.78	6.51	14.53	9.69	3.09	8.55
Il	4.67	1.71	3.25	3.30	2.30	7.73	3.55	2.64	4.84
Ap	11.33	1.54	5.64	5.78	5.09	5.95	5.66	4.43	1.37
Cc	7.00	1.09	0.59	1.75	0.34	0.41	1.16	0.34	1.09
Pr	0.84	0.09	0.19	0.21	0.13	0.60	0.19	0.34	0.15
Hm				2.59			1.05	9.09	
AFM Plotting parameters									
A	4	19	24	23	34	8	20	15	29
F	67	47	58	59	49	72	60	66	57
M	29	34	18	18	17	20	20	19	14

Table 2.17 Whole rock analyses and CIPW norms of Center II gabbroic rocks
All Center II rocks are metasomatized
* Gabbroic Xenoliths in Center II Syenite
+ Gabbro from Mink Creek Breccia Zone
Analyses by XRF methods, except S by Alphamatic Tritrator, CO2 and H2O by CHN elemental analyzer

Sample No	117*	153*	308*	608+
SiO2	47.81	48.23	46.05	49.34
TiO2	0.53	0.67	0.52	0.57
Al2O3	11.81	14.28	15.74	13.63
Fe2O3	3.87	4.23	3.79	3.89
FeO	4.08	4.40	5.00	4.76
MnO	0.17	0.17	0.17	0.18
MgO	10.36	8.44	8.44	9.89
CaO	14.71	15.36	15.36	8.88
Na2O	2.60	1.62	1.62	3.76
K2O	1.79	0.50	0.50	2.58
P2O5	0.40	0.07	0.07	0.31
S	0.01	0.03	0.02	0.00
H2O	0.99	0.90	1.26	0.09
CO2	0.11	0.22	0.22	0.77
TOTAL	99.22	99.12	98.76	98.66
CIPW Norms				
Q		0.21		
Or	10.58	2.95	2.95	15.25
Ab	7.02	13.71	12.62	22.63
An	15.27	30.22	34.20	12.69
Ne	8.12	0.00	0.59	4.98
Di	42.90	34.89	31.95	19.38
Hy	0.00	7.88	0.00	0.00
Ol	6.35	0.00	7.74	14.19
Mt	6.29	6.86	6.32	6.42
Il	1.01	1.27	0.99	1.08
Ap	0.95	0.17	0.17	0.73
Cc	0.25	5.00	0.50	1.75
Pr	0.02	0.06	0.04	0.00

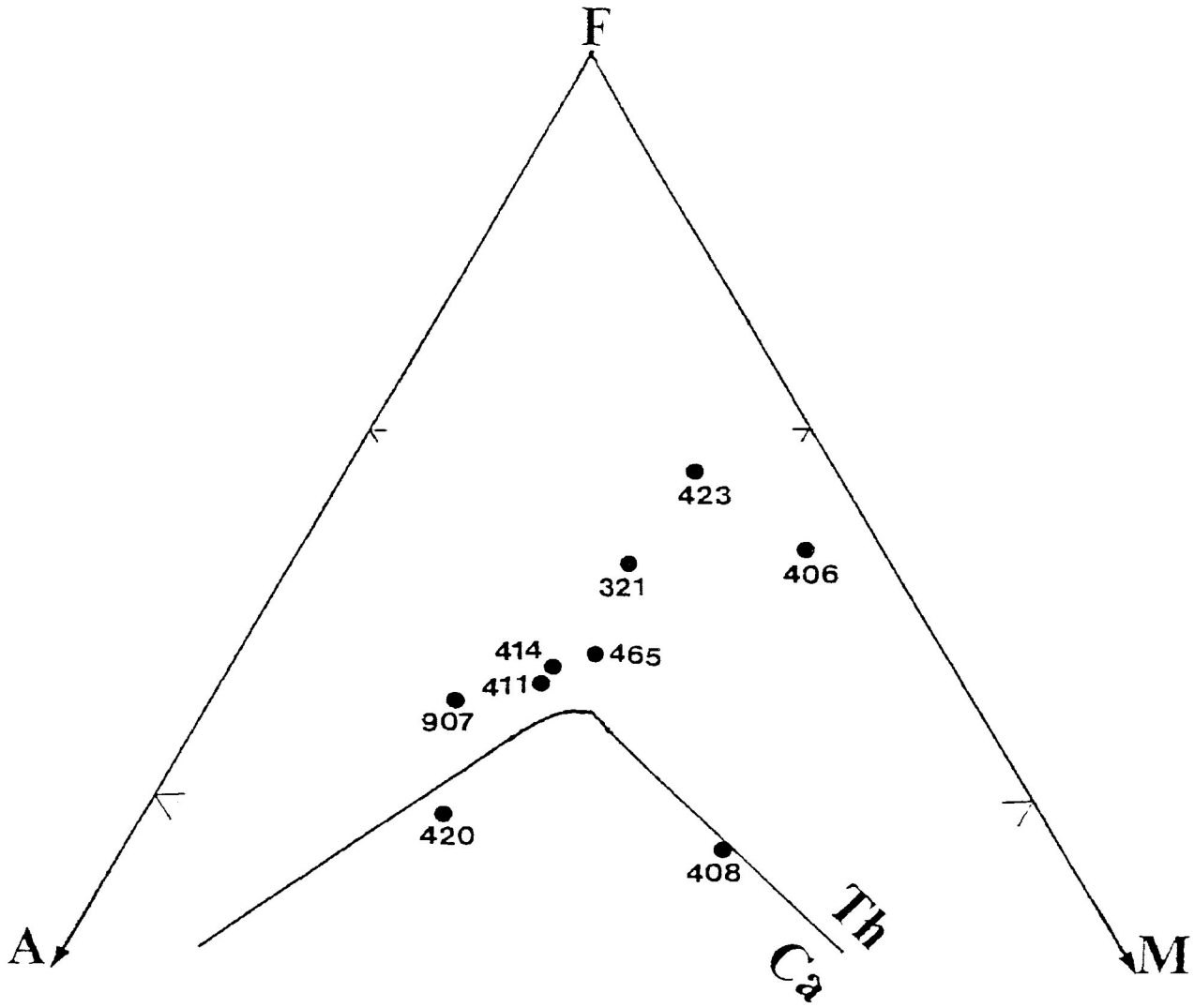

Figure 2.37 Weight percent plots of gabbroic rocks from Center I, western Coldwell. Sample C-408 is metasomatised and sample C-420 is a feldspar-rich gabbro. The calc-alkaline (Ca) and tholeiitic (Th) field boundary is after Irvine and Baragar (1971) A: $Na_2O + K_2O$, F: $FeO + 0.8998*Fe_2O_3$, and M: MgO

Figure 2.38 Variation diagrams of the Center I and II gabbroic rocks. The metasomatised samples are Center I-408, Center II-117, 153, 308, and 608.

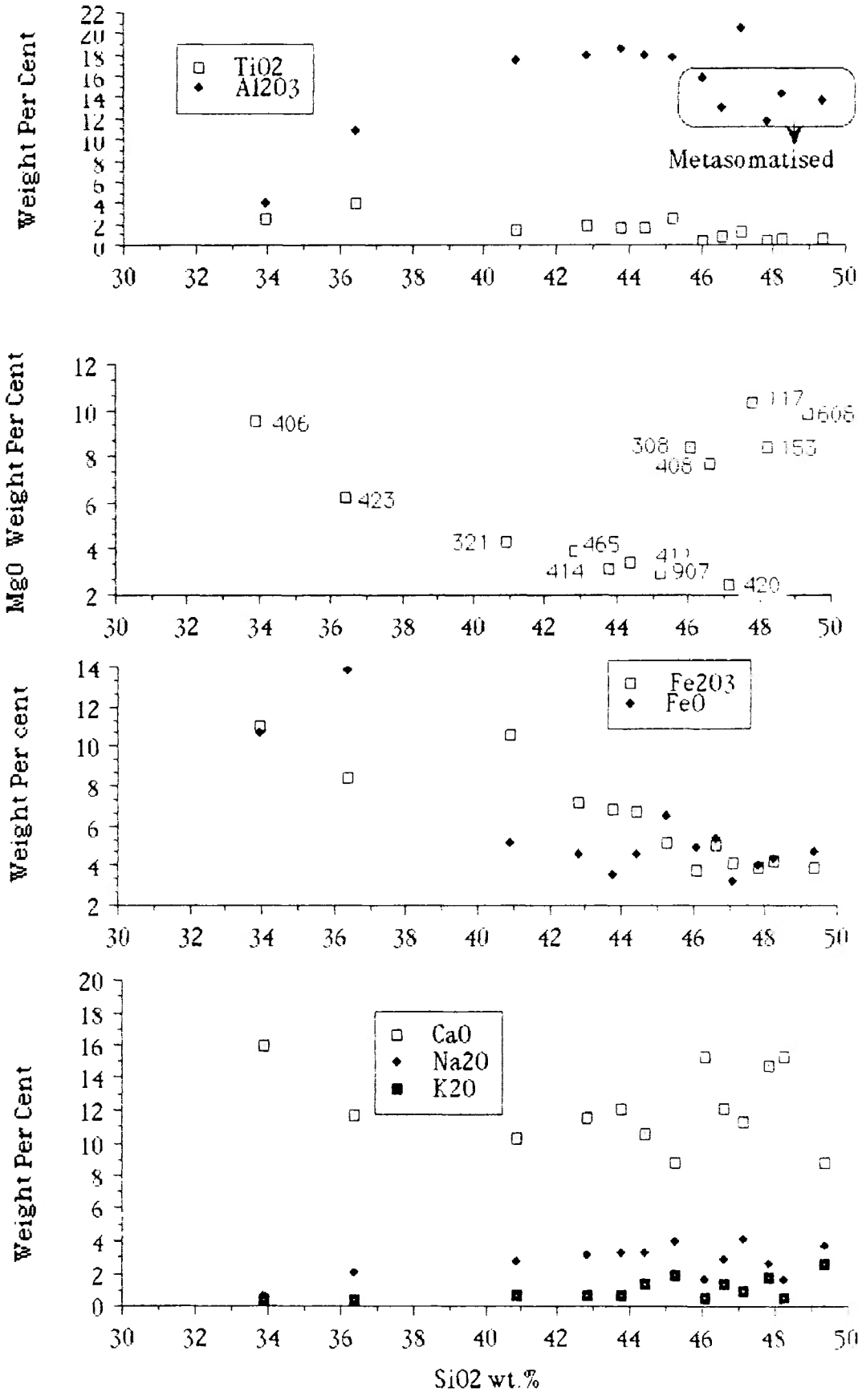
Weight Per Cent
Ti02
Al203
Metasomatised
MgO Weight Per Cent
406
423
321
465
414
907
420
117
308
153
Weight Per cent
Fe203
FeO
Weight Per Cent
CaO
Na20
K20
Si02 wt.%

(sample 406) to 47 wt. % at a location 350 meters east of the contact (sample 420). The increase is accompanied by an increase in the Al_2O_3 (4-20 wt. %), Na_2O (0.7-4 wt. %) and K_2O (0.4-0.9 wt. %) contents, and by a decrease in the MgO (16-2.5 wt. %) and total iron (22-7 wt. %) content. This observation is related to the decrease of mafic minerals and magnetites, and to the increase in the volume of plagioclases from Sample 406 to 420, and not to differentiation.

The metasomatised samples are characterized by high Al_2O_3 (12-16 wt. %), MgO (8-10 wt. %) and (CaO 12-15 wt. %)contents. These rocks, with the exception of sample 408, are xenoliths of Center II gabbros in the Center II syenite. Whether metasomatism has greatly altered the chemistry of the rocks is not yet known.

A comparative study (Table 2.18) shows that the GLI is generally similar in SiO_2 contents to other intrusive and extrusive equivalent basaltic rocks. The TiO_2 contents of the GLI are comparable to those of the Michipicoten tholeiitic basalts, Keweenawan tholeiitic basalts, and Somerset Dam troctolite-gabbro, but higher than that of the McIntosh troctolite-gabbro. Of these rocks the GLI has the lowest Al_2O_3, the highest being 20.6 wt. % Al_2O_3 of the Somerset Dam intrusion. The ranges for the GLI Fe_2O_3 overlap those for the Keweenawan suites, which have a wider range and higher maximum concentration, and are higher than those of other suites. The GLI has the highest FeO, MnO and K_2O concentrations of all rock suites. The MgO contents of the GLI are, on the average, similar to those of the Michipicoten, Keweenawan and Somerset Dam suites. The average MgO

Table 2.18 Composition of major elements of the GLI compared to other intrusive and extrusive equivalent rocks

* Troctolite and Gabbro, excluding magnetite-rich rocks (G-7 and 3)
† Quebec Mine (n=5), Michipicoten olivine tholeiite (Annells, 1974)
†† North Shore Volcanic Group, samples KW1-8 (BVSP, 1981)
~ Somerset Dam troctolite-gabbro (Mathinson, 1987)
^ McIntosh troctolite-gabbro (Mathison and Hamlyn, 1987)
Center I gabbroic rocks are not included because the analyses show a wide range of compositions.

wt. %	GLI* Range	MC† Range	KW †† Range	S. Dam~ Average	MI^ Average
SiO2	40.9-46.8	43.4-47.6	46.6-48.7	47.7	47.3
TiO2	1.2-2.5	1.1-1.6	0.72-2.3	1.9	0.5
Al203	7.1-14.1	15.2-16.7	15.2-19.2	20.6	18.9
Fe203	7.1-11.8	3.7-5.5	2.2-9.5	2.8	1.5
FeO	7.1-12.3	6.4-7.1	3-7.7	5.9	7.5
MnO	0.26-0.39	0.17-0.2	0.11-0.17	0.1	0.1
MgO	4.2-9.5	6.3-9.4	5.3-8.7	5.8	10.4
CaO	6.33-11.4	7.1-10.5	9.2-12.4	11.2	11.8
Na20	2.1-3.5	1.9-2.9	2.2-2.6	3.1	1.9
K20	0.88-2.3	0.2-1.2	0.12-0.54	0.2	0.1

content (10.4 wt. %) of the McIntosh intrusion is the highest. CaO and Na_2O are fairly similar in all rocks, with the exception of the average Na_2O content (1.9 wt. %) in the McIntosh intrusion which is the lowest.

Eastern Quartz Syenite Table 2.19 lists the compositions of major elements of the eastern quartz syenite which borders the GLI. Samples 8746 and 8750 are outcrop samples near Latvian Lake (Figure 1.5), whereas sample 61 is from core 3. Sample 8746 represents the GLI-syenite contact zone and shows lower SiO_2, Al_2O_3, Na_2O and K_2O but greater total iron, MgO, CaO and P_2O_5 contents than the eastern syenites. Sample 8750 is slightly more evolved than sample 61, and is characterized by higher SiO_2, Al_2O_3, and K_2O contents, and lesser contents of other oxides. Compositions of other quartz syenites from this unit of Center I are not available for comparison.

2.4.3 Trace Elements

Geordie Lake Intrusion

Trace element abundances of the GLI, including the eastern quartz syenite (referred to as syenite in this section), are given in Table 2.20, and summarized in Table 2.21.

Compatible Elements The average strontium (Sr) contents vary little in the various rock types of the GLI; they are between 465 and 620 ppm. The magnetite-rich troctolite (sample 7) has the lowest Sr (319 ppm)

Table 2. 19 Whole rock analyses of eastern syenites (61 and 8750) and GLI-syenite "mixed" rock (8746).
Analytical methods are similar to those of the GLI

ROCK TYPE	SN	SN	SZ-GB
Sample	61	8750	8746
SiO2	56.78	60.12	49.99
TiO2	1.01	0.86	1.40
Al2O3	14.62	15.29	13.27
Fe2O3	7.64	5.72	9.52
FeO	3.20	2.51	6.23
MnO	0.34	0.33	0.48
MgO	1.48	1.06	2.48
CaO	3.60	2.79	4.80
Na2O	4.55	4.06	3.39
K2O	4.12	4.93	3.70
P2O5	0.34	0.23	0.94
S	0.37	0.10	0.49
H2O(t)	0.00	0.81	0.99
CO2	1.14	0.18	0.07
TOTAL	99.17	98.98	97.74
CIPW Norms			
Q	9.05	11.93	6.22
Or	24.64	29.71	22.71
Ab	38.96	35.03	29.80
An	7.39	9.11	10.45
Di	0.89	1.80	5.90
Hy	3.32	1.86	4.82
Mt	7.24	6.44	14.34
Il	1.94	1.67	2.76
Ap	0.82	0.56	2.31
Cc	2.62	0.42	0.17
Pr	0.70	0.19	0.95
Hm	2.73	1.39	0.00

Table 2.20 Trace element concentrations in the various rock types from the GLI and Center I syenite
Analyses by XRF and INAA(*) methods UD: Undetected
TR: Troctolite, G: Ophitic olivine gabbro, AG: Allotriomorphic gabbro

Rock type	TR	TR	TR	TR	TR	TR	TR	TR
Sample	7	43	66	67	69	70	77	78
Sr	319	621	578	568	463	697	600	466
Ni	176	145	80.3	26	155	59	101	176
Co*	124	107	86	60	107	75	97	118
Cr*	71	12.6	4.4	1.4	16.3	20	20	9.19
Sc*	26	19	24	26	18	18	27	23
Rb	41	39.9	50.0	66.0	40.5	41	42	42.5
Ba	610	974	915	1695	861	1122	696	665
Y	28.0	30.3	37.4	57.3	33.2	18	24	20.6
Th*	2.58	6.76	7.79	11.56	9.68	4.33	3.93	3.11
Pb	21.4	30.7	26.5	37.2	25.3	19.3	24.6	23.5
Zr	98.3	120	149	245	172	76.3	65.4	93.3
Hf*	1.29	2.16	4.10	3.71	3.24	1.27	1.86	1.98
Ta*	1.61	3.85	3.79	5.18	3.59	2.46	2.54	2.58
Cu	303	3416	271	234	1757	140	284	1269
Zn	222	183	177	112	168	142	170	163

Rock type	G	G	G	AG	G	G	G	G
Sample	3	4	8	9	35	45	53	54
Sr	478	637	672	588	492	530	613	578
Ni	71.4	84.8	42.2	36.0	162	125.2	90.6	74.1
Co*	83.4	82.6	64.6	64.2	99.8	76.8	84.6	87.8
Cr*	9.24	7.69	UD	7.10	13.57	UD	6.99	11.79
Sc*	24.1	18.2	25.3	27.9	46.3	31.9	31.2	31.8
Rb	48.8	42.9	53.6	76.2	60.1	89.4	29.4	53.6
Ba	1078	1005	970	1334	441	986	631	709
Y	40.1	25.7	43.2	56.9	31.5	51.2	32.5	31.0
Th*	4.33	4.29	4.73	14.19	2.61	8.09	2.83	3.18
Pb	21.3	26.0	23.3	47.2	26.3	38.6	26.2	20.7
Zr	144	102	144	274	88	173	46.7	67.0
Hf*	2.43	2.44	2.80	4.20	1.86	3.87	1.50	1.66
Ta*	2.17	1.86	2.25	5.15	2.14	3.86	1.84	2.63
Cu	469	208	195	226	3634	3140	905	686
Zn	173	149	155	170	313	241	177	269

Table 2.20 (Cont.)

DR: Dioritic rock
WA: weakly altered rock, SA: Strongly altered rock
SN: Center I Syenite

Rock type	DR	DR	DR	WA	WA	WA	SA
Sample	27	28	29	5	64	81	30
Sr	661	525	618	538	589	512	620
Ni	109	81.6	72.4	40.2	33.3	135	435
Co	93	89.2	86.9	59.5	64.6	103	158
Cr	UD	UD	UD	5.1	UD	2.18	UD
Sc	38.7	49.1	40.2	24.7	24.8	32.5	15.5
Rb	29	45.6	40.4	39.8	52	13.3	45.3
Ba	768	632	920	1071	1614	537	2819
Y	46.8	45.4	34.4	57.4	49.5	54.8	53.7
Th	6	3.16	4.22	9.58	9.06	8.76	16.7
Pb	35	27	28.6	93.5	34.4	60.4	37.7
Zr	108	83	100	302	195	188	286
Hf	1.76	1.90	2.19	4.36	4.61	2.92	3.86
Ta	3.54	2.59	3.04	3.45	4.34	4.93	5.56
Cu	2318	555	2735	1040	248	1027	11869
Zn	236	264	244	269	186	228	111

Rock type	SA	Sn	SN
Sample	44	61	8750
Sr	465	371	411
Ni	455	55	8.8
Co	153	88.4	19.3
Cr	UD	UD	UD
Sc	8.43	13.9	9.56
Rb	90	137	196
Ba	3141	1954	1812
Y	69.2	69.5	87.6
Th	26.6	25.6	27
Pb	60.3	38.1	43.8
Zr	451	538	665
Hf	9	11	N/A
Ta	8.22	10.8	11.7
Cu	17212	1612	57.8
Zn	249	425	344

Table 2.21 Summary of trace element data (in ppm) from the GLI
UD: Undetected

Rock	Troctolite			Gabbro			Dioritic Rocks		
	Min	Max	X(n-8)	Min	Max	X(n-8)	Min	Max	X(n-3)
Sr	319	697	539	478	637	573	525	661	602
Ni	26	176	115	36	162	86	72	109	88
Co	60	124	97	64	100	80	87	93	90
Cr	1.42	71	-	UD	13.6	-	UD	UD	-
Sc	18	27.3	22.7	18	46.3	29.6	38.7	49.1	42.6
Rb	40.7	66	45.3	29.4	89.4	56.5	29	45.6	38.3
Ba	610	1694	-	441	1078	894	632	920	773
Y	18.3	57.2	31	25.7	57	39	3.16	6	4.46
Th	2.58	11.6	6.20	2.61	14.2	5.53	3.16	6	4.46
Pb	19.3	37.2	26	20.7	47.2	28.6	27	34.9	30
Zr	65.4	245	127	46.7	274	130	83	108	97
Hf	1.27	4.10	2.45	1.50	4.20	2.59	1.76	2.19	1.95
Ta	1.61	5.18	3.20	1.86	5.15	2.74	2.59	3.54	3
Cu	140	3416	959	208	3634	1183	555	2735	1869
Zn	112	222	167	149	312	206	236	264	248

Rock: Weakly Altered Rocks				Strongly Altered Rocks		Center I Syenite	
	Min	Max	X(n-3)	30	44	61	8750
Sr	512	589	546	620	465	371	411
Ni	33.3	135	69.5	435	455	54.8	8.83
Co	59.5	103	75.6	158	153	88.4	19.3
Cr	UD	5.05	-	UD	UD	UD	1.81
Sc	24.7	32.5	27.3	15.5	8.43	14	9.56
Rb	13.3	52	35	45.3	90	137	196
Ba	537	1614	-	2819	3141	1954	1812
Y	8.76	9.58	9.13	16.7	69.2	69.5	87.6
Th	8.76	9.58	9.13	16.7	26.6	25.6	27.0
Pb	34.4	93.5	62.8	45.3	60.3	38	43.8
Zr	188	301	228	286	451	538	665
Hf	2.92	4.36	3.96	3.86	9	11	N/A
Ta	3.45	4.93	4.24	5.56	8.22	11	11.7
Cu	247	1040	771	11869	17211	1611	57.8
Zn	186	269	228	111	249	425	344

concentration whereas troctolite sample 70 contains the highest Sr (697 ppm) value in the GLI. The range of the nickel (Ni) concentrations in the GLI is rather wide due to the presence of niccolite, nickeliferous pyrite and melonite ($NiTe_2$) in some samples. The average Ni concentration of the troctolite (115 ppm) is higher than in the gabbro (86 ppm), dioritic rock (88 ppm), and weakly altered rock (70 ppm), but lower than those of the strongly altered rocks (435 and 455 ppm Ni) in which numerous nickel minerals occur in the disseminated sulphides. The Co contents in all rock types are in between 60 and 124 ppm. The comparatively high Co concentrations in the strongly altered rocks is attributed to cobaltite in those samples.

The chromium (Cr) content in the troctolite varies from 9 to 20 ppm in the basal samples, 1 to 4 ppm in the upper samples, and 71 ppm in the magnetite-rich layer. In the gabbro, Cr concentrations range from 7 to 13 ppm, with the exception of two samples which contain no detectable Cr. Cr is also undetected in the dioritic rocks, strongly altered rocks, and one of the weakly altered rocks. The Cr contents in the other weakly altered rocks are essentially negligible. The average scandium (Sc) contents are fairly close among the troctolite (23 ppm), gabbro (30 ppm), and weakly altered rocks (27 ppm). The dioritic rocks contain on average 43 ppm Sc. The Sc contents in the strongly altered rocks are low, between 8.4 and 16 ppm.

Incompatible Elements The average rubidium (Rb) content in the troctolite (45 ppm) is slightly lower than in the gabbro (57 ppm), higher than in dioritic rock (38 ppm), and weakly altered rock (35 ppm). The Rb contents vary greatly in the two altered rocks, 45 versus 90 ppm. There is

no correlation between K and Rb contents in the GLI. The K/Rb ratio for the GLI ranges from 150-330 in all rock types, with the exception of the strongly altered rocks, samples 30 and 44, whose K/Rb ratios are 440 and 480, respectively. The barium (Ba) content of the GLI increases with height and is more abundant in the strongly altered rocks. The concentration of Ba varies from 610 to 1,694 ppm in the basal and magnetite-rich troctolites, and 914 to 1,695 ppm in the upper troctolites. In the basal gabbro the Ba content is between 440 and 984 ppm, whereas, in the upper section it ranges from 970 to 1,334 ppm. Dioritic rocks contain from 632 to 920 ppm Ba. The Ba contents of the strongly altered rocks are 2,819 and 3,140 ppm.

The contents of yttrium (Y) in the troctolite and gabbro are quite similar, averaging 31 and 39 ppm, respectively. The dioritic and weakly altered rocks show low Y concentrations, 45 and 9.1 ppm, respectively. Sample 30, a strongly altered rock, contains 17 ppm Y, whereas, the other sample contain between 69 and 88 ppm Y. The average thorium (Th) contents of the troctolite (6 ppm), gabbro (5.5 ppm) and dioritic rocks (4.5 ppm) are very close. Th concentrations are higher in the altered rocks, ranging from 8.8 to 27 ppm. The greater Th concentration in the altered rocks is mainly due to the presence of thorite. The lead (Pb) contents of the troctolite (26 ppm), gabbro (29 ppm) and dioritic rock (30 ppm) are similar. The Pb concentrations of the altered rocks have a wider range, from 38 to 94 ppm. The comparatively higher values are due to the presence of numerous galena grains in the altered rocks.

The average zirconium (Zr) contents in the GLI increase from the troctolite (127 ppm) and gabbro (130 ppm) to the weakly altered rocks (228

ppm). The strongly altered rock, sample 44, contains 451 ppm Zr. The average concentrations of hafnium (Hf) show an increase similar to that observed for Zr, from 2.5 ppm in the troctolite to 9 ppm in sample 44. The Zr/Hf ratio in the GLI varies from 31 to 76; the lowest ratio occurs in the ophitic gabbro containing altered olivine, skeletal magnetite and actinolite, whereas, the highest ratio is found in the magnetite-rich troctolite. The Ta content in the troctolite ranges from 1.6 to 5.2 (3.2) ppm, and generally increases from the basal to the upper sections, with the exception of the low-Ta magnetite-rich troctolite which is situated high in the stratigraphic section. The average contents of Ta in the gabbro (2.7 ppm) and dioritic rocks (3.1 ppm) are fairly close to those of the troctolite.

Chalcophile Elements Copper (Cu) contents in the GLI are variably enriched and even the least mineralized sample contains a few grains of chalcopyrite. The lowest Cu content in the troctolite is 140 ppm. The typical Cu concentration in the least mineralized gabbro ranges from 195 to 469 ppm. The altered rocks contain comparatively high Cu contents because they host disseminated chalcopyrite. It is worth-noting that some palladium minerals occur in the low-Cu content rocks such as samples 27 (248 ppm) and 28 (555 ppm). The average zinc (Zn) contents increase from troctolite (112 ppm) to gabbro (206 ppm) and to dioritic rock (248 ppm). The relatively higher Zn values, 269 and 249 ppm, in the altered rocks, are due to the presence of sphalerite.

In summary, the abundances of Sr, Rb, Co, Sc, Th, Y, Zr, Hf, and Ta are

fairly similar in the troctolite and gabbro of the GLI. This observation corroborates the evidence from the major elements that there is no differentiation relationship between the two rock types. The low concentrations of the strongly compatible elements Ni and Cr suggest that the parent magma of the GLI must be rather evolved, in agreement with conclusions derived from the mineral chemistry.

Center I Gabbroic Rocks

The trace element data from the Center I gabbroic rocks are given in Table 2.22. The "400 series" samples are tabulated in group A, whereas the other Center I gabbroic rocks are in group B. The average abundances of group A samples exclude sample C-408 because it is metasomatised. Average abundances are not given for samples with a wide range of contents.

Compatible Elements The Sr contents of group A varies quite systematically from 240 to 1,947 ppm with respect to increasing SiO_2, whereas those of group B have on average 1,448 ppm Sr. The increase of Sr in group A is generally accompanied by decreasing Ni (228 to 4.61 ppm), Cr (275 to 2 ppm), Co (89 to 37 ppm) and Sc (56 to 18 ppm) contents. In group B, the concentrations of Ni, Cr, Co, and Sc are erratic among the samples.

Incompatible Elements The average Rb content of group A (24 ppm) is lower than those of sample C-408 (60 ppm) and group B (44.5 ppm). Ba contents of group A increase from 191 to 3,531 ppm against increasing

Table 2.22 Trace element abundances (ppm) from the Center I gabbroic rocks
Analysed by XRF and INAA (*) methods
Average contents are not given for samples with a wide range of contents
++ Metasomatized + The average excludes sample C-408

Group A Sample	C-406	408++	411	414	420	423	465	466	X(n-7)+
Sr	240	571	1303	1377	1941	1011	1347	1947	-
Ni	228	113	33	22	6.30	3.64	25	4.61	-
Co*	89	58.7	70.8	47.9	33.4	97	53	37.2	61.2
Cr*	275	416	6.36	4.38	8.73	UD	UD	2.10	-
Sc*	56	57.3	25.3	20.2	16.0	79.3	22.0	17.8	33.8
Rb	36	59.7	55.9	16.5	20.4	11.8	14.2	14.29	24.1
Ba	191	673	1439	1182	2239	1603	1306	3531	-
Y	69	50.2	32.6	29.2	28.6	30.3	28	17.2	33.5
Th*	2.39	29	6.55	2.74	UD	1.43	2.74	1.59	-
Pb	25.2	0.87	UD	17.6	13.7	15.6	14.5	12.40	-
Zr	67	355	40.5	9.59	1	1.55	1	0.47	-
Ta*	1.28	7	2.93	1.3	1.5	1.5	1	1.38	1.56
Cu	2484	75	149	208	74	39	232	64.7	-
Zn	149	107	87.4	89.6	49.6	114	86.4	55.3	90.3

Group B Sample	138	321	907	1084	X(n-4)
Sr	1042	1306	1285	2161	1448
Ni	15.04	290	9.39	4.25	-
Co*	99.2	163	47.1	34.7	-
Cr*	4.52	2.25	4.57	UD	-
Sc*	51.2	28.6	40.4	15.0	33.8
Rb	19	34.8	85.0	39.1	44.5
Ba	1208	1318	3261	3583	-
Y	32	14.8	17.5	12.4	19.2
Th*	3	1.93	4.40	3.62	3.25
Pb	22.6	49.3	52	20.4	36
Zr	21	0.16	26.0	0.16	-
Ta*	1.64	0.88	2.02	1.61	-
Cu	231	6181	39.7	21	-
Zn	128	107	133	60	107

SiO_2, similar to the pattern encountered for Sr. The concentrations of Ba are between 1,200 and 1,320 ppm in two of the group B rocks, whereas, the other samples contain between 3,200 and 3,600 ppm Ba. The average Y content of group A, 34 ppm, is higher than that in group B, 19 ppm. Th contents are low in either group A or B rocks, ranging from 0 to 6.6 ppm. The metasomatised sample, however, contains 29 ppm Th. The abundances of Pb in group A vary greatly from one sample to another. Group B have on average 36 ppm Pb. Zr concentrations of group A decrease from 67 to 0.5 ppm with respect to increasing SiO_2, and there are approximately 26 ppm Zr in group B. The average Ta content of group A is 1.6 ppm. Ta contents range from 0 to 2 ppm in group B.

Chalcophile Elements Cu contents in group A are generally low, ranging from 39 to 232 ppm, with the exception of sample C-406 which contains approximately 2,484 ppm Cu. This comparatively high Cu concentration is due to the presence of chalcopyrite grains. Similarly, sample 321 of group B contains an anomalous Cu value of 6,181 ppm. The average abundances of Zn are quite similar between group A (90 ppm) and B (107 ppm) rocks.

In summary, the trace elements Sr and Ba in group A increase systematically with respect to increasing SiO_2 content of its host rock, whereas Ni, Co, Cr, Sc, Ba, Th and Zr decrease. This variation partially corresponds to changes in the modal mineralogy of the rocks and not differentiation. The metasomatised rock shows higher concentrations of Th,

Zr and Ta than its unaltered equivalents. The trace element data of group B rocks cannot be assessed further because they samples do not represent a single suite from a specific locality in western Coldwell.

Center II Gabbroic Rocks

The trace element contents of Center II gabbroic rocks are given in Table 2.23. Samples C-590, 608, 1498, and 1502 are gabbroic rocks from the Neys Peninsula, whereas samples C-117, 153, 308, and 311 are gabbroic xenoliths in Center II syenite. All Center II gabbroic rocks are metasomatised.

Compatible Elements In the Neys gabbros, Sr, Ni and Cr concentrations in samples C-590 and 608 are similar, however, only Sr and Co in samples 1498-1502 are relatively close. The former samples contain, on average, three times as much Sr (650 vs. 200 ppm) but three times less Ni (250 vs. 790 ppm) as the latter. The average Co concentration in the Neys samples is about 66 ppm, the difference between the highest and lowest values being 33 ppm. The Sc content is highest in sample 590 (78 ppm) compared to the other three (22 to 26 ppm).

In the gabbroic xenoliths, samples 117 and 153 have quite similar abundances of all compatible elements but samples 308 and 311 have fairly similar abundances only with respect to Sr, Co, and Sc contents. The Sr contents of samples 117 and 153 (623 and 548 ppm) are approximately half those of samples 308 and 311. The average Ni contents are higher in samples 117 and 153 than in the other two samples, 183 vs. 72 ppm. The Co

Table 2.23 Trace element abundances (ppm) for the Center II Gabbroic Rocks
*Analysed by INAA,others by XRF methods
+Average contents are not given for those samples with a wide range of concentrations

Center II (Neys Peninsula)

Sample	590	608	1498	1502	X(n-4)+
Sr	631	668	194	204	-
Ni	205	295	560	1018	-
Co*	68	48	69	80	66
Cr*	1064	1196	887	3473	-
Sc*	77.6	26.4	36	22.4	40.6
Rb	42	94	115	100	88
Ba	476	1112	626	569	695
Y	23.4	41	24.5	12	22.4
Th*	4.51	10.6	12.5	11	9.58
Pb	13.6	16	16	13.3	14.7
Zr	173	224	220	163	195
Ta*	2.47	5.62	4	4	4
Cu	37.7	31	41.7	76	47
Zn	56.3	97	127	64	78.5

Center II Gabbroic Xenoliths

Sample	117	153	308	311	X(n-4)+
Sr	623	548	1116	1044	-
Ni	160	206	80.5	63	-
Co*	47.6	46	54	59	51.6
Cr*	466	762	16	7.69	-
Sc*	26.4	27.2	45.2	43.5	35.5
Rb	56	81	20	27	46
Ba	731	752	846	584	728
Y	33.6	46	10	36.6	-
Th*	19	27.7	1	1.71	-
Pb	19.8	23.7	15.4	14.7	18.4
Zr	326	403	20	16	-
Ta*	6	9	0.77	0.08	-
Cu	49.5	98	47.5	635	-
Zn	77	91	48	60	69

contents are quite close in all xenolith samples, the average being 52 ppm. Samples 117 and 153 show higher Cr contents but lower average Sc contents than samples 308 and 311, 466 and 762 ppm vs. 16 and 7.7 ppm Cr., and 27 ppm vs. 44 ppm Sc.

Incompatible Elements The concentrations of the incompatible elements vary greatly between Samples 590 and 608, with the exception of the narrow range of Pb (13 to 16 ppm) and Zr (163 to 224 ppm) contents for all Neys samples. The average Rb concentration of samples 608, 1498 and 1502 is 103 ppm Rb, whereas sample 590 contains only 41.8 ppm Rb. The Th contents (10.6 to 12.5 ppm) in these samples are also fairly similar. Ta contents in samples 1498 and 1502 are the same, 4 ppm. The Y contents are similar in samples 590 (23 ppm) and 1,498 (25 ppm). The other elements show great ranges of concentration.

The incompatible element abundances, excluding Rb, in the gabbro xenoliths in samples 117 and 153 are higher than those of the Neys gabbros and other xenoliths. The great variability of the trace element abundances together with the small number of samples and the lack of information on field relationships do not permit significant conclusions to be drawn as yet from these data.

Trace Element Comparison

Table 2.24 is a comparison between the trace element contents of the GLI, represented by the troctolite and gabbro, and those of other gabbroic

Table 2.24 Comparison of trace element abundances between the GLI and other intrusive and extrusive equivalent rocks

* GLI: Geordie Lake Intrusion (This Study)
Center I "400 series" Gabbroic Rocks (This Study)
Center II Neys Gabbroic Rocks (This Study)
QM: Quebec Mine Tholeiitic Basalts, Michipicoten Island (Annels, 1974)
KW: Keweenawan North Shore Volcanic Group, KW-1 to 8 (BVSP, 1981)
S. Dam: Somerset Dam Troctolite-Olivine Gabbro (Mathison, 1987)
MI: McIntosh Troctolite-Olivine Gabbro (Mathison and Hamlyn, 1987)

\- Unavailable UD: Undetected

*	GLI Range	Center I Range	Center II Range	QM Range	KW Range	S. Dam Range	MI Range
Sr	319-697	240-1947	194-668	240-420	199-412	-	-
Ni	25.6-176	4.61-228	205-1018	150-230	90-270	5-130	54-810
Co	59.8-124	37.2-97	47.6-80.5	52-59	41.4-56.8	15-60	-
Cr	UD-71.1	UD-275	887-3473	100-310	140-387	20-140	202-830
Sc	17.9-46.3	16-79.3	22.4-77.6	36-45	22.3-32.3	-	-
Rb	29.4-89.4	11.8-56	41.8-99.6	-	1 19	-	-
Ba	441-1694	191-3531	476-1112	100-770	56-146	-	-
Y	18.3-57.2	17.2-68.9	12.1-41	0-477	-	-	-
Th	2.58-14.2	UD-6.55	4.51-12.5	-	0.33-1.83	-	-
Pb	19.3-47.2	UD-25.2	13.3-16.2	-	-	-	-
Zr	46.7-274	0.47-66.9	163-224	100-160	40-137	15-50	-
Hf	1.27-4.2	-	-	-	1.14-4.6	-	-
Ta	1.61-5.18	1.03-2.93	2.47-5.62	-	0.15-0.93	-	-
Cu	140-3634	39-2484	31-75.9	35-94	-	15-140	20-175
Zn	112-312	49.6-149	56.3-127	< 500	-	25-95	-

and volcanic equivalent rocks. The observed ranges for Sr, Ni, Co, Cr, Sc, Rb, Ba, and Y from the GLI, overlap those for the "400 series" Center I gabbros. The maximum Ni and Cr contents of Center I rocks are, however, much higher than those of GLI. Center I rocks show a wide range of Th, Pb and Zr contents.

In comparison to the tholeiitic basalts of Michipicoten Island, the GLI has higher Sr, Co, and Cu and lower Ni and Cr contents. Ba and Zr contents for the GLI overlap with those for the Michipicoten basalts. The Sr, Rb, Ba,Th, and Ta concentrations in the GLI are higher than those of the Keweenawan tholeiitic olivine basalt. The highest Ni and Cr contents of the GLI are approximately one-third and one-sixth of those of NSVG (270 ppm Ni and 390 ppm Cr). The two rock suites have similar ranges of Zr and Hf contents. The Cr content of the GLI (71 ppm) is also lower than that of the Somerset Dam (140 ppm., Mathison, 1987) and McIntosh (850 ppm., Mathison and Hamlyn, 1987).

The Rare Earth Elements (REE)

Geordie Lake Intrusion

Eight REE; La, Ce, Nd, Sm, Eu, Tb, Yb, and Lu have been determined in twenty-one samples of the GLI, including one hybrid rock from the GLI-syenite contact zone (sample 8746), and two samples from the eastern syenite (Table 2.25). Some REE data are not available due to analytical problems (marked N/A). The La and Ce concentrations from the altered and syenitic rocks are higher than those from other rocks. La/Yb

Table 2.25 Concentrations (ppm) of rare-earth elements of the GLI
Rock type abbreviations are similar to Table 2.3
*INAA +RNAA ** I+RNAA

Rock type	TR	TR	TR	G/TR	G	G	G	G
Sample	69	78	7	77	3	4	35	45
*La	66	46	55	43	76	59	55.2	91.3
+Ce	129	85	N/A	84	76	100	122	179
+Nd	53.6	33.3	53.4	N/A	74.6	48.3	N/A	82
+Sm	7.97	7.02	9.61	N/A	11.8	8.95	N/A	15
**Eu	2.43	1.97	3.48	2.18	1.61	2.34	2.76	3.71
+Tb	1.11	0.73	1.39	0.75	0.66	0.83	1.14	1.51
+Yb	3.68	1.96	4.09	N/A	1.78	2.64	N/A	4.04
+Lu	0.041	0.028	0.039	N/A	0.048	0.036	N/A	0.051
La/Yb	18	23	13	N/A	43	22		23

Rock type	G	G	AG	DR	DR	DR	WAG	WAG
Sample	53	54	9	27	28	29	5	64
*La	55.8	55	112	83.5	73	94.4	117	92
+Ce	118	11	204	151	140	190	175	159
+Nd	59.7	N/A	N/A	77.3	86.7	N/A	N/A	N/A
+Sm	10.5	N/A	N/A	13.8	14	N/A	N/A	N/A
**Eu	2.91	0.27	3.71	3.63	3.31	4.20	3.42	3.45
+Tb	1.13	0.11	1.75	1.41	1.39	1.65	1.51	1.3
+Yb	2.59	N/A	N/A	3.38	3.77	N/A	N/A	N/A
+Lu	0.031	N/A	N/A	0.044	0.050	N/A	N/A	N/A
La/Yb	22			25	19			

Rock type	WAG	WAG	SAG	SAG	SN-GB	SN	SN
Sample	67	81	30	44	8746	61	8750
*La	107	75	115	151	163	159	183
+Ce	211	150	200	307	N/A	277	N/A
+Nd	N/A	N/A	N/A	N/A	N/A	N/A	N/A
+Sm	N/A	N/A	N/A	N/A	21.4	N/A	24.8
**Eu	4.05	3.38	4.49	4.50	3.36	3.93	3.40
+Tb	1.85	1.5	1.41	2.23	N/A	1.89	N/A
+Yb	N/A	N/A	N/A	N/A	N/A	N/A	N/A
+Lu	N/A	N/A	N/A	N/A	N/A	N/A	N/A

ratios vary from 13-23 in troctolite, 22-43 in gabbro, and 19-25 in the dioritic rocks.

The chondrite-normalized distribution patterns (Figures 2.39A-D) show that all rock types are enriched in the light REE (La, Ce, Nd, and Sm). There is a substantial overlap of the REE distribution patterns of the troctolite and gabbro (Figure 2.39B). The high-silica gabbro (sample 9) shows a greater enrichment in La, Ce, and Tb than the other gabbros and troctolites. The enrichment factors for the LREE of the dioritic rocks are similar to those of the most LREE-enriched gabbro but are higher than those of the troctolite (Figure 2.39C). In the altered rocks La and Tb are more enriched than the other rock types.

Europium anomalies are absent, indicating that Eu has remained in the trivalent state. Fractionation of plagioclase, if it has occurred, is not reflected in Eu abundances.

Center I Quartz Syenite The REE distribution patterns (Figure 2.40) of the two syenites, a core sample (G-61) and surface sample (G-8746), and a hybrid rock (G-8746) show a narrow compositional range, light REE enrichment and no Eu anomaly (sample 61). The LREE concentrations, excluding Eu, are higher in the syenite than GLI.

Center I and II Gabbro Table 2.26 lists the abundances of REE of the Center I and II gabbros. The chondrite-normalized REE distribution patterns of Center I gabbro in the western contact (Figure 2.41) show an enrichment in the LREE. There is no Eu anomaly in these gabbros. The La

Figure 2.39A-D Chondrite-normalized REE distribution patterns for the troctolite (A), gabbro (B), "diorite" (C), and altered gabbroic rocks (D). Chondrite values* are those recommended by Boynton (1984).

*La: 0.31

Ce: 0.808

Nd: 0.6

Sm: 0.195

Eu: 0.0735

Yb: 0.209

Tb: 0.0474

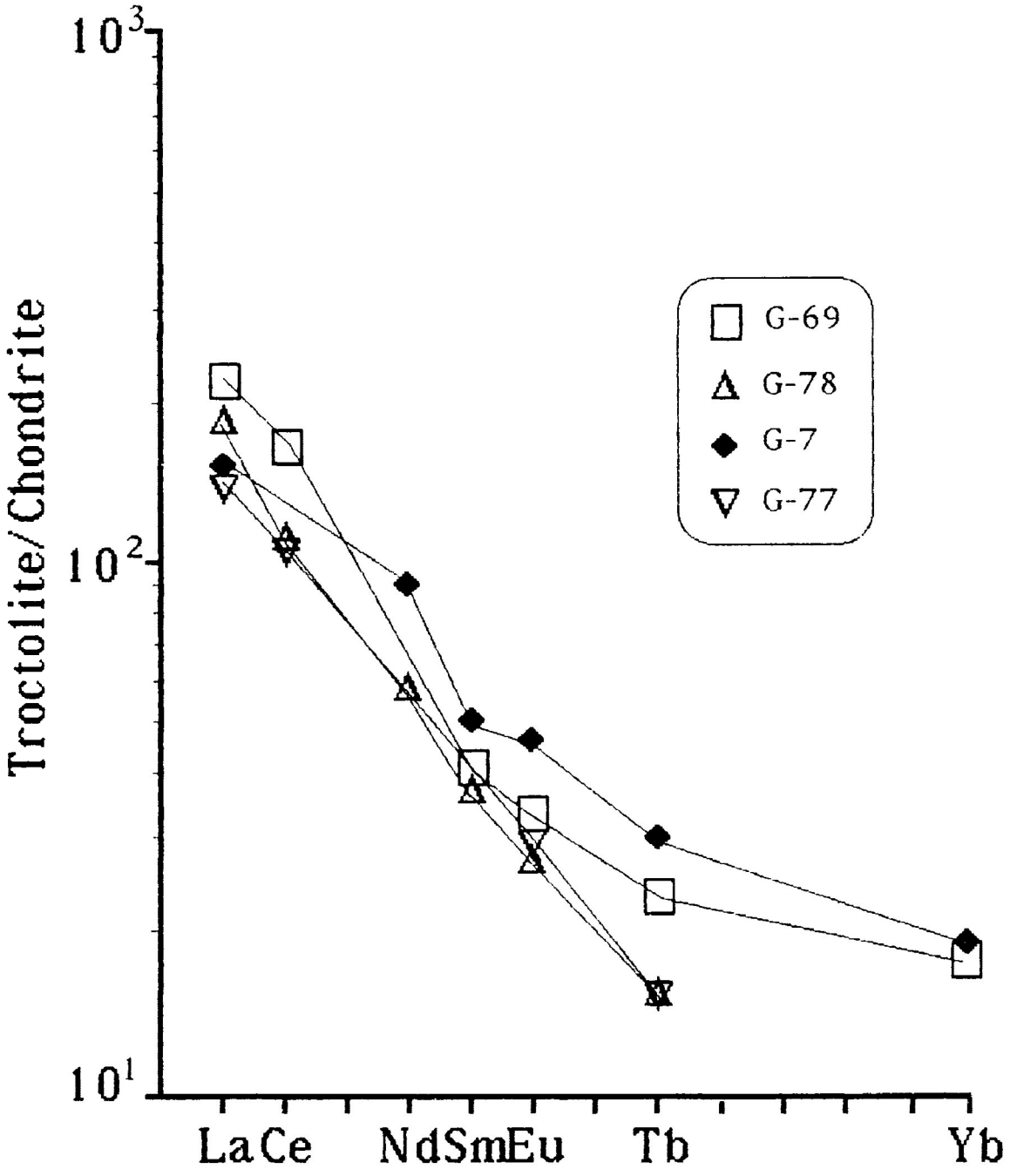

Figure 2.39A Chondrite-normalized REE distribution patterns of the troctolite

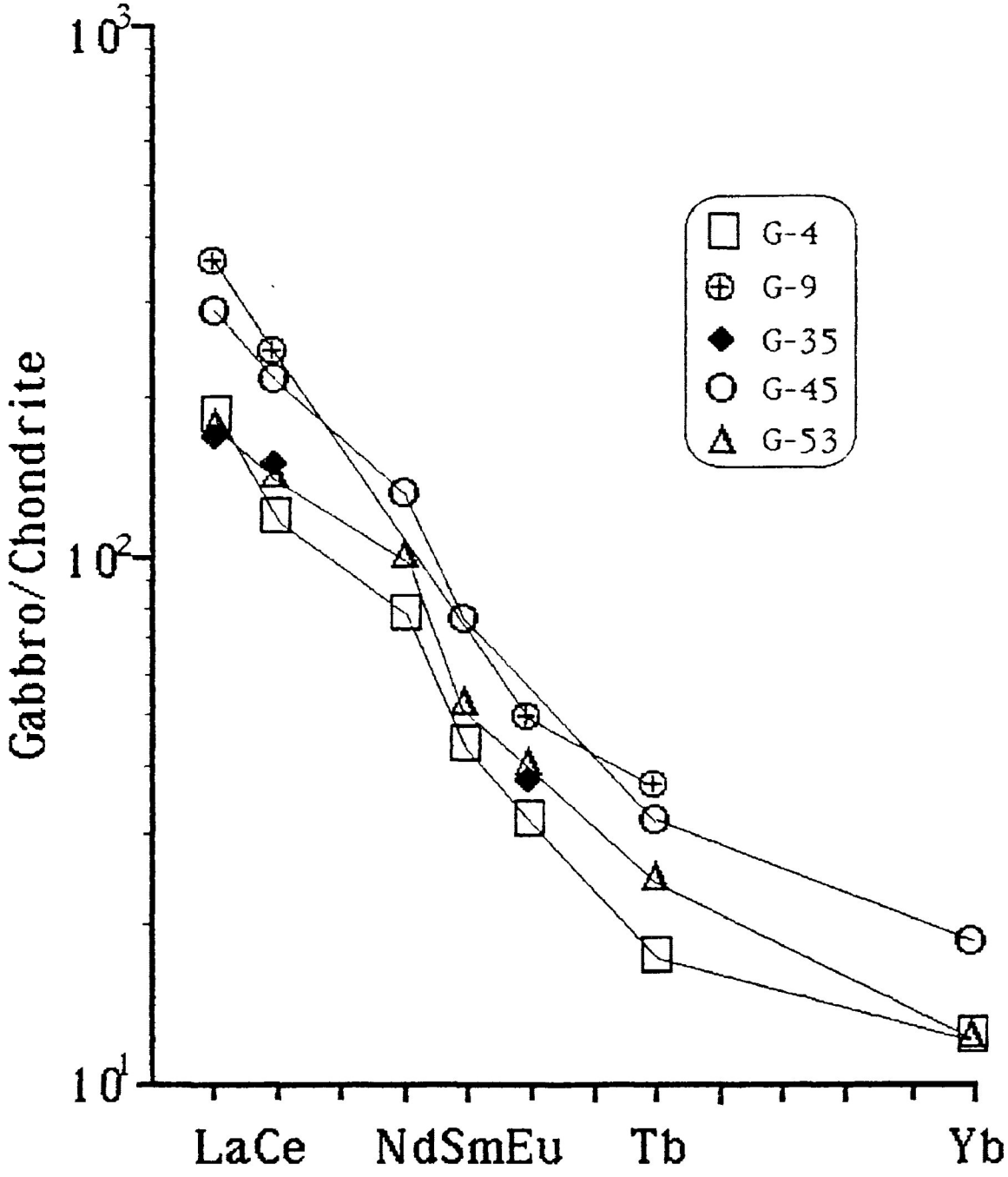

Figure 2. 39B Chondrite-normalized REE distribution patterns of the olivine gabbro

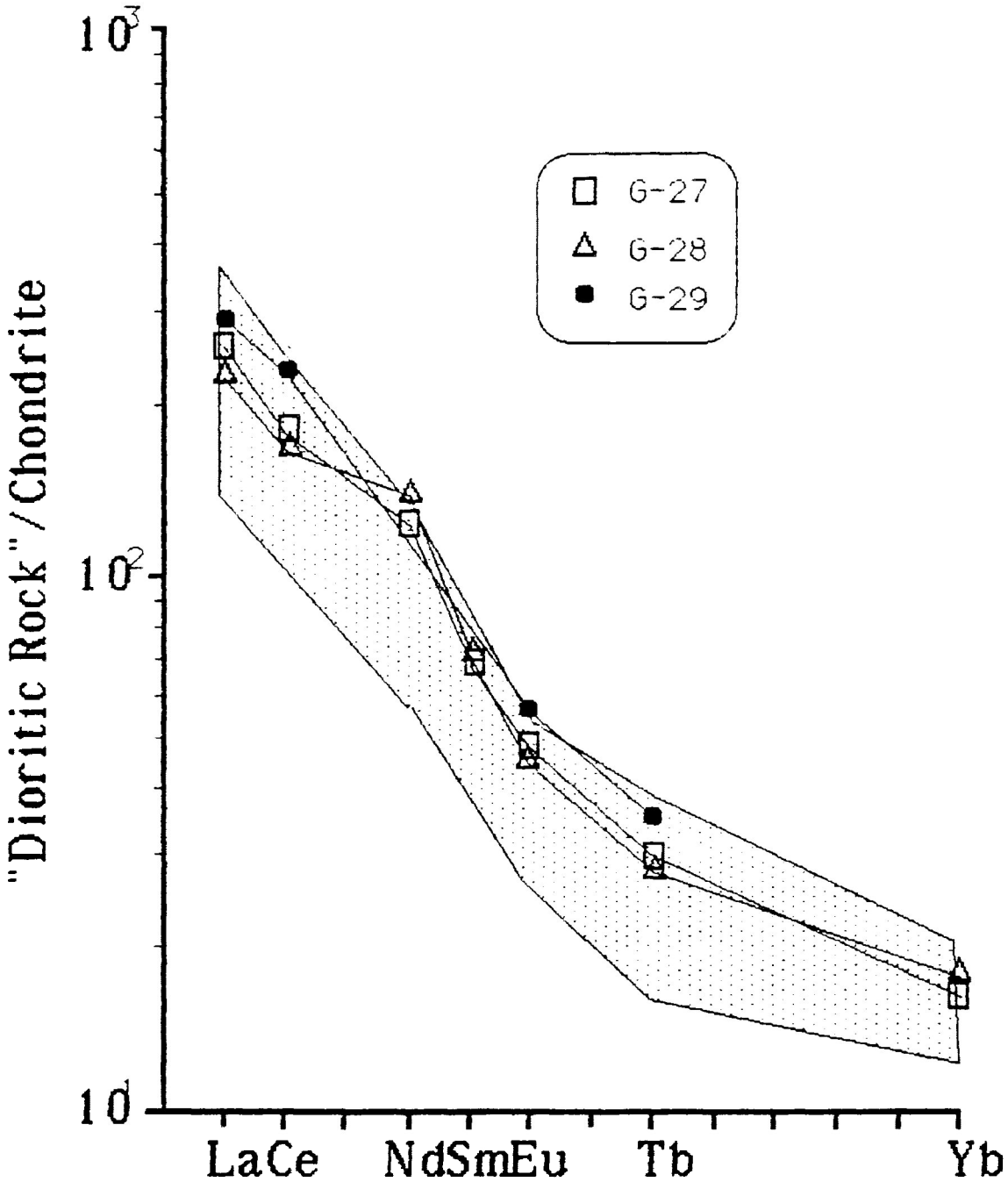

Figure 2.39C Chondrite-normalized distribution patterns of the "dioritic" rocks. The stippled area is the REE distribution patterns of the troctolite and gabbro.

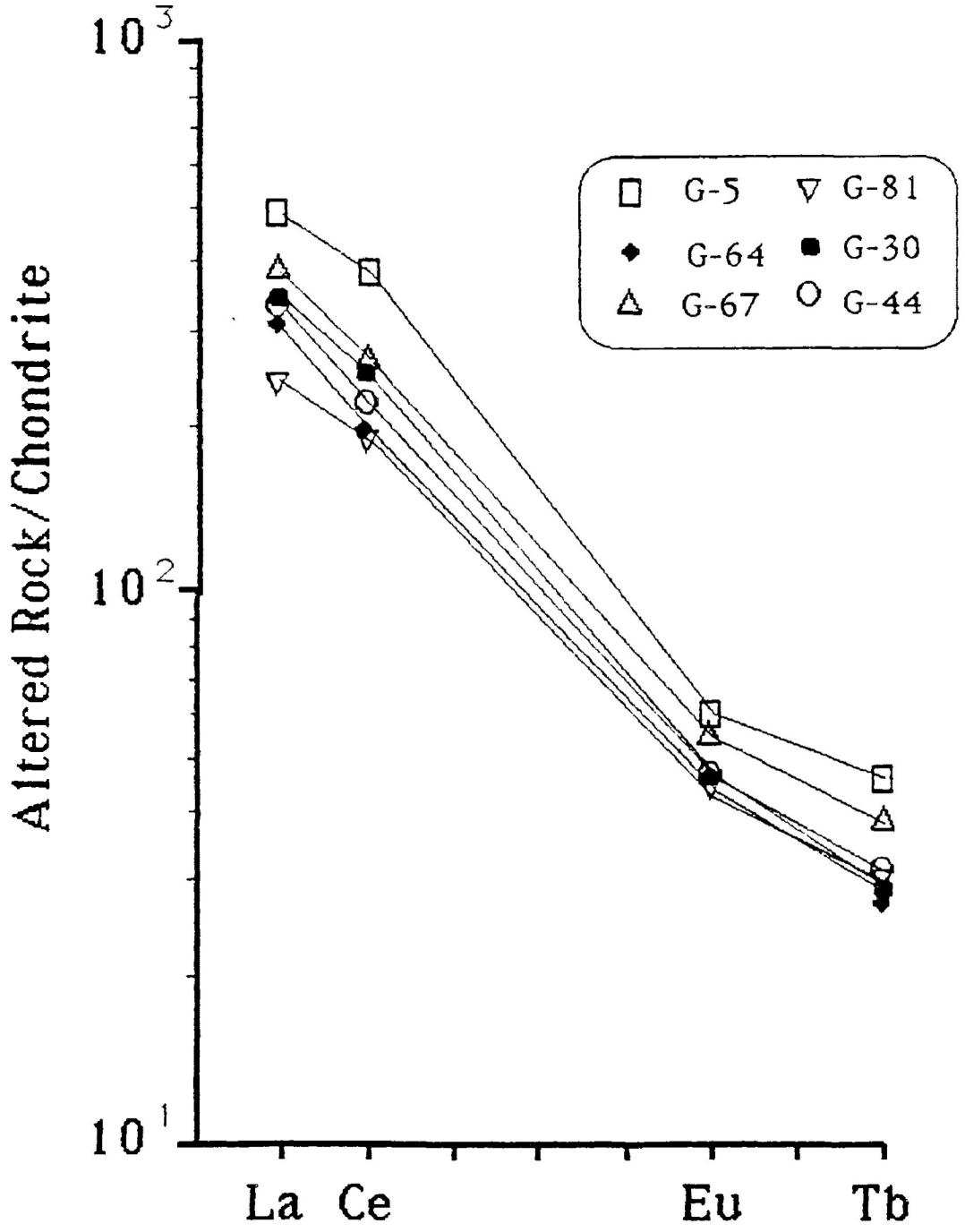

Figure 2.39D Chondrite-normalized REE distribution patterns of the altered GLI

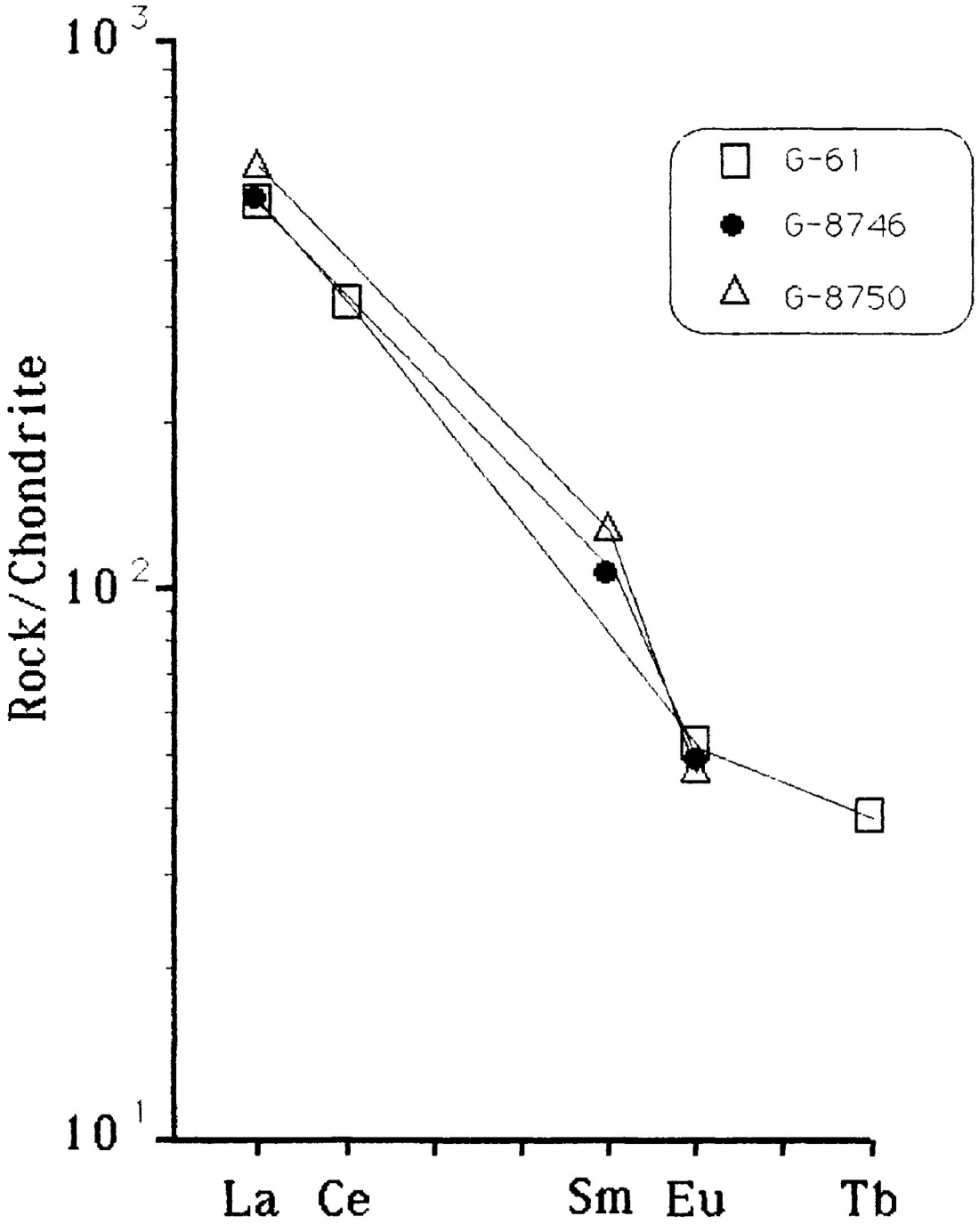

Figure 2.40 Chondrite-normalized REE distribution patterns for the mixed rock (G-8746) and eastern syenite (G-61 and 8750)

Table 2.26 Concentrations (ppm) of the rare-earth elements of Center I and II

Gabbroic rocks

*INAA +RNAA ** I+RNAA m:metasomatised

Center I	408-466 Western Gabbro					656 Bamoos Lake		
Sample	406	408 m	411	414	420	423	465	466
*La	106	108	74.8	70.6	67.8	60.1	67	50.3
+Ce	N/A	N/A	197	98.7	N/A	N/A	105	N/A
*Sm	N/A	18.2	18.2	13.4	12.9	18.5	13.7	12.7
**Eu	3.96	3.59	5.40	3.14	3.61	5.20	3.45	4.24
+Tb	1.52	N/A	1.63	0.79	N/A	N/A	0.86	N/A
+Yb	3.40	N/A	3.25	1.55	N/A	N/A	1.60	N/A
La/Yb	31		23	45			42	

Sample	138	321	907	1084	656
*La	68	46.3	51	38.6	23.6
+Ce	N/A	109	1134	69	35.6
+Sm	18.6	12.6	10.7	9.22	5.52
**Eu	4.71	4.15	5.71	3.84	1.40
+Tb	N/A	0.76	1.26	0.35	0.37
+Yb	N/A	1.55	1.51	0.18	0.20
La/Yb		30	34	214	118

Center II	590-1502: Neys				XE: Xenoliths			
Sample	590 m	608	1498 m	1502 m	XE 117 m	XE 153 m	XE 308 m	XE 311 m
*La	61	103	65	55.8	106	125	25	73
+Ce	N/A	N/A	87.5	N/A	N/A	N/A	N/A	126
+Sm	18.5	15.2	7.93	5.29	18.6	12	9	18
**Eu	4.03	2.44	1.26	0.92	2.57	1.83	2.10	4.37
+Tb	N/A	N/A	0.29	N/A	N/A	N/A	N/A	0.84
+Yb	N/A	N/A	2.26	N/A	N/A	N/A	N/A	1.96
La/Yb			29					

and Yb enrichment factors vary from approximately 150 to 350 times and 8 to 17 times chondritic abundances, respectively. La/Yb ratios in samples C-411, 414, and 465 vary from 23, to 45, and to 42, respectively, even though the samples are mineralogically similar.

The La/Yb ratios for other Center I gabbroic rocks (C-321 - 656) vary from 30 to 214. Figure 2.42 shows the chondrite-normalized REE distribution patterns of these rocks. Samples C-138, 907 and 656 show a similar pattern, whereas samples C-907 and 1084 display a positive Eu anomaly. The positive Eu anomaly suggests that there has been plagioclase accumulation during the crystallization of these gabbros. The enrichment factors against chondritic abundances for La (75), Sm (25) and Eu (17) of the Bamoos Lake gabbro (sample 656) are the lowest enrichment factors for the Center I gabbros.

The REE distribution patterns of the Center II gabbros (Figure 2.43) shows an enrichment in the light REE with the enrichment factors of La 175-325 and Eu 12-50 times chondritic abundances. Eu anomalies are not recorded in this suite of Center II gabbros. The Center II gabbroic xenoliths (Figure 2.44) display a similar distribution pattern to other Coldwell rocks, including the GLI. These are metasomatised rocks and it is not yet known if metasomatism had affected the abundance of the REE in the rocks.

All REE patterns obtained have a common characteristic, a greater enrichment factor for the LREE than the HREE. This implies that the parental magma of the gabbroic rocks was enriched in these elements. In the GLI, this enrichment may be enhanced by the high modal content of apatite. The

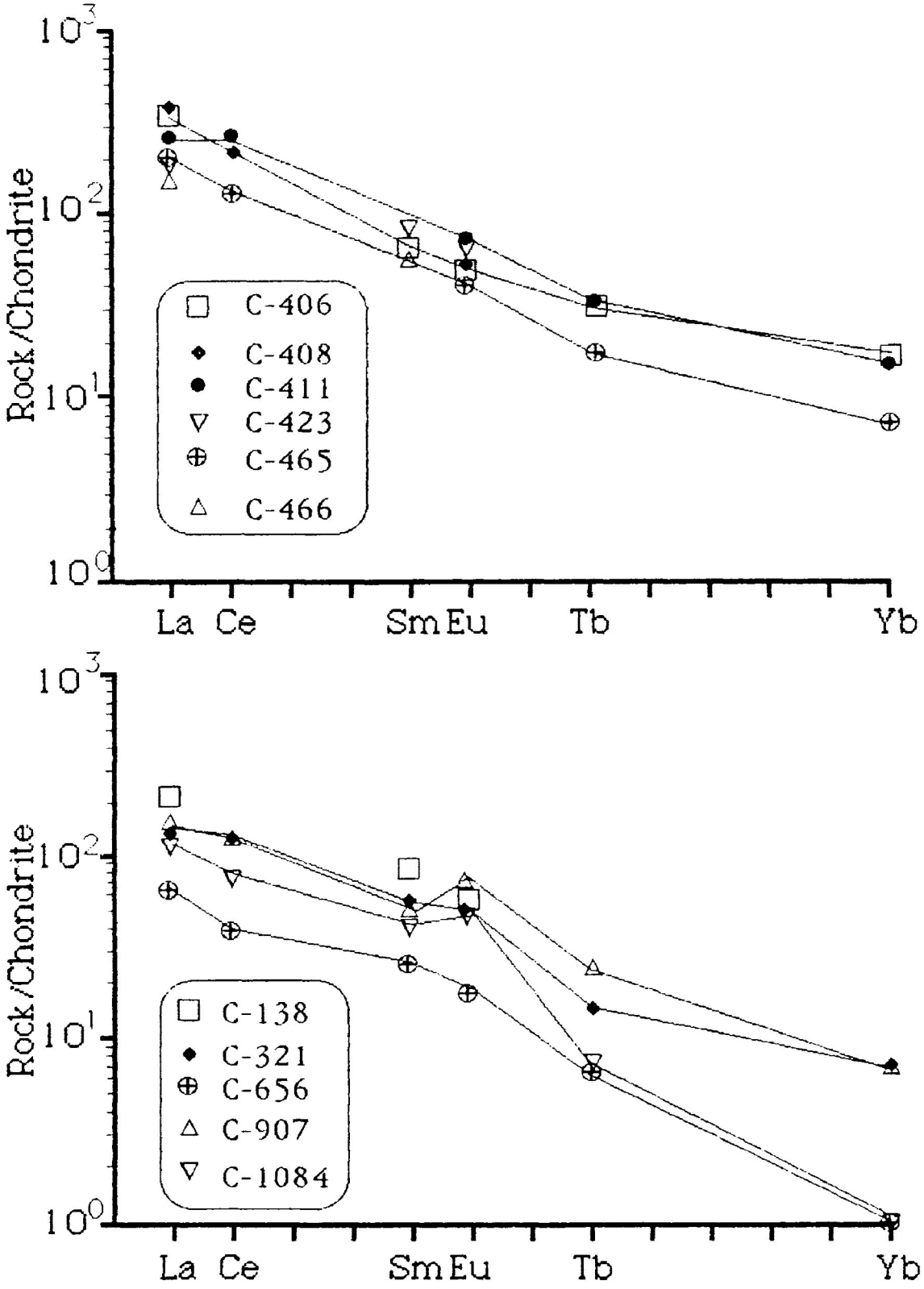

Figures 2.41/42 Chondrite-normalized REE distribution patterns for the western Center I gabbro ("400" series samples), and other Center I gabbroic rocks, Coldwell complex

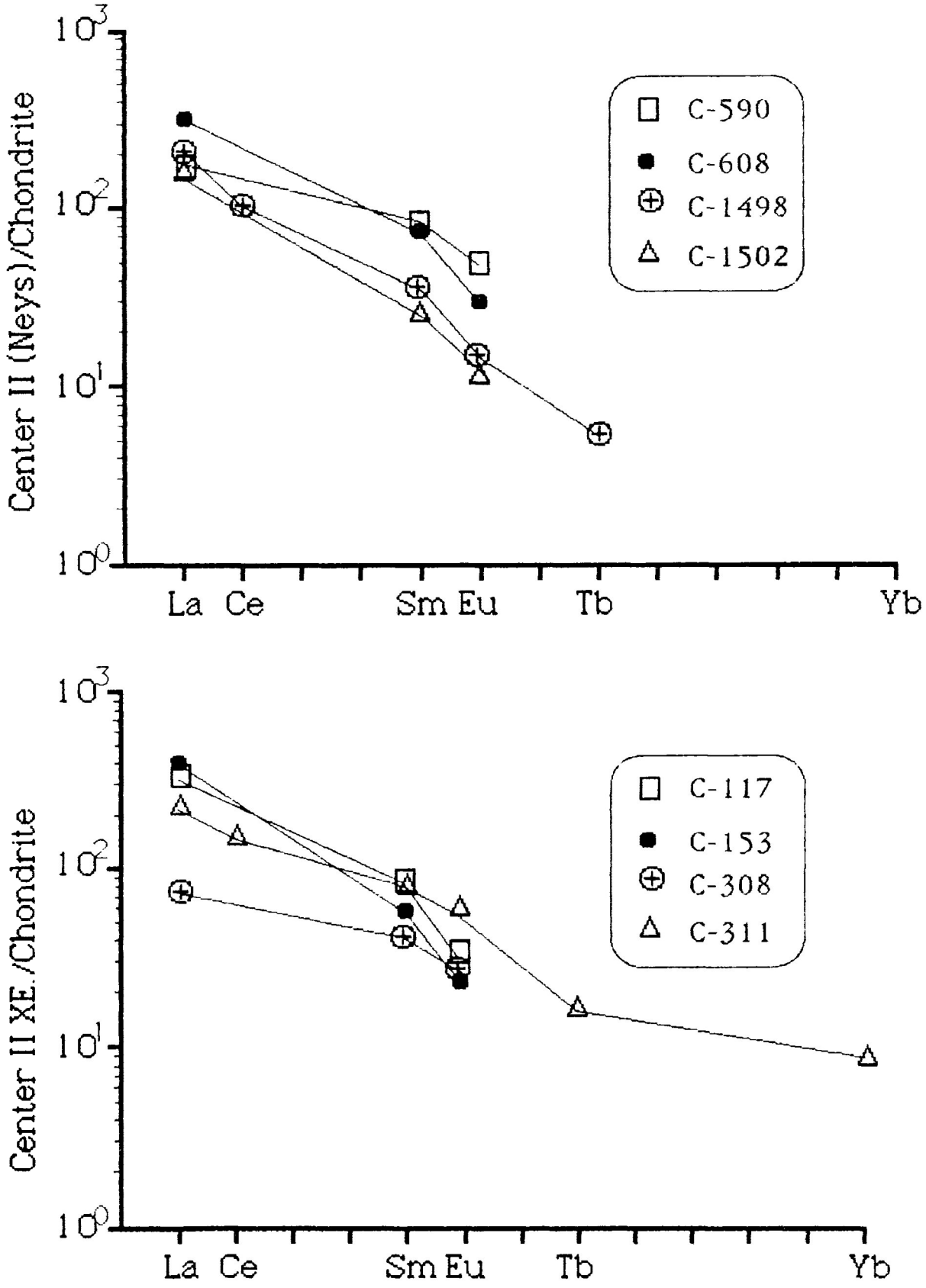

Figures 2.43/44 Chondrite-normalized REE distribution patterns for the Center II gabbros from the eastern Neys Peninsula, and the Center II gabbroic xenoliths, Coldwell complex

REE distribution patterns which show a small positive Eu anomaly (samples 907 and 1084) indicate that these rocks were formed under different conditions of crystallization from other Coldwell rocks.

The enrichment factors for the GLI overlap those for the Center I and II gabbros. These rock suites display similar patterns of light REE enrichment. In comparison to the REE patterns of the tholeiite basalts from the Keweenawan North Shore Volcanic Suite (Figure 2.45), the GLI is much more enriched in the LREE. The lowest enrichment factors of the HREE of the GLI overlap those of the more evolved NSVG. The GLI do not show any Eu anomaly, whereas the less evolved NSVG shows a positive Eu anomaly and the more evolved equivalents display a negative anomaly. The positive and negative Eu anomalies are indicative of early plagioclase accumulation and removal during crystallization, respectively.

2.5 Discussion

This section integrates all the data presented in the above sections on petrography, mineral chemistry and geochemistry, in order to assess the nature of the parent magma of the GLI. The information gathered here forms the basis for the characterisation of the platinum and Cu-sulfide mineralization which is hosted by the GLI (Chapter 3).

2.5.1 Parent Magma

The overall similarity of plagioclase, clinopyroxene and

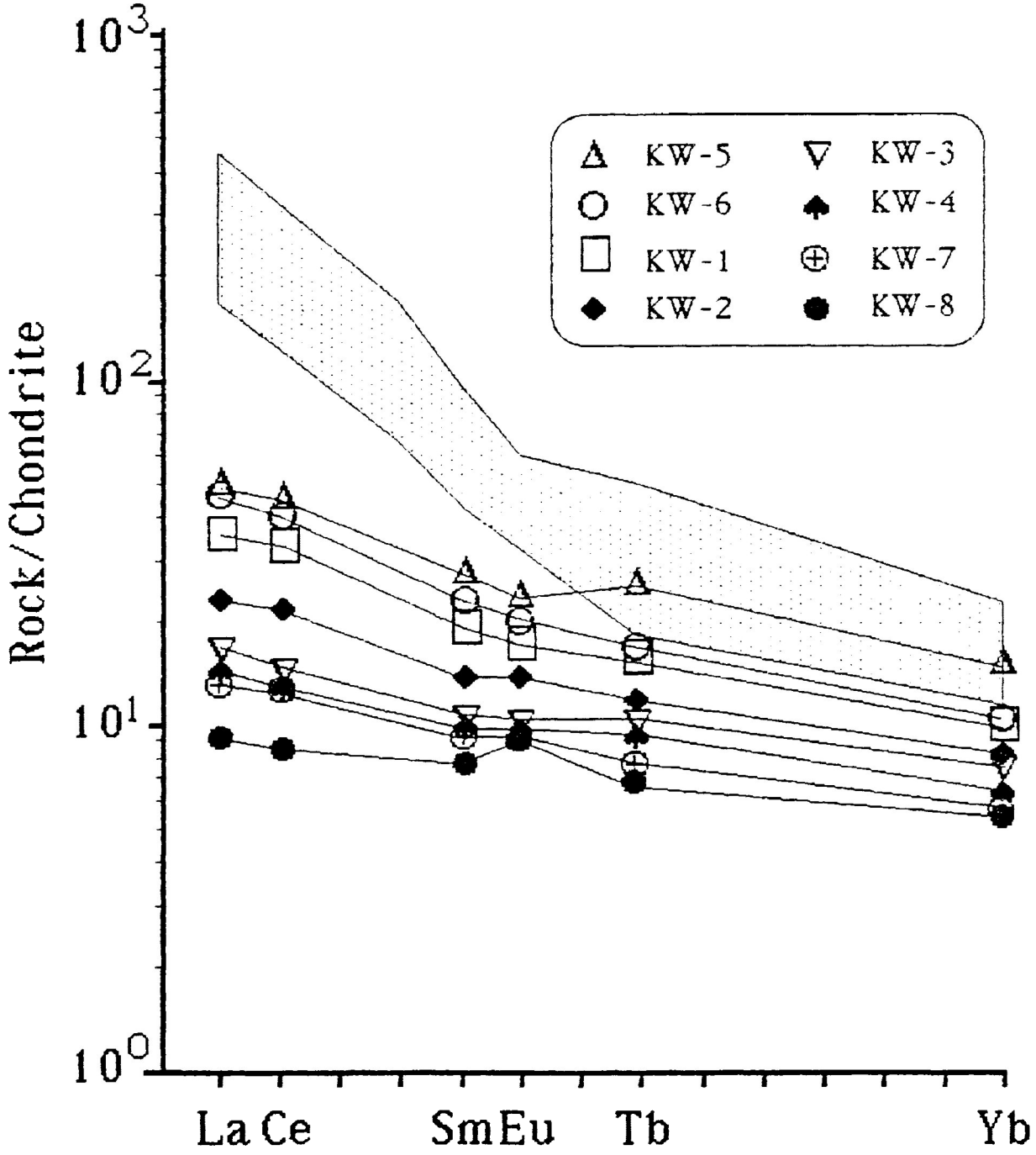

Figure 2.45 Comparison of chondrite-normalized REE distribution patterns for the GLI (stippled area) to those for the Keweenawan olivine tholeiitic basalt (Basaltic Volcanism Study Project, 1981)

titaniferous magnetite compositions in the troctolite and gabbro have demonstrated that the two rock types were derived from magmas of similar composition. This observation in turn implies that there is no differentiation relationship between the troctolite and gabbro. The textural difference is the result of different rates of cooling during the crystallization. Therefore, the parent magma of the GLI, inferred below, represents the parent magma of either rock type.

No chilled samples of the GLI exist but the inferred nature of the parent magma is a low-alumina olivine tholeiitic basalt. The absence of modal feldspathoids and alkali pyroxenes and amphiboles suggests that the GLI is not alkaline. The tholeiitic nature of the parent magma has been illustrated in the AFM diagram (Figure 2.34) and the quaternary system Di-Ab-Fo-Q (Figure 2.35). The low-alumina character is evident in the Al_2O_3 content of the GLI (Table 2.15). The tholeiitic parentage is further supported by the plot of SiO_2 against Al_2O_3 content of the clinopyroxenes (Figure 2.46), in which the majority of the compositions fall in the non-alkaline field of LeBas (1962); only a few ferroaugites and a high-alumina augite from the upper level of the ophitic gabbro in core 1 and from some of the slightly altered rocks lie in the alkaline field. In the accompanying TiO_2 against Al^{iv} diagram (LeBas, 1962) all of the clinopyroxenes of GLI are within the non-alkaline field (Figure 2.47).

The trace element data, particularly Ni and Cr, indicate that the parent magma of the GLI is more evolved than those of NSVG, the McIntosh and Somerset Dam intrusions. The minor amounts of primary amphibole in some samples suggest that the parent magma of the GLI was slightly hydrous

Figure 2.46 Plots of Al_2O_3 vs SiO_2(wt%) of the clinopyroxenes from the GLI. The boundary line between alkaline and non-alkaline fields is after LeBas (1961).

Figure 2.47 Plots of TiO_2 (wt%) vs. Al^{iv} of the clinopyroxenes from the GLI. The boundary line between alkaline and non-alkaline fields is after LeBas (1961).

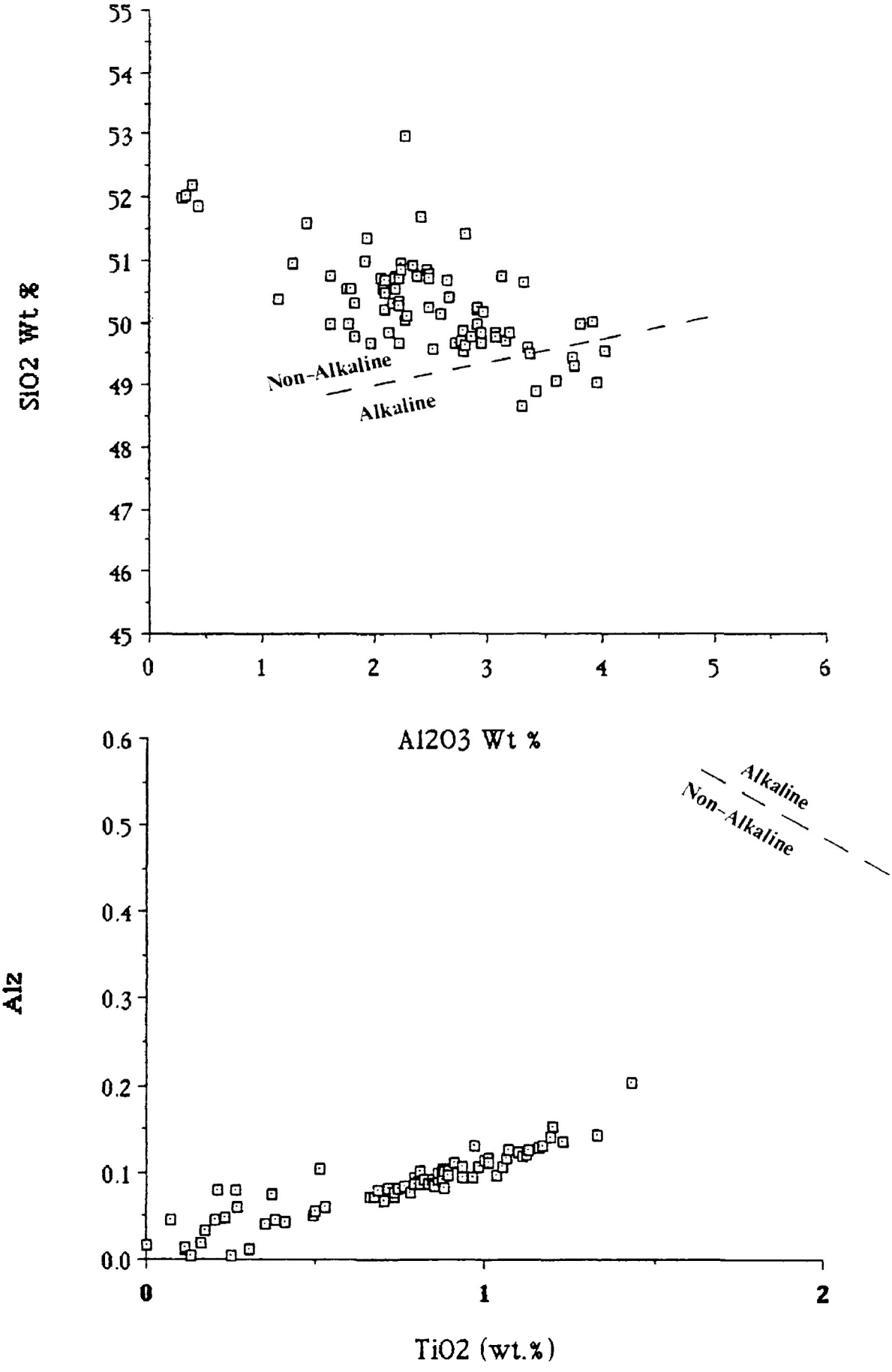
SiO2 Wt %
55
54
53
52
51
50
49
48
47
46
45
0
1
2
3
4
5
6
Non-Alkaline
Alkaline
Al2O3 Wt %
Alz
0.6
0.5
0.4
0.3
0.2
0.1
0.0
0
1
2
Alkaline
Non-Alkaline
TiO2 (wt.%)

(maximum 1.44 wt. % H_2O., Table 2.15).

2.5.2 Conditions of Crystallization

The Al_2O_3 and TiO_2 contents of clinopyroxenes are related to the temperature and pressure of crystallization of the magma. Kushiro (1960) and Wilkinson (1966) indicated that a high concentration of alumina in clinopyroxenes is related to high temperature, whereas Muir and Tilley (1964) demonstrated that high pressures could lead to an appreciable amount of alumina in pyroxenes, especially in tholeiitic magmas. Wilson (1976) stated that the relationship between pressure and alumina content in pyroxenes is valid if Al^{iv} and Al^{vi} can be accurately determined. Thompson (1974) favoured high pressure and temperature for high-alumina and high-titanium contents in pyroxenes. Based on these studies, the majority of the clinopyroxenes of the GLI were formed at relatively low pressure and temperatures. The high-alumina clinopyroxenes of the GLI are most likely to have crystallized at high temperatures but not high pressures, because the host rocks of the clinopyroxenes were emplaced at a high crustal level.

Experimental studies by Yoder and Tilley (1962) on tholeiitic basalt have demonstrated that under anhydrous conditions and at 1 atm., the temperature range of crystallization is from 1,250-1,025°C. The results of the observed mineralogy, olivine + plagioclase + clinopyroxene, agree with the modal major mineralogy of the GLI. However, the presence of primary amphiboles in the GLI points to the fact that the parent magma of the GLI must have contained small amounts of water. Under P_{H_2O}= 2 kbar, the

crystallization of the same tholeiitic basalt commenced at 1,150°C and the assemblage Amphibole + Plagioclase + Clinopyroxene + Magnetite + Glass appeared at 900°C. This seems to be a more realistic range of temperature of crystallization for the GLI because at temperatures below 900°C, clinopyroxene and glass disappeared.

Compositions of certain coexisting minerals such as plagioclase-alkali feldspar and magnetite-ilmenite pairs can be used to infer the temperature at which the minerals crystallized or equilibrated. The two-feldspar geothermometer, revised by Stormer (1975), is based on the distribution of the albite component between plagioclase and K-feldspar grains during crystallization and that the partition is believed to be sensitive to temperature. Determinative curves of temperature as a function of the albite distribution in the two feldspars are shown in Figures 2.48. The pressure range for emplacement of the Coldwell rocks falls between 1 and 2 kbar (Mitchell and Platt, 1982). The albite contents of five plagioclase-alkali feldspar pairs are plotted in the diagrams. The temperature (900°C at 1 kbar and 950°C at 2 kbar) obtained for the feldspars in sample 29 is most likely below or near the solidus temperature of the gabbro. The other feldspars, including one pair from the eastern syenite, record much lower temperatures (ca. 350°C to 450°C), thereby representing the subsolidus equilibration temperatures. These lower temperatures are consistent with the petrographic observations which show alkali-feldspars replacing plagioclase. The temperature range of crystallization of the GLI can, therefore, tentatively be constrained to between 1,150 and 900°C.

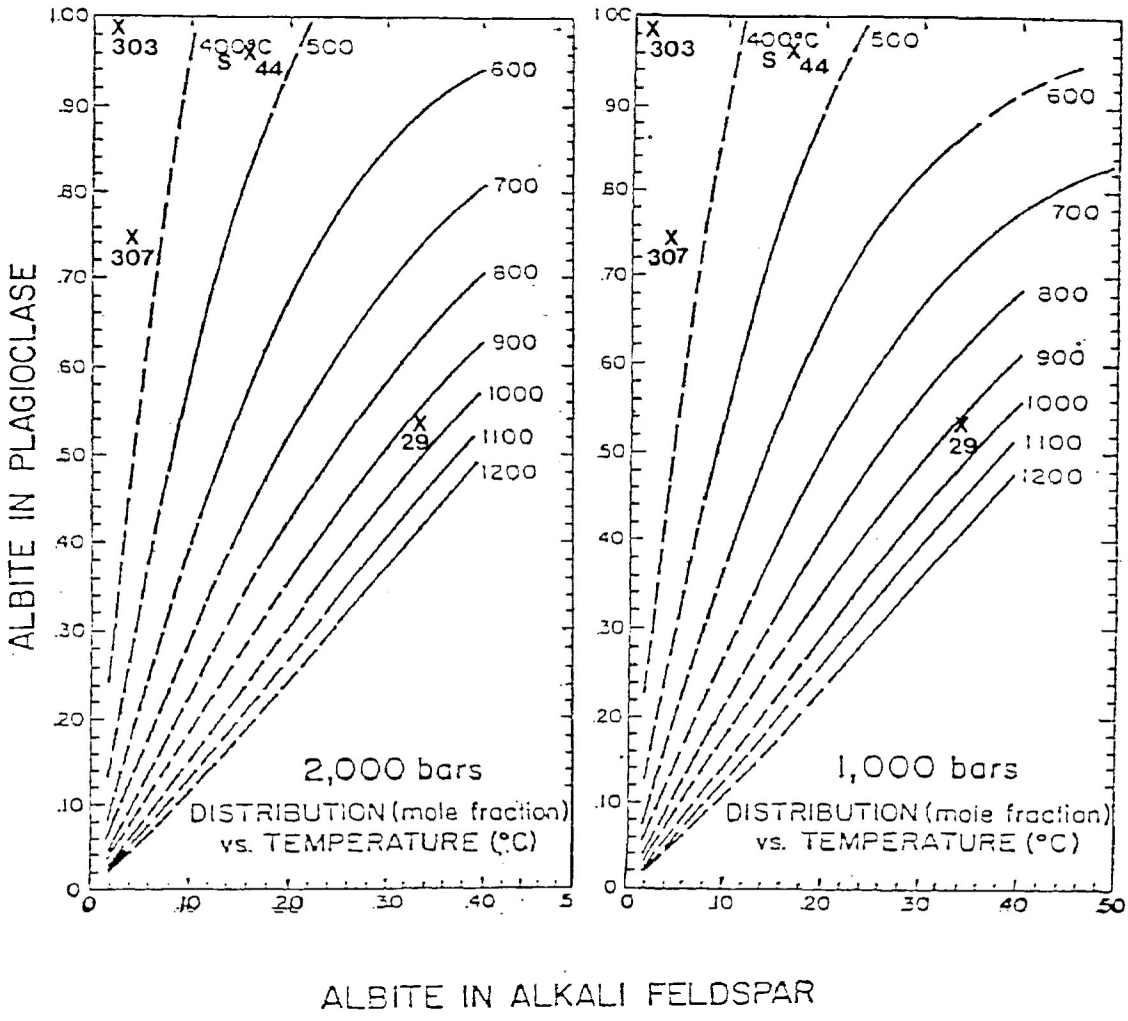

Figure 2.48 Two-feldspar geothermometer diagram (after Stormer, 1975) for the GLI and eastern syenite at 2,000 bars (A) and 1,000 bars (B). Sample 29 is a "dioritic" gabbro, samples 303 and 307 are weakly altered gabbroic rocks, and sample 44 is a strongly altered rock.

Figure 2.49 shows GLI whole rock data plotted in the ternary system Fo-Pl-Cpx. The randomly distributed data suggest that the GLI underwent non-equilibrium crystallization. The dendritic habit of the olivines in the troctolite, the ophitic texture of the gabbro, and the zoned plagioclase in both rock types attest to this non-equilibrium condition. The troctolite must have crystallized more rapidly than the gabbro in order to produce the harrisitic texture.

One major problem yet to be resolved is the origin of the alternating troctolite-olivine gabbro units. The evidence outlined earlier has indicated that each of the units represents a single batch of magma. The formation of the units must, then, be the product of successive pulses of magma. Even though the contact between the troctolite and gabbro is gradational, suggesting that the new magma and still cooling resident magma mixed, the sequence of emplacement cannot be determined as cross-cutting relationships between the troctolite and gabbro are not observed. Nevertheless, the magma pulses must have been rapid enough to inhibit fractionation in the magma and yet slow enough to prevent the formation of a sharp contact or even a thermal reaction between the units.

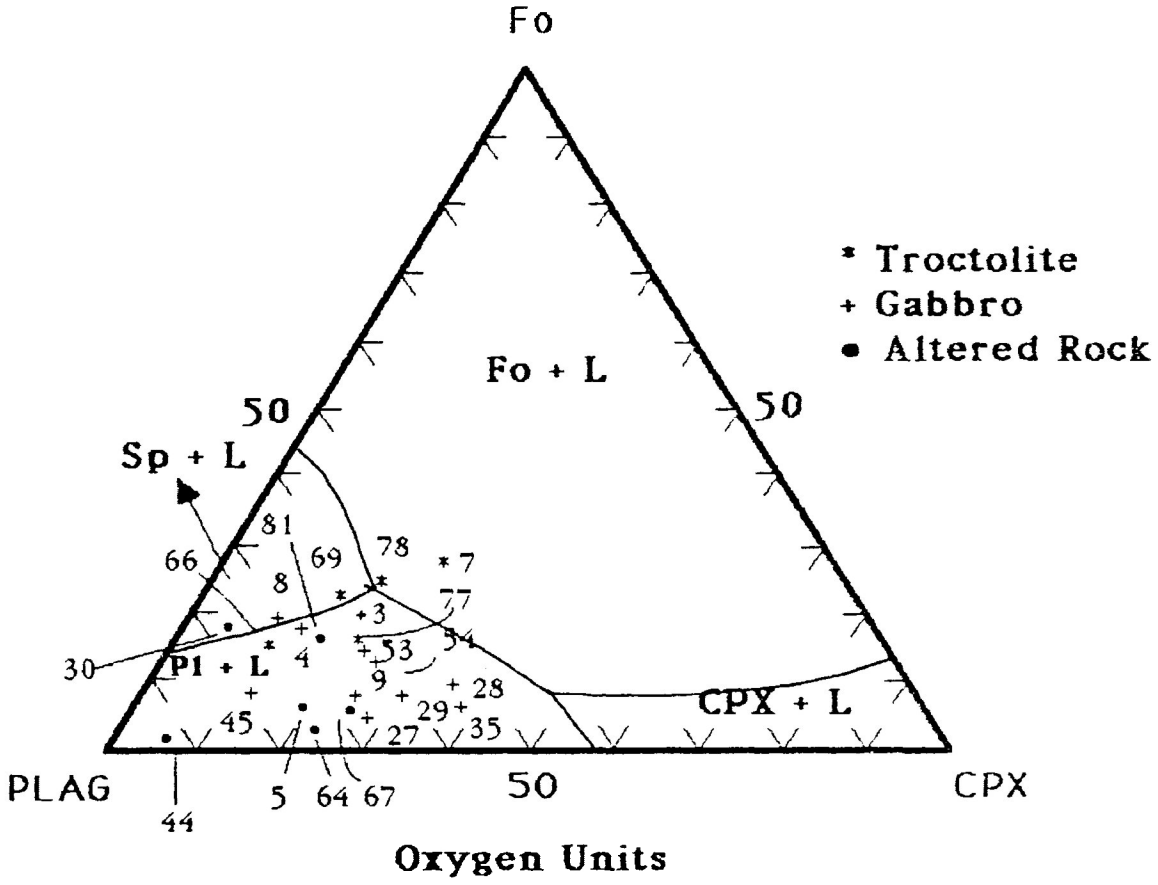

Figure 2.49 The system Fo-Pl-CPX with equivalent oxygen plots of the analysed GLI.

Symbols: * troctolite, + gabbro, and ■ altered rock

CHAPTER 3

Sulphide and Platinum-Group Element Mineralization

3.1 Introduction

The Geordie Lake Intrusion of the Coldwell complex hosts a variety of sulphides, Ag-, Ni-, and Pb-tellurides and platinum-group minerals (PGM). This chapter describes the style of the mineralization, the occurrence, texture, composition and paragenesis of the minerals, together with estimates of depositional conditions of the tellurides and PGM in terms of the partial pressure of Te_2 and S_2. The tellurides and PGM were identified using back-scattered electron imagery and energy dispersive X-ray spectrometry (EDS). This method is far more effective in recognition of these minerals than optical microscopy due to their small grain size. The accuracy of the EDS is given in Appendix II.

3.2 Style of Mineralization

Cu-sulphide mineralization in the GLI is dominated mainly by disseminated and rarely massive chalcopyrite. Scattered chalcopyrite grains of less than 1 mm across are present throughout the length of the cores but they do not host PGM. The coarser disseminated chalcopyrite grains are the most important style of mineralization because they host most of the PGM. The disseminated chalcopyrite zone or band varies from 5 cm to 5 m in

width but it is generally between 20 cm and 1 m in width. Visual estimation of the abundance of the disseminated chalcopyrite grains varies from 1 to 30 %, however, it generally falls between 10 and 15 %. In the four cores studied, disseminated mineralization becomes more apparent towards the basal sections of the GLI. The mineralization extends beyond the GLI-syenite contact and occurs as narrow bands (1 - 5 m in width) in the syenite. Melonite, hessite and altaite, but not PGM, were found in the syenite-hosted chalcopyrite grains. Bornite and pyrite are visible in many parts of the disseminated chalcopyrite bands, however, they do not form major mineralization zones. Disseminated chalcopyrite grains also grade into 1 to 3 cm thick massive chalcopyrite aggregates (Figure 3.1). This phenomenon is rare with only four examples occurring in the cores studied (samples G-30, 44, 48, and 55A). Two of these host PGM (G-30 and 55A). Tellurides and PGM occur as small grains ranging from < 5 μm across to 125 x 100 μm, but are generally between 5 and10 μm across. They are hosted mainly by chalcopyrite and rarely by bornite, magnetite or silicate minerals.

3.3 Descriptive Mineralogy and Mineral Chemistry

In this section, the order of description is sulphide, sulpharsenide and arsenide, telluride, PGM, and others. Palladium tellurides are included in the PGM section. Paragenetic relationships between the minerals are described where appropriate.

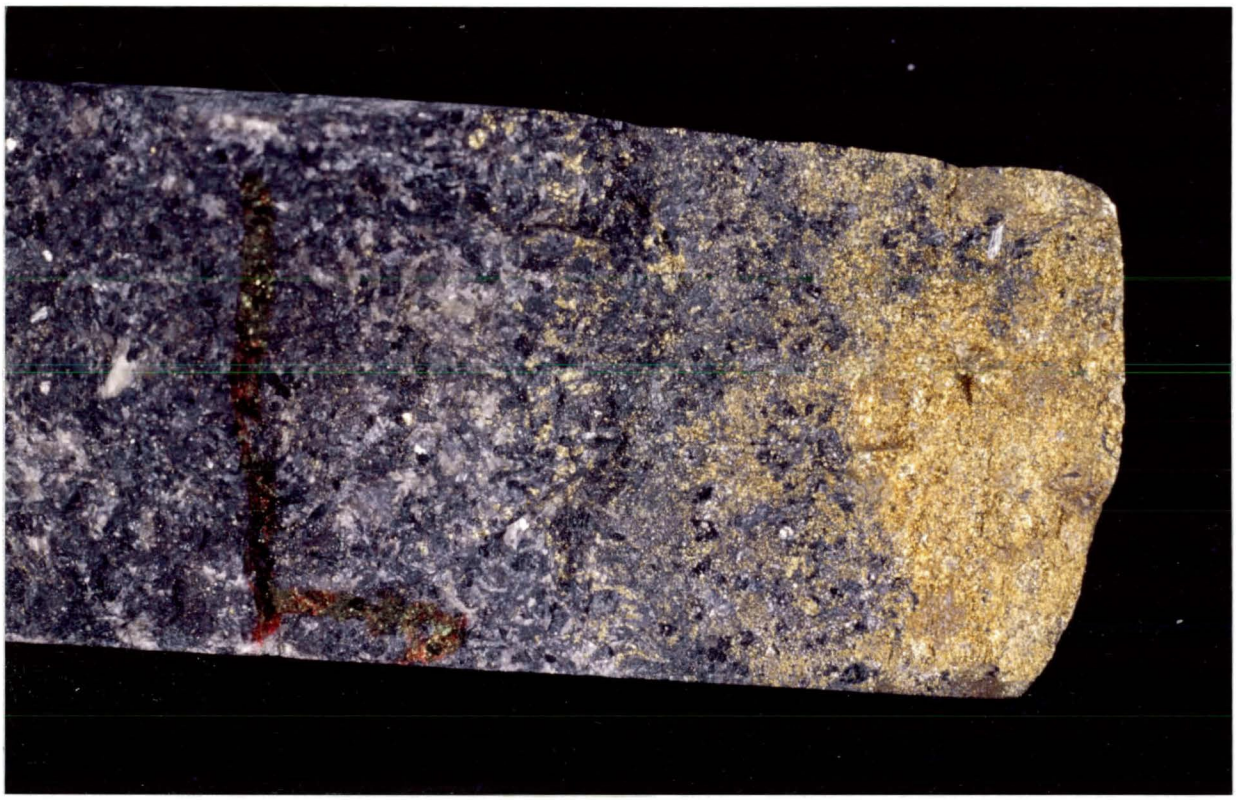

0 2 cm

Figure 3.1 The style of chalcopyrite mineralization (bright yellow) in a core slab from core 3 of the GLI, showing a gradual increase of the Cu-sulphide concentration from a few specks to massive aggregates. The host rock is an ophitic olivine gabbro (sample G-309).

3.3.1 Sulphides

Chalcopyrite ($CuFeS_2$) is the ubiquitous sulphide of the GLI. Its abundance varies throughout the cores with the greatest concentrations occurring in the basal sections. Petrographic examination shows that chalcopyrite is present as discrete grains, massive aggregates intergrown with pyrite (Figures 3.2A-D) and veinlets. Tiny chalcopyrite grains (< 1 mm across) are widely distributed throughout the unaltered gabbros. Chalcopyrite may be enclosed in feldspars and clinopyroxenes but rarely in magnetite.

Coarser-grained chalcopyrites are mostly disseminated, intergrown with and interstitial to the silicates. The grain boundaries between chalcopyrite and the silicates vary from planar to irregular. Disseminated chalcopyrite grains are also intergrown with secondary prismatic actinolites. Chalcopyrite occupies the interstices between ilmenite lamellae in magnetite that have undergone exsolution. The abundance of disseminated chalcopyrite ranges from 5 to 30 modal %, although,10 to 15 % is typical.

The comparatively rare massive chalcopyrite is hosted by the strongly altered rocks (samples 30, 44, 48, and 55A) and occurs as bands, between 1 and 3 cm in thickness. Massive chalcopyrite hosts melonite, hessite, altaite but rarely PGM (samples 30 and 55A only). Chalcopyrite veinlets in the cores are very narrow, approximately 2 mm in width. Massive chalcopyrite veinlets, between 1 and 2 cm in width, were found in the outcrop at Latvian Lake. The chalcopyrite veinlets do not contain any PGM but host a few tiny

Figure 3.2A A photomicrograph showing disseminated chalcopyrite mineralization in a gabbroic rock. The chalcopyrite grains occupy the interstices between silicate minerals, and silicate and magnetite (rounded crystals). Sample G-55B.

Figure 3.2B A chalcopyrite bleb showing a ragged grain boundary with the silicate minerals. The brown lamellae in the bleb are exsolved bornite. The small bright yellow grain (center left) is pyrite. Sample G-27

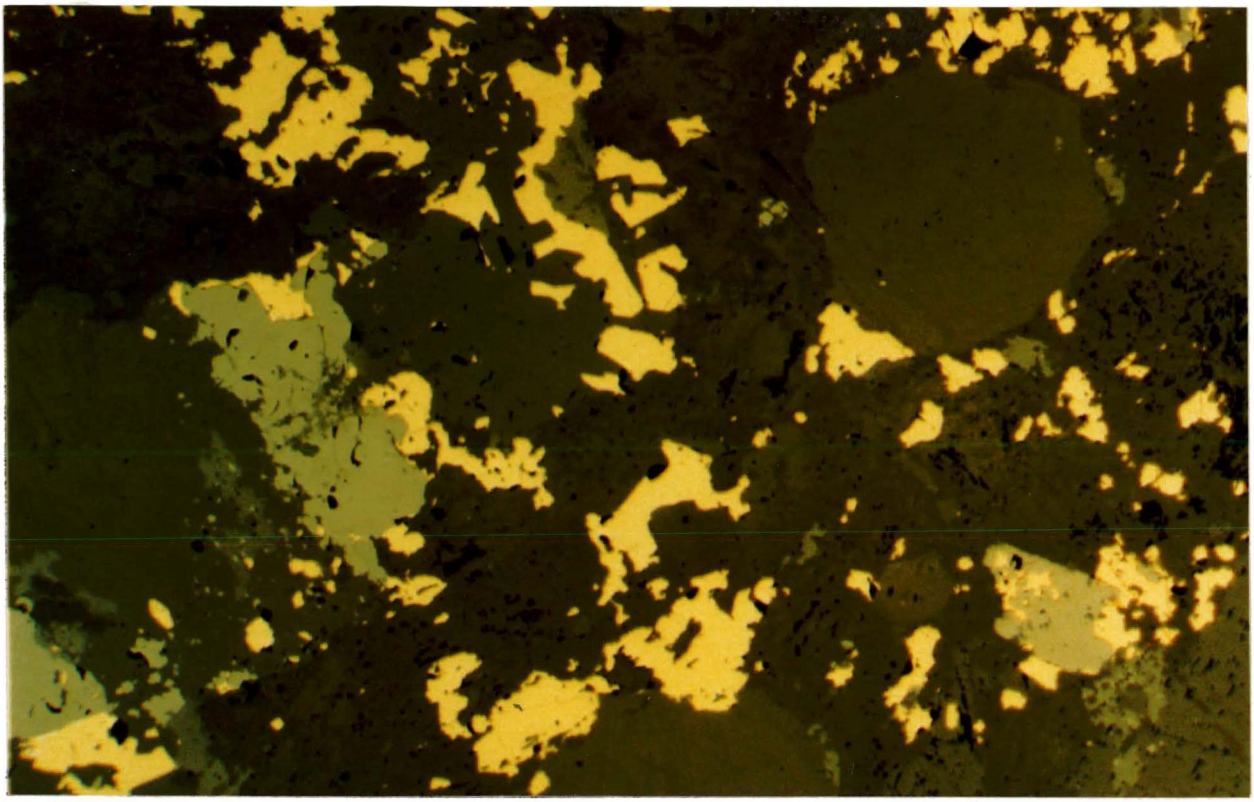
0
2mm

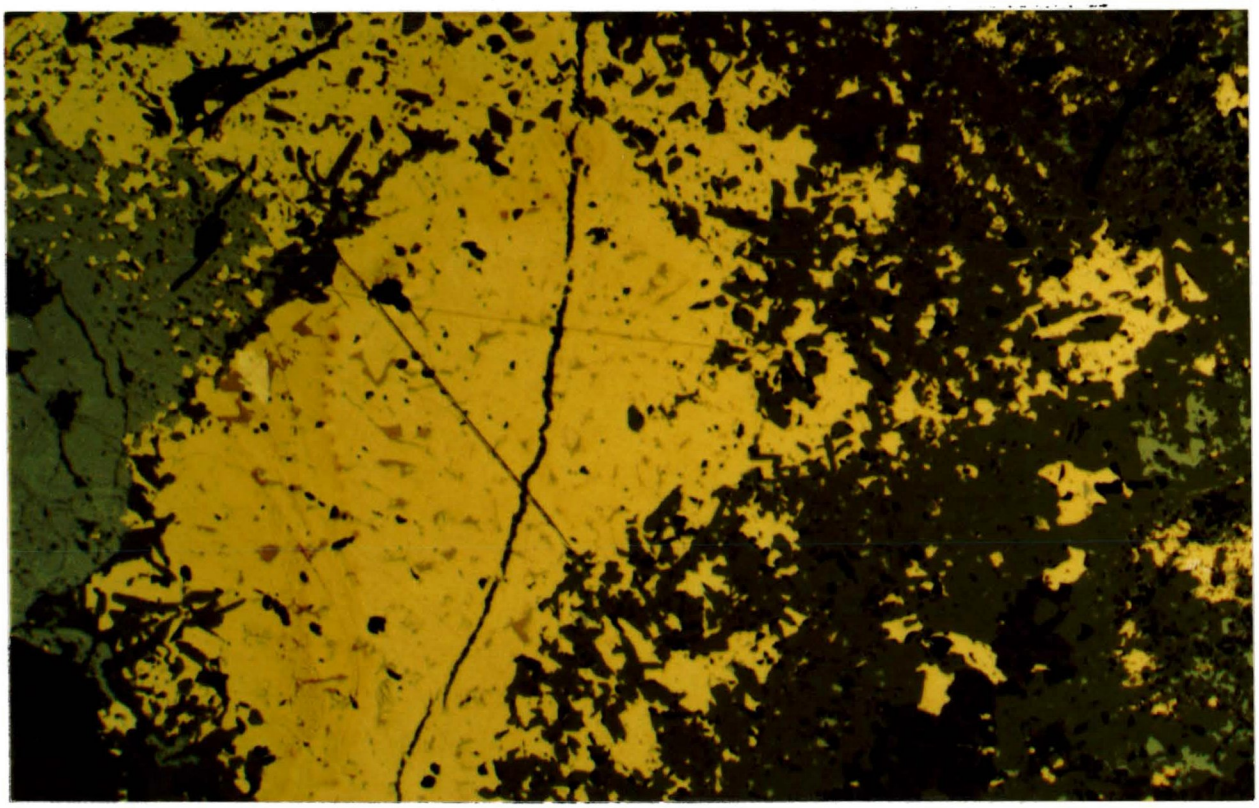
0
0.5mm

Figure 3.2C Lamellae-like chalcopyrite (CC) intergrown with anhedral pyrite (PY). This paragenesis is found only in sample 48A. Full bar= 20μm.

Figure 3.2D Chalcopyrite (white) occupying the interstices between ilmenite lamellae in a magnetite grain. The sharp boundary between the chalcopyrite and Fe-Ti oxide is indicative of infiling rather than replacement. Sample G-27. Full bar= 50 μm.

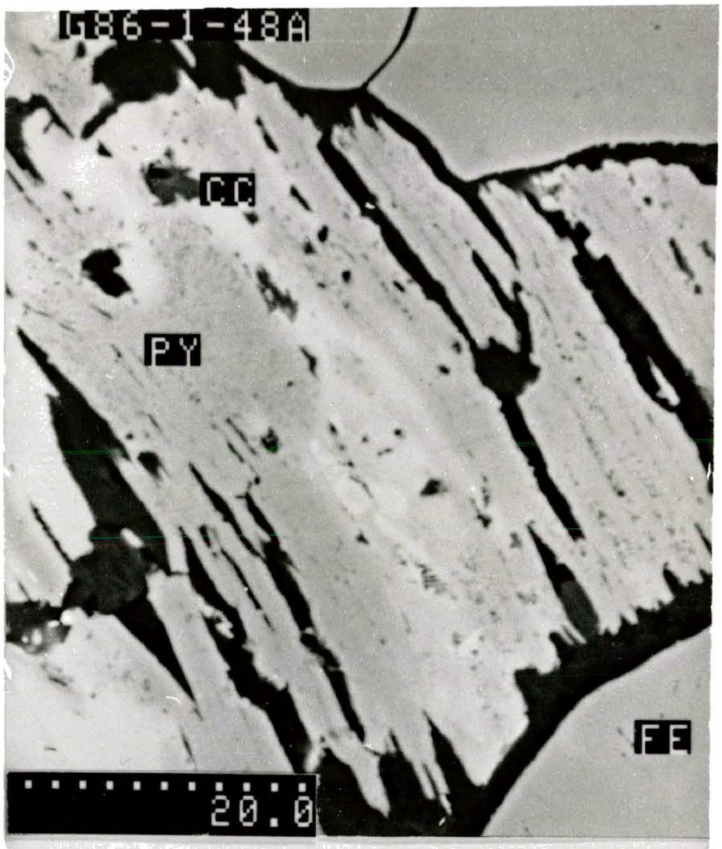
G86-1-48A
CC
PY
FE
20.0

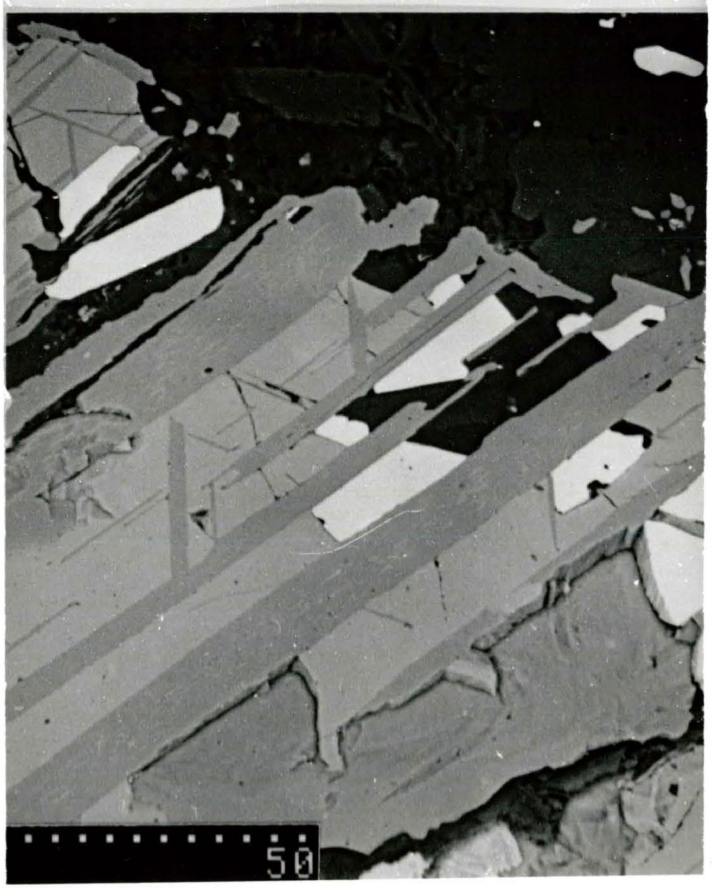
50

grains of hessite. Chalcopyrite intergrown with pyrite is rare (only in sample 48). The chalcopyrite lamellae (5-10 μm in width) are irregular (Figure 3.2C).

The observed textures of chalcopyrite indicate the following relative order of deposition:

1. the small chalcopyrite grains in the plagioclase represent early trapping of the sulphide melt during plagioclase crystallization;

2. the interstitial coarse-grained disseminated chalcopyrites were most likely precipitated following the crystallization of the primary magnetite;

3. chalcopyrite intergrown with secondary actinolite and infilling of magnetite occurred at subsolidus temperatures; and

4. final chalcopyrite mineralization formed veinlets.

Chalcopyrite compositions do not show any variation with respect to paragenesis and host rock type (Table 3.1). Minor elements (Zn, Co, Ni, and Mn) were not detected.

Bornite (Cu_5FeS_4) is rather common. It occurs as exsolved lamellae, as a replacement of chalcopyrite, and as interstitial grains in the sulphides. In the disseminated sulphides, the lamellae are generally very narrow and short, less than 0.5 mm in width and 2 mm in length. In the massive chalcopyrite, exsolved bornite lamellae form a vermicular/worm-like texture (Figure 3.3). Replacement bornites are common in the disseminated and

Table 3.1 Electron microprobe and energy dispersive (*) analyses of chalcopyrite from the GLI and Center I syenite (S)

Sample	14*		25		30+		31	
	Atm.%	Wt.%	Atm.%	Wt.%	Atm.%	Wt.%	Atm.%	Wt.%
Cu	25.85	35.33	24.78	34.42	25.15	34.71	24.68	34.20
Fe	24.77	29.75	24.76	30.09	24.73	29.87	24.53	29.74
S	49.37	34.04	50.47	35.05	50.12	34.59	50.76	35.17
TOTAL Wt%		99.12		99.56		99.17		99.11

Sample	34		35		37		38	
	Atm.%	Wt.%	Atm.%	Wt.%	Atm.%	Wt.%	Atm.%	Wt.%
Cu	24.44	34.07	24.13	33.47	24.41	34.05	24.23	33.64
Fe	25.17	30.69	24.51	29.75	24.84	30.33	25.43	30.89
S	50.39	35.11	51.36	35.63	50.75	35.40	50.29	34.90
TOTAL Wt%		99.86		98.85		99.77		99.50

Sample	43		44+		47*		48A	
	Atm.%	Wt.%	Atm.%	Wt.%	Atm.%	Wt.%	Atm.%	Wt.%
Cu	24.38	34.23	24.06	33.93	24.81	34.45	24.86	34.84
Fe	24.29	29.84	24.35	30.04	24.52	29.92	24.58	30.15
S	51.33	36.03	51.59	36.36	50.41	35.32	50.56	35.42
TOTAL Wt%		100.09		100.32		100.02		100.40

Sample	48B*		50*		51		55B	
	Atm.%	Wt.%	Atm.%	Wt.%	Atm.%	Wt.%	Atm.%	Wt.%
Cu	24.64	34.14	24.05	33.26	25.24	35.11	24.29	34.08
Fe	24.63	30.00	25.11	30.52	24.47	29.79	24.78	30.42
S	50.73	35.47	50.54	35.26	50.26	34.96	50.94	35.74
TOTAL Wt%		99.62		99.41		99.91		100.24

Sample	56*		60 (S)		80*		302**	
	Atm.%	Wt.%	Atm.%	Wt.%	Atm.%	Wt.%	Atm.%	Wt.%
Cu	23.77	33.55	24.58	33.98	25.10	34.78	23.97	33.24
Fe	24.48	30.36	24.99	30.23	24.44	29.77	25.43	30.85
S	51.75	36.84	50.42	34.85	50.46	35.29	50.60	35.08
TOTAL Wt%		100.75		99.06		99.84		99.17

Sample	CW-3++	
	Atm.%	Wt.%
Composition		
Cu	24.84	34.68
Fe	25.02	30.56
S	50.14	35.00
TOTAL Wt%		100.23

\+ Massive chalcopyrite
++ Chalcopyrite veinlet
** Small grains, PGM-free host rock
Others are disseminated chalcopyrites

Figure 3.3 Exsolved bornite lamellae exhibiting vermicular/ worm-like texture. The euhedral grey crystals are magnetite. The light brown patches in the magnetite grains are residuals of carbon coating. Sample CW-1.

Figure 3.4A Subhedral pyrite grains in chalcopyrite showing sutured grain boundaries. The silicate mineral (dark brown) is actinolite. Sample G-55B.

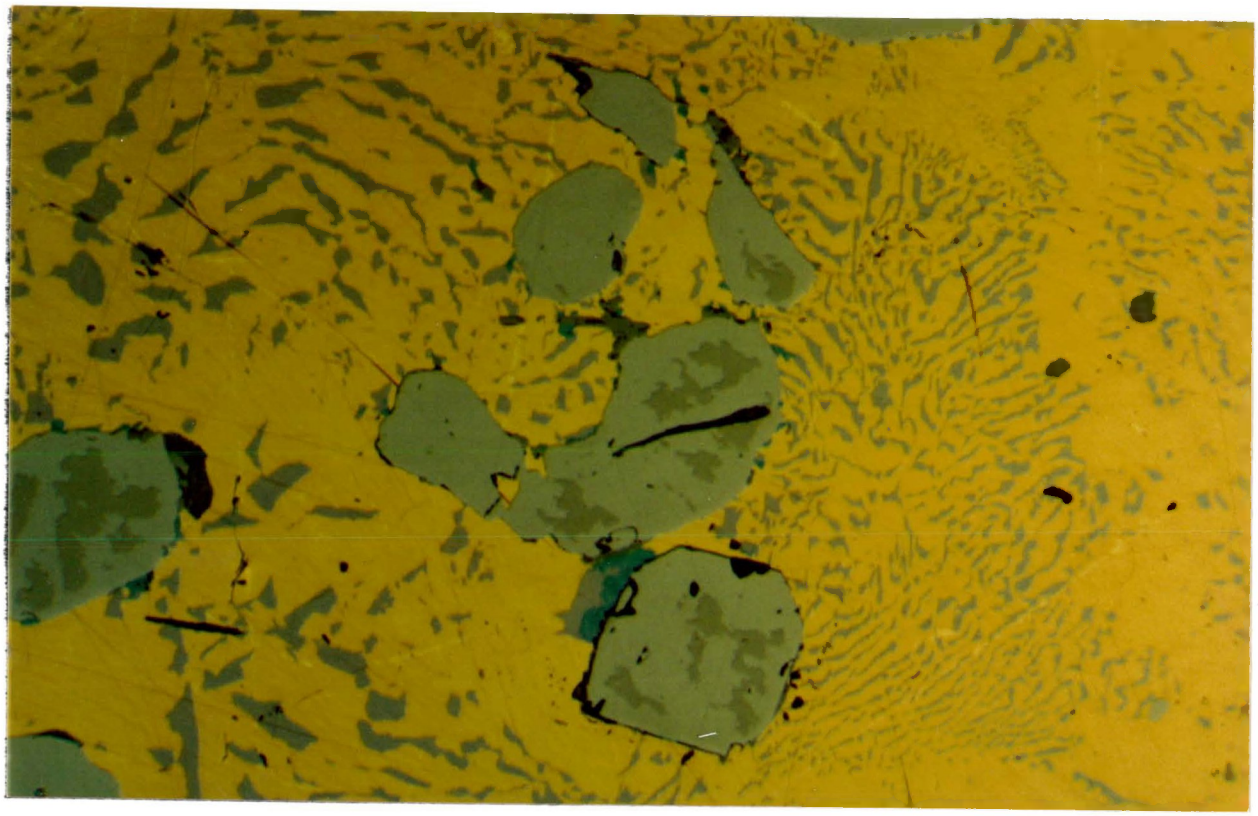

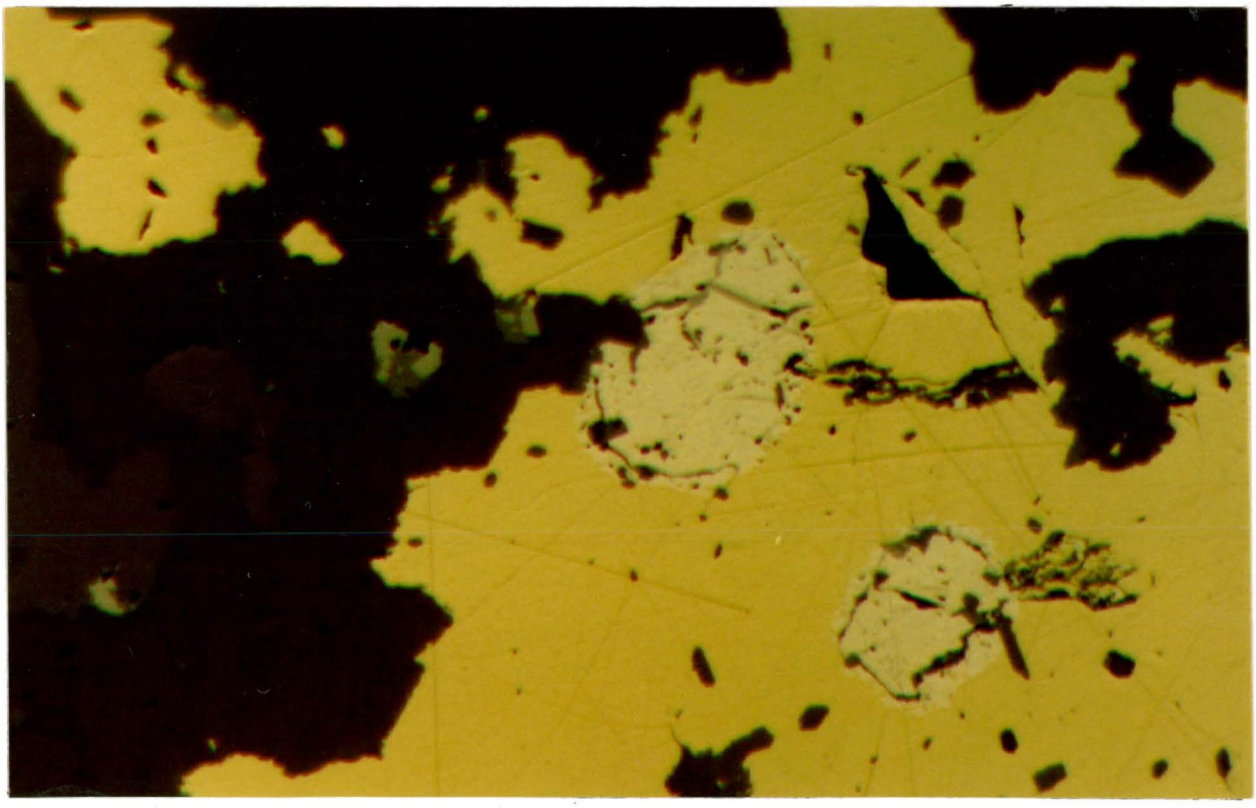

0 4mm

massive chalcopyrite. The replacement occurs at the periphery of the host mineral and along the grain boundary between chalcopyrite and PGM (Figures 3.15A-B). Interstitial bornites are fine-grained (< 1 mm across) and uncommon (1% modal). It is difficult to ascertain whether these bornites are primary or secondary phases that completely pseudomorph the chalcopyrite. Bornite is replaced by niccolite (Figure 3.8B).

Bornite composition (Table 3.2) is constant regardless of paragenesis. Zn, Co, Ni and Mn were not detected.

Pyrite (FeS_2) occurs in all rock types of the GLI and Center I syenite. It is comparatively less common than chalcopyrite and bornite and is observed only in nine out of twenty-nine polished thin sections. Pyrite occurs as anhedral to subhedral inclusions (15 μm to 2 mm across) in chalcopyrite (Figures 3.4A and C), as rod-like crystals in a coarse-grained olivine (Figure 3.4B), and as veinlets (Figure 3.4D). The pyrite inclusions have sutured boundaries with the host chalcopyrite and adjacent silicate mineral but they are not exsolved phases. One pyrite inclusion was found to be intergrown with exsolved bornite. Pyrite veinlets occur in a chalcopyrite grain in sample G-48, and range from approximately 0.05 to 0.1 mm in width. Pyrites in the three modes of occurrence do not contain any exsolved phases.

The paragenetic sequence of pyrite is difficult to determine, since subhedral/euhedral pyrites can occur at any stage of deposition (Craig and

Table 3.2 Electron microprobe and EDS (*) analyses of bornite.

Sample	14*		25		35		51	
	Atm.%	Wt.%	Atm.%	Wt.%	Atm.%	Wt.%	Atm.%	Wt.%
Cu	51.54	64.13	46.09	59.65	47.37	60.42	49.70	62.94
Fe	9.90	10.83	11.40	12.92	10.82	12.08	9.89	10.95
S	38.56	24.21	42.50	27.50	41.81	26.66	40.32	25.53
Zn							0.08	0.10
TOTAL Wt%		99.17		100.07		99.16		99.52

Sample	56*		80*		CW-3	
	Atm.%	Wt.%	Atm.%	Wt.%	Atm.%	Wt.%
Cu	48.11	61.84	49.87	63.34	48.74	63.38
Fe	10.35	11.69	10.06	11.23	10.17	11.57
S	41.54	26.94	40.07	25.68	41.02	26.67
TOTAL Wt%		100.47		100.25		101.62

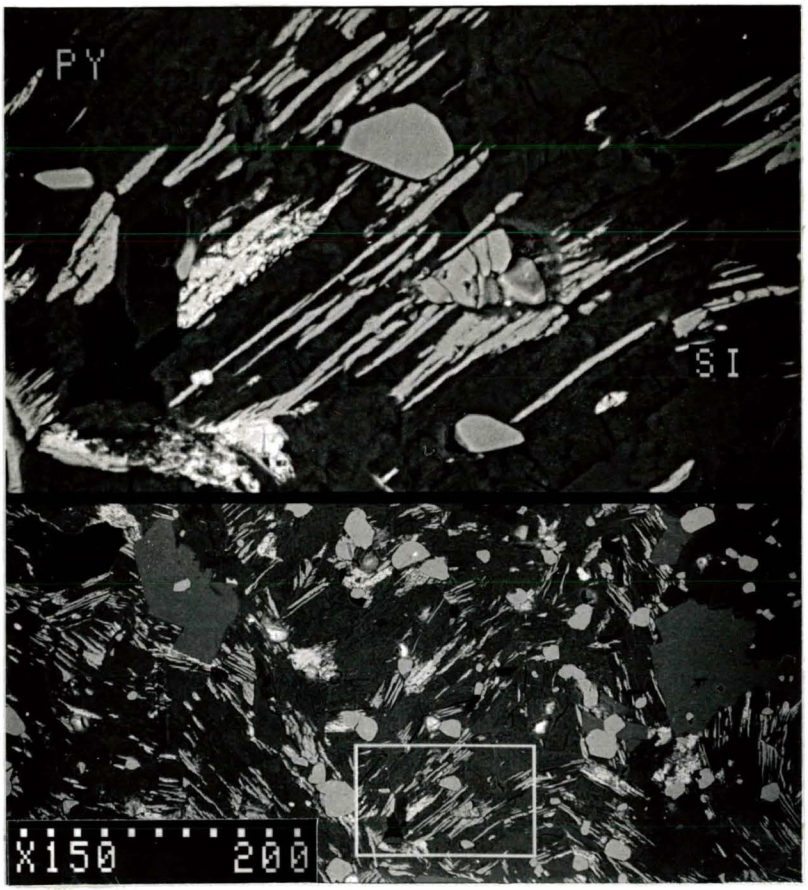

Figure 3.4B Rod-like pyrite lamellae in serpentinized olivine. The subrounded crystals are magnetite. Sample 42. Full bar scale in µm.

Figure 3.4C Anhedral pyrite grains intergrown with exsolved bornite (dark brown) in massive chalcopyrite. The grey subrounded crystals are magnetite. Sample CW-1.

Figure 3.4D Pyrite veinlets cutting through massive chalcopyrite. The euhedral to subhedral grains are magnetite. A narrow and discontinued pyrite veinlet (left corner) partially filled the crack in the chalcopyrite. Sample G-48.

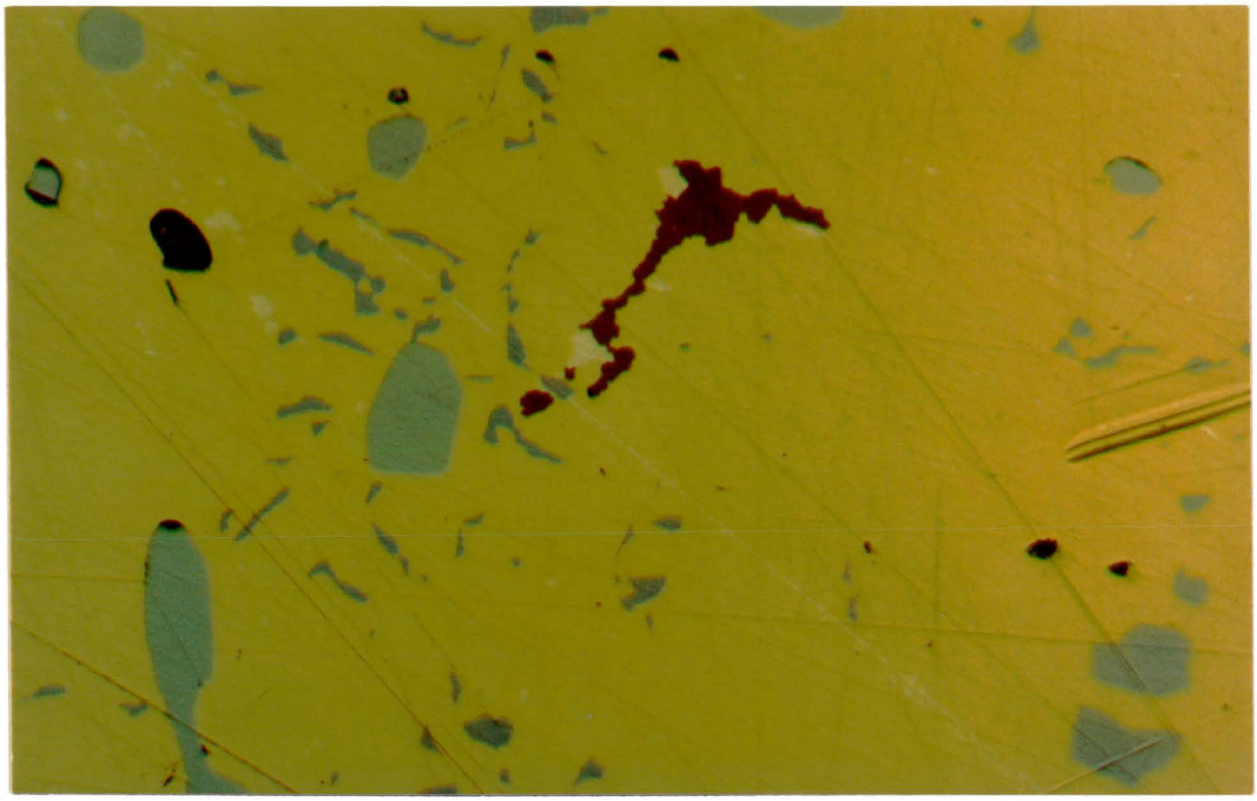

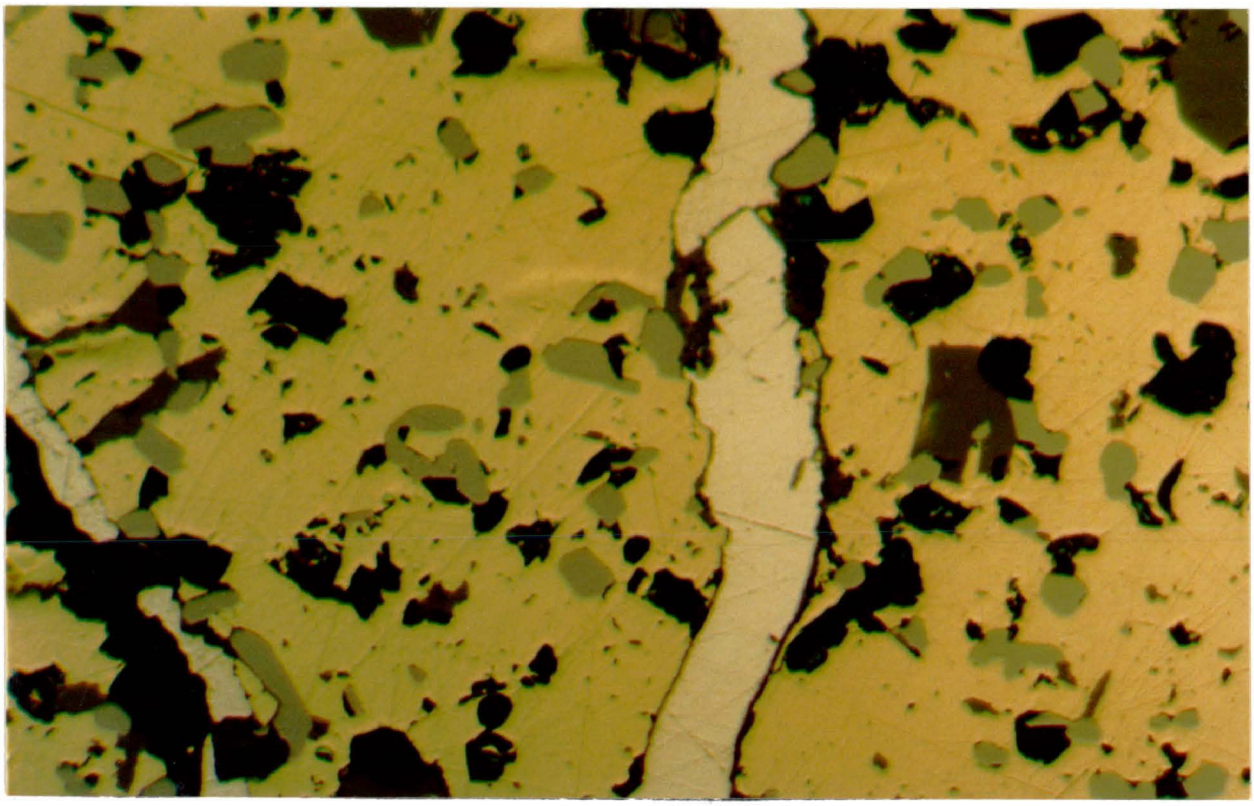

0 0.5mm

Vaughan, 1981). The last pyrite forms veinlets cutting chalcopyrite masses.

Pyrite compositions (Table 3.3) show variation in the amounts of substitution of Fe by Ni, Mn and Zn, and rarely by Co, with the exception of those occurring in the massive sulphides (samples 48A and B) and in the GLI-syenite mixed rock (sample 60) which are pure FeS_2.

Galena (PbS) is ubiquitous and primarily occurs as tiny anhedral inclusions in chalcopyrite blebs. It is commonly found replacing hessite and melonite (Figures 3.5A-B). These observations indicate that galena is a late crystallizing sulphide. The composition of galena was not determined quantitatively. Energy dispersive microanalysis did not indicate the presence of silver.

Siegenite $(Co,Ni)_3S_4$, Millerite (NiS), Sphalerite (ZnS), and Chalcocite (Cu_2S) are minor sulphides which were rarely observed (1-6 samples). Their compositions are given in Table 3.4.

Siegenite is present only in troctolite (22) and altered gabbro (30, 36, 48A and 55). The rarity is perhaps more apparent rather than real because of the similar appearance of the mineral to pyrite in the back scattered images. Siegenite occurs as discrete anhedral grains forming a granular texture with millerite and chalcopyrite (Figure 3.6A), and in some instances contains exsolved pentlandites (Figure 3.6B). The compositions of siegenite agree with the ideal formula, $(Co, Ni)_3S_4$.

Table 3.3 Electron microprobe and energy dispersive spectrometry (*) analyses of pyrites from the GLI
All analyses included Zn, Co, Mn, and Ni

Sample	37		37		37		38	
	Atm.%	Wt.%	Atm.%	Wt.%	Atm.%	Wt.%	Atm.%	Wt.%
Fe	33.01	46.57	27.53	38.59	28.11	38.63	33.31	46.53
S	66.99	54.01	67.08	53.73	66.70	52.38	66.69	53.24
Co					0.20	0.28		
Mn								
Ni			5.39	7.96	5.00	7.24		
TOTAL Wt%		100.58		100.27		98.53		99.76

Sample	47*		48A		48B*		50*	
	Atm.%	Wt.%	Atm.%	Wt.%	Atm.%	Wt.%	Atm.%	Wt.%
Fe	32.56	45.12	33.08	46.78	31.78	44.42	32.84	46.63
S	67.10	53.40	66.92	54.06	67.92	54.51	66.60	54.29
Zn							0.34	0.56
Mn							0.21	0.30
Ni					0.31	0.45		
TOTAL Wt%		99.02		100.83		99.38		101.77

Sample	55B		60	
	Atm.%	Wt.%	Atm.%	Wt.%
Fe	32.55	46.43	33.47	47.20
S	67.45	54.98	66.53	53.61
TOTAL Wt%		101.40		100.81

Figure 3.5A-B Back-scattered electron images of galena replacement of hessite (top) and melonite (bottom). Full scale bar in μm.

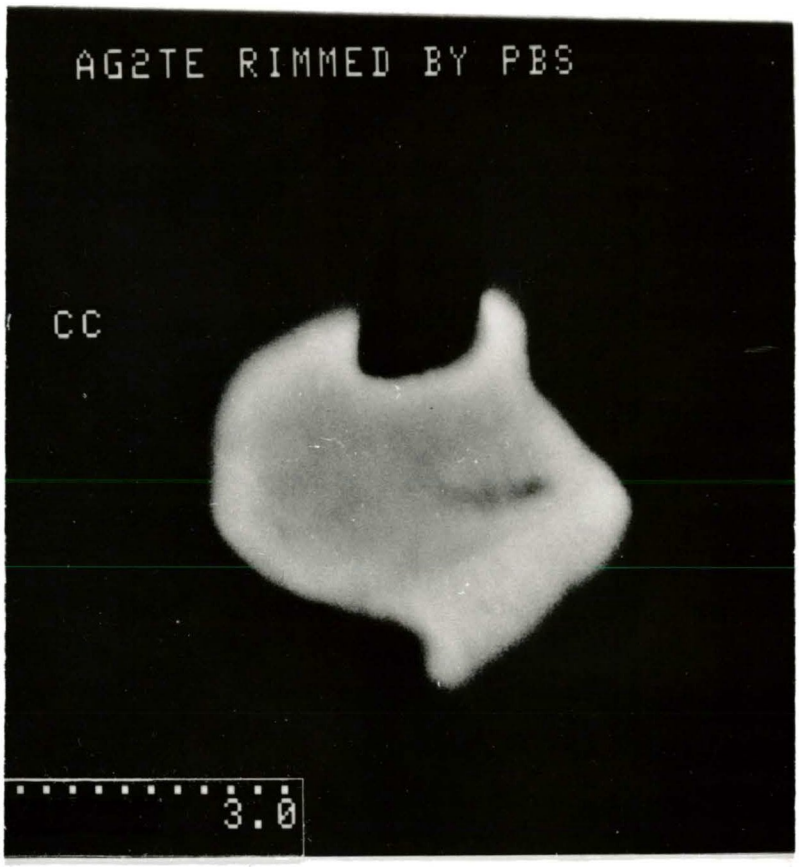
AG2TE RIMMED BY PBS
CC
3.0

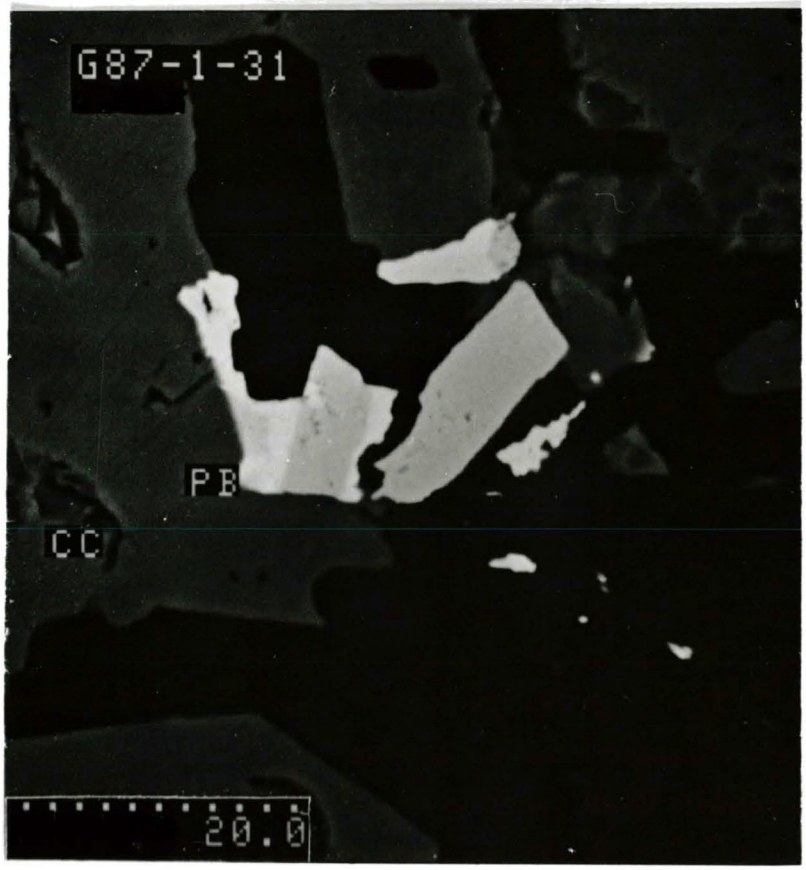
G87-1-31
PB
CC
20.0

Table 3.4 Electron microprobe and energy dispersive spectrometry (*) analyses of siegenite, millerite, sphalerite and chalcocite from the GLI

Siegenite

Sample	22*		55B	
	Atm%	Wt.%	Atm%	Wt.%
Co	21.22	28.86	23.55	32.5
Ni	20.34	27.56	17.72	24.45
S	57.4	42.21	57.96	43.38
Fe	1.41	1.81	0.77	1
TOTAL Wt%		100.44		101.33

Millerite

Sample	37		43	
	Atm.%	wt.%	Atm.%	wt.%
Ni	26.75	36.83	47.59	61.92
S	56.95	42.53	50.05	35.32
Fe	10.18	13.3	0.22	0.28
Co	6.11	8.42	1.81	2.35
Cu			0.33	0.46
TOTAL		101.08		100.32

Sphalerite

Sample	30		37		48A*	
	Atm%	wt%	Atm%	wt%	Atm%	wt%
Zn	40.50	54.79	40.26	55.28	41.21	56.93
S	52.38	34.89	51.91	35.09	50.80	34.42
Fe	3.53	4.11	7.78	9.20	7.99	9.43
Cu	3.59	4.78				
TOTAL		98.56		99.62		100.77

Chalcocite

Sample	CW-1					
	Atm.%	Wt.%	Atm.%	Wt.%	Atm.%	Wt.%
Cu	64	78.2	63.78	77.64	63.64	77.71
S	35.9	21.93	36.22	22.05	35.95	21.95
Fe	0.1	0.11			0.41	0.44
TOTAL		100.24		99.68		100.09

Figure 3.6A(left) Siegenite (right, CoNiS) with exsolved pentlandite, co-existing with millerite (NiS) and chalcopyrite (CC). Sample G-48A.

Figure 3.6B(Right) Siegenite with exsolved pentlandite which displays crystallographic orientation.

Figure 3.7A (Left) Euhedral cobaltite showing an octahedral habit on the margin of chalcopyrite (CC). Sample G-30.

Figure 3.7B (Right) Cobaltite (CT) replacement of chalcopyrite (CC). Sample G-30.

Full scale bar in μm.

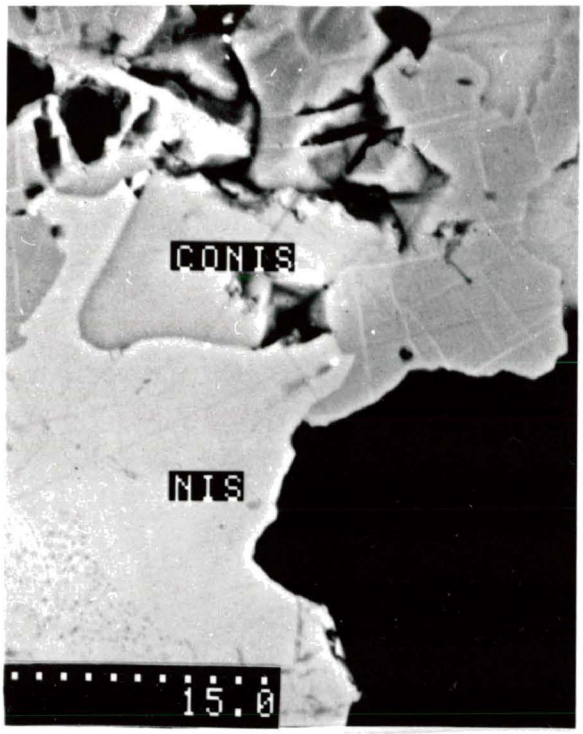
CONIS
NIS
15.0

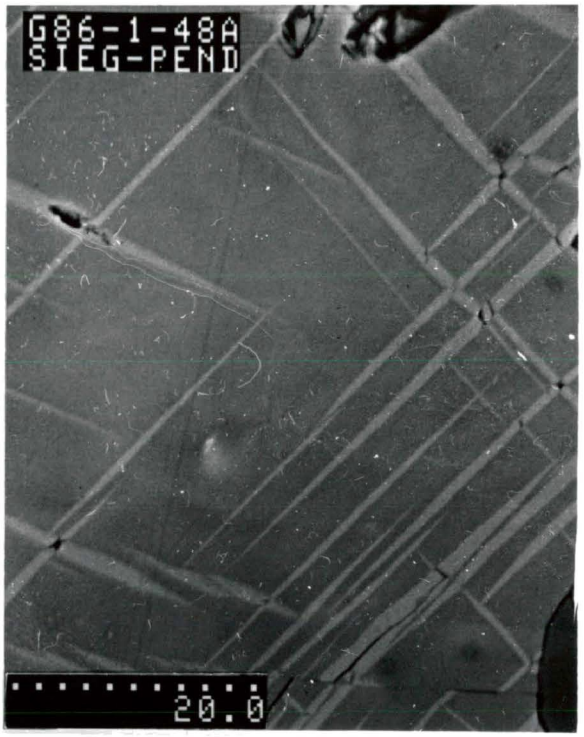
G86-1-48A
SIEG-PEND
20.0

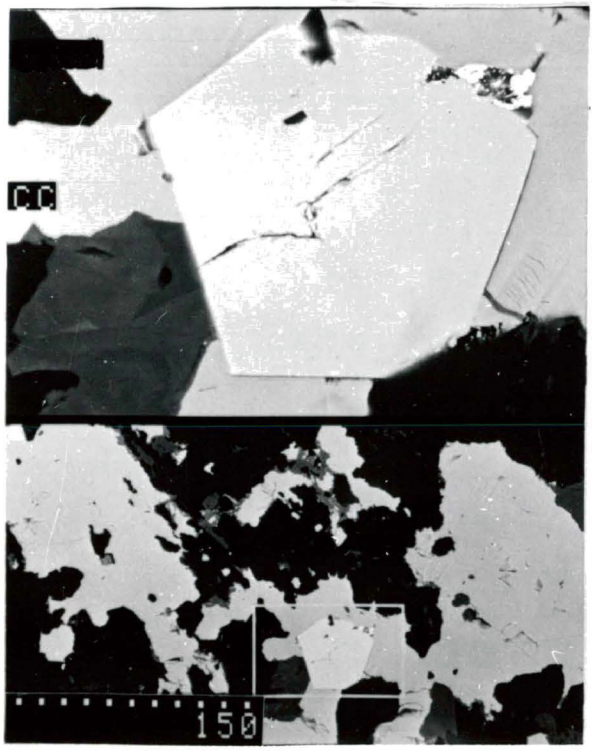
CC
150


CC
CT
15.0

Millerite (NiS) occurs as tiny inclusions in chalcopyrite blebs, as anhedral grains intergrown with chalcopyrite (Figure 3.6A), and as a fracture-filling phase in chalcopyrite. Sample 43 shows minor substitutions of Ni by Fe, Co, and Cu, whereas in sample 37 major substitution of Ni by Fe and Co has occurred.

Sphalerite (ZnS) is present as tiny subhedral grains associated with chalcopyrite. The compositions of the ZnS grains in the massive chalcopyrite show significant replacement of Zn by Fe.

Chalcocite (Cu_2S) occurs as lamellae, only in the massive chalcopyrite veinlets at the GLI outcrop on Latvian Lake. Analyses of Cu_2S show minor substitution of Cu by Fe. Cu_2S is a common hypogene and supergene copper sulphide mineral (Craig, 1982). The absence of Cu_2S in the subsurface massive chalcopyrite and the sample location of the observed Cu_2S indicate that it is a product of supergene processes.

3.3.2 Sulpharsenide and Arsenide

Cobaltite (CoAsS) and Niccolite (NiAs) are the only sulpharsenide and arsenide observed and are present in 8 samples. Cobaltite occurs as discrete inclusions in chalcopyrite, euhedral crystals cutting grain boundaries with chalcopyrite and secondary amphibole, and as a replacement of chalcopyrite (Figures 3.7A-B). Cobaltite inclusions are

Figure 3.8A A niccolite (NC) grain showing complex intergrowth with cobaltite (CB), chalcopyrite (CP), electrum (AuAg), and galena (GL). SC: silicate mineral. Sample G-30.

Figure 3.8B Niccolite replacement of chalcopyrite and bornite (BR). A small palladium antimonide (Pd-Sb) occurs at the margin of chalcopyrite. Sample G-20.

Full bar scale in μm.


X1.00K 30

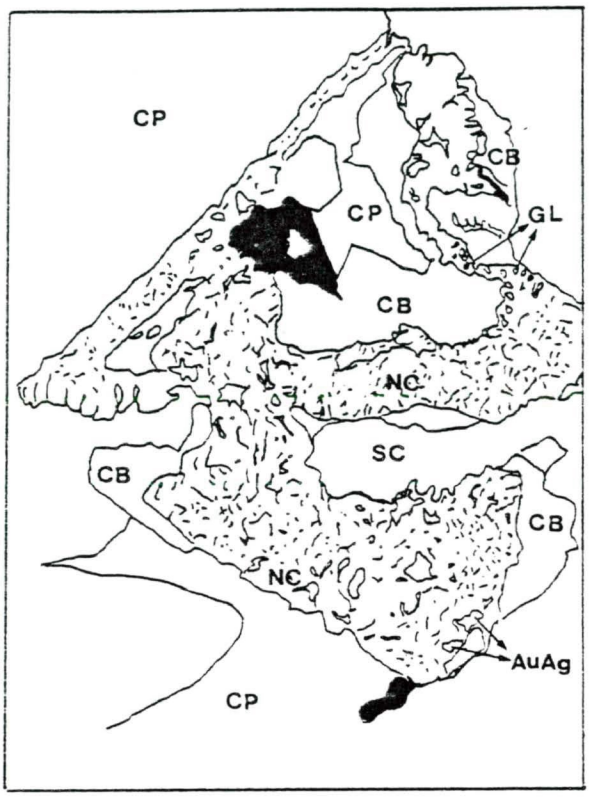
CP
CB
CP
GL
CB
NC
SC
CB
CB
NC
AuAg
CP

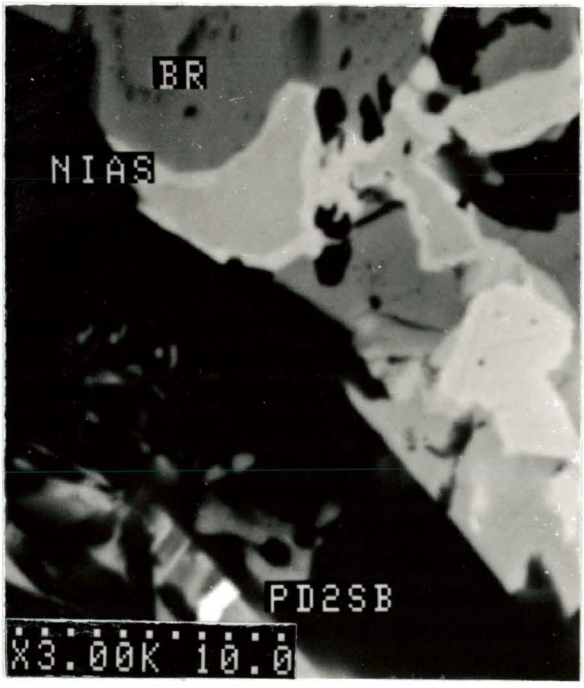
BR
NIAS
PD2SB
X3.00K 10.0

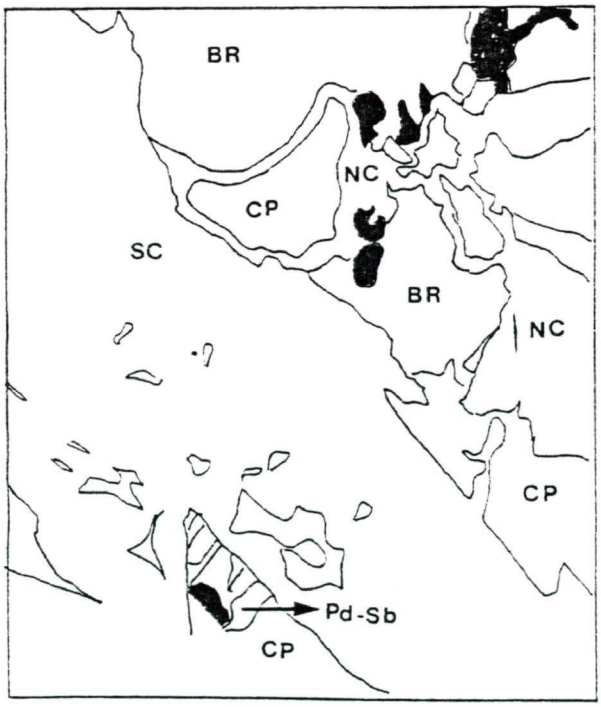
BR
NC
CP
SC
BR
NC
CP
Pd-Sb
CP

small, ranging from 10 to 20 μm in width. The euhedral cobaltite exhibits an octahedral habit (50 μm across) and occurs at grain boundaries between chalcopyrite and actinolite. Figure 3.15D shows a small subhedral cobaltite crystal (10 μm) intergrown with kotulskite and hessite. The compositions of cobaltites (Table 3.5) show significant substitution of Co by Fe and Ni.

Niccolite occurs as discrete grains between magnetite and amphibole crystals, as small inclusions in, and a replacement phase of, chalcopyrite, and as discontinuous veinlets in magnetites. The discrete niccolite grains are anhedral (10 to 15 μm across) and present only in sample G-22. One of these grains is rimmed by a palladium nickel arsenide. Niccolite inclusions in chalcopyrite are small, approximately from 5 to 10 μm across. A relatively coarser-grained niccolite in sample G-30 (50 μm across) forms complex relationships with chalcopyrite, cobaltite, electrum, galena, and actinolite (Figure 3.8A) making it difficult to ascertain the paragenetic sequence for these minerals. Niccolite is found to replace chalcopyrite and possibly bornite (Figure 3.8B). Only one analysis of niccolite (Table 3.6) was obtained because the majority of niccolite grains are very small. The composition shows minor substitutions of As by Fe, Zn, Co, and S.

3.3.3 Tellurides

Hessite ($AgTe_2$) is ubiquitous and more than thirty discrete grains of hessite have been found in samples 26 and 27. It generally occurs

Tables 3.5 and 3.6 Electron microprobe analyses of cobaltite and niccolite from the GLI

Cobaltite

Sample	30		37		55	
	Atm.%	wt.%	Atm.%	wt.%	Atm.%	wt.%
Co	21.57	22.87	21.47	23.03	24.00	25.98
As	32.73	44.12	32.09	48.39	33.56	46.17
S	33.00	19.05	35.47	18.68	34.00	19.97
Fe	4.15	4.17	3.34	3.40	3.26	3.35
Ni	8.53	9.00	7.36	7.90	5.17	5.60
TOTAL		99.21		101.40		101.06

Niccolite

Sample	51	
	Atm.%	wt.%
Ni	52.66	46.84
As	41.82	47.29
Fe	3.85	3.25
Zn	0.19	0.18
Co	1.15	1
S	0.11	0.06
TOTAL		98.62

as fine-grained (5 - 10 μm) crystals in disseminated and massive chalcopyrite (Figure 3.9), silicate and bornite. The coarsest hessite (17 x 17 μm) exhibits an octahedral habit and co-exists with chalcopyrite and silicate minerals. This hessite also penetrates the interstices between the sulphide and silicate. Hessite may be intergrown with palladium antimonide (Figure 3.19) and is replaced by galena (Figure 3.5A).

The composition of the hessite is essentially pure Ag_2Te (Table 3.7A) with minor substitution of Ag by Ni and Co, and of Te by As and Sb. Numerous hessites in massive sulphide veinlets were not analysed due to their small grain size.

An unnamed silver telluride was found in samples 46 and 62, and occurs as discrete grains (4 x 2 μm) in a chalcopyrite. The mineral has the composition Ag_3Te_2 (Table 3.7B). This mineral has only previously been reported by Chizhikov and Shchastlivyi (1970), who indicated that it is formed by a peritectic reaction in the system Te-Ag.

Melonite ($NiTe_2$) is the second most abundant telluride and occurs as discrete grains in pyroxene, altered olivine, chalcopyrite, and bornite (Figures 3.10A-C). In the silicate minerals, melonite varies from small equant (5 -10 μm) to prismatic grains (4 x 15 μm). Some melonites are intergrown with chalcopyrite grains. In the disseminated sulphides, coarse-grained melonite (75 x 100 μm) occurs as subhedral to euhedral crystals forming sharp grain boundaries with chalcopyrite blebs

Figure 3.9 Back-scattered images of fine-grained (top, white) and coarse-grained subhedral (bottom) crystals of hessite. Both photomicropgraphs show that the hessites form on the margins of chalcopyrite (CC). The coarse-grained hessite also fills the grain boundaries between chalcopyrite (grey) and silicate (black) minerals. Samples G-55B (top) and G-28 (bottom). Full scale bar in μm.

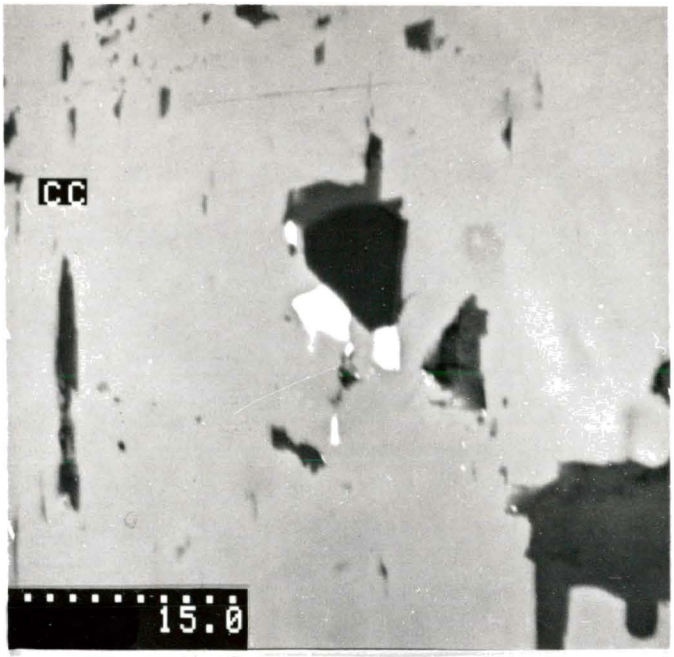
CC
15.0

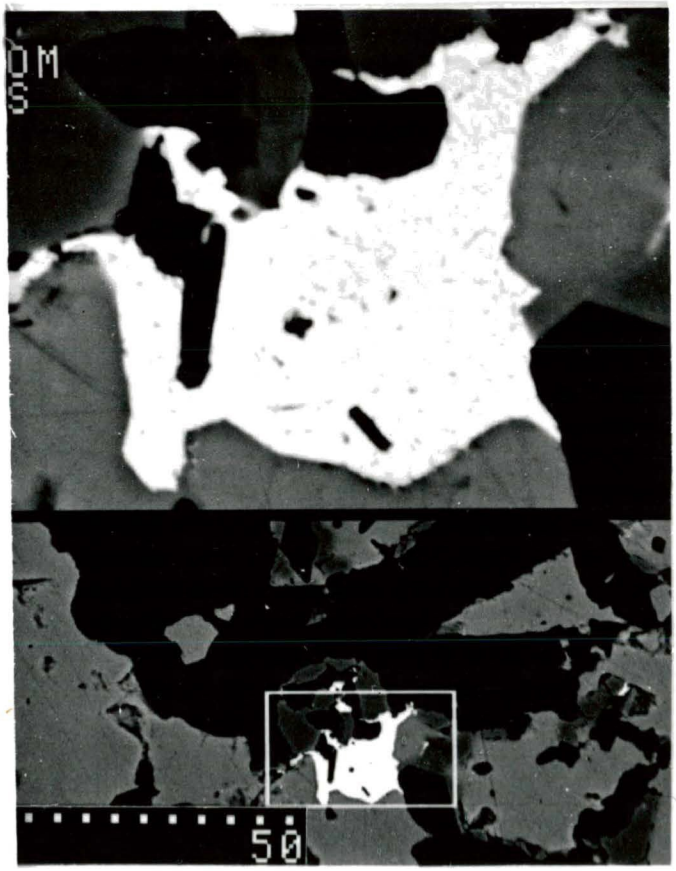
OM
S
50

Table 3.7A EDS analyses of hessite from the GLI
Stoichiometry (Wt.%): Ag: 62.86, Te: 37.14

Sample	26		28		30		30		37	
	Atm.%	Wt.%	Atm.%	Wt.%	Atm.%	Wt.%	Atm.%	Wt.%	Atm.%	Wt.%
Ag	65.96	62.37	64.9	60.66	67.09	61.98	65.49	62.63	66.63	63.26
Te	34.04	38.08	32.3	35.71	32.91	35.96	33.82	38.26	33.37	37.48
Sb			1.17	1.23						
As			1.63	1.06						
Co							0.69	0.36		
TOTAL Wt%		100.45		98.66		97.93		101.26		100.74

Sample	46		50		55		66	
	Atm.%	Wt.%	Atm.%	Wt.%	Atm.%	Wt.%	Atm.%	Wt.%
Ag	63.80	59.85	65.28	61.69	67.01	63.71	65.32	61.81
Te	35.25	39.11	33.56	37.52	32.99	37.10	33.69	37.72
Ni			1.14	0.59				
As	0.95	0.62					0.53	0.35
Co							0.46	0.24
TOTAL Wt%		99.59		99.80		100.81		100.12

Table 3.7B EDS analyses of Ag3Te2
Stoichiometry (Wt %): Ag: 55.91, Te: 44.09

Sample	46		62	
	Atm. %	Wt. %	Atm. %	Wt. %
Ag	60.18	55.61	61.29	57.28
Te	39.82	43.53	38.71	42.79
TOTAL Wt%		99.14		100.07

Figure 3.10 Back-scattered electron images of melonite showing different modes of occurrence; prismatic (top left) and euhedral to subhedral grains forming a granular texture with subrounded magnetite grains (top right). The melonite forms between chalcopyrite (CC)-silicate (black) boundary. Sample G-48A (left top) and G-31 (middle and bottom).

Full scale bar in µm.

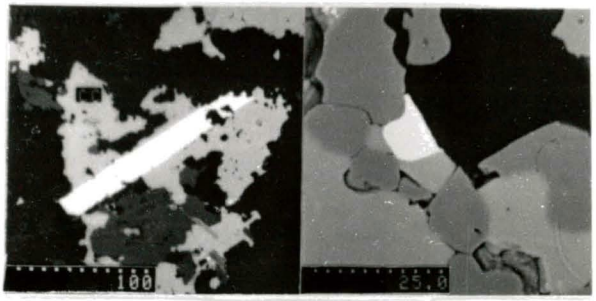
100
25.0

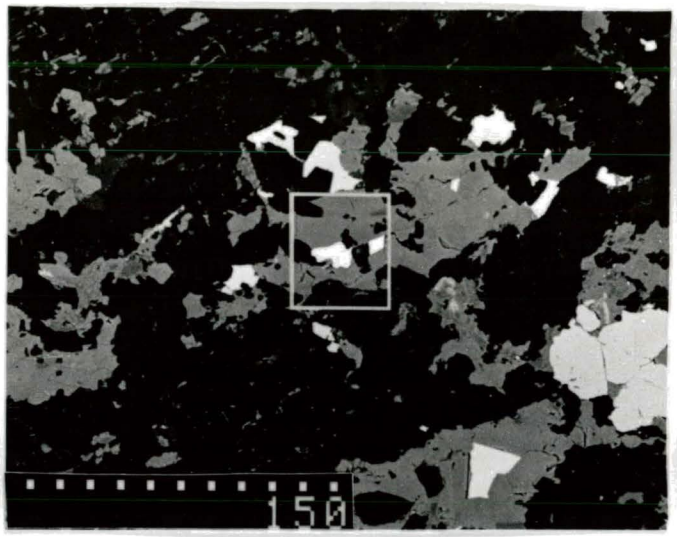
150

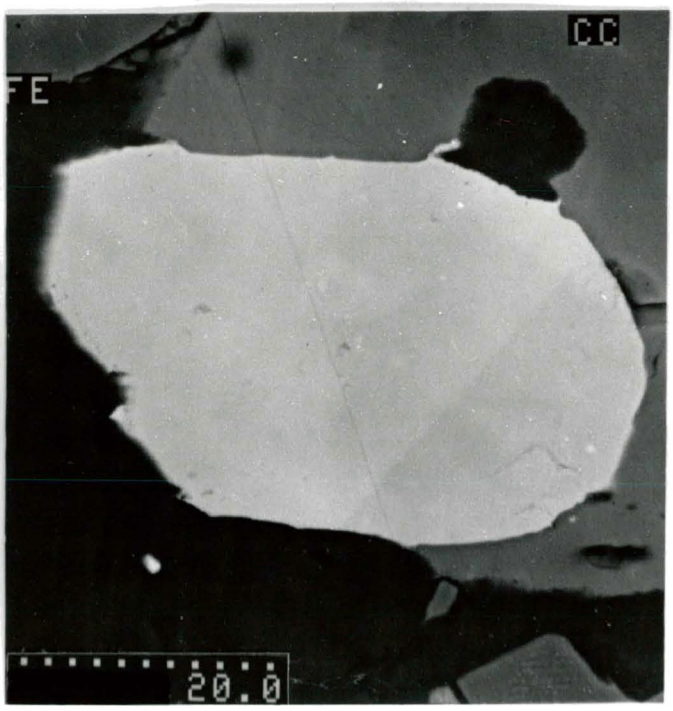
CC
FE
20.0

and silicate minerals. This melonite also infills the narrow interstices between chalcopyrite and silicate/magnetite in a texture similar to that exhibited by hessite. There is no evidence of replacement. These textural relationships suggest that coarse-grained melonites crystallized contemporaneously with, or immediately after, the initial deposition of the disseminated sulphides Other coarse-grained melonite crystals are replaced by hessite and altaite (Figure 3.12C), and by galena (Figure 3.5B).

Melonite compositions (Table 3.8) show that pure $NiTe_2$ is found only in a few grains and that substitution of Ni by Pd, Co, and of Te by Bi by varying amounts occurred in most samples. Substitution of Pd by Ni varies from 2 to 10 wt.%. Melonites of similar composition have been reported from the Kambalda nickel deposit, Australia (Hudson, 1986) and the Ivrea-Verbano basic complex, Italy (Garuti and Rinaldi, 1986). Melonite and merenskyite are considered to form complete solution (Vermaak and Hendriks, 1976). The compositions of palladian melonite from the GLI plot on the melonite-merenskyite join in the Pd-Ni-Te system (Figure 3.11).

Altaite (PbTe) is present in all rock types. It occurs as discrete crystals (< 6 μm) in silicate and chalcopyrite, and as a replacement mineral (Figures 3.12A-B). Altaite typically replaces melonite but rarely hessite. Figure 3.12B shows a single example of altaite and hessite replacing melonite.

The compositions of altaite (Table 3.9) show that it is essentially pure PbTe with a minor substitution by Ag in one of the grains in sample 18. In

Table 3.8 EDS analyses of melonite from the GLI

Stoichiometry Wt% Ni:18.7, Te:81.3

Sample	18		18		18		18		18	
	Atm%	Wt%	Atm%	Wt%	Atm%	Wt%	Atm%	Wt%	Atm%	Wt%
Ni	33.39	18.86	28.34	15.84	18.65	9.90	19.25	10.29	18.73	9.94
Te	63.82	78.35	65.64	79.73	68.54	79.08	67.72	78.68	67.90	78.30
Pd	2.79	2.85	4.66	4.72	11.01	10.59	9.82	9.51	10.03	9.64
Co			1.36	0.76	1.80	0.96	3.22	1.73	3.34	1.78
TOTAL Wt%		100.06		101.06		100.53		100.21		99.66

Sample	36		36		36		36		37	
Ni	32.12	17.44	29.16	16.31	29.41	16.31	22.52	12.49	29.17	16.01
Te	67.88	80.07	67.22	81.69	67.49	81.34	66.80	80.55	68.61	81.78
Pd			0.53	0.54			0.60	0.61	0.81	0.80
Co			3.08	1.73	3.10	1.73	9.55	5.32	1.41	0.77
Ag							0.53	0.54		
TOTAL Wt%		97.50		100.26		99.38		99.50		99.36

Sample	37		37		38		38		38	
Ni	25.04	13.60	26.75	14.68	32.02	17.79	30.83	17.14	29.30	15.95
Te	66.93	79.00	66.13	78.88	67.25	81.19	66.48	80.30	67.59	79.96
Pd	6.92	6.81	5.65	5.61			0.66	0.66	1.59	1.57
Co	1.11	0.60	1.47	0.82	0.72	0.40	2.03	1.13	1.52	0.83
TOTAL Wt%		100.01		99.99		99.38		99.23		98.31

Sample	38		38		38		47		47	
Ni	28.52	15.63	22.45	12.15	21.64	11.67	26.76	14.70	26.76	15.00
Te	66.37	79.07	66.33	78.01	67.32	78.90	66.69	79.64	66.73	81.29
Pd	3.31	3.29	9.88	9.69	9.70	9.48	3.28	3.26	2.13	2.16
Co	1.38	0.76	1.33	0.72	1.34	0.73	3.27	1.80	4.38	2.47
TOTAL Wt%		99.18		100.57		100.78		99.41		100.92

Sample	47		47		48		48		48	
Ni	26.69	14.57	26.39	14.67	23.67	12.61	22.82	12.14	31.60	17.22
Te	66.51	78.88	66.25	80.04	66.12	76.55	65.85	76.11	68.40	80.99
Pd	2.95	2.92	3.57	3.60	9.11	8.80	8.61	8.30		
Co	3.85	2.11	3.78	2.11			1.53	0.82		
Bi					1.09	2.07	1.18	2.23		
TOTAL Wt%		98.48		100.42		100.03		99.60		98.21

Sample	48		48		50		50	
Ni	22.21	11.59	31.14	16.94	32.86	18.42	33.76	18.87
Te	65.77	74.57	67.47	79.80	67.14	81.79	66.24	80.47
Pd	10.64	10.05	1.40	1.38				
Bi	1.38	2.57						
TOTAL Wt%		98.77		98.12		100.21		99.35

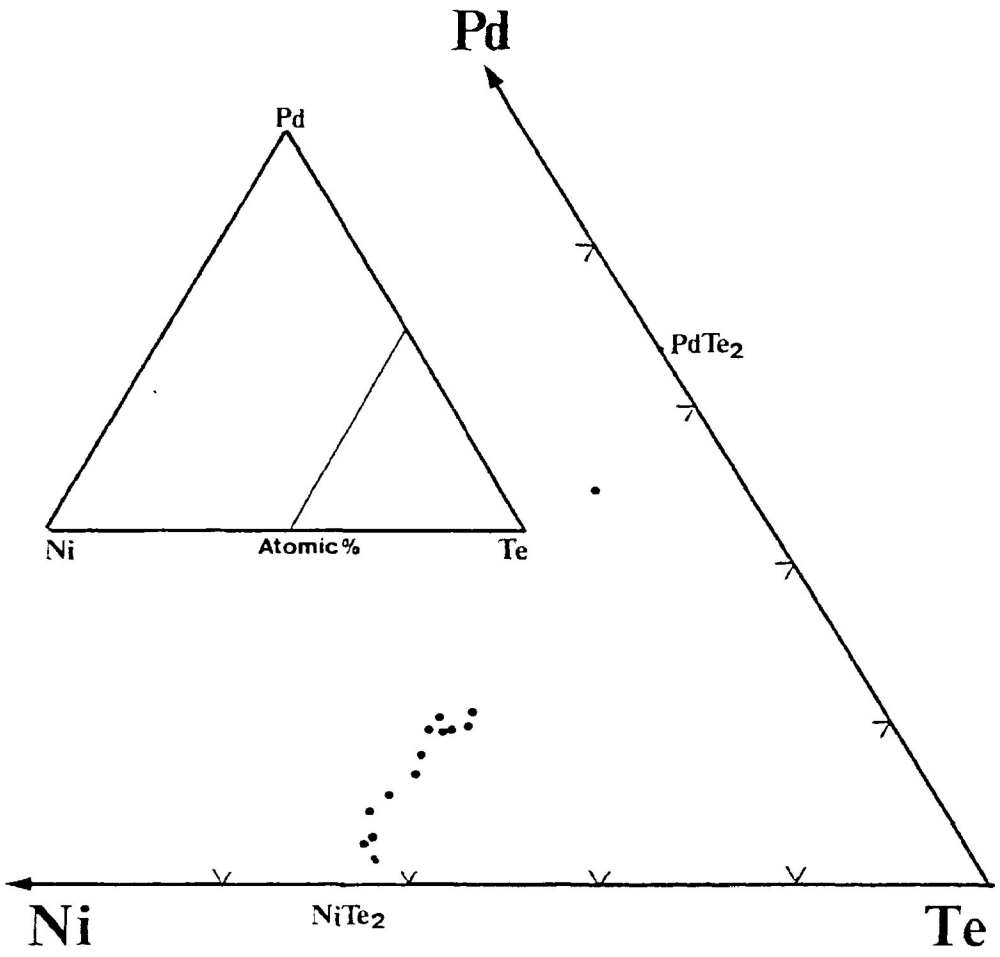

Figure 3.11 Compositions of palladian melonite plot on the $NiTe_2$-$PdTe_2$ tie-line in the ternary system Pd-Ni-Te. The maximum Pd content in the melonite from the GLI is 11 atomic percent.

Figure 3.12A-B Back-scattered electron images of altaite (AT) modes of occurrence as a small inclusion in chalcopyrite (Top image; smaller white grain on right) and as a replacement phase of melonite (Bottom image; ML, sample G-50). Altaite replacement extends to cracks in the melonite. Image (A) also shows a prismatic hessite, and (B) illustrates hessite replacement (?) of melonite.
Full scale bar in μm.


AG2TE-PBTE
CC
15.0

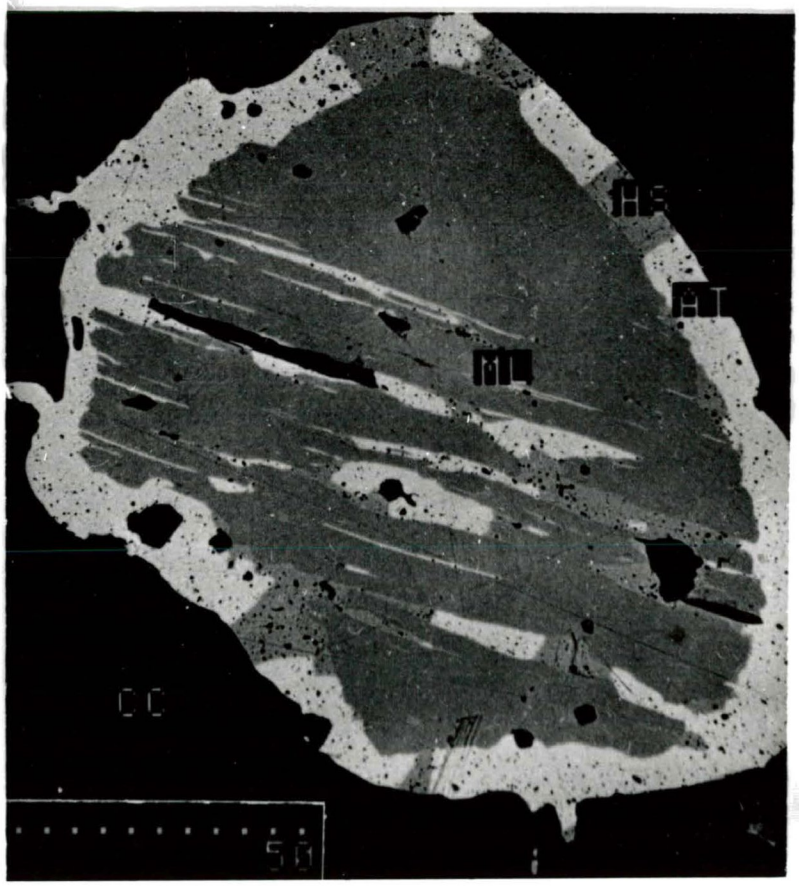
CC
50

Table 3.9 EDS analyses of altaite from the GLI
Stoichiometry (Wt%) Pb: 62, Te: 38

Sample	18		18		36	
	Atm.%	Wt%	Atm.%	Wt%	Atm.%	Wt%
Pb	48.36	60.13	50.79	63.03	51.41	63.74
Te	50.46	38.64	49.21	37.63	48.59	37.11
Ag	1.18	0.76				
TOTAL Wt%		99.54		100.69		100.84

Sample	37		50	
	Atm.%	Wt%	Atm.%	Wt%
Pb	49.44	62.78	51.58	63.27
Te	50.56	37.81	48.42	36.58
Ag				
TOTAL Wt%		100.59		99.85

contrast, altaite found in the Ivrea-Verbano basic complex (Italy) contains up to 9 atomic % Ag (Garuti and Rinaldi, 1986). The Ag-poor altaite of the GLI is attributed to its late crystallization; most Ag combined with Te to form hessite which formed earlier than altaite.

3.3.4 The Platinum-Group Minerals (PGM)

Sperrylite is the only platinum mineral observed in the GLI. It occurs small monomineralic inclusions (< 5 μm across) in chalcopyrite and silicate. Sample 55B, a sulphide-mineralized gabbro, contains more than ten sperrylite grains in a coarse chalcopyrite grain. Other samples only contain between 2 and 4 grains. The small grain size precluded quantitative analysis. Nevertheless, semi-quantitative analyses indicate that most sperrylite grains are composed of Pt and As with elemental ratios close to 1:2.

Pd-Bi-Te Minerals (Table 3.10A) are classified according to the known phases in the system Pd-Bi-Te (Figure 3.13). Each of the end member phases kotulskite (PdTe), merenskyite ($PdTe_2$), and michenerite (PdBiTe), is represented by a mineral from the GLI whose composition is close to the ideal formula. The three grains from sample 30, which plot between PdBi and PdTe, are considered to be Bi-rich kotulskite. This variety of kotulskite has been found in other deposits. For example, the compositions of the bismuthian kotulskites from the Sudbury area are 37-38

Table 3.10A EDS analyses of Pd-Bi-Te minerals from the GLI
Host minerals are disseminated chalcopyrites, with the exception of sample 30, which is massive chalcopyrite
S: Sample number

S		Pd	Ag	Ni	Bi	Te	TOTAL	Formula Mineral
24	A %	46.56	6.34		3.49	43.52		PdTe
	W %	41.67	5.83		6.14	46.71	100.35	Kotulskite
30		43.98	5.14		23.18	27.69		Bi-PdTe
		34.79	4.12		36.02	26.26	101.19	
30		48.51			16.13	35.36		Bi-PdTe
		39.48			25.79	34.52	99.79	
30		48.29			16.5	35.21		Bi-PdTe
		38.99			26.16	34.09	99.24	
37		24.17		7.37		67.66		PdTe2
		22.16		3.61		72.03	97.8	Merenskyite
59		26.99			18.02	47.74		PdBiTe-PdTe2
		27.25			28.92	45.32	101.49	
30		31.69		0.36	35.95	32		PdBiTe
		22.23		0.14	49.53	26.92	98.82	Michenerite
								Palladium bismuthotelluride
55B		41.89	5.87		34.08	18.17		
		30.36	4.31		48.51	15.79	98.97	
55B		44.18	2.85		37.11	15.86		
		31.93	2.09		52.67	13.75	100.44	
55B		48	2.66		35.11	11.94		
		35.56	1.97		50.45	11.95	99.93	

Table 3.10B Compositions of palladium bismuthotelluride from Finland.
(after Vuorelainen et al., 1982)

S		Pd	Ag	Ni	Bi	Te	TOTAL
1*	Wt.%	37.6	0.48	0.6	19.1	43.1	102.83
2**		33.11		0.08	43.5	20.41	99.45
3+		33.65		0.03	50.4	14.12	99.6

*plus 0.59 Pt, 0.2 Au, 0.39 Cu, 0.39 As, and 0.38 Sb
**plus 0.77 Pt, 0.12 Cu, 0.3 Fe, 0.04 S, and 0.77 Sb
**plus 0.77 Pt, 0.12 Cu, 0.02 S, and 0.49 Sb

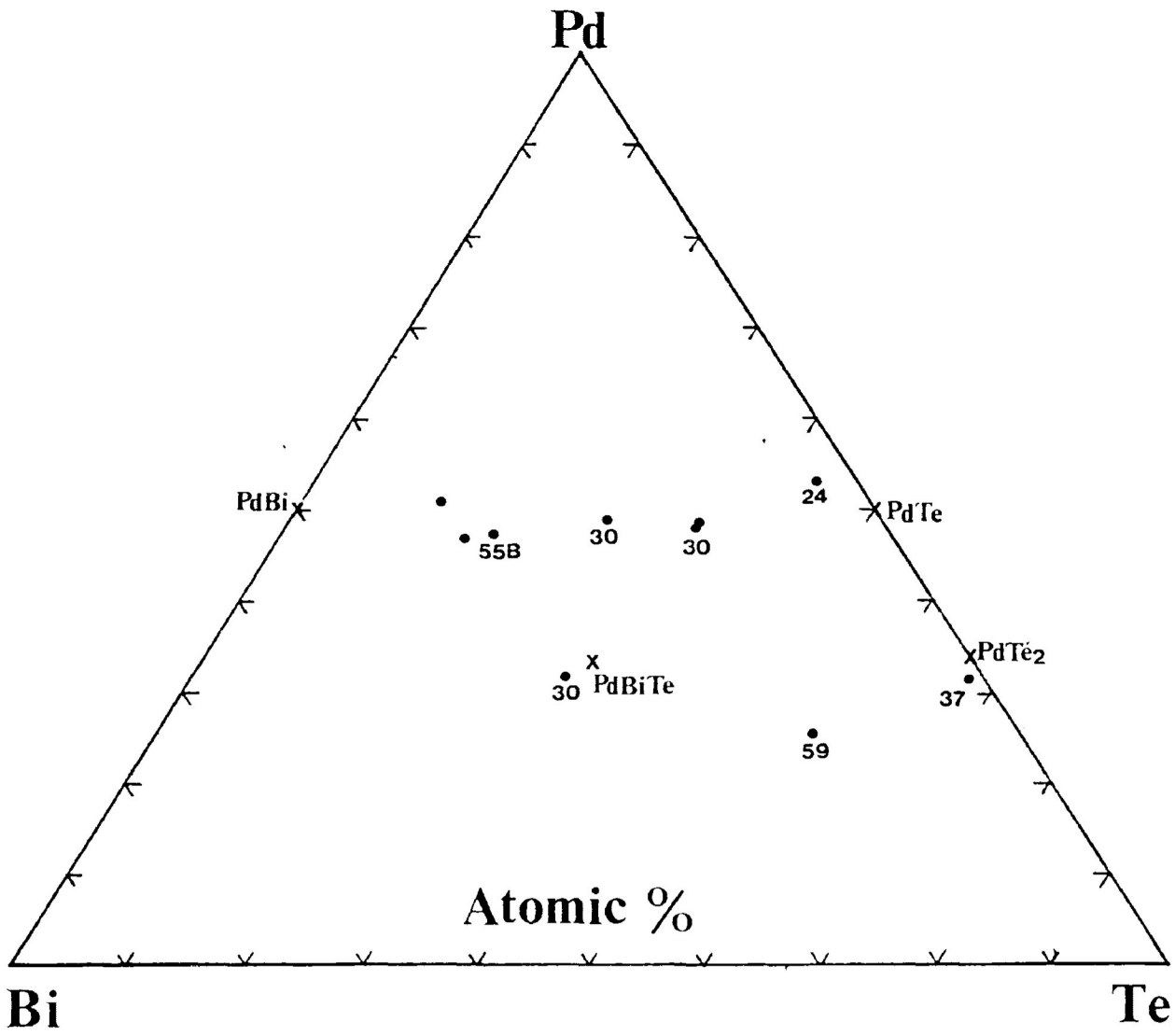

Figure 3.13 Compisitions of Pd-Bi-Te minerals from the GLI plot in the ternary system Pd-Bi-Te.

PdTe: kotulskite, $PdTe_2$: merenskyite,

PdBi: polarite, PdBiTe: michenerite

wt. % Pd, 33-35 wt. % Bi., and 26-28 wt. % Te (Cabri and Laflamme, 1976). Sample 59 is an intermediate phase in the michenerite- merenskyite solid solution series. Pd-Bi-Te minerals from sample 55B are tentatively regarded as palladium bismuthotellurides, since their compositions and those reported by Vuorelainen *et al*, (1982) are quite similar (Table 3.10B).

Kotulskite (PdTe) and Bi-rich PdTe: The kotulskite in sample 24 (troctolite-gabbro transitional rock) has a composition closest to the ideal formula PdTe. This subhedral PGM (7 x 10 μm) occurs at the margin of chalcopyrite and is intergrown with sopcheite (Figure 3.14C). The Bi-rich kotulskite grains (sample 30) occur as interstitial grains (9 x 12 μm) between chalcopyrite and silicate, as oval inclusions (< 5 μm) in chalcopyrite, and as an intergrowth with hessite and cobaltite (Figures 3.14A-B and D). The interstitial grain is euhedral against the chalcopyrite but is irregular with the silicate.

Merenskyite ($PdTe_2$): This mineral was only found in a highly altered and recrystallized rock suspected to be originally Center I syenite (sample 37). The PGM occurs as a minute grain (3 μm across) at the margin of chalcopyrite. This Bi-free merenskyite contains a substantial amount of Ni. This substitution is common, for example, the merenskyite from the Sudbury area contains 6.1 wt. % Ni (Cabri and Laflamme, 1976). Pt-bearing merenskyite appears to be common in other deposits such as the Bushveld complex (Vermaak and Hendriks, 1976; Kinloch, 1982) and Levak West,

Figure 3.14A A Bi-rich kotulskite (white) occurs on the margin of chalcopyrite (light grey). It is euhedral on the Cu sulfide but anhedral against the silicate mineral (black). Sample G-30.

Figure 3.14B A fine-grained oval Bi-rich kotulskite hosted by chalcopyrite. Sample G-31.

Figure 3.14C A kotulskite (right) fringing chalcopyrite is intergrown with sopcheite (left) which is enclosed in the altered silicate groundmass. The grain boundary between the two minerals are not clearly visible, however, kotulskite is slightly darker than sopcheite. Both minerals also rim the margins of the chalcopyrite grains. Sample G-24.

Figure 3.14D Bi-rich kotulskite (BIPDTE) grains are intergrown with cobaltite (CO) and hessite (labelled AGTE) on a chalcopyrite-silicate boundary. The hessite also occurs at the corner of chalcopyrite, magnetite (FE) and silicate. Sample G-30.

Full scale bar in μm.

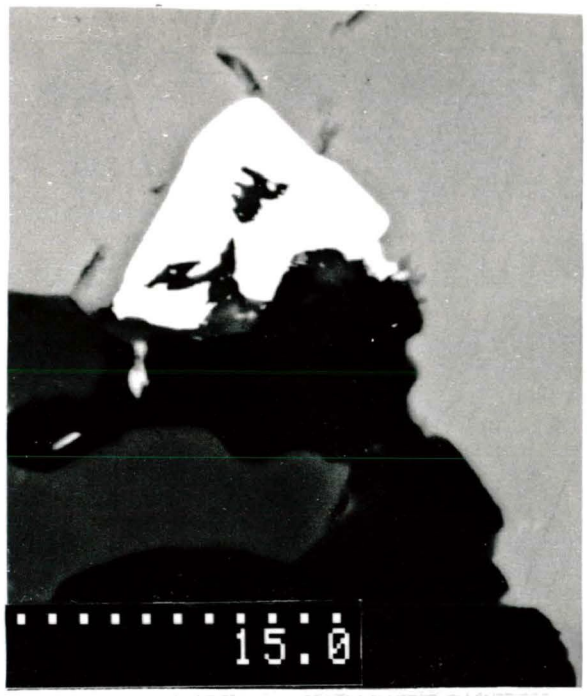
15.0

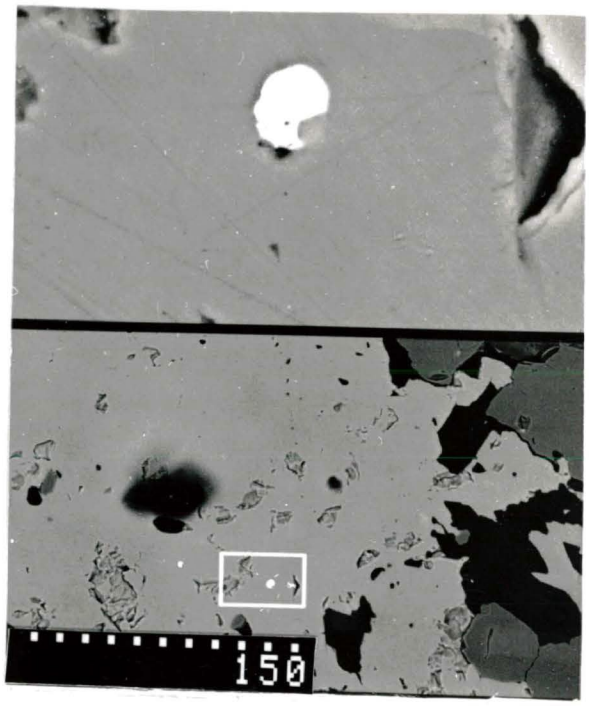
150

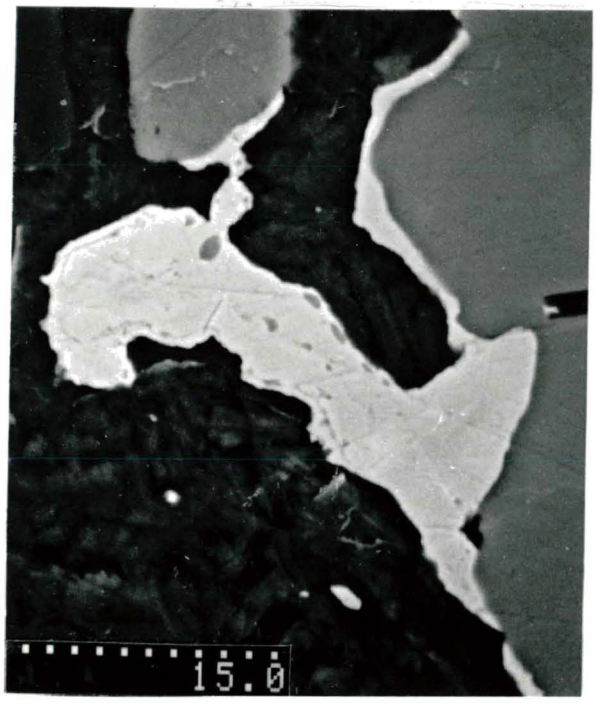
15.0

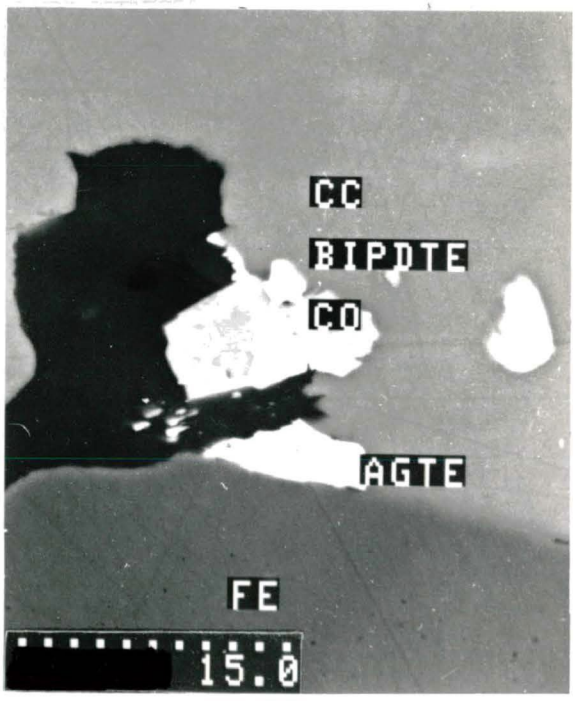
CC
BIPDTE
CO
AGTE
FE
15.0

Sudbury (Cabri and Laflamme, 1976).

Michenerite (PdBiTe): An anhedral michenerite (7 x 10 μm) is intergrown with hessite which occurs at the margin of chalcopyrite. The michenerite grain is mostly enclosed in a silicate groundmass. The composition of this michenerite is close to the ideal formula Pd-Bi-Te (Table 3.10A). Michenerite forms a complete solid solution series with merenskyite (Vermaak and Hendriks, 1976). The intermediate composition is represented by $Pd_{1.5}BiTe_{2.65}$ (sample 59) which plots slightly below the $PdTe_2$-PdBiTe join of the Pd-Bi-Te system (Figure 3.13).

Palladium bismuthotelluride ?: This palladium mineral is present as small inclusions (10 x 4 μm) in disseminated chalcopyrites and as an intergrowth with hessite partially enclosed by chalcopyrite and altered silicate mineral. The palladium mineral exhibits euhedral faces with the hessite but has an irregular grain boundary with the silicate mineral.

The compositions of these palladium minerals (Table 3.10A) vary from $(Pd_{7.1}Ag)_{\Sigma 8.1}(Bi_{5.8}Te_{3.1})_{\Sigma 8.9}$, to $(Pd_{7.75}Ag_{0.5})_{\Sigma 7.8}(Bi_{6.51}Te_{2.78})_{\Sigma 9.29}$, and to $(Pd_{9.02}Ag_{0.5})_{\Sigma 9.52}(Bi_{6.6}Te_{2.24})_{\Sigma 8.84}$. The first two are relatively similar to the palladium bismuthotellurides $[Pd_7(Bi,Te)_8]$ from Finland (Table 3.10B, after Vuorelainen *et al*, 1982), who also suggested that there might be a solid solution series between PdTe and PdBi. The palladium minerals from the GLI, however, contain considerable amounts of Ag, but lack Pt or any of the other elements present in those from Finland.

Sopcheite ($Pd_3Ag_4Te_4$) in the GLI is the third reported Canadian

occurrence; the first and second occurrences being those at Levak West (Sudbury) and Lac-des-Iles, Ontario (Dunning *et al.*, 1984), respectively. Three sopcheite grains were found in the GLI. An anhedral sopcheite grain (10 x 20 μm) occurs between the grain boundary of silicate and bornite replacement of the host chalcopyrite (Figures 3.15A-B) in a sheared gabbro (sample 14). The second grain (25 x 45 μm) is intergrown with kotulskite and enclosed by silicates but not chalcopyrite (Figure 3.15C) in a troctolite-gabbro transitional rock (sample 24). The third grain occurs as a subhedral grain (7 x 10 μm) enclosed in a chalcopyrite bleb. The host rock of this sopcheite is a chalcopyrite-disseminated gabbro (sample 27). The sopcheites from the Lac-des-Iles are intergrown with merenskyite and rimmed by kotulskite (Dunning *et al.*, 1984), and, hence, a different paragenesis to that of the GLI.

The two compositions of the sopcheite (Table 3.11) essentially agree with the ideal formula $Pd_3Ag_4Te_4$, with a small amount of substitution of Pd by Co in the former sample. The compositions of sopcheite from the Lac-des-Iles, Ontario, $Pd_{3.05}Ag_4(Te_{3.92}Bi_{0.03})\Sigma 3.95$ and Monchergork, USSR, $Pd_{2.96}(Ag_{3.78}Fe_{0.18}Cu_{0.02}Ni_{0.01})\Sigma 3.99(Te_{4.04}Bi_{0.01})\Sigma 4.05$, and $(Pd_{2.74}Fe_{0.25})\Sigma 2.99(Ag_{3.79}Fe_{0.21})\Sigma 4Te_{4.02}$ (Dunning *et al.*, 1984) are, in general, similar to those of the GLI.

Paolovite (Pd_2Sn) occurs as two anhedral grains (maximum 6 x 10 μm), rimmed by electrum, in a bornite bleb (Figure 3.16) which is hosted by a troctolite (sample 33) containing serpentinized dendritic olivine. Five

Figure 3.15A Anhedral sopcheite grain (white) surrounded by bornite (light grey) which replaces the original host chalcopyrite. The black inclusion bordering the sopcheite is a silicate mineral. Sample G-27.

Figure 3.15B Coarse- and fine-grained sopcheites (white) occur on the margin of bornite (BR) which has replaced the margin of the chalcopyrite. Sample G-14.

Figure 3.16 Anhedral grains of exsolved paolovite in bornite. The paolovites are rimmed by electrum (white). Sample G-33.

Figure 3.17A (Right) A small inclusion of palladium arsenide (white) in magnetite which lacks ilmenite lamellae (later stage magnetite). Sample G-22.

Full scale bar in μm.

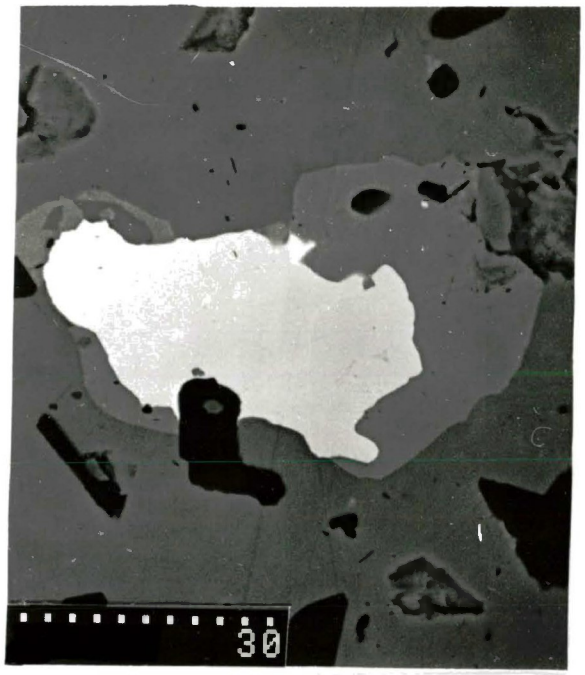
30

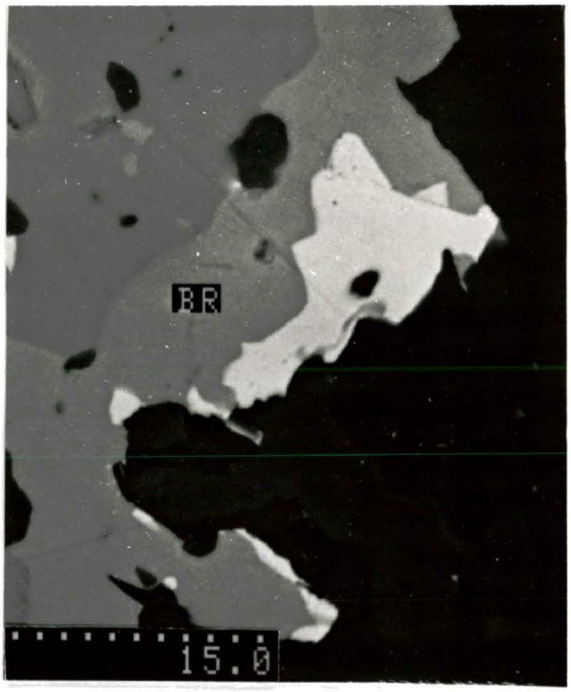
BR
15.0


15.0


100

Table 3.11 EDS analyses of sopcheite from the GLI

Sample	Grain		Pd	Ag	Te	Co	TOTAL
14	1	Atomic %	27.54	34.73	37.21	0.51	
		Wt. %	25.3	32.4	41.1	0.26	99.05
24	2	Atomic %	28.48	34.35	37.17		
		Wt.%	26.5	32.4	41.5		100.39

anhedral paolovite grains (1 to 3 μm across) were found in chalcopyrite hosted by a moderately altered gabbro (sample 55C). The irregular grain boundary between paolovite and the host chalcopyrites (Figure 3.16) demonstrates that the former is an exsolved phase.

The compositions of the paolovite (Table 3.12) do not deviate significantly from the ideal Pd_2Sn. The paolovite in sample 55C contains a considerable amount of As. This grain becomes Sn-rich at the rim, suggesting that it might have been a Pd-As mineral prior to replacement by Sn. Paolovite from the Merensky Reef contains 5 wt. % Pt (Cabri and Laflamme, 1981).

Pd-As (± Ni, Sb) minerals are present in troctolite (samples 20, 22 and 33) and gabbro (samples 27 and 55A-C). The dendritic olivines in the troctolites are serpentinized but hydrous minerals are scarce. Gabbro 27 and 55B and C host disseminated sulphides, sample 55 is massive chalcopyrite.

Table 3.12 EDS analyses of paolovite from the GLI.

Sample	Grain		Pd	Sn	As	TOTAL
33	1	Atomic %	66.89	33.11		
		Wt. %	64.1	35.4		99.42
	2	Atomic %	66.08	33.92		
		Wt. %	64.3	36.8		101.07
55C	3	Atomic %	66.11	18.98	14.91	
		Wt. %	68.3	21.9	10.8	100.96
Stoichiometry (Wt.%)			Pd: 64.2	Sn: 35.8 (Cabri and Laflamme, 1981)		

The Pd-As minerals occur as small spherical inclusions (< 2 μm across) in late magnetite grains lacking ilmenite exsolution lamellae, as a discrete grain (3 x 7 μm) intergrown with a subhedral niccolite in the silicate groundmass, and as a comparatively coarse (0.15 x 0.55 mm) interstitial palladium arsenide exhibiting a distinct grain boundary against the chalcopyrite and an irregular boundary against the silicate mineral (Figures 3.17A-C). This texture appears to be common in the PGM of the GLI.

Although eleven Pd-As minerals are present in five samples, only the coarsest grain is large enough for microanalysis (Table 3.13). The composition of this mineral, expressed as atomic proportions, is $(Pd_{2.05}Ni_{0.86})_{\Sigma 2.91}(As_{1.32}Sb_{0.2})_{\Sigma 1.52}$, which is close to the ideal formula of palladoarsenide (Pd_2As). Substitution of As by Sb in palladoarsenide has

Figure 3.17B A prismatic palladium arsenide intergrown with an unknown anhedral arsenide mineral (right) in a silicate groundmass.

Figure 3.17C Palladium arsenide showing a fairly planar boundary with the margin of the chalcopyrite but having a ragged boundary with the silicate mineral. Sample G-27.

Full scale bar in μm

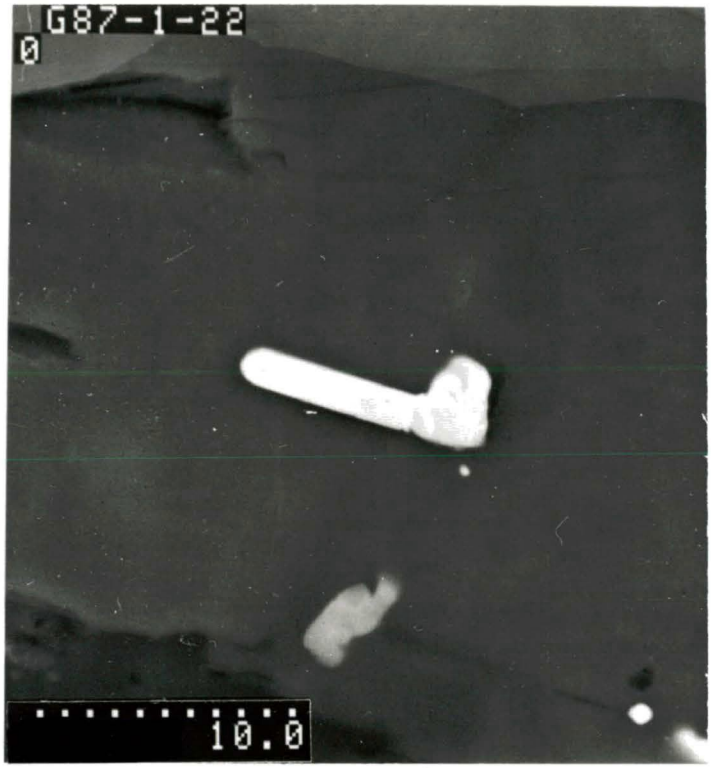
G87-1-22
0
10.0

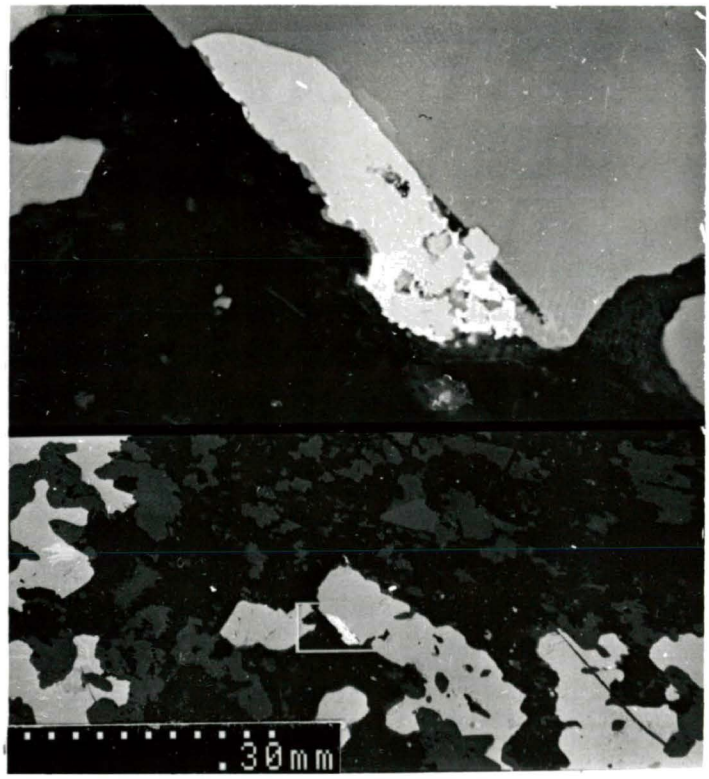
.30mm

Table 3.13 EDS analysis of a Pd-As (± Ni, Sb) Mineral from the GLI. Other samples, which contain this kind of PGM but not analysed, are 20, 22, 33, 55A, and 55B/C.

Sample 27	Pd	As	Ni	Sb	TOTAL
Atomic %	46.22	29.87	19.39	4.52	
Wt. %	55.9	25.4	12.9	6.25	100.5

been reported by Hudson (1986). Analyses of palladoarsenide from various localities compiled by Cabri and Laflamme (1981), however, contain little (0.23 wt.%) or no Ni.

Guanglinite (Pd_3As) occurs as tiny subhedral crystals, approximately 7 μm across, between silicate and chalcopyrite grain boundaries. The host rock (sample 55B) is a moderately altered gabbro which contains disseminated chalcopyrite. The compositions of guanglinite are essentially Pd_3As with minor substitution of As by Bi (Table 3.14). However, its Pd contents (75.5-77.5 wt. %) are lower than the ideal 81 wt. %.

Palladium Antimonides are present in troctolite (samples 20, 22, 33, and 42) and gabbro (sample 28), which are among the least chalcopyrite-mineralized samples. The palladium antimonides occur as discrete subhedral grains (3 x 7μm) in clinopyroxene, as small grain (< 5 μm across) at the margin of a chalcopyrite grain, and as an intergrown phase

Table 3.14 EDS analyses of guanglinite from the GLI.

Sample 55B		Pd	As	Bi	TOTAL
Grain 1	Atomic %	73.8	23.68	2.5	
	Wt. %	75.5	17.1	5.51	98.06
Grain 2	Atomic %	70.59	22.93	2.41	
	Wt. %	77.5	17.7	5.2	100.36
Stoichiometry (Wt%)		Pd: 81	As: 19	(Cabri and Laflamme, 1981)	

with hessite (Figure 3.18A-C). Figure 3.18D shows co-existing palladium antimonide, palladium arsenide and chalcopyrite. The paragenetic sequence of these minerals is, however, difficult to determine due to small grain size.

The compositions of palladium antimonide (Table 3.15) show that analysis 3 is close to the ideal formula of mertieite I and that analysis 4 is close to stibiopalladinite. However, Cabri (1981) stated that mertieite I and II and stibiopalladinite can be distinguished from one another only by X-ray diffraction analysis. Other Pd-Sb analyses do not correspond to the known phases, including isomertieite ($Pd_{11}Sb_2As_2$). The small grain size of the minerals precluded X-ray diffraction analyses.

3.3.5 Other Minerals

Au-Ag alloys are small (± 5 μm across), enclosed in chalcopyrite and magnetite, and present in troctolite (samples 22 and 33) and syenite (sample

Figure 3.18A-D Photomicrographs showing different modes of occurrence of palladium antimonide; subrounded grains in clinopyroxene (top left., sample G-28); small grains on the margin of chalcopyrite* (top right., sample G-22); intergrowth with hessite (bottom left., sample G-28), and replacement of, or intergrown with, palladium arsenide and bornite* (bottom right, sample G-33).

* sketched below.

The anhedral grey crystals in sample 22 are magnetite lacking ilmenite lamellae. The bright inclusion in a magnetite (right corner) is a palladium arsenide (Figure 3.17A).

Full scale bar in μm.

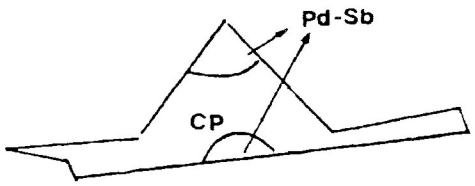

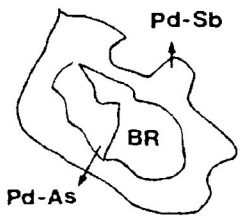

Not to scale

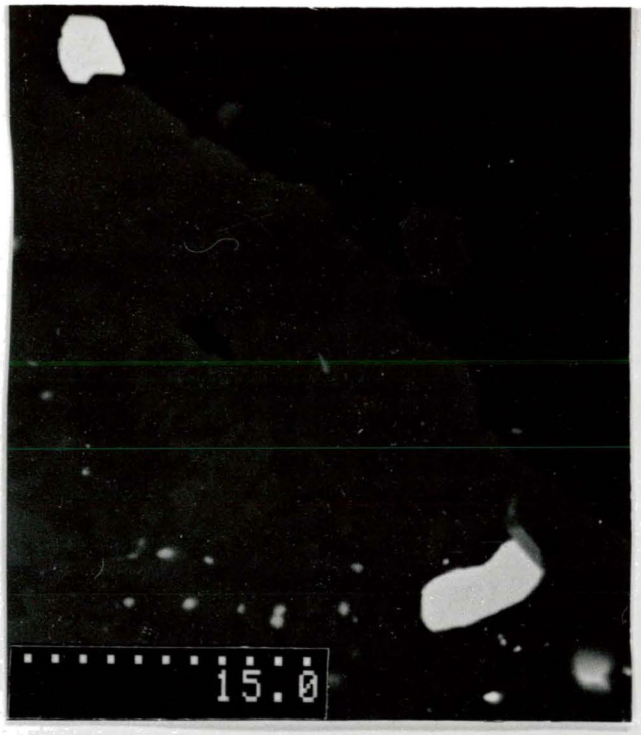
15.0

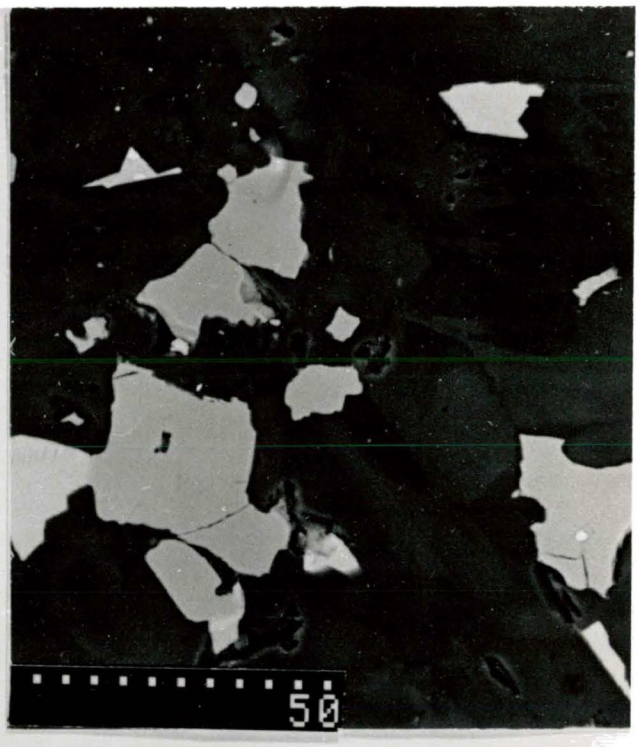
50

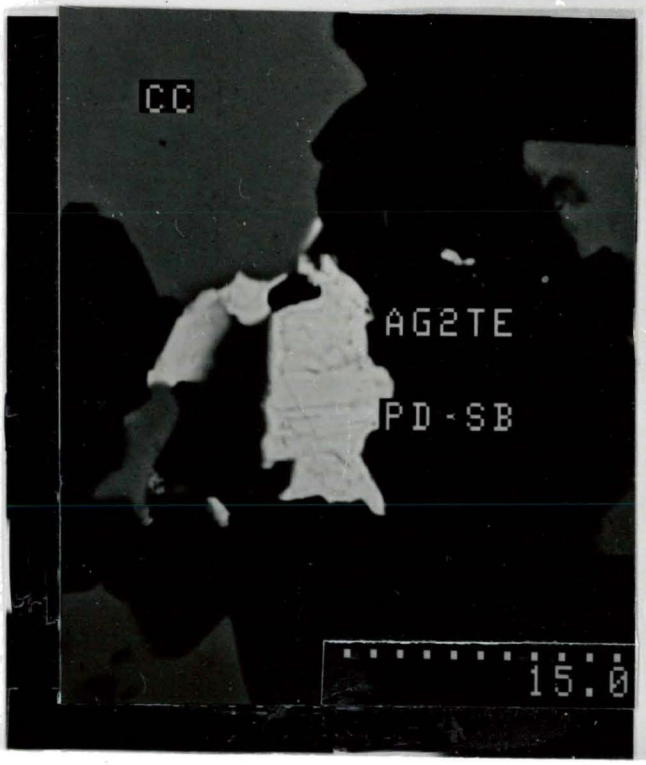
CC
AG2TE
PD-SB
15.0

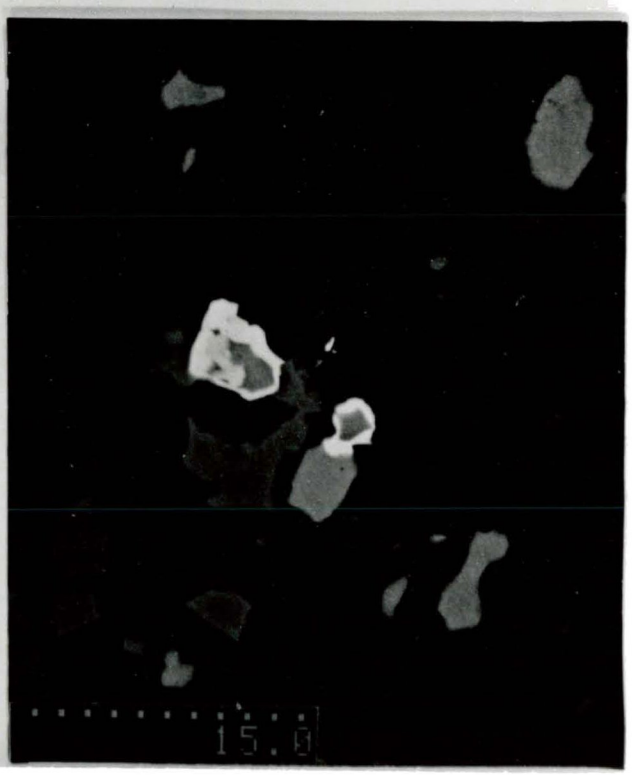
15.0

Table 3.15 EDS analyses of Palladium antimonite from the GLI
S: Sample number

	S		Pd	Ag	As	Sb	Te	Co	TOTAL
1	22	Atom%	69.58	0.9	4.07	25.45			
		Wt.%	68.27	0.89	2.81	28.57			100.54
2	22		73.5			25.56		0.94	
			69.19			27.53		0.49	97.21
3	28		73.6		4.54	21.86			
			71.22		3.09	24.21			98.52
4	28		71.38		7.11	20.84	0.67		
			70.06		4.92	23.41	0.78		99.17
5	42		74.66			25.34			
			72.02			27.98			100

Analysis	Formula	Pd:Sb
1	$(Pd_{2.78}Ag_{0.04})\Sigma 2.82\ (Sb_{1.02}As_{0.16})\Sigma 1.18$	2.39
2	$(Pd_{2.94}Co_{0.04})\Sigma 2.98 Sb_{1.02}$	2.92
3	$Pd_{2.94}(Sb_{0.87}As_{0.18})\Sigma 1.05$	2.8
4	$Pd_{2.86}(Sb_{0.83}As_{0.28}Te_{0.03})\Sigma 1.14$	2.51
5	$Pd_{2.99}Sb_{1.01}$	2.95

Ideal Formula of palladium antimonide (Cabri, 1981)	Pd:Sb
Mertieite I: $(Pd,Cu)_{5+x}(Sb,As)_{2-x}$, or $(Pd,Cu)_{11}(Sb,As)_4$	2.75
Mertieite II: $(Pd,Cu)_8(Sb,As)_3$	2.67
Stibiopalladinite: $(Pd,Cu)_{5+x}(Sb,As)_{2-x}$, or $(Pd,Cu)_{8+x}(Sb,As)_{3+x}$	2.59-2.64

50). The latter rock is recrystallized and hosts the only chalcopyrite bleb in which the gold-silver alloy occurs. The chalcopyrite is surrounded by secondary amphiboles. The compositions of the alloy (Table 3.16) indicate that alloys from samples 22 and 33 are electrum (> 20 wt.% Ag). Compositions plotted in the system Au-Ag-Te demonstrate that all are Au-Ag alloys (Figure 3.19).

Table 3.16 EDS analyses of Au-Ag alloy

Sample	Grain		Au	Ag	Te	TOTAL
22	1	Atomic %	33.9	42.97	23.13	
		Wt. %	45.04	31.27	19.9	96.21
33	2	Atomic %	44.39	55.61		
		Wt. %	58.21	39.94		98.15
22	3	Atomic %	67.15	28.59	4.26	
		Wt. %	78.15	18.22	3.2	99.57

Naumannite (Ag_2Se), Lead-Antimonide, and **Clausthalite (PbSe)** were recognized by their characteristic X-ray spectra (Figures 3.20-22) and by semi-quantitative analysis. Clausthalite is the only PbSe mineral (Cooper *et al.*, 1974). Clausthalite is a replacement phase of a Bi-bearing melonite grain in sample 46. Numerous naumannite grains (< 5 μm across) are present in the disseminated chalcopyrite grains in sample 55B. Lead antimonide also occurs as fine-grained crystals in chalcopyrite blebs in samples 42 and 55C.

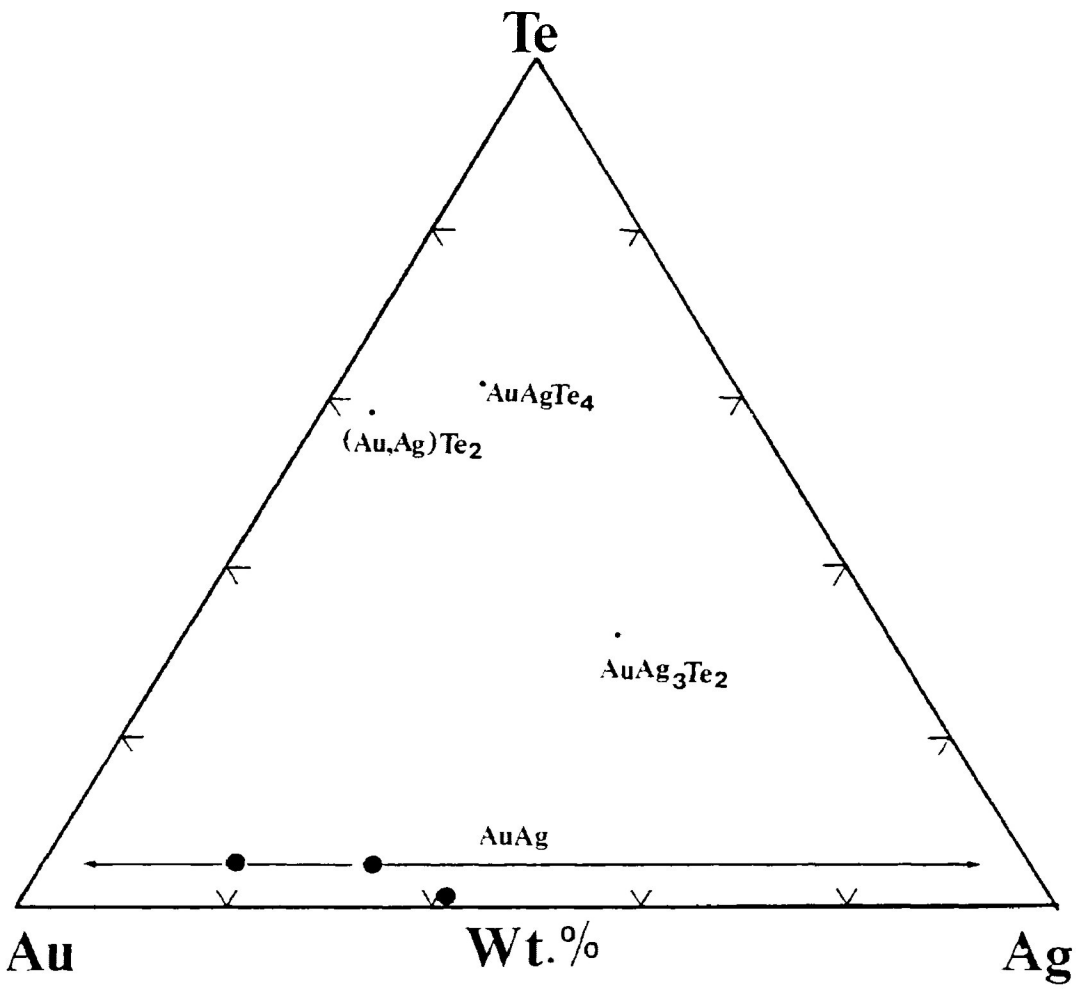

Figure 3.19 Compositions (wt%) of Au-Ag minerals from the GLI plot in the ternary system Au-Ag-Te. The data plot in the Au-Ag alloy field. $AuAg_3Te_2$: petzite, $(Au, Ag)Te_2$: krennerite, $AuAgTe_4$: sylvanite. The diagram is after Kelley and Goddard (1969).

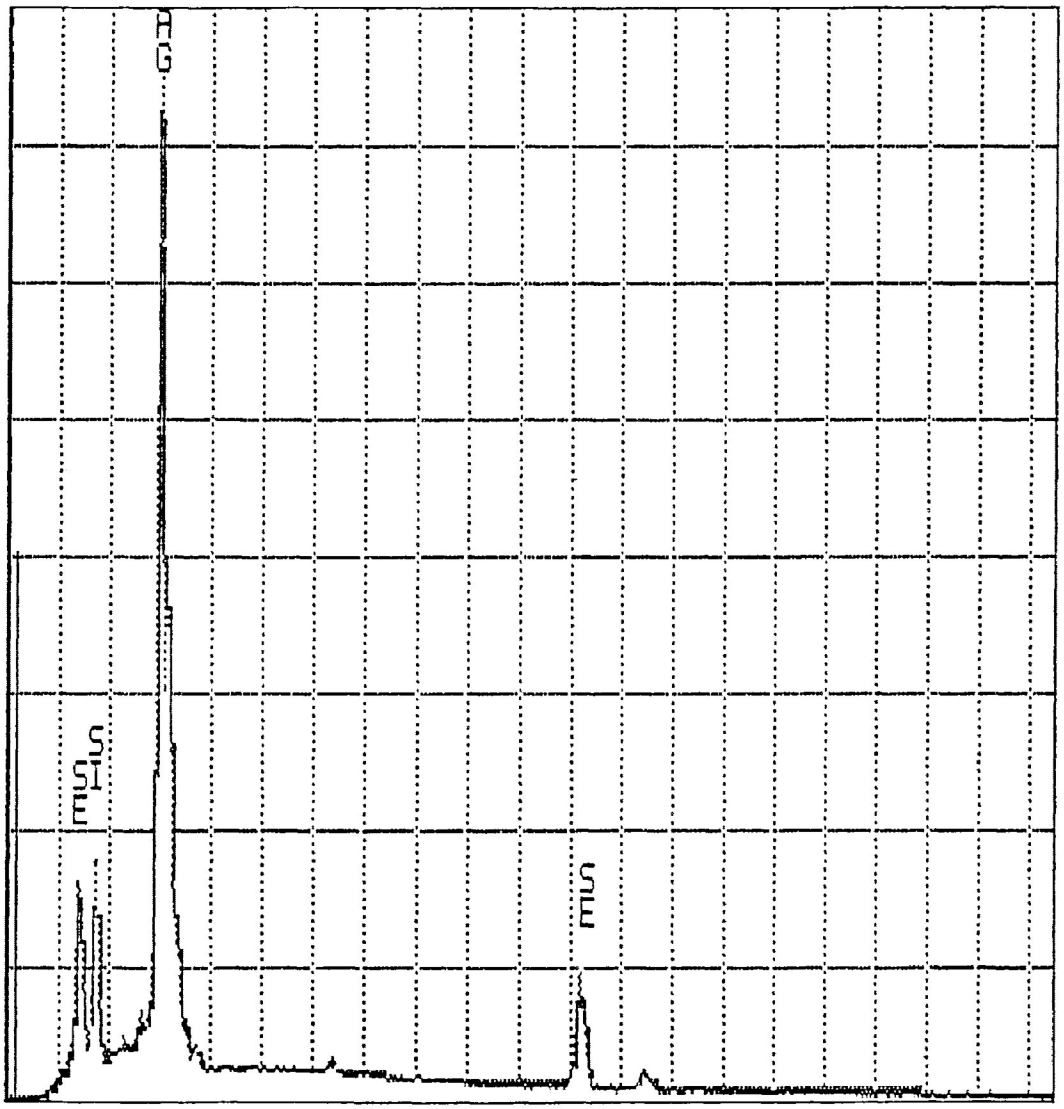

Figure 3.20 The spectrum of naummanite. The Si peak is an interference from the host silicate mineral. Sulphur is absent.

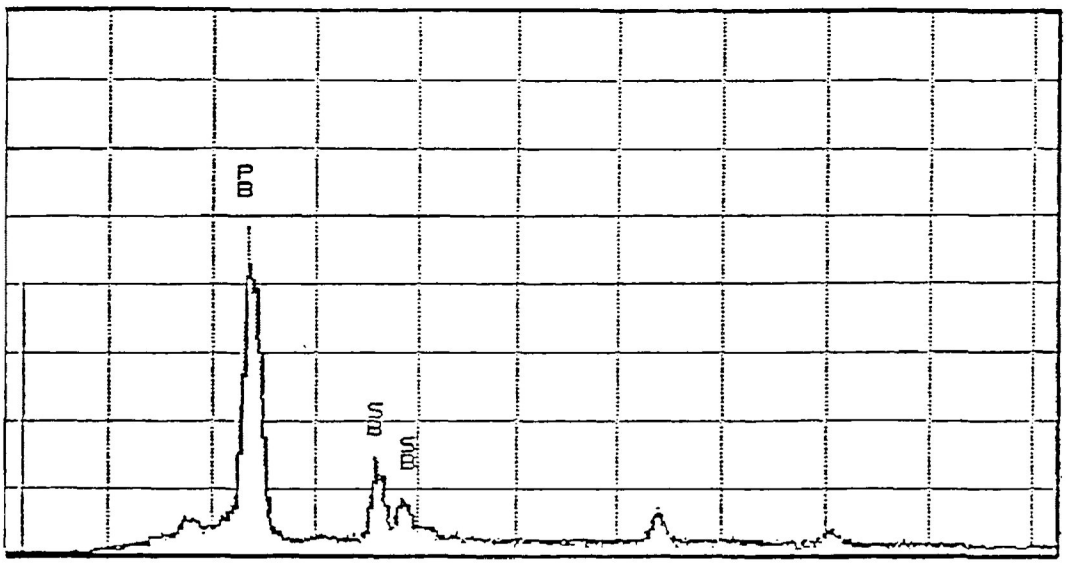

Figure 3.21 The spectrum of lead antimonide from the GLI. Sample G-55C.

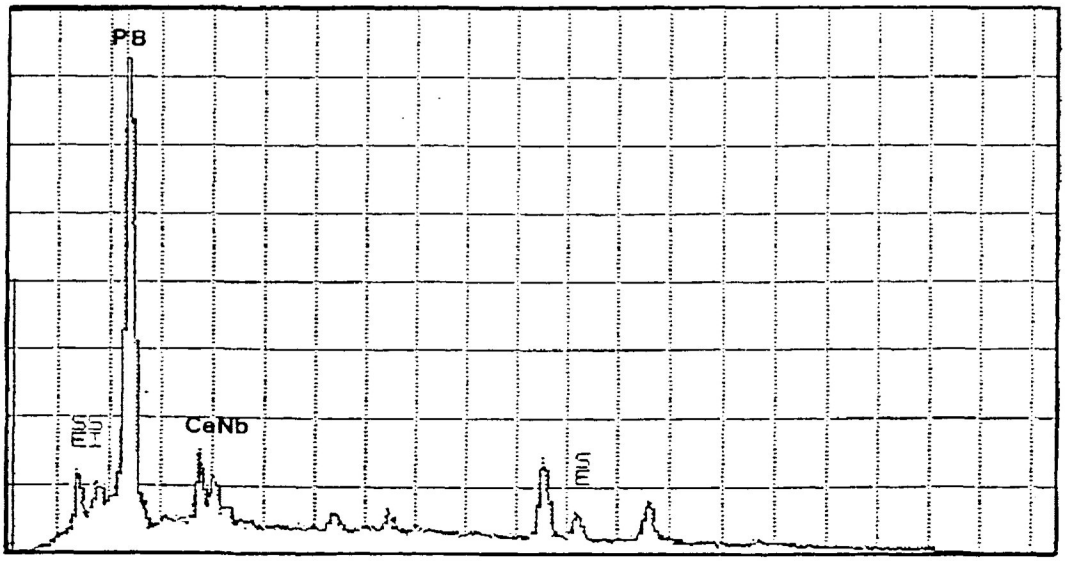

Figure 3.22 The spectrum of clausthalite (PbSe) which occurs adjacent to a Ce-Nb mineral. Sample G-46.

A silver sulphide suspected to be **acanthite (Ag_2S)** is present in a weakly sulphide-mineralized syenite (sample 60) in contact with the GLI. The "acanthite" occurs as an nanhedral and ragged grain (4 x 10 μm) fringing upon chalcopyrite grain and has a cribriform appearance. The composition of this silver-sulphide is (atomic/wt. %): Ag (62.42/83.24) and S (37.58/14.9). Low analytical totals result in a poor stoichiometry (Ag:S 1.6) Acanthite is a mineral that forms at low temperatures, < 170 °C (Boyle, 1968).

3.3.6 New Minerals ?

A probable new palladium mineral ($Pd_{1.6}As_{1.5}Ni$) was found in an altered and weakly sulphide-mineralized troctolite (sample 80). Two grains (15 x 50 μm and 1.5 μm across) are present in a silicate groundmass (Figure 3.23), in which the larger crystal appears to be a fracture-filling phase of the silicate. This PGM is intergrown with two bands of palladium arsenides (1.5 μm in width). The atomic/weight percentage of the larger PGM is 38.96/48.89 Pd, 36.75/32.47 As, and 24.29/16.82 Ni. The total weight % (98.18) is, however, slightly low.

A silver-antimonide ($AgSb_4$) occurs as a small anhedral inclusion (3 x 5 μm) in galena which borders chalcopyrite and silicate mineral. The host rock (sample 38) is a recrystallized and mineralized syenite. The composition of this mineral is (atomic and weight %) 19.21/17.04 Ag and 80.79/80.89 Sb. The total weight % (97.93) is rather low due to the small grain size.

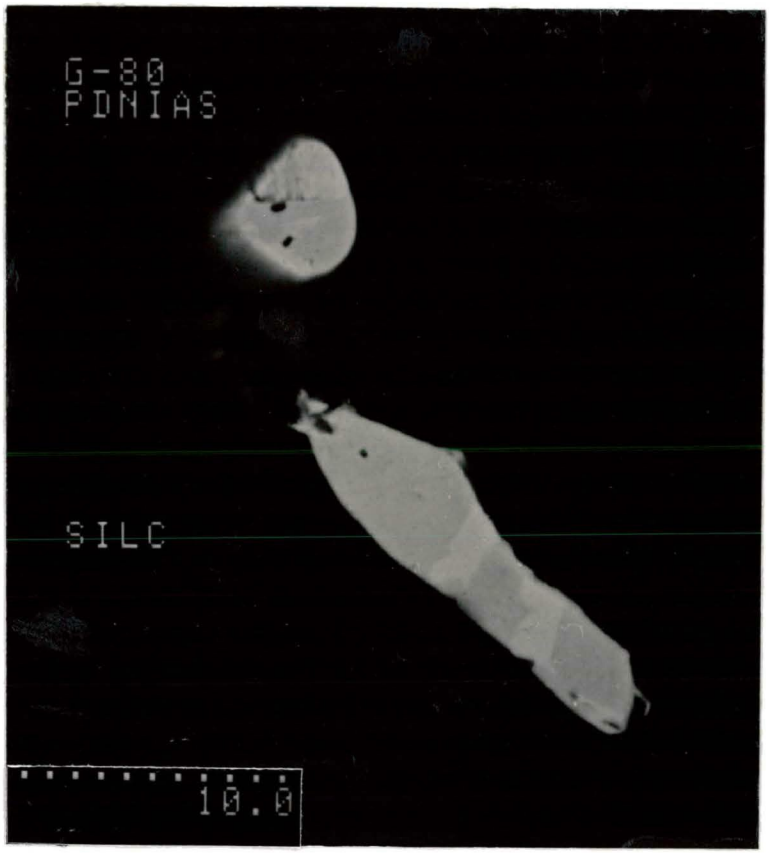

Figure 3.23 Back-scattered electron image of Pd-Ni-As, the probable new PGM from the GLI. The larger grain appears to set in a fracture of a silicate mineral. It also has two (white) bands of palladium arsenide whose stoichiometry could not be determined due to small size. The smaller grain is most likely intergrown with palladium arsenide. The silicate mineral may be an altered clinopyroxene. Sample G-80.

Full scale bar in μm.

A number of significant features of the mineralization in the GLI can be noted:

1. Chalcopyrite is the dominant Cu-sulphide mineral forming mainly disseminated but rarely massive mineralization. Early chalcopyrite and some pyrite display segregation textures.

2. Pyrrhotite is absent, and pentlandite is a subordinate sulphide only occurring as an exsolved phase in siegenite. Pyrrhotite and pentlandite are the principal hosts of PGM in other major deposits (Chapter 4).

3. The PGM are dominated by palladium minerals; sperrylite is the only platinum mineral found. Ir-, Rh-, and Os-based PGM are absent.

4. Although disseminated chalcopyrite hosts most of the PGM, particularly samples 55B and C, few are present in the massive chalcopyrite. Some samples hosting disseminated (G-30A, 44A) and also massive chalcopyrite (G-44B and 48A/B) are PGM-free. In contrast, some sperrylite and palladium antimonide grains are present in the silicate groundmass with no obvious association with any sulphide mineral. The host rock is deuterically altered but lacks hydrous and sulphide minerals and contains neither quartz nor carbonate.

3.4 Paragenesis

The paragenetic sequence of the sulphides, sulpharsenide, niccolite, tellurides, PGM, and electrum is shown in Figure 3.24. The chalcopyrite

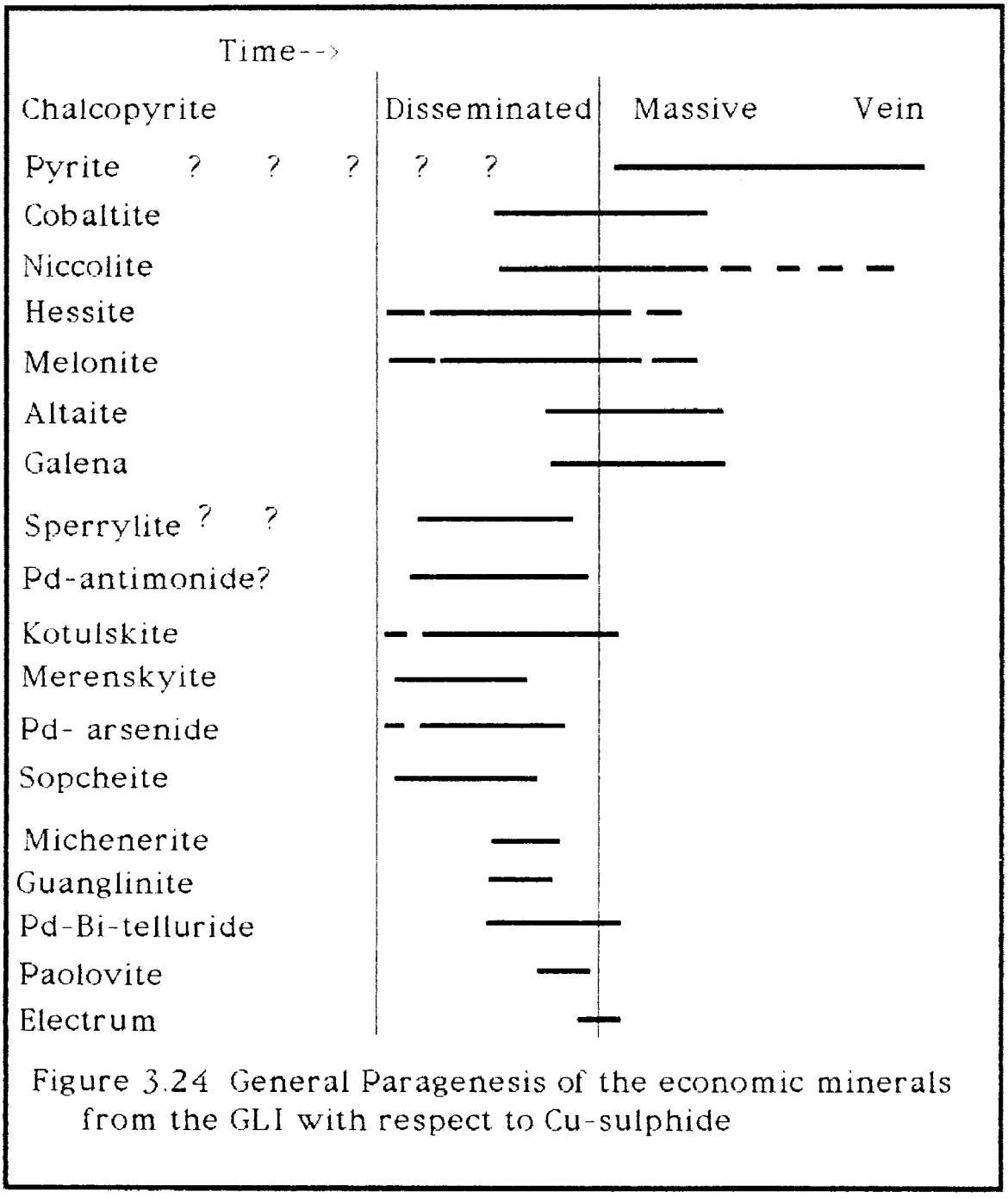

Figure 3.24 General Paragenesis of the economic minerals from the GLI with respect to Cu-sulphide

deposition spans the entire period of mineralization of the GLI (section 3.3.1). While the latest pyrite deposition is indicated by veinlets cutting massive chalcopyrite, the timing of the deposition of the earlier pyrite cannot be accurately determined (page 157). The deposition of the disseminated chalcopyrite was followed by cobaltite and niccolite as replacements of chalcopyrite.

Palladium antimonide, some sperrylite, and the probable new mineral (Pd-Ni-As), which are hosted by silicate minerals and not chalcopyrite, may be the earlier phases among the PGM and tellurides to precipitate. Palladium antimonide and sperrylite, however, continued to precipitate even after the onset of the deposition of hessite and melonite, because palladium antimonide is intergrown with hessite, and is either intergrown with, or a replacement of, palladium arsenide which is hosted by chalcopyrite. Small sperrylite inclusions also occur in disseminated chalcopyrite (sample 55B).

Mostert *et al.* (1982) stated that the PGM of the Impala Mine crystallized after the chalcopyrite because they occur mostly on the margins of the Cu sulphide. Vermaak and Hendriks (1976) indicated that minerals which are euhedral in chalcopyrite but irregular against the silicate matrix crystallized after the solidification of the silicate, while the sulphide was still in a molten state. This relationship is observed in the GLI where coarse-grained melonite, hessite, kotulskite, palladium arsenide, sopcheite, and merenskyite occur as euhedral to anhedral crystals between disseminated chalcopyrite and silicate. The tellurides and PGM, also rim the Cu sulphide and fill in the interstices between the chalcopyrite and silicate, suggesting a

later deposition than the Cu sulphide. It appears that the initial deposition of the coarse-grained tellurides and PGM was contemporaneous with, or slightly earlier than, the disseminated chalcopyrite, and that the tellurides and PGM continued to precipitate after the deposition of the Cu sulphide. These PGM ended their precipitation before the crystallization of the massive chalcopyrite and formation of chalcopyrite veinlets, since no PGM were found in these Cu sulphides. The presence of melonite and hessite in the massive chalcopyrite demonstrates that the tellurides continued to deposit until the main Cu sulphide mineralization ceased. The size and abundance of the tellurides are, however, diminished in the massive chalcopyrite.

Michenerite, paolovite, palladium bismuthotelluride, and guanglinite, which occur as oval and anhedral inclusions in chalcopyrite, or in late magnetite in the case of fine grained palladium arsenide, are interpreted to have exsolved from their host. Altaite replaces melonite, and galena replaces hessite and melonite, thus the two lead minerals form later than melonite and hessite. Altaite and galena are also present in massive chalcopyrite. Electrum, which rims paolovite, represents the latest stage of precious metal mineralization.

In summary, the general paragenetic sequence of mineralization of the GLI commenced with fine-grained chalcopyrite crystallization together with sperrylite and palladium antimonide, followed by, in no particular order, disseminated chalcopyrite blebs, coarse-grained melonite, hessite and PGM, and later by massive chalcopyrite, fine-grained melonite and hessite, altaite, and galena. Crystallization terminated with the formation of electrum,

chalcopyrite and pyrite veinlets. Bornite exsolution occurred upon cooling and chalcocite was formed by supergene processes.

3.5 Conditions of Deposition

3.5.1 Temperature

In this section, "fixed point" geothermometers and textural relationships between the sulphides and tellurides/PGM described earlier are used to constrain the range of depositional temperatures of the disseminated chalcopyrites, coarse-grained tellurides and PGM. The melting points of hessite (959°C), kotulskite (720°C), altaite (977°C), and merenskyite (740°C) have been reported by (Chizhikov and Shchatlivyi, 1970) and Hoffman and MacLean (1976). These are maximum temperatures of crystallization, and for synthetic minerals they are usually higher than those occurring in natural assemblages (Gilbert and Park, 1981) as indicated by the compositions and textural relationships of these minerals. For example, hessite is intergrown with kotulskite, therefore, its maximum temperature must be equal to or lower than 720°C. Altaite replaced hessite, suggesting that it was formed below 720°C.

Disseminated chalcopyrites infilled the interspaces between the ilmenite exsolution lamellae in magnetite, indicating that the Cu-sulphides were deposited after the temperature of equilibration of the magnetite-ilmenite pairs (average 608° ± 35°C., Chapter 2). Therefore, the temperature

of deposition of the disseminated chalcopyrite must be below 608° ± 35°C. This temperature is close to the upper stability temperature of chalcopyrite, 557°C (Craig, 1974). Coarse-grained melonite and hessite, kotulskite, merenskyite, sopcheite, and palladium arsenide, which occurred with the chalcopyrites, hence, were most likely precipitated at 557°C and lower. This deduction agrees with the experimental results of Hoffman and MacLean (1976), who, on the basis of the phase relations between merenskyite and michenerite, have shown that the Bi-rich portion of the solid-solution michenerite melts incongruently at 489° ± 3°C, and the Te-rich portion (merenskyite) melts at 501° ± 3°C to Bi-rich kotulskite and liquid. Kotulskites in the GLI are Bi-rich (Table 3.10A), thus, the maximum deposition temperature of this palladium telluride, plus hessite and sopcheite which are intergrown with kotulskite, is approximately 501°C. Michenerite formed at temperature ≤ 489°C, which is also the deposition temperature of paolovite and guanglinite. The maximum stability of the low temperature chalcocite is about 435 °C (Craig, 1982). Coarse-grained tellurides and PGM are not associated with this Cu sulphide, which is a supergene phase in the GLI (section 3.3.1), therefore, they most likely formed at ≥ 435 °C. Paolovite has been experimentally determined to form from hydrothermal chloride solutions at temperatures of 300° to 400°C (Genkin and Evstigneeva, 1986). PGM from a hydrothermal environment were considered to have formed within the temperature interval 270° and 400°C (Mihalik *et al*, 1974). The PGM from the GLI is a (late) magmatic deposit (section 3.6), therefore, its temperature of mineralization is likely

higher than those of hydrothermal deposits. The mineralization of the disseminated chalcopyrite, coarse-grained tellurides and PGM from the GLI, therefore, appears to be within the temperature interval 557° and 400°C. The maximum temperature, however, may not be applicable to the palladium antimonide, sperrylite, and the probable new minerals which are not hosted by chalcopyrite and are not intergrown with other PGM. Late stage massive chalcopyrite mineralization, which is telluride- and PGM-free (sample 44), might occur at a lower temperature than the main stage of mineralization.

3.5.2 Tellurium and Sulphur Fugacities

The conditions of deposition of the sulphides, tellurides, and most PGM in terms of the prevailing fugacities (equal to partial pressures in this thesis) of sulphur and tellurium, were inferred from the predominance diagrams for the systems Pb-PbS-PbTe, Ag-Ag_2S-Ag_2Te-Ag_5Te_3 (or $Ag_{18}Te_{11}$), Pd-PdS-PdTe-$PdTe_2$, Ni-NiS-NiTe-$NiTe_2$, and the Cu-sulphide systems. The PdTe and $PdTe_2$ represent the other PGM (including the palladium antimonide intergrowth with hessite), for which their thermodynamic data are not available. The diagrams were constructed, using the Facility for the Analysis of Chemical Thermodynamics (FACT) computer program (McGill University), at 550°, 500°, 450° and 400°C, in order to cover the temperature range of mineralization. The influence of variation in $P(O_2)$ on mineral stability is negligible because all common

oxides, except those of Fe, are unstable with respect to either sulphides or tellurides (Afifi *et al*, 1988). In the construction of the predominance diagrams, non-solid phases were suppressed and it was assumed that activities of all solid phases are 1 because there are no thermodynamic data for solid solutions.

Four isothermal predominance diagrams at 550°, 500°, 450° and 400°C, superimposing different systems are depicted in Figures 3.25-3.28. The upper and lower limits of $P(Te_2)$ are set by the stability of hessite, because stuetzite (Ag_5Te_3) is absent in the mineral assemblage and argentite (Ag_2S) is a supergene phase. The upper limit of $P(S_2)$ is defined by the phase boundary between bornite plus pyrite and digenite (Cu_9S_5), the latter being absent in the GLI. The position of the boundary between bornite plus pyrite and digenite, however, is approximate because thermodynamic data for their reaction are unavailable. The lower limit of $P(S_2)$ is defined by pyrite and pyrrhotite boundary, since pyrrhotite is absent. Hence, the stippled area bounded by the stability fields of these minerals represents the $P(Te_2)$ and $P(S_2)$ conditions at which the tellurides, PGM and sulphides were deposited.

The mineralogy of the sulphides, tellurides and PGM supports the constraints on the extent of the depositional conditions. The compounds outside of the region such as Pd_4S and PdS_2, heazlewoodite (Ni_3S_2), empressite (NiTe), unnamed Ni_2Te_3, stuetzite (Ag_5Te_3), and native Ni, Pd, Ag, and Pb, are absent in the studied samples. These compounds cannot normally co-exist in equilibrium with the phases in the region. Vaesite (NiS_2) and PdS, which are within the shaded area, were not observed.

Figure 3.25-28 The superimposed predominance diagrams of the sulphides, tellurides and PGM at 550°C, 500°C, 450°C, and 400°C. The stippled areas are depositional conditions.

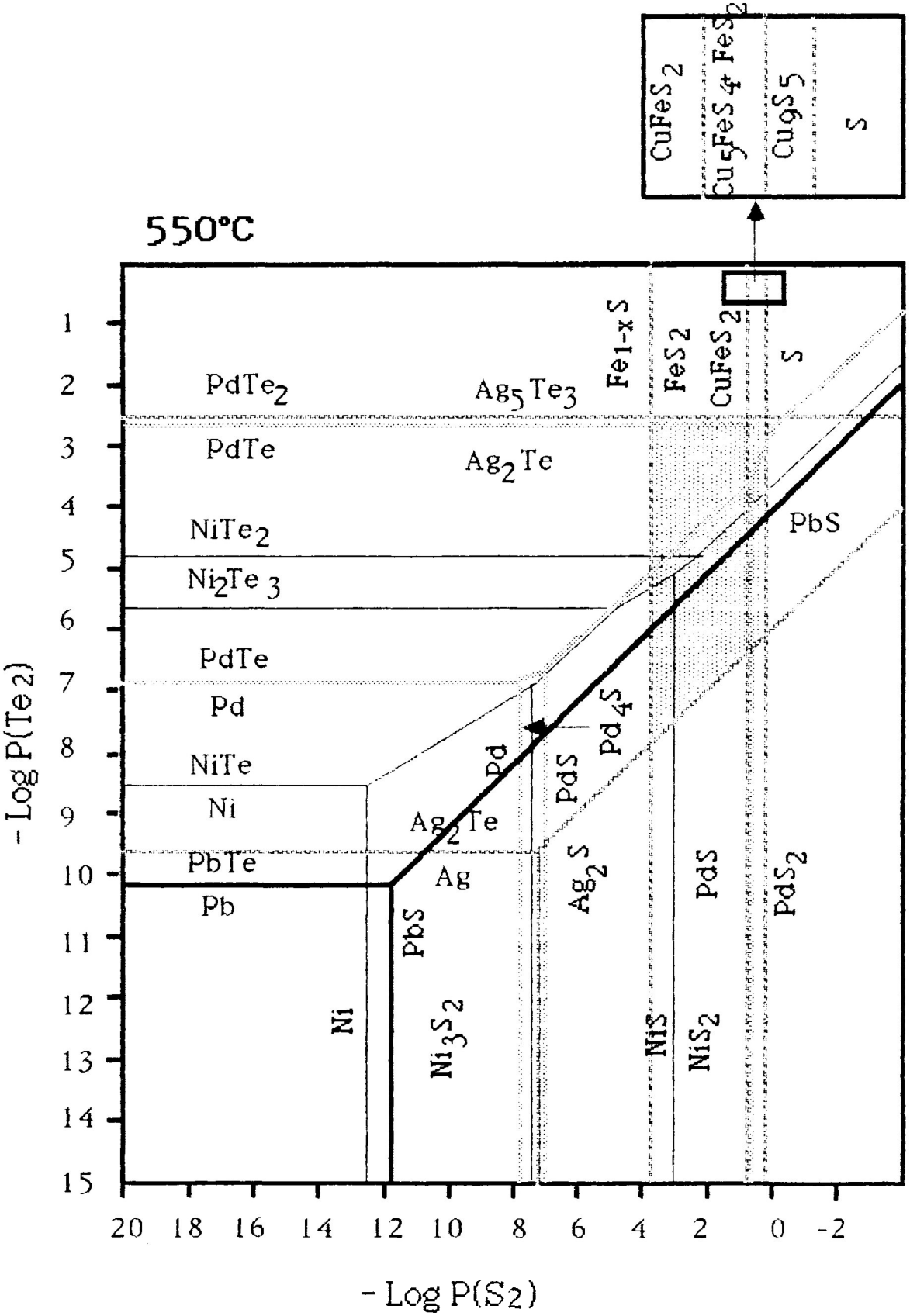
550°C
CuFeS2
Cu5FeS4 + FeS2
Cu9S5
S
PdTe2
Ag5Te3
Fe1-xS
FeS2
CuFeS2
S
PdTe
Ag2Te
NiTe2
Ni2Te3
PbS
PdTe
Pd
NiTe
Ni
Ag2Te
PbTe
Pb
Ag
Pd
PdS
Pd4S
Ag2S
PdS
PdS2
PbS
Ni
Ni3S2
NiS
NiS2
1
2
3
4
5
6
7
8
9
10
11
12
13
14
15
20 18 16 14 12 10 8 6 4 2 0 -2
- Log P(Te2)
- Log P(S2)

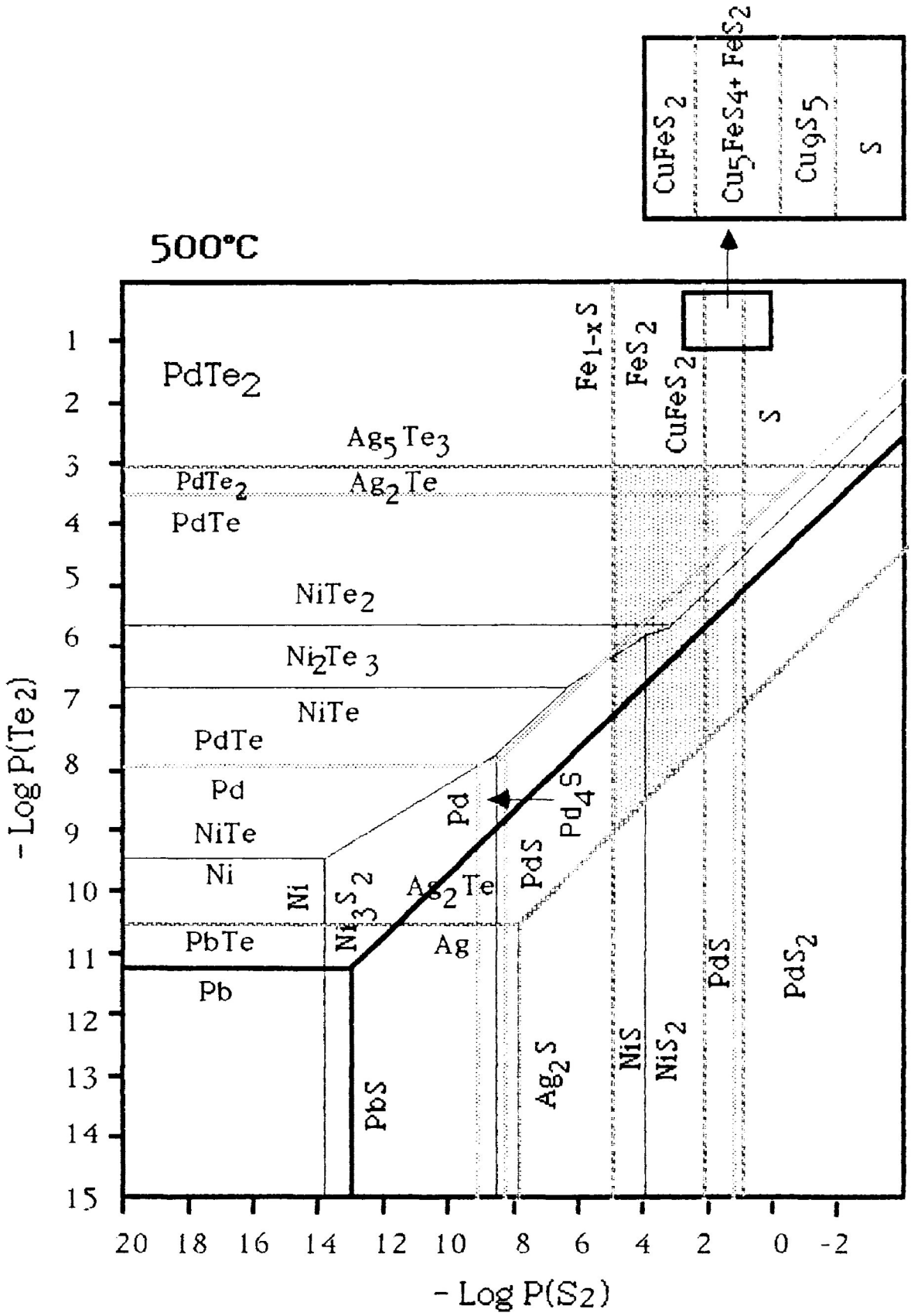
500°C
CuFeS2
Cu5FeS4+ FeS2
Cu9S5
S
PdTe2
Fe1-xS
FeS2
CuFeS2
S
Ag5Te3
PdTe2
Ag2Te
PdTe
NiTe2
Ni2Te3
NiTe
PdTe
Pd
NiTe
Ni
Ni
Ni3S2
Ag2Te
Pd
PdS
Pd4S
PbTe
Ag
Pb
PbS
Ag2S
NiS
NiS2
PdS
PdS2
- Log P(Te2)
- Log P(S2)
1
2
3
4
5
6
7
8
9
10
11
12
13
14
15
20
18
16
14
12
10
8
6
4
2
0
-2

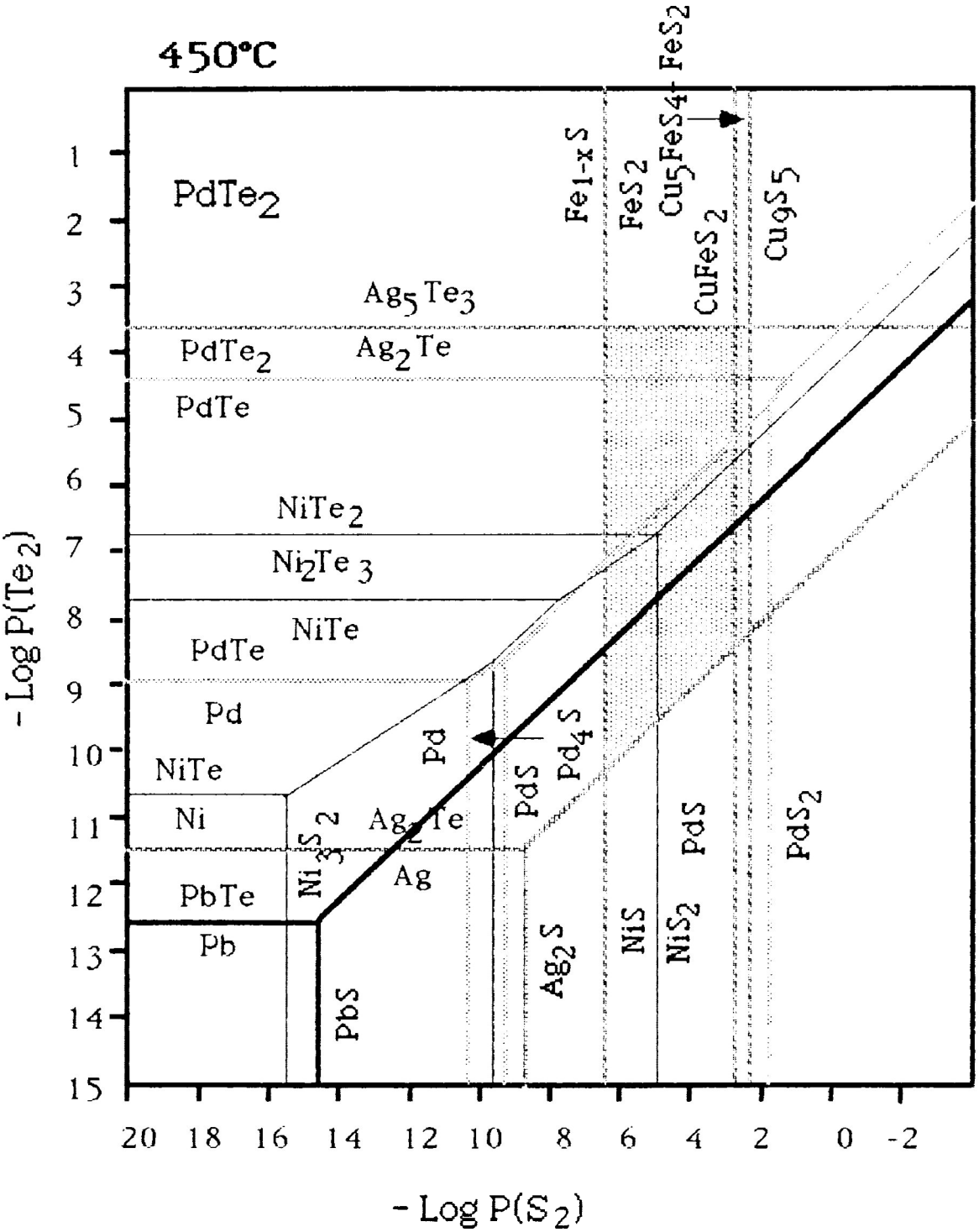
450°C
FeS2
PdTe2
Fe1-xS
FeS2
Cu5FeS4
CuFeS2
Cu9S5
Ag5Te3
PdTe2
Ag2Te
PdTe
NiTe2
Ni2Te3
NiTe
PdTe
Pd
NiTe
Ni
Ni3S2
Ag2Te
Ag
PbTe
Pb
PbS
Pd
PdS
Pd4S
Ag2S
NiS
NiS2
PdS
PdS2
- Log P(Te2)
- Log P(S2)
1
2
3
4
5
6
7
8
9
10
11
12
13
14
15
20
18
16
14
12
10
8
6
4
2
0
-2

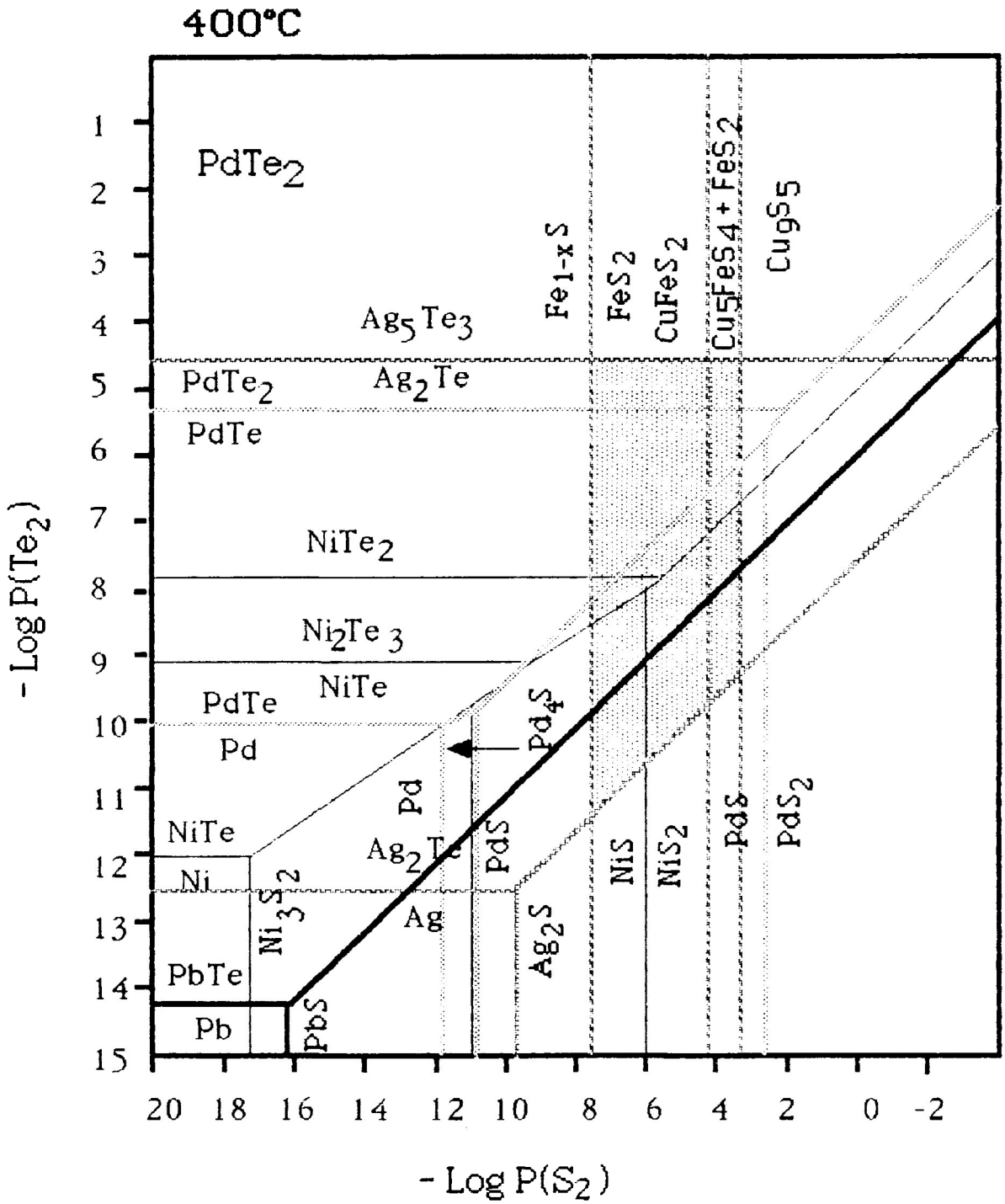
400°C
PdTe2
Ag5Te3
Fe1-xS
FeS2
CuFeS2
Cu5FeS4 + FeS2
Cu9S5
PdTe2
Ag2Te
PdTe
NiTe2
Ni2Te3
NiTe
PdTe
Pd
Pd4S
Pd
NiTe
Ag2Te
PdS
Ni
Ni3S2
Ag
Ag2S
NiS
NiS2
PdS
PdS2
PbTe
Pb
PbS
- Log P(Te2)
- Log P(S2)
1
2
3
4
5
6
7
8
9
10
11
12
13
14
15
20
18
16
14
12
10
8
6
4
2
0
-2

These minerals may have been overlooked but are most likely absent. PdS is the ideal composition for vysotskite, which is the end-member composition of the braggite and vysotskite (Pd, Pt, Ni)S solid-solution series (Cabri *et al*, 1978). PdS is not yet known to exist in nature.

The paragenetic sequence of the sulphides and tellurides were used to indicate the most likely pathway and temperature or range of temperatures of mineral deposition, which in turn indicate the changes of $P(Te_2)$ and $P(S_2)$. The pathway must have started from a point between the pyrite and chalcopyrite field bounded by the lower limit of merenskyite and upper limit of hessite, and moved towards the bornite + pyrite field at any angle between the limits shown by the arraows in Figures 3.29. Mineralization at the GLI, however, did not occur isothermally as indicated by the observed textural relationships between the minerals. For example, the replacement galena did not crystallize contemporaneously with the replaced tellurides. The 550°C diagram, therefore, represents the conditions at which merenskyite, kotulskite, melonite, hessite, pyrite and chalcopyrite formed. Michenerite and other PGM formed at temperature ≤ 489°C (page 205). The depositional temperatures of the early hessite and melonite and PGM can, therefore, be constrained between 450° and 550°C. Galena and altaite replace melonite, hence, they could not have formed at the same conditions. Hence, the 450 and 400°C diagrams are most likely the conditions of the late stage mineralization.

From the above observations, it appears that mineralization started between 550° - 450°C with the deposition of chalcopyrite, coarse-grained

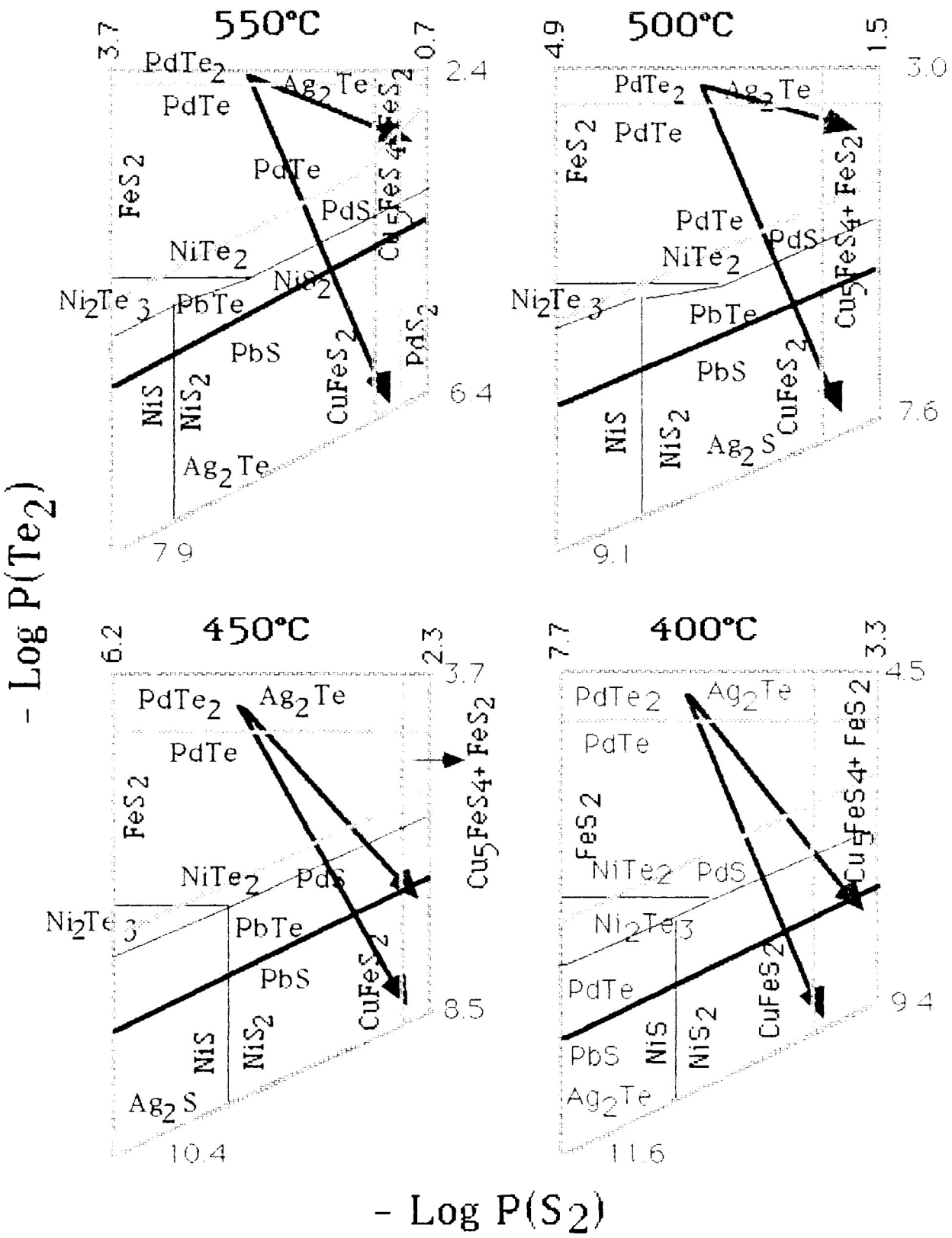

Figure 3.29 Possible pathways of mineralization for the GLI from temperature interval 550° and 400°C.

melonite and hessite, followed by palladium tellurides and perhaps other PGM and tellurides, and ended between 450° and 400°C, when galena and altaite started crystallizing and replacing the earlier formed melonite and hessite. Late stage mineralization includes formation of massive chalcopyrite and sulphide veinlets. Accordingly, the $P(Te_2)$ changed from -2.4 ± 0.13 bar to between -6.4 and -9.7 bar, and the $P(S_2)$ from -3.7 and -0.8 to between -4.5 and -2.3 bar. Hence, during deposition, the tellurium was being depleted from the mineralizing fluids. In contrast, sulfur fugacity appeared to increase. These phenomena are consistent with the observed mineralogy, in which late stage massive chalcopyrite contain only few and fine-grained tellurides.

3.6 Speculation on the Mechanism of Mineralization

Spherical inclusions of sulphide (chalcopyrite in the GLI) in the feldspars represent early trapped sulphide droplets in the silicate melt (Ramdohr, 1980). Chalcopyrite encloses euhedral magnetite grains without corroding them, suggesting that this sulphide was magmatic (Loucks, 1987). Gruenewaldt (1976) stated that crystallization of Fe-rich olivine and clinopyroxene together with magnetite would reduce the solubility of sulphur in the crystallized portion of the magma thereby causing the formation of the sulphide droplets. These observations point to the segregation of sulphide droplets during the crystallization of the GLI.

These droplets then coalesced into sulphide melt. During segregation, the sulphide melt also collected palladium, copper and other chalcophilic elements. The importance of sulphide as a Pd-carrier has been stressed by Crocket *et al.* (1976), who have demonstrated that Pd is more chalcophilic than Pt and, therefore, it tends to partition into the sulphide melt. The association of most tellurides and PGM with chalcopyrite in the GLI fits this hypothesis.

Precipitation of the primary silicate minerals and skeletal magnetite grains during the crystallization of the GLI promoted subsequent chalcopyrite and PGM deposition. Experimental studies by Haughton *et al.*, (1974) have indicated that sulphur is complexed with Fe^{2+} in mafic magmas, thus, the decrease of the Fe^{2+} content of the silicate liquid lowers sulphur solubility and results in the precipitation of sulphide minerals. This stage is represented by the disseminated chalcopyrite and PGM deposition in the GLI. Deposition of the disseminated sulphide decreased the activity of FeS, hence causing oxidation of iron and precipitation of magnetite. This magnetite forms a second or subsequent generation and lacks exsolved ilmenite (Figure 3.3). These ilmenite-poor magnetite grains (Table 2.14) are euhedral to subhedral and set in a groundmass of massive chalcopyrite, thus indicating that this massive chalcopyrite precipitated after the deposition of the magnetite. The melt from which this chalcopyrite crystallized was, however, already depleted in the PGM, which had been precipitated in the earlier phase of sulphide deposition. There appears to have been cyclic depositions of magnetite and chalcopyrite in the formation of the

mineralization of the GLI.

The disseminated chalcopyrites, which occupy silicate interstices, did not replace the silicate minerals along grain boundaries (Figure 3.2A). Their abundance can also be correlated with the amount of subsolidus actinolite, amphibole, and biotite. The PGM-bearing host rocks did not undergo pervasive alteration and contain no secondary minerals such as quartz and carbonates which are typical of hydrothermal deposits; many plagioclases and clinopyroxenes have remained unaltered (Sections 2.3.2 and 2.3.4). These characteristics indicate that the sulphide melt and the residual silicate fluid might have existed concurrently. The mineralization of the GLI, thus, appears to have occurred at the later stage of solidification of the GLI induced by the precipitation of magnetite and involved cyclic depositions of magnetite and chalcopyrite. The alteration of the mineralized rocks is interpreted to result from the circulation of deuteric or residual magmatic fluids.

CHAPTER 4

COMPARATIVE STUDIES, SUMMARY, AND RECOMMENDATIONS

4.1 Comparisons to Other Platinum Deposits

Sulphide and platinum mineralization in the Two Duck Lake area of the Coldwell complex has been reported by Wilkinson (1983) and Watkinson *et al.* (1983). The host rock varies from magnetite-rich banded gabbro, which consists of several sub-units of fine-grained to medium-grained sub-ophitic gabbros, to pegmatitic gabbro-monzonite. The main silicate minerals are olivine (Fo_{56-59}), plagioclase (An_{45-55}), and clinopyroxene ($Di_{24}Hd_{72}Ae_4$- $Di_{35}Hd_{61}Ae_4$). The magnetite grains are equant with exsolved ilmenite lamellae.

The sulphide occurs as disseminated grains in the magnetite layers, which are rather randomly distributed throughout the banded gabbro. In decreasing order of abundance, the sulphides are pyrrhotite, chalcopyrite, cubanite, pentlandite, pyrite and bornite. Hollingworthite and merenskyite occur in association with pyrrhotite, chalcopyrite, and cubanite. Selenide minerals have also been reported. Silicate minerals in contact with the sulphide grains are altered; plagioclase is saussuritized, clinopyroxene is uralitized, and olivine is replaced by serpentine, chlorite and magnetite. Watkinson and Dahl (1987) reported the presence of sperrylite, michenerite, mertieite II, stannopalladinite, kotulskite, zvyiagintsevite [$(Pd, Pt)_3(Pd,Sn)$], and atokite. Mitchell *et al.* (1989) reported the presence of a rhenium

mineral $(Re, Mo)_2S_3$.

The silicate mineral compositions of the banded gabbros are similar to those of the GLI, even though the textures of the two rock types are different. The magnetite-rich layers in the banded gabbro host most of the disseminated sulphide mineralization, whereas the magnetite-rich rocks from the GLI are PGM-free. In addition, the sulphides of the banded gabbro contain pyrrhotite, cubanite and platinum minerals which are absent in the GLI. The host rocks of these two deposits vary little with respect to the texture but they are significantly different in terms of PGM and sulphide assemblages.

The Roby zone of the western gabbro in the Lac-des-Iles mafic-ultramafic complex, northwestern Ontario, hosts sulphide and platinum deposit (Dunning 1979; Watkinson and Dunning, 1979; Sweeny and Edgar, 1988). The zone consists mainly of layered gabbro (70%), norite (20%), clinopyroxenite and anorthosite (10%). The gabbro is composed of cumulus plagioclase, intercumulus clinopyroxene, and orthopyroxene ($En_{72-82.5}$); the compositions of the other silicate minerals were not given.

Sulphide mineralization in the Roby zone, in decreasing order of abundance, consists of pyrite, chalcopyrite, pentlandite, pyrrhotite, millerite, violarite, sphalerite, and galena. The sulphides occur as intercumulus blebs and are most abundant in some of the clinopyroxenite and norite. (Watkinson and Dunning, 1979) reported that vysotskite (Pd, Pt, Ni)S is the most abundant PGM and occurs as discrete anhedra or in lamellar

intergrowth with pentlandite and in chalcopyrite. In contrast, Sweeny and Edgar (1988) stated that kotulskite is the most common PGM, followed by merenskyite and the braggite series. Other PGM present are sperrylite, moncheite, stillwaterite, and Pt-Fe(-Au) alloys.

The Roby zone gabbro of the Lac-des-Iles is different from the GLI in that it is layered and contains orthopyroxene. Pyrrhotite and vysotskite are absent in the GLI. Pyrite is the prominent sulphide in Roby but it is subordinate in the GLI. Chalcopyrite and pentlandite host most of the PGM in the Roby zone gabbro, in contrast, pentlandite in the GLI occurs only as an exsolved phase of siegenite and does not host PGM.

The PGE-Cu-Ni sulphide mineralization of the New Rambler Mine in Wyoming (McCallum *et al.*, 1976., and Loucks, 1987) resembles that of the GLI in that disseminated chalcopyrite is the main sulphide mineralization, palladium tellurides (Pd-Bi-Te) predominate over platinum minerals. Sulphide deposition was induced by early magnetite precipitation, and the mineralization resulted from magmatic processes. The New Rambler ores, however, are hosted by multiple cyclic units of layered mafic-ultramafic rocks such as harzburgite, and orthopyroxenite which grade upward through gabbronorite to quartz-diorite. The presence of pyrrhotite is a major distinction between these two deposits.

The J-M Reef of the Stillwater complex has recently been reinvestigated by Todd *et al.*(1982). The Reef, between 1 and 3 m thick

and about 40 km long, is defined as the platinum and palladium-rich stratigraphic interval. It is characterized by disseminated sulphides and is situated in the basal part of the anorthosite 1 subzone of troctolite-anorthosite zone I. The ore zone is most commonly hosted by troctolite and rarely by norite, two-pyroxene gabbro, peridotite, and anorthosite. All rocks are cumulates. The troctolite consists of olivine (Fo_{74-67}), plagioclase (An_{88-83}) and post cumulus augite and bronzite. The major sulphide minerals, in order of abundance, are chalcopyrite, pyrrhotite, and pentlandite, the others are cubanite, violarite, pyrite and millerite. The sulphides are interstitial to euhedral plagioclase and are locally included in the feldspars. The most abundant PGM are moncheite, cooperite, braggite, and Pt-Fe alloy. Other PGM are palladium minerals and Pt-Pd alloy. The PGM are adjoined or included in the major sulphides.

The troctolite, including the two-pyroxene gabbro, of the J-M Reef is compositionally less evolved than that of the GLI. The sulphides include pyrrhotite which is absent in the GLI, and the PGM are dominated by platinum minerals, in contrast to the predominance of palladium minerals in the GLI.

The two best-developed platinum deposits in the Bushveld complex are the UG-2 layer and Merensky Reef (Sharpe, 1982). Both are associated with ultramafic rocks such as chromitite (chromite, orthopyroxene, and plagioclase) and pyroxenite, respectively. The platinum-group mineralogy of the UG-2 chromitite layer consists mostly of laurite, cooperite, Pt-Ir-Rh-Cu

sulphide, braggite, Pt-Pb-Cu sulphide, vysotskite, Pt-Fe, Pd-Cu, Pd-Pb and Pd-Hg alloys (McLaren and De Villiers, 1982). Associated sulphides are pentlandite, chalcopyrite, pyrrhotite, and pyrite. The PGM in the Merenskyite Reef, although vary in terms of modes of occurrence and compositions from one locality to another, are dominated mainly by braggite, cooperite, laurite, and Pt-Fe alloy, whereas palladium minerals such as merenskyite, kotulskite and michenerite constitute a small fraction of the total assemblage (Vermaak and Hendriks, 1976; Kingston and El-Dosuky, 1982).

The petrology and PGM of these two well-known deposits are very different from those of the GLI. They are associated with layered mafic-ultramafic rocks, and consist mainly of platinum rather than palladium minerals. The mineralization is a product of early magmatic segregation and settling of the sulphides and PGM. In contrast, the GLI is hosted by evolved troctolite and gabbro, and the mineralization occurred at the later stages of magmatic processes. Chromite is absent from the GLI.

From the above comparisons, it is concluded that the platinum-group element mineralization of the GLI is distinct from that of other deposits in terms of petrology and ore mineralogy. The predominance of palladium over platinum minerals is characteristic of the GLI and it may be explained by the hypothesis of Naldrett and Cabri (1976) who stated that the trend of the Pt/(Pt+Pd) ratio is to decrease with increasing differentiation of the host rocks, and that Pt is incorporated preferentially with respect to Pd in early

forming silicates and oxides (chromite). If this is the case, the less evolved portion of the magma, from which the GLI was derived, might contain the missing Ir and Pt elements. The existence of such rocks (co-magmatic with the GLI), however, cannot be proved at present.

4.2 Summary

The Geordie Lake Intrusion consists of troctolite and gabbro. The troctolite is characterized by coarse-grained dendritic olivine and plagioclase with small amounts of clinopyroxene, whereas the gabbro is composed of (ophitic) clinopyroxene, plagioclase and olivine. Despite textural and mineralogical differences, the petrochemistry of the two rock types indicate that there is no differentiation relationship between them. The data also suggest that the parent magma of the GLI was a relatively evolved low-alumina tholeiite. Neither cryptic nor rhythmic layering has been observed.

Cu-sulphide mineralization in the GLI consists mainly of disseminated and rarely massive chalcopyrite. The disseminated Cu sulphides tend to become coarser and more abundant towards the basal sections of the intrusion which is in contact with a syenitic rock. Pyrite is notably rare, pentlandite occurs as a minor exsolution phase, and pyrrhotite is absent. The PGM are dominated by palladium minerals such as kotulskite, merenskyite, palladium bismuthotelluride, sopcheite, paolovite palladium arsenide, guanglinite, and palladium antimonide. Sperrylite is the only platinum mineral found.

The paragenesis suggests that the deposition of chalcopyrite spans the entire period of mineralization. The majority of the tellurides and PGM were precipitated during and after the formation of the disseminated chalcopyrite. Textural relationships between the tellurides/PGM and silicate minerals, together with the inferred temperatures of deposition indicate that mineralization occurred at a later stage in the formation of the GLI. The occurrence of PGM in silicate minerals, the similarity in the mineralogy and mineral chemistry of PGM-bearing and PGM-free rocks, and the absence of pervasive alteration preclude extensive hydrothermal processes as being responsible for the mineralization. The relatively evolved nature of the GLI accounts for the predominance of palladium over platinum minerals. The GLI is unique in the sense that its petrology, geochemistry and mineralization are different to that of other PGE deposits found at the Coldwell complex and elsewhere.

4.3 Recommendations

This thesis has made some contributions to unravelling a small portion of the Geordie Lake Intrusion and its mineralization. Future research should include:

1. Field investigation, including geophysics, of the exact relationships between the GLI and syenitic rocks.

2. Petrological and geochemical studies of the remaining four drill cores in order to examine the lateral extension of the various rock types and

mineralization.

3. Sulphur isotopic studies which may indicate the source of the sulphur, thereby providing additional evidence of the processes leading to mineralization.

4. Radiometric age determination of the GLI and surrounding syenite.

5. Investigation of the sulphide/PGE mineralization in the gabbroic rocks in other localities of the Coldwell complex. These investigations will define the origin of the GLI and mineralization more rigorously, and may also be used to assess the economic potential of the deposits.

"...we seldom understand rocks as well as we think and never as well as we should."

Alexander R. McBirney, 1985.

References

Afifi, A. M., Kelly, W. C., and Essene, E. J., 1988, Phase Relations among Tellurides, Sulfides, and Oxides: II. Apllications to Telluride-Bearing Ore Deposits: Econ. Geol., v. 83, p. 395-404.

Annells, R. N., 1974, Kewenawan Volcanic Rocks of Michipicoten Island, Lake Superior, Ontario: Geol. Surv. Canada Bull. 218, 141p.

Atkins, F. B., 1969, Pyroxenes of the Bushveld Intrusion, South Africa: J. of Petrol., v. 10, p. 222-249.

Aubut, A. J., 1977, The Geology of the Southwest Margin of the Coldwell Complex: Unpublished BSc (Honours) Thesis, Lakehead University, Thunder Bay, Ontario, 115 p.

Basaltic Volcanism Study Project (1981) *Basaltic Volcanism on the Terrestrial Planets* Pergamon Press, Inc., New York. 1286 p.

Bell, K., and Blemkinsop, J., 1980, Ages and Initial 87Sr/86Sr Ratios from Alkalic Complexes, Ontario: Ontario Geological Survey Misc. Paper 93, p. 16-23.

Bell, K., and Blemkinsop, J., and Watkinson, D. H., 1979, Rb/Sr Geochronology of Alkalic Complexes, Ontario: Ontario Geological Survey Misc. Paper 87, p. 69-78.

Boone, C. M., 1969, Origin of Clouded Red Feldspars: Petrologic Contrast in a Granitic Porphyry Intrusion: Am. J. Sci. v. 267, p. 633-668.

Boynton, W. C., 1984, Cosmochemistry of the Rare-Earth Elements; Meteorite Studies *in* Henderson, P., ed., Rare Earth Element Geochemistry, El Sevier, p. 63-107.

Brown, G.E., 1982, Olivines and Silicate Spinels, *in* Orthosilicates, Reviews in Mineralogy, v. 5, Ed. Ribbe, P.H., MSA, p. 275-329.

Buddington, A. F., and Lindsley, D. H., 1964, Iron-Titanium Oxide Minerals and Synthetic Equivalents: J. Petrol. 5, Part 2, p. 310-357.

Cabri, L. J., and Harris, D. C., and Gait, R. L., 1973, Michenerite (PdBiTe) Redefined and Froodite ($PdBi_2$) Confirmed from the Sudbury Area: Canadian Mineralogist, v. 11, p. 903-912.

Cabri, L. J., and Laflamme, J. H., 1976, The Mineralogy of the Platinum-Group Elements from Some Copper-Nickel Deposits of the Sudbury Area, Ontario: Econ. Geol. v. 71, p. 1159-1195.

Cabri, L. J., and Laflamme, J. H., 1981, Analyses of Minerals containing Platinum-Group Elements *in* Platnum-Group Elements: Mineralogy, Geology, Recovery, CIM Special Volume 23, p. 151-176.

Cabri, L. J., and Laflamme, J. H., Stewart, J. M., Turner, K., and Skinner, B.J., 1978, On Cooperite, Braggite, and Vysotskite: American Mineralogist, v. 63, p. 832-839.

Card, K. D., Church, W. R., Franklin, J. M., Frarey, M. J., Robertson, J. A., West, G. F., and Young, G. M., 1972, The Southern Province, *in* Variations in Tectonic Styles in Canada (Ed. Price, R.A., and Douglas, R. J): Geol. Assoc. of Canada Special Paper 11, p. 335-380.

Chaudhuri, S., Brookins, D.G. and Fenton, M.D., 1971, Rubidium-strontium Whole Rock and Mineral Ages of the Coldwell, Ontario Syenites: Geological Society of America, North-Central Meeting, Lincoln, NE, Abstracts with Programs, 255.

Chizhikov, D. M., and Shchastlivyi, V. P., 1970, Tellurium and Tellurides: Collet's (Publishers) Ltd, London and Wellingborough, p. 205-219 and p. 251-259.

Chou, I-Ming, 1978, Calibration of Oxygen Buffers at Elevated P and T using the Hydrogen Fugacity Sensor: Amer. Mineral. v. 63, p. 690-703.

Cooper, W. C., Bennett, K. G., and Croxton, F. C., 1974, The History, Occurrence, and Properties of Selenium *in* Zingaro, R. A., and Cooper, W. C., eds., Selenium and Selenide: Van Nostrand Reinhold Company, New York, p. 1-26.

Craig, J. R., 1982, The Cu-Fe-S System, *in* Sulfide Phase Equilibria: Sulfide Mineralogy, Reviews in Mineralogy Volume 1 (Ed. Ribbe, P.H), MSA, p. 64-76.

Craig, J. R., and Vaughan, D. J., 1981, Ore Microscopy and Ore Petrography: John Wiley and Sons, New York, 393p.

Crocket, J. H., Teruta, Y., Garth, J., 1976, The Relative Importance of Sulfides, Spinels, and Platinoid MInerals as Carriers of Pt, Pd, Ir, and Au in the Merensky Reef at Western Platinum Ltd, near Marikana, South Africa: Econ. Geol. v. 71, p. 1308-1323.

Currie, K. L., 1980, A Contribution to the Petrology of the Coldwell Alkaline Complex, Northern Ontario: Geological Survey of Canada Bulletin 287, 43p.

Currie, K. L., Eby, N. G., and Gittins, J., 1986, The Petrology of the Mont Saint Hilaire Complex, Southern Quebec: An Alkaline Gabbro-Peralkaline Syenite Association: Lithos, v. 19, p. 65-81.

Czamanke, G.K., Ishihara, S., and Atkin, S.A., Chemistry of Rock-Forming Minerals of the Cretaceous-Paleocene Batholith in Southwestern Japan and Implications for Magma Genesis, JGR. v. 86(B11) p. 10431-10469.

Deer, W. A., Howie, R. A., and Zussman, J., 1978, Rock-Forming Minerals, Volume 2A, Single-Chain Silicates: John Wiley & Sons, New York, 668p.

Donaldson, Colin H., 1976, An experimental Investigation of Olivine Morphology: Contrib. Mineral. Petrol., v. 57, p. 187-213.

Dunning, G. R., 1979, The Geology and Platinum-Group Mineralization of the Roby Zone, Lac-des-Iles Complex, Northwestern Ontario: Unpublished MSc Thesis, Carleton University, 129p.

Dunning, G. R., Laflamme, J. H., and Criddle, A. J., 1984, Sopcheite: A Second Canadian Occurrence, from the Lac-Des-Iles Complex, Ontario: Can. Mineral. v. 22, p. 233-237.

Elthon, D., 1987, Petrology of Gabbroic Rocks from the Mid-Cayman Rise Spreading Center: J. Geophysc. Res., v. 92, No. B1, p. 658-682.

FACT Guide to Operations: 1985, Ed. Bale, C. W., Thompson, W. T., and Pelton, A. D., McGill University.

Fairbairn, H. W., Bullwinkel, J. M., Pinson, W. H., and Hurley, P. M., 1959, Age Investigation of Syenites from Coldwell, Ontario: Proceedings of the Geological Society of Canada, 11, p. 141-144.

Garuti, G., and Rinaldi, R., 1986, Mineralogy of Melonite-Group and Other Tellurides from the Ivrea-Verbano Basic Complex, Western Italian Alps: Econ. Geol. v. 81, p. 1213-1217.

Genkin, A. D., and Evstigneeva, T. L., 1986, Associations of Platinum-Group Minerals of the Noril'sk Copper-Nickel Sulfide Ores: Econ. Geol. v. 81, p. 1203-1212.

Guilbert, J. M., and Park, C. F. Jr., 1986, Geothermometry, Geobarometry, and Isotopic Studies *in* The Geology of Ore Deposits: W. H. Freeman and Company, New York, p. 251-294.

Grant, S. M., 1988, Diffusion Models for Corona Formation in Metagabbros from the Western Grenville Province, Canada: Contrib. Mineral Petrol., v. 98, p. 49-63.

Green, J. C., 1983, Geologic and Geochemical Evidence for the Nature and Development of the Middle Proterozoic (Keweenawan) Midcontinent Rift of North America: Tectonophysics, 94, p. 413-437.

Griffin, W. L., and Heier, K. S., 1973, Petrological Implications of Some Corona Structures: Lithos, v. 6, p. 315-335.

Halls, H. C., 1978, The Late Precambrian Central North American Rift System-A Survey of Recent Geological and Geophysical Investigations, *in* Neumann, E. R., and Ramberg, T. B., eds., Tectonics and Geophysics of Continental Rifts: NATO Advanced Study Institute Series C., v. 37, p. 111-123

Haughton, D. R., Roeder, P. L., and Skinner, B. J., 1974, Solubility of Sulfur in Mafic Magmas: Econ. Geol. v. 69, p. 451-467.

Hawthorne, F. C., 1982, Crystal Chemistry of the Amphiboles, *in* P. H. Ribbie (Ed.), Amphiboles: Petrology and Experimental Phase Relations, Mineralogical Society of America Reviews in Mineralogy v. 9A., Chapter 1, pp 1-95.

Heaman, L.M. and Machado, M., 1987, Isotope Geochemistry of the Coldwell Alkaline Complex, I, U-Pb Studies on Accessory Minerals: Geological Assoc. of Canada and Mineralogical Assoc. of Canada Joint Annual Meeting, Program with Abstracts, v. 12.

Hoffman, E., and MacLean, W. H., 1976, Phase Relations of Michenerite and Merenskyite in the Pd-Bi-Te System: Econ. Geol. v. 71, p. 1461-1468.

Hudson, D. R., 1986, Platinum-Group Minerals from the Kambalda Nickel Deposits, Western Australia: Economic Geology, v. 81, Number 5, p. 1218-1225.

Jago, B. C., 1980, Geology of a Portion of the Western Contact Margin, the Coldwell Complex: Unpublished BSc (Honours) Thesis, Lakehead University, Thunder Bay, Ontario, 98 p.

Joeston, R., 1986, The Role of Magmatic Reaction, Diffusion and Annealing in the Evolution of Coronitic Microstructure in Troctolitic Gabbro from Risor, Norway: Mineralogical Magazine, v. 50, p. 441-467.

Kelly, W. C., and Goddard, E. N., 1969, Telluride Ores of Boulder County, Colorado: The Geological Society of America Memoir 109, 237p.

Kingston, G. A., and El-Dosuky, B. T., 1982, A Contribution on the Platinum-Group Mineralogy of the Merensky Reef at the Rustenburg Platinum Mine: Econ. Geol., v. 77, p. 1367-1384.

Kinloch, E. D., 1982, Regional Trends in the Platinum-Group Mineralogy of the Critical Zone of the Bushveld Complex, South Africa: Econ. Geol. v. 77, p. 1328-1347.

Klasner, J. S., Cannon, W.F. and van Schmus, W.R.., 1982, The Pre-Keweenawan Tectonic History of Southern Canadian Midcontinent Rift, *in* Geology and Tectonics of the Lake Superior Basin: Geological Society of America Memoir 156, p. 27-46.

Kushiro, I., 1960, Si-Al Relation in Clinopyroxenes from Igneous Rocks: Am. J. Sci., v. 258, p. 548-554.

Laderoute, D., 1988, The Petrography, Geochemistry and Petrogenesis of Alkaline Dyke Rocks from the Coldwell Alkaline Complex, NW Ontario: Unpublished MSc Thesis, Lakehead University, Thunder Bay, Ontario, 318p.

Leake, B. E., 1978, Nomenclature of Amphiboles: Can. Mineral. v. 16, Part 4, p. 501-520.

LeBas, M. J., 1962, The Role of Aluminum in Igneous Clinopyroxenes with Relation to Their Parentage: Amer. J. Sci., v. 260, p. 267-288.

Lilley, F.E.M. 1964, An Analysis of the Magnetic Features of the Port Coldwell Intrusive: Unpublished MSc Thesis, University of Western Ontario, London.

Lister, G. F., 1966, The Composition and Origin of Selected Iron-Titanium Deposits: Econ. Geol. v. 61, p. 257-274.

Loucks, R. R., 1987, Magmatic PGE-Cu-Ni Sulfide Mineralization and Generalized Petrology and Structure of the Early Proterozoic Mullen Creek Layered Mafic-Ultramafic Intrusion, Medicine Bow Mountains, Wyoming: Unpublished Report, Purdue University, 36p.

Lukosius-Sanders, J., 1988, Petrology of Syenites from Centre III of the Coldwell Alkaline Complex, Northwest Ontario: Unpublished Msc Thesis, Lakehead University, Thunder Bay, Ontario, 110 p.

Lum, H. K., 1973, Petrology of the Eastern Gabbro and Associated Sulfide Mineralization of the Coldwell Alkalic Complex, Ontario: Unpublished Honours BSc. Thesis, Carleton University, Ontario, 65 p.

Mathison, C.I., 1975, Magnetites and Ilmenites in the Somerset Dam Layered Basic Intrusion, Southeastern Queensland: Litho, v. 8, p. 93-111.

Mathison, C.I., 1987, Cyclic Units in the Somerset Dam Layered Gabbro Intrusion, Southeastern Queensland, Australia: Lithos, v. 20, p. 187-205.

Mathison, C.I., and Hamlyn, P.R., 1987, The McIntosh Layered Troctolite-Olivine Gabbro Intrusion, East Kimberley, Western Australia: J. Petrol., v. 28, p. 211-234.

McBirney, A. R., 1984, Igneous Petrology: Freeman, Cooper and Co., San Francisco, 441p.

McCallum, I. S., Raedeke, L. D., and Mathez, E. A., 1980, Investigations of the Stillwater Complex: Part I. Stratigraphy and Structure of the Banded Zone: American Journal of Science, v. 280-A, p. 59-87.

McCallum, M. E., Loucks, R. R., Carlson, R. R., Cooley, E. F., and Doerge, T. A., 1976, Platinum Metals Associated with Hydrothermal Copper Ores of the New Rambler Mine, Medicine Bow Mountains, Wyoming: Econ. Geol. v. 71, p. 1429-1450.

McGill, M. K., 1980, The Coldwell Complex Western Margin-Petrology and Intrusive Relationships: Unpublished BSc (Honours) Thesis, Lakehead University, Thunder Bay, Ontario, 98 p.

McLaren, C. H., and De Villiers, J. P. R., 1982, The Platinum-Group Chemistry and Mineralogy of the UG-2 Chromitite Layer of the Bushveld Complex: Econ. Geol., v. 77, p. 1348-1366.

Mihalik, P., Jacobsen, B. E., and Hiemstra, S. A., 1974, Platinum-Group Minerals from a Hydrothermal Environment: Econ. Geol. v. 69, p. 257-262.

Mitchell, R. H., and Platt, R. G., 1978, Mafic Mineralogy of Ferroaugite Syenite from the Coldwell Alkaline Complex, Ontario, Canada: Journal of Petrology, v. 19, Part 4, p. 627-651.

_____ 1982, Mineralogy and Petrology of Nepheline Syenites from the Coldwell Alkaline Complex, Ontario, Canada: Journal of Petrology, v. 23, Part 2, p. 186-214.

Mitchell, R. H., Laflamme, J.H., and Cabri, L. J., 1989, Rhenium Sulfide from the Coldwell Complex, Northwestern Ontario, Canada: Mineralogical Magazine (in press).

Mitchell, R. H., Platt, R. G., and Cheadle, S. P., 1983, A Gravity Study of the Coldwell Complex, Northwestern Ontario and Its Petrological Significance: Canadian Journal of Earth Sciences, v. 20, No.11, p. 1631-1638.

Morimoto, N., 1988, Nomenclature of Pyroxenes: Scheiz. Mineral. Petrogr. Mitt. v. 68, p. 95-111.

Mostert, A. B., Hofmeyr, P. K., and Potgieter, G. A., 1982, The Platinum-Group Mineralogy of the Merensky Reef at the Impala Platinum Mines, Bophuthatswana: Econ. Geol., v. 77, p. 1385-1394.

Muir, I. D., and Tilley, C. E., 1964, Basalts from the Northern Part of the Rift zone of the Mid-Atlantic Ridge: J. Petrology, v. 5, p. 409-434.

Naldrett, A. J., and Cabri, L. J., 1976, Ultramafic and Related Mafic Rocks: Their Classification and Genesis with Special Reference to the Concentrations of Nickel Sulfides and Platinum Group Elements: Econ. Geology, v. 71, p. 1131-1158.

Patterson, G.C., Scott, J. F., Mason, J. K., and Schnieders, B. R., MacTavish, A. D., Dutka, R. J. A., Kennedy, M. C., White, G. D., and Hinz, P., 1987, Report of Activities (1986) Regional and Resident Geologists: Ontario Geological Survey Miscellaneous Paper 134, p. 113-115.

Platt, R. G., and Mitchell, R. H., 1982, Rb-Sr Geochronology of the Coldwell Complex, Northwestern Ontario, Canada: Canadian Journal of Earth Sciences, v. 19, p. 1796-1801.

Prichard, H. M., and Tarkian M., Platinum and Palladium Minerals from Two PGE-rich Localities in the Shetland Ophiolite Complex: The Canadian Mineralogist, v. 26, p. 979-990.

Puskas, F.P., 1967, The Geology of the Port Coldwell Area: Ont. Dept. Mines Open File Rpt. 5104, Thunder Bay, Ont.

Ramdohr, P., 1980, The Ore Textures *in* The Ore Minerals and Their Intergrowths, Pergomon Press, Toronto, p. 81-258.

Robins, B., 1972, Crescumulate Layering in a Gabbroic Body on Seiland, Northern Norway: Geol. Mag. v. 109, p. 532-541.

Sharpe, M. R., Nobel Metals in the Marginal Rocks of the Bushveld Complex: Econ. Geol. v. 77, p. 1286-1295.

Simkin, T., and Smith, J.V., 1970, Minor-element Distribution in Olibine: J. Geol., v. 78, p. 304-325.

Stormer, J. C. Jr., 1975, A Practical Two-feldspar Geothermometer: Amer. Mineral., v. 60, p. 667-674.

Streckeisen, A.,1976, To Each Plutonic Rock Its Proper Name: Earth Science Reviews, v. 12, p. 1-33.

Sweeny, J. M., and Edgar, A. D., 1988, The Geochemistry, Origin, and Economic Potential of Platinum Group Element Bearing Rocks of the Lac des Iles Complex, Northwestern Ontario: Ontario Miscellaneous Paper 140, p. 68-77.

Todd, S. G., Keith, D. W., Le Roy, L. W., Schissel, D. J., Mann, E. L., and Irvine, T. N., 1982, The J-M Platinum-Palladium Reff of the Stillwater Complex: I. Stratigraphy and Petrology: Economic Geology, v. 77, No. 6, p. 1454-1480.

Tyson R. M., and Chang, L. L. Y., 1984, The Petrology and Sulfide Mineralization of the Partridge River Troctolite, Duluth Complex, Minnesota:Canadian Mineralogist, v. 22, Part 1, p. 23-38.

van der Merve, M. J., 1976, The Layered Sequence of the Potgietersrus Limb of the Bushveld complex: Economic Geology, v. 71, No. 7, p. 1337-1351.

Vemaak, C. F., and Hendriks, L. P., 1976, A Review of the Mineralogy of the Merensky Reef, with specific to New Data on the Precious Metal Mineralogy: Econ. Geol. v. 71, No. 7, p. 1244-1269.

von Gruenewaldt, G., Sharpe, M. R., and Hatton, C. J., 1985, The Bushveld Complex: Introduction and Review: Economic Geology, v. 80, No. 4, p. 803-812.

Vuorelainen, Y., Hakli, A., Hanninen, E., Papunen, Reino, J., and Tornroos, R., 1982, Isomertieite and Other Platinum-Group Minerals from the Konttijarvi Layered Mafic Intrusion, Northern Findland: Econ. Geol. v. 77, p. 1511-1518.

Wager, L. R., and Brown, G. M., 1965, Layered Igneous Rocks: W. H. Freeman and Co., San Francisco, 585 p.

Walker, J. W. R., 1967, Geology of the Jackfish-Middleton Area: Ont. Dept. Mines Geol. Rpt. 50, 41p.

Watkinson, D. H., and Dahl, R., 1987, Platinum-Group Mineral Precipitation from Fluids in Pegmatitic Gabbro: Two Duck Lake Intrusion, Coldwell Complex, Ontario, Canada: Geo-Platinum '87, p. 237.

Watkinson, D. H., and Dunning, G. R., 1979, Geology and Platinum-Group Mineralization, Lac-Des-Iles Complex, Northwestern Ontario: The Canadian Mineralogist, v. 17, pp.453-462.

Watkinson, D. H., Whittaker, P. J., and Jones, P. L., 1983, Platinum Group Elements in the Eastern Gabro, Coldwell Complex, Northwestern Ontario: OGS Misc. Paper 113, p. 183-191.

Weiblen, P. W., and Morey, G. B., 1980, A Summary of the Stratigraphy, Petrology, and Structure of the Duluth Complex: American Journal of Science, v. 280-A, p. 88-133.

Wilkinson, S. J., 1983, Geology and Sulphide Mineralization of the Margin Phases of the Coldwell Complex, Northwestern Ontario: Unpublished MSc Thesis, Carleton University, Ottawa, Ontario, 113 p.

Williams, H., Turner, F. J., and Gilbert, C. M., 1982, Petrography: An Introduction to the Study of Rocks in Thin Sections: Freeman and Co., New York, 606 p.

Wilson, A. F., 1976, Aluminium in Coexisting Pyroxenes as a Sensitive Indicator of Changes in Metamorphic Grade within the Mafic Granulite Terrane of the Fraser Range Western Australia: Contr. Miner1 Petrol., v. 38, p. 255-277.

Wones, D. R., and Gilbert, M. C., 1982, Amphiboles in the Igneous Environment, *in* P. H. Ribbe, ed., Amphiboles: Petrology and Experimental Phase Relations: Mineralogical Society of America Reviews in Mineralogy v. 9B, p. 335-383.

Yoder, H. S., and Tilley, C. E., 1962, Origin of Basalt Magmas: An Experimental Study of Natural and Synthetic Rock Systems: J. of Petrology, v. 3, p. 342-532.

APPENDIX I

WHOLE-ROCK ANALYSES

1. Rock Powder

All rock powders were prepared by the writer following these procedures:

1. Remove all weathered surfaces using a diamond-impregnated saw blade
2. Reduce samples into chips by either a hydraulic compressor or a tungsten hammer
3. Clean the tungsten shatterbox by grinding with quartz sand
4. Wash the shatterbox and dry with acetone
5. Pre-contaminate the box by grinding a few chips of the next sample
6. Repeat (4)
7. Pulverize the sample

Pulverizing procedures (3 through 7) were repeated for each sample. In addition, similar rocks were pulverized successively, i.e. all gabbros were pulverized before syenites. These procedures minimized contamination.

2. XRF Methods

The compositions of major oxides* and some trace elements were determined by XRF methods by Laurentian University and Nuclear Activation Services Ltd., Hamilton, Ont. The latter laboratory analysed the following samples: G-3, 4, 28, 29, 30, 43, 53, 54, 61, 70, 77, and 78. The accuracy of these methods is given in Table A.1.

*FeO was determined by titration methods by Eleanor Jensen of Lakehead University.

*Sulphur was determined by the writer (Center I and II samples) and Henry Connors (Geordie Lake samples) using the Leco Induction Furnace Model 523 coupled with an automatic titrator. The detection limit is approximately 0.04 wt %.

*Hydrogen and carbon were determined by Keith Pringnitz (Center I and II samples) and Henry Connors (Geordie Lake samples) at Lakehead University using the CHN analyser Model 240XA made by Control Equipment Corporation.

The accuracy of these methods is approximately ± 2 %.

3. Neutron Activation Analysis Methods

Sample preparation, counting and calculation were performed by the writer. Maureen Downey performed the post-irradiation procedures, i.e.,

transferring samples to counting vials and radiochemical separation. Shelley Moogk performed some of the radiochemical separation.

Approximately 0.1 g of rock powder is double wrapped in an aluminum packet measuring approximately 1 cm^2. As many as twenty of these packets, including five or six packets containing rock-standard powders, were put into a small aluminum vial for irradiation. The rock standards are PCC-1, G-2 and STM-1.

The aluminum vial containing individually wrapped sample and standard packets was irradiated in a thermal neutron flux of 4×10^{13} $n/cm^2/sec$ in the McMaster University Nuclear Reactor for five hours (INAA) or twenty four hours (RNAA). The concentration of the following trace and rare-earth elements was determined by the INAA method: Thorium, Tantalum, Hafnium, Scandium, Cobalt, Chromium, Lanthanum, Samarium and Europium. Samarium, Europium, Cerium, Neodymium, Ytterbium, and Lutetium were determined by the RNAA method.

The gamma-ray spectrometer used in this experiment consists of an APTEC NRD PHYGE coaxial spectrometer (1.85 KeV FWHM at 1331 KeV) with a Tennelec Tc 242 Spectroscopy amplifier coupled to a NUCLEAR DATA ND-66 multichannel analyser. A printer is also connected to the analyser to print out the experimental data such as date and time of experiment, positions of peak markers and number of counts for analysed elements. The sample-detector distance is determined by the sample shelf level in which

every sample has a dead time of less than 10 %.

The measure of photopeak areas is done by locating the left- and right-channel markers on either side of the centre of the peak that are above the background. The net peak area, translated into counts, is automatically calculated by a computer program for the full-energy integration method in the analyser.

The element concentrations were calculated using the APL computer programs written by Dr. R. H. Mitchell. The calculation method is based on the comparative approach*. The accuracy of these methods are given in Table A.2.

* $X(\text{sample})/X(\text{standard}) = A_X e^{+\lambda t(\text{sample})} / A_X e^{+\lambda t(\text{standard})}$

where

$X(\text{sample})$ = weight of element X is sample

$X(\text{standard})$ = weight of element X in standard rock

A_X = activity (counts/s) of a radionuclide X at time t

λ = decay constant ($0.693/t_{0.5}$) of the radionuclide

t = decay time after the end of irradiation (λ and t are in the same unit)

Table A.1 Accuracy of XRF methods
*Concensus values are after Abbey (1983)

	Concensus value*	Analyses G2	Analyses G2	Concensus value*	Analyses AGV-1	Analyses AGV-1
SiO2	69.22	69.42	69.21	59.61	59.8	59.9
TiO2	0.48	0.49	0.49	1.06	1.07	1.07
Al2O3	15.4	15.29	15.26	17.19	17.17	17.16
Fe2O3	2.67	2.68	2.67	6.82	6.59	6.6
MnO	0.03	0.03	0.03	0.1	0.1	0.1
CaO	1.96	2.03	2.01	4.94	5.02	5.02
MgO	0.75	0.79	0.78	1.52	1.58	1.59
Na2O	4.06	4.1	4.1	4.32	4.25	4.36
K2O	4.46	4.37	4.4	2.92	2.93	2.91
P2O5	0.13	0.15	0.16	0.51	0.51	0.51

	Concensus value*	G2	G2	Concensus value*	GSP-1	Concensus value*	AGV-1
Ni	3.5	5.76	6.05	9	14.7	15	19.6
Cu	10	10.8	10.6	33	32.7	59	59.1
Zn	84	83.5	87.2	105	103	86	85
Pb	30	31.7	31.7	54	53	33	36.2
Zr	300	306	300	500	509		
Y	11	10.5	10.8	29	26.36		
Sr	480	474	476	240	235		
Rb	170	171	171	250	254		
Ba	1900	1907	1864	1300	1268		

Abbey, S., 1983, Studies in "standard samples" of silicate rocks and minerals 1969-1982:GSC Paper 83-15, 114p.

APPENDIX II
ANALYSES OF MINERAL COMPOSITIONS

All analyses of mineral compositions, with the exception of the olivine standard, were performed by the author using the Hitachi 750 SEM Energy Dispersive X-ray Spectrometry (EDS) at Lakehead University and the JOEL Superprobe Electron Microprobe (EMP) at Dalhousie University. The EMP is equipped with 4 wavelength spectrometers and a Tracor Northern Si(Li) energy dispersive detector.

1. Olivine, telluride, platinum-group mineral and some sulphide compositions were analysed using EDS attached to a scanning electron microscope. The operating conditions were: accelerating voltage of 15 kV, beam current of 0.38 nA, and spot size of approximately 2 µm. The olivine standard used was PL40. The accuracy and precision for MgO, SiO_2, and FeO are shown in Table A.3. The standards for the telluride, PGM and sulphide are synthetic materials. The counting time ranges from 60 to 240 seconds. The analytical data were obtained using the Tracor Northern ZAF computer programmes. The accuracy (± stoichiometry value) of the tellurides and PGM are: -0.4 (Te), -0.7 (Ni), -0.25 (Ag in hessite), -0.1 and +0.1 (Pd) and -0.4 and +1 (Sn) in paolovite, and -4.5 (Pd) in guanglinite.

2. Plagioclase, alkali-feldspar, clinopyroxene, amphibole, biotite, magnetite and ilmenite, and sulphide mineral compositions were analysed using the electron microprobe. The operating conditions were; acceleration voltage 15 KV, beam current of 5 nA, and spot size of approximately 1 µm. The standard minerals used and the accuracy of the method are given in Table A.4.

Table A.2 Accuracy of trace element analyses by INAA and RNAA

INAA

Element	Th		Ta		Hf		La	Eu	
Standard	G2	STM-1	G2	STM-1	G2	STM-1	G2	G2	STM-1
(ppm)	25	33	0.8	19	8	27	92	1.4	3.47
Analyses									
1	24.4	33.3	0.74	19.05	8.12	26.97	91.37	1.4	3.43
2	25.6	32.7	0.86	18.95	7.89	27.03	92.63	1.4	3.51
3	24.89	35.46	0.79	19.7	7.68	26.77	90.62	1.36	3.48
4	25.12	30.71	0.81	18.93	8.34	27.24	93.41	1.44	3.46
5	25.18	31.75	0.8	19.18	7.98	27.17	96.19	1.4	3.48
6	24.82	34.3	0.8	18.83	8.02	26.83	87.99	1.4	3.46
7	26.91	33.31	0.72	18.73	8.59	27.54		1.49	3.43
8	23.23	32.69	0.88	19.28	7.45	26.48		1.32	3.51

Element	Co	Sc	Cr
Standard	PCC-1	PCC-1	PCC-1
(ppm)	110	9	2800
Analyses			
1	112	9.16	2797
2	108	8.84	2802
3	109	8.94	2736
4	111	9.06	2865

RNAA

Element	Ce	Sm		Nd		Tb		Yb		Lu
Standard	G-2	G-2	STM-1	G-2	STM-1	G-2	STM-1	G-2	STM-1	STM-1
(ppm)	160	7.2	12.6	58	0.84	0.5	1.5	0.86	4.57	0.65
Analyses										
1	146	6.24	12.4	66.9	0.8	0.44	1.42	0.84	5	0.63
2	176	8.3	12.78	50	0.88	0.56	1.59	0.88	4.2	0.67
3	162	6.76	12.2	52.7	0.87	0.43	1.53		5	0.66
4	158	7.67	13	64	0.81	0.58	1.55		3.9	0.64

Table A.3 Accuracy and precision of olivine (P140) analyses by EDS
Data compiled by Al McKenzie (Lakehead Univ. SEM Laboratory)

Analyses	MgO	SiO2	FeO	TOTAL
Standard	51.47	41.23	7.28	99.98
1	51.29	41.04	7.34	98.27
2	50.9	41.25	7.41	99.16
3	51.01	41.02	7.46	98.69
4	50.47	41.6	7.21	98.54
5	50.96	41.14	7.29	98.02
6	50.67	41.65	7.18	100.55
7	50.99	41.61	6.86	101.97
8	51.1	41.24	7.1	100.19
9	50.9	41.36	7.13	98.51
10	50.81	41.99	6.64	101.69
11	50.84	41.82	6.82	101.82
12	50.91	41.46	6.94	101.33
13	51.36	41.74	6.58	99.82
14	50.54	41.74	7.13	98.57
15	50.79	41.65	7.12	100.95
16	50.9	41.74	6.85	100.24
17	50.37	41.3	7.32	99.12
Average	50.87	41.47	7.08	99.9
STD	0.23	0.29	0.25	
Accuracy	-0.6	0.24	-0.2	
Precision	0.45	0.57	0.51	

Table A.4 Accuracy of mineral analyses by electron microprobe

	Standard value	Analysis 1	2	3	4	Average	Accuracy	Standard Mineral
SiO2	40.37	40.44	40.31	40.89	40.54	40.55	+ 0.18	Jadeite
TiO2	4.72	4.85	4.85	4.68	4.9	4.82	+ 0.1	Kaersutite
Al2O3	14.9	14.48	14.64	14.74	14.39	14.56	- 0.34	Jadeite
FeO	10.9	10.65	10.52	10.57	10.34	10.52	- 0.38	Magnetite
MgO	12.8	12.53	13.04	12.92	13.19	12.92	+ 0.12	Kaersutite
CaO	10.3	9.89	10.25	10.11	10.17	10.11	- 0.19	Kaersutite
Na2O	2.6	2.79	2.68	2.6	2.91	2.75	+ 0.15	Jadeite
K2O	2.04	2.15	1.99	2.09	2.4	2.16	+ 0.12	Sanidine
TOTAL	98.63	97.78	98.28	98.6	98.84			

APPENDIX III

COMPOSITIONS OF PLAGIOCLASE, CLINOPYROXENE, AMPHIBOLE, AND MAGNETITE-ILMENITE PAIR FROM THE GLI AND OF BIOTITE FROM CENTER II, COLDWELL COMPLEX

FELDSPAR ANALYSES

Rock Type	G		G		AG				
	CORE	RIM	CORE	RIM	CORE	RIM	DUSTY	CORE	RIM
Sample No.	1	1	2	2	5	5	5	5	5
SiO2	54.97	57.78	55.28	58.52	56.34	65.48	66.59	56.33	67.32
Al2O3	27.96	26.57	27.99	25.76	26.66	21.28	19.4	27.38	20.53
FeO	0.67	0.52	0.69	0.54	0.55	0.062	0.18	0.48	0.17
CaO	10.89	8.74	10.62	7.95	9.59	1.19	0.71	9.69	1.35
Na2O	5.56	6.79	5.48	7.46	6.29	10.7	10.76	6.42	11.05
K2O	0.05	0.25	0.46	0.16	0.41	0.9	0	0.25	0.02
TOTAL	100.1	100.65	100.52	100.39	99.84	99.612	97.64	100.55	100.44
Structural Formula based on Thirty-two Oxygens									
Si	9.908	10.293	9.932	10.436	10.164	11.520	11.893	10.087	11.732
Al	5.943	5.581	5.930	5.417	5.671	4.415	4.059	5.782	4.219
Fe3+	0.100	0.078	0.104	0.081	0.083	0.091	0.027	0.072	0.025
Ca	2.106	1.671	2.047	1.521	1.856	0.225	0.136	1.862	0.252
Na	1.945	2.348	1.911	2.583	2.203	3.654	3.731	2.232	3.738
K	0.012	0.057	0.106	0.036	0.094	0.202	0.000	0.057	0.004
Mol. Percent End Members									
Anorthite	51.83	40.99	50.37	36.74	44.69	5.5	3.52	44.85	6.32
Albite	47.89	57.62	47.03	62.38	53.04	89.54	96.48	53.77	93.57
Orthoclase	0.28	1.4	2.6	0.88	2.27	4.96	0	1.38	0.11

Rock Type	G		TR			TR		TR	
	CORE	MANTLE	NEAR. C	W.ALT			DUSTY	CORE	RIM
Sample No.	9	9	11	11	11	13	13	18	18
SiO2	61.45	61.19	54.73	55.49	55.71	54.7	67.69	54.77	66.66
Al2O3	23.75	25.51	27.36	26.41	27.72	28.12	19.97	28.19	21.16
FeO	0.28	0.33	0.55	0.81	0.46	0.59	0.15	0.39	0.1
CaO	5.01	1.27	10.45	10.1	9.97	10.96	0.35	10.42	1.77
Na2O	8.69	6.93	5.92	6.5	6.06	5.76	12.3	5.52	10.83
K2O	0.21	4.08	0.2	0	0	0	0	0.04	0
TOTAL	99.39	99.31	99.21	99.31	99.92	100.13	100.46	99.33	100.52
Structural Formula based on Thirty-two Oxygens									
Si	10.946	10.940	9.958	10.088	10.023	9.867	11.806	9.917	11.623
Al	4.989	5.378	5.870	5.662	5.881	5.981	4.107	6.019	4.351
Fe3+	0.034	0.049	0.084	0.123	0.069	0.089	0.022	0.059	0.015
Ca	0.958	0.244	2.040	1.970	1.925	2.121	0.066	2.024	0.331
Na	3.005	2.405	2.091	2.294	2.117	2.017	4.164	1.940	3.666
K	0.048	0.931	0.047	0.000	0.000	0.000	0.000	0.009	0.000
Mol. Percent End Members									
Anorthite	23.87	6.8	48.83	46.2	47.62	51.26	1.55	50.94	8.28
Albite	74.93	67.17	50.06	53.8	52.38	48.74	98.45	48.83	91.72
Orthoclase	1.19	26.02	1.11	0	0	0	0	0.23	0

FELDSPAR ANALYSES

Rock Type	TR	G							G
			CORE	RIM	CORE	RIM	MANTLE	DUSTY	
Sample No.	22	26	26	26	26	26	26	26	27
SiO2	54.2	55.75	55.48	58.22	55.77	59.64	63.83	62.82	55.79
Al2O3	27.66	27.39	27.31	25.87	26.83	25.17	22.55	22.67	27.89
FeO	0.59	0.48	0.7	0.44	0.63	0.57	0.3	0.13	0.65
CaO	10.39	9.53	9.79	7.43	9.22	6.88	3.4	3.67	9.8
Na2O	5.29	6.23	6.16	7.1	5.78	7.58	9.49	9.34	6.1
K2O	0.35	0.12	0	0.1	0.77	0	0.09	0	0.36
TOTAL	98.48	99.5	99.44	99.16	99	99.84	99.66	98.63	100.59
Structural Formula based on Thirty-two Oxygens									
Si	9.927	10.079	10.041	10.477	10.124	10.631	11.286	11.218	9.986
Al	5.974	5.839	5.829	5.490	5.743	5.291	4.702	4.774	5.887
Fe3+	0.090	0.073	0.106	0.066	0.096	0.085	0.044	0.019	0.097
Ca	2.042	1.849	1.936	1.435	1.796	1.316	0.645	0.703	1.882
Na	1.881	2.186	2.164	2.480	2.037	2.623	3.257	3.269	2.119
K	0.082	0.028	0.000	0.023	0.179	0.000	0.020	0.000	0.082
Mol. Percent End Members									
Anorthite	50.98	45.5	47.21	36.43	44.77	33.4	16.44	17.7	46.08
Albite	46.97	53.82	52.79	62.99	50.78	66.6	83.04	82.3	51.9
Orthoclase	2.04	0.68	0	0.58	4.45		0.52	0	2.02

Rock Type	G				G				
				MANTLE				FINE INTERST.	
Sample No.	27	27	27	27	28	28	28	28	28
SiO2	57.18	55.59	55.93	58.31	55.47	56.18	56.57	55.52	57.26
Al2O3	26.88	27.84	27.92	26.2	28	27.48	27.48	28.26	26.85
FeO	0.46	0.7	0.72	0.56	0.45	0.68	0.55	0.46	0.68
CaO	8.55	9.79	9.62	7.5	9.93	9.46	9.21	9.91	8.57
Na2O	6.57	5.76	5.86	7.56	6.27	6.47	6.58	6.25	7.07
K2O	0.34	0.57	0.53	0.17	0.13	0.36	0.21	0.14	0.1
TOTAL	99.98	100.25	100.58	100.3	100.25	100.63	100.6	100.54	100.53
Structural Formula based on Thirty-two Oxygens									
Si	10.241	9.989	10.008	10.395	9.961	10.054	10.102	9.936	10.221
Al	5.677	5.899	5.891	5.508	5.929	5.799	5.787	5.964	5.652
Fe3+	0.069	0.105	0.108	0.084	0.068	0.102	0.082	0.069	0.102
Ca	1.643	1.887	1.847	1.435	1.913	1.816	1.765	1.903	1.641
Na	2.284	2.009	2.035	2.616	2.186	2.248	2.281	2.171	2.450
K	0.078	0.131	0.121	0.039	0.030	0.082	0.048	0.032	0.023
Mol. Percent End Members									
Anorthite	41.02	46.86	46.13	35.08	46.34	43.8	43.1	46.34	39.89
Albite	57.04	49.89	50.85	63.98	52.94	54.21	55.73	52.88	59.55
Orthoclase	1.94	3.25	3.03	0.95	0.72	1.98	1.17	0.78	0.55

FELDSPAR ANALYSES

Rock Type	G		G						
	CORE	RIM							
Sample No.	28	28	29	29	29	29	29	29	29
SiO2	56.92	64.58	56.29	55.73	55.87	55.81	53.14	55.68	55.56
Al2O3	26.7	20.42	27.36	28.03	28.01	27.93	27.83	28.03	27.89
FeO	0.62	0.14	0.62	0.72	0.57	0.74	0.68	0.72	0.63
CaO	8.68	1.47	9.63	10.09	9.73	9.95	9.15	9.89	9.84
Na2O	6.75	9.92	6.39	5.89	6.04	6.03	6.43	6.18	6.27
K2O	0.34	0.79	0.24	0.51	0.25	0.44	0.23	0.2	0.21
TOTAL	100.01	97.32	100.53	100.97	100.47	100.9	97.46	100.7	100.4
Structural Formula based on Thirty-two Oxygens									
Si	10.193	11.645	10.077	9.955	9.994	9.969	9.836	9.960	9.965
Al	5.638	4.342	5.776	5.904	5.908	5.883	6.075	5.913	5.899
Fe3+	0.093	0.021	0.093	0.108	0.085	0.111	0.105	0.108	0.0946
Ca	1.668	0.284	1.850	1.934	1.867	1.907	1.817	1.898	1.894
Na	2.347	3.472	2.221	2.042	2.097	2.091	2.310	2.146	2.183
K	0.078	0.182	0.055	0.116	0.057	0.100	0.054	0.046	0.048
Mol. Percent End Members									
Anorthite	40.75	7.22	44.83	47.25	46.43	46.53	43.45	46.41	45.9
Albite	57.35	88.16	53.83	49.91	52.15	51.02	55.25	52.48	52.93
Orthoclase	1.9	4.62	1.33	2.84	1.42	2.45	1.3	1.12	1.17

Rock Type	G		G						
	CORE	MANTLE							
Sample No.	29	29	30	30	30	30	30	30	30
SiO2	56.07	61.97	61.15	60.21	59.2	59.79	60.97	60.34	60.7
Al2O3	27.87	20.73	24.52	24.76	25.12	25.33	23.86	24.49	24.66
FeO	0.59	0.75	0.49	0.53	0.51	0.41	0.43	0.46	0.52
CaO	9.65	1.49	5.54	6.19	6.48	6.35	5.19	5.63	5.98
Na2O	6.54	3.55	8.45	8.41	7.84	8.6	9.1	8.63	8.73
K2O	0.23	10.17	0.71	0.63	0.23	0.21	0.34	0.18	0.31
TOTAL	100.95	98.66	100.86	100.73	99.38	100.69	99.89	99.73	100.9
Structural Formula based on Thirty-two Oxygens									
Si	9.978	11.430	10.796	10.673	10.606	10.589	10.852	10.753	10.719
Al	5.848	4.509	5.104	5.176	5.307	5.290	5.008	5.146	5.135
Fe3+	0.088	0.116	0.072	0.079	0.077	0.061	0.064	0.069	0.077
Ca	1.843	0.295	1.049	1.177	1.246	1.207	0.991	1.076	1.133
Na	2.259	1.271	2.895	2.894	2.727	2.957	3.144	2.985	2.993
K	0.052	2.395	0.160	0.143	0.053	0.048	0.077	0.041	0.070
Mol. Percent End Members									
Anorthite	44.35	7.44	25.56	27.94	30.94	28.65	23.52	26.23	27
Albite	54.39	32.08	70.54	68.68	67.75	70.22	74.64	72.77	71.33
Orthoclase	1.26	60.48	3.9	3.39	1.31	1.13	1.83	1	1.67

FELDSPAR ANALYSES

Rock Type	G					G			
			DUSTY	DUSTY	DUSTY				
Sample No.	30	30	30	30	30	35	35	35	35
SiO2	60.05	60.94	62.98	63.68	67.13	55.34	55.32	55.5	55.89
Al2O3	24.9	24.25	22.59	20.84	19.5	28.6	28.18	28.33	28.08
FeO	0.5	0.5	0.87	0.35	0.25	0.6	0.57	0.63	0.53
CaO	6.2	5.55	3.53	2.45	0.57	10.62	10.38	10.92	10.29
Na2O	8.34	8.1	9.8	9.69	11.83	5.89	5.8	5.57	6.21
K2O	0.27	0.96	0.26	1.19	0.09	0.09	0.45	0.56	0.15
TOTAL	100.26	100.3	100.03	98.2	99.37	101.14	100.7	101.51	101.15
Structural Formula based on Thirty-two Oxygens									
Si	10.670	10.820	11.155	11.452	11.834	9.863	9.907	9.878	9.951
Al	5.217	5.077	4.718	4.420	4.054	6.011	5.951	5.946	5.895
Fe3+	0.074	0.074	0.129	0.053	0.037	0.090	0.085	0.094	0.079
Ca	1.182	1.057	0.671	0.473	0.108	2.031	1.995	2.085	1.966
Na	2.877	2.792	3.369	3.383	4.048	2.038	2.016	1.925	2.146
K	0.061	0.218	0.059	0.273	0.020	0.021	0.103	0.127	0.034
Mol. Percent End Members									
Anorthite	28.69	25.99	16.36	11.45	2.58	49.66	48.48	50.4	47.41
Albite	69.83	68.65	82.2	81.93	96.93	49.84	49.02	46.52	51.77
Orthoclase	1.49	5.35	1.43	6.62	0.49	0.5	2.5	3.08	0.82

Rock Type	G					G	TR		
		INTERST.	CORE	RIM	RIM	DUSTY		CORE	RIM
Sample No.	35	35	35	35	35	38	43	43	43
SiO2	58.3	59.36	55.81	55.87	59.49	66.2	54.63	54.02	54.69
Al2O3	26.52	25.88	27.83	26.84	25.79	20.28	28.11	28.9	28.71
FeO	0.57	0.5	0.6	0.38	0.4	0.45	0.8	0.84	0.5
CaO	8.2	7.49	10.34	7.72	6.73	1.36	10.37	10.9	10.31
Na2O	7.33	7.58	5.95	7.46	8.57	7.73	6.1	5.94	5.86
K2O	0.14	0.14	0.23	0.07	0.21	4.08	0.07	0.1	0.42
TOTAL	101.06	100.95	100.76	98.34	101.19	100.1	100.08	100.7	100.49
Structural Formula based on Thirty-two Oxygens									
Si	10.327	10.493	9.975	10.178	10.503	11.733	9.825	9.706	9.807
Al	5.540	5.394	5.866	5.766	5.369	4.239	5.962	6.123	6.071
Fe3+	0.085	0.074	0.090	0.058	0.059	0.067	0.120	0.126	0.075
Ca	1.559	1.421	1.983	1.509	1.275	0.259	2.001	2.101	1.984
Na	2.521	2.601	2.064	2.638	2.937	2.660	2.130	2.072	2.040
K	0.032	0.032	0.053	0.016	0.047	0.923	0.016	0.023	0.096
Mol. Percent End Members									
Anorthite	37.91	35.04	48.36	36.24	29.93	6.73	48.25	50.07	48.15
Albite	61.32	64.18	50.36	63.37	68.96	69.23	51.36	49.38	49.52
Orthoclase	0.77	0.78	1.28	0.39	1.11	24.04	0.39	0.55	2.34

FELDSPAR ANALYSES

Rock Type	TR			TR			G		TR
	MANTLE	CORE	MANTLE						NEAR C
Sample No.	43	43	43	44	44	44	45	45	51
SiO2	63.25	53.97	62.39	67.63	68.15	63.61	56.22	56.66	54.99
Al2O3	23.09	28.12	23.08	20.39	20.06	20.58	25.93	26.26	27.43
FeO	0.42	0.86	0.4	0.23	0.15	0.18	0.85	0.82	0.68
CaO	4.31	10.69	4.12	0.65	0.49	0.14	8.97	8.89	10.55
Na2O	9.55	6.02	9.66	12.01	12.06	1.7	6.49	6.77	5.57
K2O	0.1	0.08	0.09	0.18	0.12	13.35	0.29	0.21	0.1
TOTAL	100.72	99.74	99.74	101.09	101.03	99.56	98.75	99.61	99.32
Structural Formula based on Thirty-two Oxygens									
Si	11.106	9.782	10.058	10.725	11.798	11.635	10.235	10.224	9.982
Al	4.781	6.011	4.824	4.169	4.095	4.439	5.567	5.588	5.871
Fe3+	0.062	0.130	0.059	0.033	0.022	0.028	0.130	0.124	0.103
Ca	0.812	2.079	0.784	0.121	0.091	0.028	1.752	1.721	2.055
Na	3.255	2.118	3.324	4.042	4.053	0.604	2.294	2.371	1.963
K	0.022	0.019	0.020	0.040	0.027	3.117	0.067	0.048	0.023
Mol. Percent End Members									
Anorthite	19.85	49.31	18.98	2.88	2.18	0.73	42.59	41.56	50.85
Albite	79.6	50.25	80.53	96.18	97.18	16.1	55	57.27	48.58
Orthoclase	0.55	0.44	0.49	0.95	0.64	83.17	1.64	1.17	0.57

Rock Type	TR	G					G		
					RIM	INTERST.	CORE	RIM	CORE
Sample No.	51	53	53	53	53	53	54	54	54
SiO2	56.39	52.65	54.39	54.12	54.8	54.53	54.16	57.11	55.35
Al2O3	27.04	28.5	27.99	29.01	28.49	28.56	28.69	26.81	27.89
FeO	0.59	0.75	0.88	0.62	0.77	0.66	0.63	0.69	0.73
CaO	9.72	10.2	10.31	11.59	10.93	10.87	11.2	8.79	10.45
Na2O	6.36	5.6	5.87	5.18	5.28	5.33	5	6.6	5.63
K2O	0	0.18	0.17	0.15	0.34	0.21	0.44	0.28	0.23
TOTAL	100.1	97.88	99.61	100.67	100.61	100.16	100.12	100.28	100.28
Structural Formula based on Thirty-two Oxygens									
Si	10.126	9.710	9.858	9.715	9.829	9.818	9.769	10.214	9.944
Al	5.726	6.198	5.983	6.141	6.026	6.064	6.102	5.654	5.909
Fe3+	0.089	0.116	0.134	0.093	0.116	0.099	0.095	0.103	0.110
Ca	1.873	2.018	2.005	2.232	2.103	2.100	2.168	1.687	2.014
Na	2.217	2.005	2.065	1.805	1.838	1.863	1.751	2.291	1.964
K	0.000	0.042	0.039	0.034	0.078	0.048	0.101	0.064	0.053
Mol. Percent End Members									
Anorthite	45.79	49.64	48.78	54.82	52.32	52.35	53.92	41.73	49.97
Albite	54.21	49.32	50.26	44.34	45.74	46.45	43.56	56.69	48.72
Orthoclase	0	1.04	0.96	0.84	1.94	1.2	2.52	1.58	1.31

FELDSPAR ANALYSES

Rock Type	G RIM	G INTERST.				SN	TR		TR
Sample No.	54	54	55B	55B	55B	60	62	64	64
SiO2	55.57	57.26	68.38	68.3	68.63	66.85	54.84	55.72	56.87
Al2O3	28.36	27.33	20.23	21.1	20.68	20.85	27.63	27.73	27.05
FeO	0.66	0.77	1.33	0.28	0.18	0.24	0.47	0.6	0.53
CaO	10.49	9.03	1.21	1.09	1.01	1.37	10.41	9.82	9.01
Na2O	5.43	6.5	10.2	10.69	10.77	10.13	5.6	5.52	6.43
K2O	0.49	0.13	0.15	0.13	0.13	0.73	0.03	0.29	0.31
TOTAL	101	101.02	101.5	101.59	101.4	100.17	98.98	99.68	100.2
Structural Formula based on Thirty-two Oxygens									
Si	9.911	10.164	11.791	11.730	11.795	11.688	9.977	10.029	10.182
Al	5.964	5.721	4.114	4.273	4.191	4.299	5.928	5.885	5.711
Fe3+	0.985	0.114	0.192	0.040	0.026	0.035	0.072	0.090	0.079
Ca	2.007	1.720	0.224	0.201	0.186	0.257	2.032	1.896	1.731
Na	1.880	2.240	3.414	3.564	3.593	3.438	1.978	1.929	2.235
K	0.112	0.030	0.033	0.029	0.029	0.163	0.003	0.067	0.071
Mol. Percent End Members									
Anorthite	50.19	43.11	6.1	5.29	4.89	6.66	50.58	48.72	42.88
Albite	47.02	56.15	93	93.95	94.36	89.11	49.24	49.56	55.37
Orthoclase	2.79	0.74	0.9	0.75	0.75	4.23	0.17	1.71	1.76

Rock Type	TR					TR			
		CORE	RIM	DUSTY	DUSTY				MANTLE
Sample No.	64	64	64	64	64	70	70	70	70
SiO2	58.71	59.14	61.73	61.88	66.48	53.13	53.47	59.01	61.01
Al2O3	25.66	25.65	23.42	21.71	19.95	29.04	29.13	25.51	24.49
FeO	0.62	0.57	0.41	1.26	0.21	0.62	0.7	0.58	0.2
CaO	7.21	7.18	3.61	4.72	0.76	11.72	11.6	7.03	5.22
Na2O	6.96	7.1	7.93	8.94	8.32	4.65	4.69	7.22	8.43
K2O	0.68	0.25	0.23	0.22	3.05	0.15	0.25	0.2	0.11
TOTAL	99.84	99.89	97.33	98.73	98.77	99.31	99.84	99.55	99.46
Structural Formula based on Thirty-two Oxygens									
Si	10.500	10.540	11.125	11.110	11.825	9.659	9.672	10.547	10.851
Al	5.412	5.391	4.977	4.597	4.185	6.225	6.213	5.377	5.136
Fe3+	0.093	0.085	0.062	0.189	0.031	0.094	0.106	0.867	0 030
Ca	1.384	1.373	0.070	0.909	0.145	2.286	2.251	1.348	0.996
Na	2.416	2.456	2.774	3.116	2.873	1.641	1.647	2.505	2.910
K	0.155	0.057	0.053	0.050	0.693	0.035	0.058	0.046	0.025
Mol. Percent End Members									
Anorthite	34.98	35.33	19.8	22.31	3.91	57.7	56.91	34.57	25.33
Albite	61.1	63.21	78.7	76.46	77.42	41.42	41.63	64.25	74.03
Orthoclase	3.93	1.46	1.5	1.24	18.67	0.88	1.46	1.17	0.64

FELDSPAR ANALYSES

Rock Type	TR	TR					TR		
	DUSTY	CORE	RIM	CORE	RIM	RIM	CORE	RIM	RIM
Sample No.	70	77	77	77	77	77	78	78	78
SiO2	61.26	53.15	59.54	52.99	58.66	61.89	53.73	58.1	61.07
Al2O3	19.51	29.17	24.7	29.39	25.28	23.36	28.46	26.39	23.76
FeO	4.11	0.68	0.59	0.76	0.59	0.51	0.74	0.62	0.5
CaO	0.74	11.59	6.26	11.89	7	4.68	10.91	7.72	5.1
Na2O	9.78	4.66	7.86	4.6	7.71	8.42	4.85	7.23	8.3
K2O	1.94	0.25	0.11	0.42	0.13	0.14	0.54	0.22	0.17
TOTAL	97.34	99.5	99.06	100.05	99.37	99	99.23	100.28	98.9
Structural Formula based on Thirty-two Oxygens									
Si	11.103	9.646	10.681	9.588	10.528	11.032	9.774	10.358	10.914
Al	4.170	6.243	5.225	6.271	5.350	4.910	6.105	5.548	5.007
Fe3+	0.623	0.103	0.089	0.115	0.089	0.076	0.113	0.093	0.075
Ca	0.144	2.257	1.205	2.308	1.348	0.895	2.129	1.477	0.978
Na	3.441	1.642	2.737	1.616	2.686	2.914	1.713	2.502	2.880
K	0.449	0.058	0.025	0.097	0.030	0.032	0.125	0.050	0.039
Mol. Percent End Members									
Anorthite	3.57	57.04	30.37	57.4	33.17	23.3	53.67	36.65	25.1
Albite	85.3	41.5	69	40.19	66.1	75.87	43.17	62.11	73.91
Orthoclase	11.13	1.46	0.64	2.41	0.73	0.83	3.16	1.24	1

Rock Type	TR	G					G	G	
	MANTLE			CORE	RIM	DUSTY		CORE	RIM 1
Sample No.	78	81	81	81	81	81	MR-5	201	201
SiO2	61.64	54.82	56.57	55.5	63.61	61.14	57.13	59.59	60.58
Al2O3	23.44	28.4	27.71	28.09	22.34	24.28	26.26	25.53	24.98
FeO	0.52	0.74	0.72	0.75	0.34	0.48	0.59	0.49	0.57
CaO	4.6	10.75	9.16	10.26	2.97	5.3	8.32	7.07	6.43
Na2O	8.45	5.25	6.19	5.5	9.58	8.27	6.46	7.17	7.61
K2O	0.09	0.42	0.2	0.16	0.13	0.12	0.32	0.54	0.15
TOTAL	98.74	100.38	100.55	100.26	98.97	99.59	99.08	100.39	100.32
Structural Formula based on Thirty-two Oxygens									
Si	11.002	9.847	10.086	9.946	11.296	10.860	10.336	10.577	10.720
Al	4.948	6.016	5.826	5.936	4.678	5.058	5.602	5.344	5.212
Fe3+	0.078	0.111	0.107	0.113	0.051	0.071	0.089	0.073	0.084
Ca	0.884	2.072	1.752	1.973	0.566	1.010	1.615	1.347	1.221
Na	2.937	1.831	2.142	1.913	3.303	2.852	2.269	2.471	2.614
K	0.021	0.096	0.046	0.037	0.030	0.027	0.074	0.122	0.034
Mol. Percent End Members									
Anorthite	23	51.81	44.47	50.29	14.52	25.97	40.8	34.18	31.55
Albite	76.46	45.78	54.38	48.78	84.73	73.33	57.33	62.72	67.57
Orthoclase	0.54	2.41	1.16	0.93	0.76	0.7	1.87	3.11	0.88

FELDSPAR ANALYSES

Rock Type	G	G				TR		G	G
	RIM 2	FINE	CORE	RIM	DUSTY	CORE	RIM		
Sample No.	201	204	204	204	204	205	205	208	208
SiO2	62.23	58.61	55.72	56.27	68.87	54.29	58.13	56.16	57.33
Al2O3	24.23	25.01	26.88	26.52	19.58	27.76	25.53	27.5	26.64
FeO	0.37	0.52	0.64	0.67	0.11	0.72	0.58	0.59	0.41
CaO	5.25	7.43	9.57	9.22	0.4	10.76	7.77	9.83	8.36
Na2O	8.03	6.66	5.9	5.88	11.37	5.21	6.76	6.01	6.6
K2O	0.05	1.27	0.32	0.74	0	0.46	0.5	0.04	0.09
TOTAL	100.16	99.5	99.03	99.3	100.33	99.2	99.27	100.13	99.43
Structural Formula based on Thirty-two Oxygens									
Si	10.964	10.560	10.117	10.193	11.959	9.887	10.465	10.070	10.301
Al	5.034	5.314	5.756	5.665	4.009	5.961	5.420	5.815	5.644
Fe3+	0.055	0.078	0.097	0.102	0.016	0.110	0.087	0.089	0.062
Ca	0.993	1.419	1.865	1.792	0.075	2.102	1.501	1.891	1.612
Na	2.746	2.329	2.080	2.068	3.833	1.842	2.362	2.092	2.302
K	0.011	0.292	0.074	0.171	0.000	0.107	0.115	0.009	0.021
Mol. Percent End Members									
Anorthite	26.46	35.11	46.39	44.45	1.91	51.89	37.72	47.37	40.96
Albite	73.24	57.65	51.76	51.3	98.09	45.47	59.39	52.4	58.52
Orthoclase	0.3	7.23	1.85	4.25	0	2.64	2.89	0.23	0.53

Rock Type	G	TR		G		AG		G	G
	DUSTY	CORE	RIM						CORE
Sample No.	208	209	209	302	302	303	303	304	307
SiO2	67.24	56.04	57.61	55.55	54.69	65.22	68.31	57.53	57.26
Al2O3	20.81	27.08	26.15	28	28.33	18.34	19.97	26.7	27.1
FeO	0.14	0.69	0.71	0.71	0.7	0.09	0.48	0.54	0.6
CaO	1.51	9.84	8.5	10.39	10.9	0.07	0.18	8.37	8.77
Na2O	10.63	5.99	6.25	5.27	5.11	0.1	11.39	6.1	6.46
K2O	0.05	0	0.02	0.49	0.39	16.77	0	0.81	0.4
TOTAL	100.38	99.64	99.24	100.41	100.12	100.59	100.33	100.05	100.59
Structural Formula based on Thirty-two Oxygens									
Si	11.709	10.104	10.370	9.964	9.857	11.972	11.879	10.300	10.209
Al	4.273	5.757	5.550	5.923	6.021	3.970	4.095	5.637	5.698
Fe3+	0.020	0.104	0.107	0.107	0.106	0.014	0.070	0.081	0.090
Ca	0.282	1.904	1.642	2.000	2.108	0.014	0.034	1.608	1.678
Na	3.593	2.096	2.184	1.835	1.788	0.036	3.842	2.120	2.236
K	0.011	0.000	0.005	0.112	0.090	3.930	0.000	0.019	0.091
Mol. Percent End Members									
Anorthite	7.26	47.58	42.86	50.66	52.88	0.35	0.87	41.08	41.89
Albite	92.46	52.42	57.02	46.5	44.86	0.9	99.13	54.18	55.84
Orthoclase	0.29	0	0.12	2.84	2.25	98.76	0	4.73	2.27

FELDSPAR ANALYSES

Rock Type	G		G			TR		SN	
	RIM	MANTLE			DUSTY				
Sample No.	307	307	402	402	402	404	407	410	410
SiO2	63.03	65.63	55.33	55.03	59.58	54.46	55.43	65.07	69.18
Al2O3	23.22	18.83	27.73	27.95	25.36	28.77	28.4	18.74	20.16
FeO	0.37	0.27	0.47	0.45	0.42	0.68	0.39	0.23	0.12
CaO	4.07	0.15	10.43	10.59	7.21	11.74	10.64	0.06	0.28
Na2O	8.43	0.4	5.59	5.51	7.87	5.19	5.52	1.56	10.9
K2O	0.8	14.66	0.17	0.65	0	0	0	14.79	0.07
TOTAL	99.92	99.94	99.72	100.18	100.44	100.84	100.38	100.45	100.71
Structural Formula based on Thirty-two Oxygens									
Si	11.120	11.970	9.988	9.920	10.570	9.763	9.928	11.894	11.937
Al	4.831	4.050	5.903	5.942	5.306	6.082	5.998	4.039	4.102
Fe3+	0.055	0.041	0.071	0.068	0.062	0.102	0.059	0.035	0.017
Ca	0.770	0.029	2.020	2.048	1.373	2.258	2.045	0.012	0.052
Na	2.887	0.142	1.959	1.928	2.710	1.806	1.919	0.554	3.651
K	0.180	3.414	0.039	0.150	0.000	0.000	0.000	3.452	0.015
Mol. Percent End Members									
Anorthite	20.07	0.82	50.27	49.64	33.61	55.56	51.58	0.29	1.39
Albite	75.23	3.95	48.75	46.73	66.39	44.44	48.42	13.78	98.19
Orthoclase	4.7	95.23	0.98	3.63	0	0	0	85.93	0.41

Pyroxene analyses and structural formulae

Rock Type	G			G			G			G
	CORE 1	RIM 1	FINE 1	CORE 2	RIM 2	2	AT 5	AT 5	AT 5	9
SiO2	49.53	49.12	49.86	50.72	49.63	50.80	49.85	49.99	51.36	48.89
TiO2	0.21	0.14	0.2	0.88	0.51	0.88	0.07	0.17	0.13	1.20
Al2O3	4.03	4	3.07	2.48	4.87	2.47	3.19	2.90	1.92	3.42
FeO	23.52	25.29	23.92	11.5	20.36	11.31	22.69	23.68	20.53	11.69
MnO	0.57	0.53	0.62	0.31	0.53	0.32	0.72	0.64	0.56	0.29
MgO	8.83	7.63	8.58	13.03	10.84	12.99	9.26	8.54	10.65	12.98
CaO	11.94	12.02	11.85	21.35	11.67	21.57	11.37	11.62	12.23	21.08
Na2O	0.89	0.73	0.64	0.46	1.12	0.46	0.84	0.62	0.56	0.56
TOTAL	99.52	99.46	98.74	100.73	99.53	100.8	97.99	98.16	97.9	100.11
Structural Formulae based on Six Oxygens										
Si	1.919	1.924	1.955	1.896	1.893	1.897	1.954	1.9667	1.996	1.846
Al(iv)	0.081	0.076	0.045	0.104	0.107	0.103	0.046	0.033	0.005	0.152
Al(vi)	0.104	0.109	0.097	0.005	0.112	0.006	0.102	0.101	0.084	0.000
Ti	0.006	0.004	0.006	0.025	0.015	0.025	0.002	0.005	0.041	0.034
Fe3(vi)	0.067	0.056	0.049	0.033	0.083	0.033	0.064	0.047	0.042	0.039
Fe2+	0.696	0.773	0.736	0.326	0.567	0.320	0.680	0.732	0.625	0.328
Mn	0.019	0.018	0.021	0.010	0.017	0.010	0.024	0.021	0.018	0.009
Mg	0.511	0.446	0.502	0.727	0.617	0.724	0.542	0.501	0.617	0.731
Ca	0.497	0.505	0.499	0.856	0.478	0.864	0.478	0.491	0.510	0.854
Na	0.067	0.056	0.049	0.033	0.083	0.033	0.064	0.047	0.042	0.041
Mol. Percent End Members										
Wo.	25.92	26.21	27.06	43.97	24.56	44.40	26.23	27.26	29.35	43.63
Fs	42.73	46.81	43.37	17.37	36.13	17.05	41.08	43.18	35.73	17.47
En.	31.35	26.98	29.57	38.66	39.31	38.55	32.69	29.56	35.27	38.90
Ae	13.69	11.36	9.59	3.88	17.70	3.85	12.83	9.29	7.68	4.77
Di	49.78	56.23	53.76	29.79	39.42	29.49	48.38	53.85	46.46	29.51
Hd	36.52	32.41	36.65	66.33	42.88	66.66	38.63	36.86	45.86	65.72
Ti-Px	4.32	3.22			8.33					
CATS	48.31	53.25			44.3					
Ae	47.36	43.53			47.37					

Rock Type G; Gabbro, TR: Troctolite, AT: Altered rock

Pyroxene analyses and structural formulae

	TR	TR CORE	RIM	TR AT	G	G				
	11	13	13	18	26	27	27	27	27	27
SiO2	50.38	50.69	51.87	52.98	49.84	51.01	49.98	49.67	49.87	50.86
TiO2	0.49	1.05	0.52	0.25	0.79	0.73	0.67	0.88	1.00	0.85
Al2O3	1.14	2.64	3.42	2.26	2.11	1.90	1.61	1.96	2.78	2.45
FeO	15.16	11.76	16.27	18.04	11.88	12.88	14.56	12.41	12.06	11.86
MnO	0.48	0.31	0.69	0.51	0.29	0.45	0.44	0.43	0.35	0.38
MgO	10.06	12.65	15.09	12.82	12.26	11.73	10.40	11.52	12.06	12.26
CaO	21.21	21.09	10.34	12.01	21.34	20.95	21.36	20.58	21.13	20.93
Na2O	0.60	0.59	0.90	0.56	0.48	0.55	0.55	0.48	0.53	0.50
TOTAL	99.52	100.78	99.1	99.43	98.99	100.2	99.57	97.93	99.78	100.09
Structural Formula based on Six Oxygens										
Si	1.940	1.894	1.941	1.996	1.904	1.927	1.920	1.918	1.887	1.912
Al(iv)	0.052	0.106	0.060	0.004	0.095	0.074	0.073	0.082	0.113	0.088
Al(vi)	0.000	0.010	0.091	0.097	0.000	0.011	0.000	0.007	0.011	0.020
Ti	0.014	0.030	0.015		0.023	0.021	0.019	0.026	0.029	0.024
Fe3(vi)	0.037	0.043	0.065	0.041	0.034	0.040	0.034	0.036	0.039	0.037
Fe2+	0.444	0.325	0.444	0.528	0.344	0.367	0.427	0.365	0.343	0.337
Mn	0.016	0.010	0.022	0.016	0.001	0.014	0.014	0.014	0.011	0.012
Mg	0.578	0.705	0.842	0.721	0.699	0.661	0.596	0.664	0.681	0.687
Ca	0.877	0.845	0.415	0.486	0.875	0.849	0.880	0.853	0.858	0.844
Na	0.045	0.043	0.065	0.041	0.036	0.040	0.041	0.036	0.039	0.037
Mol. Percent End Members										
Wo.	45.77	43.90	22.53	27.92	44.96	44.29	45.70	44.35	44.42	43.85
Fs	23.55	17.70	26.81	30.47	18.16	19.88	22.67	19.75	18.62	18.45
En.	30.68	38.40	50.84	41.60	36.87	35.82	31.63	35.90	36.96	37.69
Ae	4.95	5.04	15.00	7.81	4.01	4.70	4.55	4.20	4.54	4.36
Di	41.28	29.96	29.34	38.98	31.68	34.01	39.85	34.00	31.98	31.43
Hd	53.77	65.00	55.65	53.21	64.31	61.29	55.61	61.80	63.48	64.20

Ti-Px
CATS
Ae

Pyroxene analyses and structural formulae

			G						G
	27	27	28	28	28	28	28	28	29
SiO2	50.35	50.87	49.52	50.29	50.33	50.21	50.54	50.33	50.56
TiO2	0.76	0.85	1.17	0.83	0.89	0.82	0.84	0.89	0.68
Al2O3	2.20	2.23	3.37	2.20	2.16	2.08	2.06	2.16	1.78
FeO	12.65	12.97	12.02	12.61	12.56	12.66	11.79	12.56	12.66
MnO	0.41	0.38	0.32	0.41	0.36	0.40	0.36	0.36	0.39
MgO	11.74	11.76	11.87	11.60	11.88	11.69	12.50	11.88	11.86
CaO	20.69	20.87	21.13	21.14	21.29	21.30	21.36	21.29	21.47
Na2O	0.48	0.48	0.57	0.46	0.54	0.59	0.50	0.54	0.44
TOTAL	99.28	100.41	99.97	99.54	100	99.75	99.95	100	99.84
Structural Formula based on Six Oxygens									
Si	1.916	1.915	1.870	1.913	1.899	1.906	1.907	1.904	1.919
Al(iv)	0.084	0.085	0.130	0.087	0.101	0.093	0.092	0.096	0.080
Al(vi)	0.015	0.014	0.020	0.011	0.011	0.000	0.000	0.000	0.000
Ti	0.022	0.024	0.033	0.024	0.025	0.023	0.024	0.025	0.019
Fe3(vi)	0.035	0.035	0.042	0.034	0.036	0.043	0.035	0.040	0.031
Fe2+	0.367	0.374	0.338	0.367	0.326	0.359	0.336	0.358	0.370
Mn	0.013	0.012	0.010	0.013	0.012	0.013	0.012	0.012	0.013
Mg	0.667	0.661	0.669	0.658	0.696	0.662	0.704	0.670	0.671
Ca	0.845	0.844	0.856	0.863	0.867	0.868	0.865	0.086	0.874
Na	0.036	0.035	0.042	0.034	0.036	0.044	0.037	0.040	0.032
Mol. Percent End Members									
Wo.	43.87	43.78	44.36	44.66	44.86	45.27	44.73	44.91	45.09
Fs	19.95	20.31	18.68	19.82	17.59	19.24	17.85	19.17	19.50
En.	36.18	35.91	36.96	35.51	37.55	35.50	37.42	35.91	35.41
Ae	4.20	4.18	4.95	3.94	4.14	4.90	4.17	4.52	3.65
Di	34.04	34.62	31.92	34.41	30.58	33.42	30.95	33.24	34.21
Hd	61.75	61.21	63.13	91.65	65.28	61.68	64.88	62.25	62.14
Ti-Px			34.87						
CATS			21.22						
Ae			43.91						

Pyroxene analyses and structural formulae

				G					G
	29	29	29	30	30	30 (C)	30 (R)	35	35 (C)
SiO2	50.75	51.59	50.25	51.88	52.01	52.05	52.21	49.06	49.43
TiO2	0.86	0.53	0.93	0.16	0.11	0.11	0.00	1.33	1.19
Al2O3	2.17	1.38	2.48	0.43	0.29	0.32	0.37	3.59	3.74
FeO	12.00	11.47	12.23	13.77	12.42	12.62	12.25	12.05	11.71
MnO	0.39	0.37	0.41	0.78	0.81	0.84	0.80	0.40	0.35
MgO	12.77	12.18	11.95	9.93	10.50	9.87	10.42	11.94	12.12
CaO	21.14	21.90	21.49	23.74	24.24	24.17	24.10	21.01	21.13
Na2O	0.48	0.68	0.62	0.38	0.28	0.28	0.34	0.49	0.60
TOTAL	100.56	100.1	100.36	101.07	100.66	100.26	100.49	99.87	100.27
Structural Formula based on Six Oxygens									
Si	1.903	1.939	1.893	1.966	1.971	1.981	1.978	1.856	1.858
Al(iv)	0.096	0.061	0.107	0.019	0.013	0.014	0.017	0.144	0.142
Al(vi)	0.000	0.000	0.004	0.000	0.000	0.000	0.000	0.017	0.024
Ti	0.024	0.015	0.026	0.005	0.003	0.003	0.000	0.038	0.034
Fe3(vi)	0.034	0.050	0.045	0.014	0.004	0.016	0.019	0.036	0.044
Fe2+	0.342	0.311	0.340	0.409	0.373	0.381	0.363	0.346	0.325
Mn	0.012	0.012	0.013	0.025	0.026	0.027	0.026	0.013	0.011
Mg	0.714	0.683	0.672	0.562	0.594	0.560	0.589	0.674	0.680
Ca	0.851	0.883	0.869	0.965	0.986	0.987	0.980	0.853	0.852
Na	0.035	0.050	0.045	0.028	0.021	0.021	0.025	0.036	0.044
Mol. Percent End Members									
Wo.	43.90	46.61	45.32	49.76	50.40	51.10	50.71	43.92	44.18
Fs	18.15	16.71	18.39	21.17	19.15	19.80	18.81	19.01	18.04
En.	37.95	36.68	36.29	29.07	30.45	29.10	30.48	37.07	37.77
Ae	4.06	5.41	5.13	2.83	2.09	2.15	2.56	4.31	5.22
Di	31.04	29.61	31.90	40.94	37.80	39.62	37.18	31.43	30.64
Hd	64.90	64.98	62.97	56.23	60.11	58.23	60.26	63.25	64.14
Ti-Px								41.88	33.26
CATS								18.34	23.37
Ae								39.78	43.37

Pyroxene analyses and structural formulae

				TR		G		TR	G
	35 (R)	35 (C)	35 (R)	43	43	45	45	51	53
SiO2	50.33	50.23	50.03	50.56	49.73	50.06	49.59	49.77	49.79
TiO2	0.45	1.01	0.51	0.86	1.01	0.81	0.91	1.23	1.07
Al2O3	4.37	2.99	3.92	2.17	2.76	2.27	2.51	3.07	2.85
FeO	16.68	11.68	16.01	11.73	11.45	12.78	13.04	11.58	11.45
MnO	0.81	0.32	0.81	0.44	0.38	0.54	0.49	0.31	0.38
MgO	12.46	12.46	11.35	12.32	12.31	12.78	12.53	12.93	12.88
CaO	12.34	21.33	16.11	21.26	21.07	20.36	20.49	21.48	21.38
Na2O	1.05	0.44	0.93	0.54	0.51	0.38	0.41	0.48	0.38
TOTAL	98.49	100.46	99.67	99.88	99.22	99.98	99.97	100.85	100.18
Structural Formula based on Six Oxygens									
Si	1.910	1.884	1.895	1.908	1.888	1.895	1.881	1.863	1.874
Al(iv)	0.090	0.116	0.105	0.092	0.112	0.101	0.112	0.136	0.126
Al(vi)	0.106	0.016	0.070	0.004	0.011	0.000	0.000	0.035	0.001
Ti	0.013	0.029	0.015	0.024	0.029	0.023	0.026	0.000	0.030
Fe3(vi)	0.077	0.032	0.068	0.040	0.038	0.024	0.024	0.033	0.028
Fe2+	0.452	0.335	0.439	0.331	0.326	0.377	0.384	0.328	0.333
Mn	0.026	0.010	0.026	0.014	0.012	0.017	0.016	0.010	0.012
Mg	0.705	0.697	0.641	0.694	0.697	0.722	0.709	0.722	0.723
Ca	0.503	0.858	0.655	0.861	0.858	0.827	0.834	0.863	0.864
Na	0.077	0.032	0.068	0.040	0.038	0.028	0.030	0.035	0.028
Mol. Percent End Members									
Wo.	26.87	44.09	34.56	44.82	44.43	42.25	42.51	44.09	44.08
Fs	28.58	18.13	26.60	17.82	17.71	19.81	20.19	17.46	17.63
En.	44.56	37.78	38.84	37.36	37.86	37.93	37.30	38.45	38.29
Ae	15.39	3.79	10.70	4.54	4.39	3.36	3.60	4.04	3.23
Di	33.06	31.20	36.29	30.83	30.47	33.16	33.85	29.97	30.50
Hd	51.55	65.01	53.01	64.63	65.13	63.49	62.55	65.99	66.27
Ti-Px	8.32		9.55						
CATS	41.62		45.64						
Ae	50.06		44.81						

Pyroxene analyses and structural formulae

	53	53 (F)	G 54	54 (C)	54 (R)	G 55B	55B	55B (A)	SN AT 60	60
SiO2	49.86	52.67	50.43	49.67	50.70	50.75	51.70	50.66	48.67	50.18
TiO2	1.13	0.19	1.05	1.16	0.87	0.35	0.30	0.38	0.27	0.23
Al2O3	2.93	1.04	2.66	2.94	2.08	3.12	2.41	3.32	3.30	2.95
FeO	11.30	25.99	12.25	11.80	12.31	21.10	21.06	20.33	21.15	21.73
MnO	0.37	1.55	0.41	0.39	0.42	0.78	0.74	0.73	1.52	1.52
MgO	12.80	15.14	12.42	12.69	12.32	10.26	10.39	10.57	9.18	9.50
CaO	21.48	1.91	21.02	21.22	21.17	11.88	11.72	11.79	11.58	11.87
Na2O	0.38	0.21	0.31	0.37	0.41	0.53	0.54	0.67	0.72	0.79
TOTAL	100.25	98.7	100.55	100.24	100.28	98.77	98.86	98.45	96.39	98.77
Structural Formula based on Six Oxygens										
Si	1.975	2.026	1.893	1.871	1.902	1.959	1.989	1.953	1.939	1.951
Al(iv)	0.126	0.026	0.107	0.129	0.092	0.041	0.011	0.047	0.061	0.049
Al(vi)	0.004	0.073	0.011	0.002	0.000	0.101	0.098	0.104	0.094	0.086
Ti	0.032	0.006	0.030	0.033	0.025	0.010	0.009	0.011	0.008	0.007
Fe3(vi)	0.028	0.016	0.023	0.027	0.024	0.040	0.040	0.050	0.056	0.060
Fe2+	0.328	0.821	0.362	0.345	0.357	0.642	0.638	0.606	0.650	0.647
Mn	0.012	0.051	0.013	0.012	0.013	0.026	0.024	0.024	0.051	0.050
Mg	0.718	0.869	0.696	0.713	0.690	0.591	0.596	0.608	0.546	0.551
Ca	0.867	0.079	0.847	0.858	0.874	0.492	0.484	0.488	0.495	0.495
Na	0.028	0.016	0.023	0.027	0.030	0.040	0.040	0.050	0.056	0.060
Mol. Percent End Members										
Wo.	44.25	5.15	43.25	43.76	44.81	27.21	27.93	27.14	27.01	27.43
Fs	17.47	46.08	19.44	18.34	18.81	37.90	37.24	36.36	39.67	39.21
En.	38.27	48.77	37.32	37.91	36.38	34.89	34.83	36.49	33.32	33.37
Ae	3.23	14.59	2.73	3.18	3.40	7.94	7.78	9.98	11.19	11.63
Di	30.33	41.50	33.31	31.56	32.93	47.94	47.66	44.93	48.27	47.74
Hd	66.43	43.92	63.96	65.25	63.67	44.13	44.56	45.09	40.55	40.63
Ti-Px									7.43	
CATS									41.25	
Ae									51.32	

Pyroxene analyses and structural formulae

			TR		TR		TR		G
	60	64	70	70	77	77	78	78	81
SiO2	49.32	50.31	50.11	50.16	49.54	50.71	49.60	50.74	50.92
TiO2	0.26	0.73	0.96	0.98	1.12	0.87	0.97	0.81	0.93
Al2O3	3.75	1.81	2.28	2.59	2.77	2.20	3.35	2.18	2.34
FeO	22.42	17.86	13.15	12.39	12.32	11.83	11.20	11.29	11.29
MnO	1.51	0.47	0.41	0.40	0.41	0.38	0.36	0.39	0.36
MgO	9.00	10.37	11.41	11.85	11.97	12.43	12.75	13.17	12.96
CaO	11.83	21.01	21.13	21.10	21.24	20.95	21.31	20.68	21.00
Na2O	0.94	0.46	0.38	0.59	0.42	0.48	0.35	0.34	0.47
TOTAL	99.03	103.02	99.83	100.06	99.79	99.85	99.89	99.6	100.27
Structural Formula based on Six Oxygens									
Si	1.920	1.922	1.905	1.894	1.879	1.911	1.869	1.912	1.906
Al(iv)	0.080	0.078	0.095	0.106	0.121	0.089	0.131	0.088	0.094
Al(vi)	0.092	0.004	0.007	0.009	0.003	0.009	0.018	0.009	0.009
Ti	0.008	0.021	0.027	0.028	0.032	0.025	0.028	0.023	0.026
Fe3(vi)	0.071	0.034	0.028	0.043	0.031	0.035	0.026	0.025	0.034
Fe2+	0.659	0.441	0.390	0.348	0.360	0.338	0.328	0.331	0.320
Mn	0.050	0.015	0.013	0.013	0.013	0.012	0.012	0.013	0.011
Mg	0.523	0.591	0.647	0.668	0.677	0.699	0.717	0.740	0.724
Ca	0.494	0.861	0.862	0.855	0.865	0.847	0.862	0.836	0.843
Na	0.071	0.034	0.028	0.043	0.031	0.035	0.026	0.025	0.034
Mol. Percent End Members									
Wo.	26.30	44.77	44.37	44.60	44.43	43.96	43.87	42.88	43.65
Fs	41.11	23.60	20.93	19.00	19.29	18.27	17.61	17.65	17.26
En.	32.59	31.63	34.70	36.41	36.28	37.77	38.52	39.47	39.09
Ae	14.41	3.92	3.28	5.02	3.59	4.14	3.04	3.00	4.05
Di	47.74	41.06	36.39	32.56	33.47	31.25	30.41	29.98	29.39
Hd	37.84	55.03	60.33	62.41	62.94	64.61	66.54	67.02	66.56
Ti-Px	5.34								
CATS	45.12								
Ae	49.54								

Pyroxene analyses and structural formulae

	81 (A)	81(A)	G MR5	MR5	MR5	G RIM NO 201	URLT 201	TR 205	G 208	TR 209
SiO2	49.98	51.44	49.98	49.79	49.69	49.72	49.05	50.75	50.55	50.49
TiO2	0.37	0.41	0.66	0.71	0.87	1.06	1.43	0.70	0.78	0.87
Al2O3	3.81	2.80	1.76	1.81	2.70	3.15	3.96	1.60	1.74	2.09
FeO	20.92	16.99	13.10	13.41	11.67	12.13	12.55	12.11	13.78	11.58
MnO	0.59	0.65	0.34	0.33	0.22	0.33	0.36	0.36	0.41	0.32
MgO	10.26	13.36	11.33	11.16	11.91	12.20	11.51	11.70	11.71	13.26
CaO	11.99	11.92	21.06	21.15	21.51	20.41	20.54	21.19	21.33	20.82
Na2O	0.93	0.68	0.38	0.42	0.41	0.48	0.46	0.67	0.52	0.57
TOTAL	98.85	98.25	98.61	98.78	98.98	99.48	99.86	99.08	100.82	100
Structural Formula based on Six Oxygens										
Si	1.925	1.957	1.926	1.918	1.896	1.884	1.797	1.932	1.909	1.900
Al(iv)	0.075	0.043	0.074	0.082	0.104	0.116	0.203	0.068	0.078	0.093
Al(vi)	0.098	0.083	0.006	0.000	0.017	0.025	0.098	0.004	0.000	0.000
Ti	0.011	0.012	0.019	0.021	0.025	0.030	0.039	0.020	0.022	0.025
Fe3(vi)	0.070	0.050	0.028	0.031	0.030	0.035	0.033	0.050	0.025	0.034
Fe2+	0.605	0.491	0.394	0.401	0.342	0.349	0.352	0.336	0.397	0.323
Mn	0.019	0.021	0.011	0.011	0.007	0.011	0.011	0.012	0.013	0.010
Mg	0.590	0.758	0.651	0.641	0.678	0.690	0.629	0.665	0.660	0.744
Ca	0.496	0.487	0.871	0.874	0.881	0.830	0.808	0.866	0.864	0.841
Na	0.070	0.050	0.028	0.031	0.030	0.035	0.033	0.050	0.038	0.042
Mol. Percent End Members										
Wo.	26.53	26.72	44.73	45.02	45.11	42.71	40.58	45.67	44.34	43.33
Fs	37.21	28.79	20.83	21.15	18.42	19.26	21.32	18.26	20.92	17.15
En.	36.27	44.49	34.43	33.83	36.48	38.02	38.10	36.07	34.74	39.52
Ae	13.89	9.93	3.25	3.55	3.50	4.36	4.66	5.56	4.33	4.85
Di	43.61	35.39	36.47	37.10	32.38	32.16	34.21	31.74	35.96	28.79
Hd	42.51	54.68	60.28	59.35	64.13	63.18	61.13	62.70	59.71	66.35
Ti-Px	7.99					33.41	23.17			
CATS	40.23					27.56	57.58			
Ae	51.98					39.03	19.25			

Pyroxene analyses and structural formulae

	G	G		G	G	G	TR
			COARSE			COARSE	FINE
	302	303	303	304	307	402	407
SiO2	50.24	50.95	49.65	50.76	49.69	50.71	50.97
TiO2	1.11	0.50	1.10	0.86	1.03	0.79	0.74
Al2O3	2.91	1.27	2.79	2.36	2.20	2.04	2.22
FeO	11.66	14.04	12.30	11.31	14.49	13.22	12.06
MnO	0.33	0.48	0.37	0.32	0.45	0.42	0.39
MgO	12.70	11.14	12.23	12.92	10.54	11.50	12.04
CaO	21.30	21.59	21.14	21.39	21.01	21.27	21.71
Na2O	0.44	0.53	0.56	0.54	0.44	0.62	0.58
TOTAL	100.69	100.5	100.14	100.46	99.85	100.57	100.71
Structural Formula based on Six Oxygens							
Si	1.882	1.933	1.876	1.900	1.903	1.913	1.917
Al(iv)	0.118	0.057	0.124	0.100	0.097	0.087	0.083
Al(vi)	0.010	0.000	0.000	0.004	0.002	0.004	0.015
Ti	0.031	0.014	0.031	0.024	0.030	0.022	0.029
Fe3(vi)	0.032	0.029	0.041	0.039	0.033	0.045	0.042
Fe2+	0.334	0.407	0.348	0.315	0.432	0.372	0.337
Mn	0.011	0.015	0.012	0.010	0.015	0.013	0.012
Mg	0.710	0.631	0.689	0.722	0.602	0.647	0.642
Ca	0.856	0.879	0.857	0.859	0.863	0.861	0.876
Na	0.032	0.039	0.041	0.039	0.033	0.045	0.042
Mol. Percent End Members							
Wo.	43.85	45.46	44.32	44.48	44.57	45.02	45.93
Fs	17.95	21.39	18.67	16.88	23.14	20.07	18.62
En.	38.20	33.15	37.01	38.64	32.28	34.91	35.45
Ae	3.78	4.32	4.74	4.51	3.79	5.16	4.85
Di	30.76	37.52	31.95	29.02	40.17	34.61	32.78
Hd	65.46	58.16	63.31	66.46	56.04	60.23	62.38

Ti-Px
CATS
Ae

Compositions of amphiboles from the GLI

Sample	2	5	9	9	18	22(R)	22(R)	22(R)	26	26	26	28	28
SiO2	42.5	41.9	42.1	41.9	42.9	47.0	49.6	51.6	45.5	42.3	41.9	43.1	42.1
TiO2	1.96	2.75	2.46	2.71	0.41	0.41	0.39	0.43	0.08	2.27	2.14	1.88	2.10
Al2O3	7.66	9.50	9.68	8.96	11.36	7.08	4.61	2.53	7.45	9.08	8.90	8.64	9.41
Fe2O3	3.02	0.68	0.42	1.71	6.01	11.86	11.90	5.16	5.46	2.70	0.93	1.32	1.52
FeO	13.1	16.6	16.8	15.1	13.9	5.6	4.3	10.6	13.4	14.2	15.3	14.0	14.3
MnO	0.27	0.29	0.26	0.30	0.45	0.69	0.66	0.60	0.42	0.24	0.27	0.36	0.29
MgO	12.8	10.5	10.5	11.3	9.4	13.0	14.3	13.8	10.9	11.2	11.2	12.3	11.5
CaO	11.2	11.3	11.4	11.3	11.6	10.3	10.2	11.4	11.8	11.1	11.2	11.3	11.4
Na2O	3.28	2.69	2.73	2.78	2.42	1.71	1.13	0.72	1.53	2.70	3.02	3.04	2.71
K2O	1.55	1.82	1.90	1.70	0.18				0.24	1.44	1.46	1.59	1.55
TOTAL	97.4	98.0	98.2	97.8	98.7	97.7	97.1	96.8	96.8	97.2	96.3	97.7	97.0

Structural Formula based on Twenty-three Oxygens

Si	6.457	6.374	6.389	6.371	6.393	6.850	7.180	7.557	6.862	6.429	6.455	6.513	6.414
Al(iv)	1.372	1.626	1.611	1.605	1.607	1.150	0.787	0.437	1.138	1.571	1.545	1.487	1.586
Al(vi)		0.078	0.122		0.389	0.066			0.186	0.057	0.070	0.052	0.103
Ti	0.224	0.315	0.281	0.310	0.046	0.045	0.042	0.047	0.009	0.260	0.248	0.214	0.241
Fe3+	0.346	0.078	0.048	0.196	0.674	1.300	1.297	0.569	0.619	0.309	0.108	0.150	0.174
Fe2+	1.664	2.111	2.129	1.920	1.736	0.686	0.519	1.295	1.694	1.806	1.965	1.773	1.825
Mn	0.347	0.037	0.033	0.039	0.057	0.085	0.081	0.074	0.054	0.031	0.035	0.046	0.037
Mg	2.902	2.381	2.387	2.560	2.097	2.818	3.094	3.020	2.438	2.537	2.573	2.766	2.619
Ca	1.827	1.846	1.854	1.845	1.858	1.605	1.576	1.791	1.911	1.805	1.841	1.831	1.863
Na	0.966	0.794	0.804	0.819	0.700	0.483	0.317	0.204	0.447	0.796	0.902	0.890	0.801
K	0.300	0.353	0.368	0.330	0.034				0.046	0.279	0.287	0.306	0.301

Sample	28	28(R)	28(R)	29(R)	30(R)	30(F)	30(F)	30	30(R)	35	35(F)	43(R)	43(F)
SiO2	43.2	52.5	53.4	53.9	45.5	43.4	45.0	43.7	42.9	39.7	47.9	48.1	45.0
TiO2	2.02	0.17	0.06	0.25	0.34	0.24	0.34	1.86	0.44	4.72	0.29	0.12	0.14
Al2O3	8.61	2.03	1.82	1.64	6.64	6.14	7.26	7.97	7.65	14.60	5.53	6.28	9.44
Fe2O3	1.81	2.13	2.57	3.42	5.22	7.16	6.27	5.76	6.01	3.17	4.93	3.88	4.95
FeO	14.4	13.1	11.4	10.1	19.3	18.2	18.6	14.4	20.5	7.8	13.4	14.1	14.8
MnO	0.32	0.61	0.54	0.53	0.75	0.75	0.70	0.45	0.74	0.14	0.76	0.42	0.41
MgO	12.1	13.8	15.0	15.8	7.6	7.2	7.6	10.5	6.0	12.7	11.6	11.4	9.7
CaO	11.3	12.0	12.2	12.2	11.6	11.3	11.6	10.9	11.5	10.3	12.0	12.2	11.9
Na2O	3.09	0.59	0.52	0.51	1.11	1.24	1.51	2.26	1.35	2.77	1.10	1.01	1.70
K2O	1.47	0.17	0.14	0.18	1.04	0.80	0.63	1.50	1.03	2.00	0.29	0.13	0.15
TOTAL	98.4	97.2	97.7	98.7	99.2	96.6	99.6	99.4	98.3	97.9	97.9	97.7	98.2

Structural Formula based on Twenty-three Oxygens

Si	6.491	7.703	7.724	7.696	6.910	6.806	6.797	6.543	6.673	5.836	7.116	7.133	6.718
Al(iv)	1.509	0.297	0.276	0.276	1.090	1.135	1.203	1.406	1.327	2.164	0.884	0.867	1.282
Al(vi)	0.016	0.054	0.035		0.100		0.090		0.075	0.366	0.084	0.230	0.379
Ti	0.228	0.019	0.007	0.027	0.039	0.028	0.038	0.209	0.051	0.522	0.032	0.013	0.016
Fe3+	0.205	0.235	0.280	0.368	0.597	0.846	0.713	0.649	0.704	0.351	0.552	0.433	0.556
Fe2+	1.807	1.610	1.383	1.199	2.455	2.393	2.350	1.804	2.673	0.953	1.666	1.743	1.849
Mn	0.041	0.076	0.066	0.064	0.096	0.100	0.090	0.057	0.098	0.017	0.096	0.053	0.052
Mg	2.703	3.006	3.230	3.369	1.714	1.691	1.718	2.332	1.399	2.790	2.570	2.528	2.148
Ca	1.825	1.885	1.889	1.868	1.894	1.906	1.879	1.750	1.917	1.619	1.906	1.931	1.897
Na	0.900	0.168	0.146	0.141	0.327	0.377	0.443	0.656	0.407	0.790	0.317	0.290	0.492
K	0.282	0.032	0.025	0.033	0.201	0.160	0.122	0.286	0.204	0.375	0.055	0.024	0.029

Compositions of amphiboles from the GLI

Sample	43	43 (R)	44 (R)	44 (R)	44 (R)	45 (R)	45 (R)	55B (F)	64 (R)	70 (F)	81 (R)	81
SiO2	42.6	53.6	50.1	51.7	51.1	50.4	50.2	44.5	51.5	40.7	47.7	47.8
TiO2	2.45	0.25	0.41	0.37	0.18	0.28	0.52	0.45	0.39	0.26	0.55	0.65
Al2O3	8.55	1.57	2.84	1.78	1.98	3.22	3.15	8.94	1.64	11.01	6.24	5.79
Fe2O3	1.91	7.97	2.35	3.40	2.29	5.29	4.26	3.76	2.72	6.38	6.83	5.96
FeO	14.8	6.2	16.6	16.0	17.4	14.6	14.3	18.9	20.1	15.1	11.7	13.2
MnO	0.37	0.60	0.89	0.94	0.87	0.83	0.79	0.57	0.76	0.57	0.63	0.59
MgO	11.4	16.1	10.8	11.3	11.0	11.5	11.9	7.6	9.0	8.1	11.7	11.4
CaO	11.0	11.3	11.8	11.8	12.2	12.0	12.0	11.8	11.7	11.3	11.4	11.6
Na2O	3.17	0.37	0.64	0.40	0.47	0.54	0.51	1.56	0.19	2.40	1.26	1.28
K2O	1.36	0.07	0.25	0.15	0.16	0.21	0.31	0.64	0.17	0.53	0.30	0.31
TOTAL	97.8	98.1	96.8	97.9	97.7	98.9	98.0	98.9	98.2	96.5	98.5	98.7

Structural Formula based on Twenty-three Oxygens

Si	6.467	7.633	7.542	7.669	7.636	7.414	7.431	6.736	7.740	6.304	7.012	7.053
Al(iv)	1.529	0.263	0.458	0.311	0.349	0.558	0.550	1.264	0.259	1.696	0.988	0.947
Al(vi)			0.047							0.314	0.093	0.059
Ti	0.279	0.027	0.046	0.041	0.020	0.031	0.058	0.051	0.044	0.030	0.061	0.072
Fe3+	0.218	0.854	0.266	0.379	0.258	0.586	0.474	0.428	0.308	0.744	0.755	0.662
Fe2+	1.882	0.739	2.092	1.981	2.171	1.797	1.769	2.392	2.527	1.956	1.440	1.630
Mn	0.048	0.072	0.114	0.118	0.110	0.103	0.099	0.073	0.097	0.075	0.078	0.074
Mg	2.578	3.411	2.435	2.500	2.455	2.511	2.619	1.724	2.025	1.880	2.573	2.499
Ca	1.783	1.724	1.908	1.870	1.957	1.886	1.897	1.911	1.889	1.876	1.802	1.829
Na	0.932	0.102	0.187	0.115	0.136	0.154	0.146	0.458	0.055	0.721	0.359	0.366
K	0.263	0.013	0.048	0.028	0.031	0.039	0.059	0.124	0.033	0.104	0.056	0.058

Sample	204	205	302	303	303	307	402	407
SiO2	42.3	42.0	42.6	43.5	43.3	43.4	40.4	45.2
TiO2	1.39	2.90	2.83	2.11	2.10	2.55	0.87	2.99
Al2O3	7.78	9.56	9.35	8.19	8.24	8.82	10.45	8.54
Fe2O3	7.84	1.85	1.58	3.52	2.94	1.44	4.07	1.63
FeO	17.7	12.5	15.4	14.1	14.1	14.0	21.0	10.1
MnO	0.52	0.27	0.26	0.35	0.32	0.30	0.54	0.24
MgO	6.9	12.1	11.0	11.6	11.7	12.3	6.2	14.2
CaO	10.3	11.0	11.2	11.3	11.1	11.4	11.8	11.5
Na2O	1.78	2.61	2.77	2.49	2.85	2.80	2.09	2.12
K2O	1.43	1.62	1.41	1.52	1.39	1.51	1.54	1.52
TOTAL	98.0	96.5	98.4	98.6	98.1	98.5	98.9	98.0

Structural Formula based on Twenty-three Oxygens

Si	6.547	6.371	6.414	6.521	6.524	6.482	6.279	6.554
Al(iv)	1.420	1.629	1.586	1.447	1.462	1.518	1.721	1.446
Al(vi)		0.082	0.073			0.034	0.019	0.048
Ti	0.162	0.331	0.320	0.238	0.238	0.286	0.102	0.337
Fe3+	0.914	0.211	0.178	0.397	0.333	0.162	0.476	0.182
Fe2+	2.298	1.593	1.936	1.764	1.771	1.743	2.728	1.256
Mn	0.068	0.035	0.033	0.044	0.041	0.038	0.071	0.030
Mg	1.591	2.748	2.459	2.588	2.632	2.736	1.430	3.151
Ca	1.716	1.796	1.808	1.812	1.792	1.825	1.957	1.825
Na	0.534	0.768	0.808	0.724	0.832	0.811	0.630	0.610
K	0.283	0.314	0.271	0.291	0.267	0.288	0.305	0.288

Compositions of magnetite-ilmenite pairs from the GLI

Sample	1		2		5		9		11		13	
	Mt	Il	Mt	Il	Mt	Il	Mt	Il	Mt	Il	Mt	Il
TiO2	5.81	49.9	1.30	49.2	9.06	49.2	1.82	49.8	1.70	50.7	2.30	50.7
Al2O3	0.09	0.06	0.35	0.09	0.10	0.09	0.13	0.06	1.04	0.09	2.96	0.09
Cr2O3	0.23	0.15	0.17	0.16	0.21	0.16	0.20	0.19	0.33	0.16	0.38	0.16
Fe2O3	57.6	5.02	66.9	5.68	51.0	5.12	65.5	5.73	63.7	4.51	61.1	4.51
FeO	35.6	41.2	32.1	39.4	38.0	40.0	32.3	40.6	31.9	43.3	32.7	43.3
MnO	0.63	3.32	0.39	4.36	1.00	3.87	0.34	3.80	0.33	1.52	0.34	1.52
MgO	0.08	0.09	0.07	0.18	0.10	0.11	0.10	0.10	0.14	0.39	0.41	0.39
TOTAL	100.1	99.8	101.3	99.2	99.6	98.7	100.4	100.4	99.2	100.7	100.2	100.7
Structural Formulae												
Ti	0.167	0.950	0.037	0.943	0.261	0.948	0.052	0.943	0.049	0.955	0.065	0.955
Al	0.004	0.002	0.016	0.003	0.005	0.003	0.006	0.002	0.047	0.003	0.131	0.003
Cr	0.007	0.003	0.005	0.003	0.006	0.003	0.006	0.004	0.010	0.003	0.011	0.003
Fe3+	1.655	0.096	1.905	0.109	1.468	0.099	1.883	0.109	1.844	0.085	1.727	0.085
Fe2+	1.138	0.873	1.016	0.839	1.217	0.857	1.032	0.854	1.026	0.906	1.027	0.906
Mn	0.020	0.071	0.013	0.094	0.032	0.084	0.011	0.081	0.011	0.032	0.011	0.032
Mg	0.005	0.003	0.004	0.007	0.006	0.004	0.006	0.004	0.008	0.015	0.023	0.015

Sample	18		22		25		26		27A		27B	
	Mt	Il	Mt	Il	Mt	Il	Mt	Il	Mt	Il	Mt	Il
TiO2	1.80	49.1	1.37	47.4	1.37	48.7	1.26	46.5	1.10	48.3	1.48	48.3
Al2O3	0.53	0.07	0.38	0.02	0.47	0.24	0.73	0.06	0.54	0.13	0.28	0.11
Cr2O3	0.27	0.18	0.14	0.09	0.20	0.18	0.17	0.12	0.24	0.22	0.21	0.24
Fe2O3	64.5	5.03	66.5	7.23	66.3	7.17	66.9	3.38	67.0	7.36	67.50	6.86
FeO	32.1	40.8	32.4	39.0	32.1	40.0	32.6	38.4	31.8	39.3	32.6	39.1
MnO	0.39	2.57	0.26	2.85	0.36	3.28	0.30	2.69	0.39	3.49	0.37	3.95
MgO	0.09	0.34	0.00	0.40	0.08	0.21	0.04	0.34	0.10	0.27	0.12	0.12
TOTAL	99.7	98.2	101.0	97.5	100.9	99.9	102.0	96.6	101.3	99.2	102.7	98.7
Structural Formulae												
Ti	0.005	0.948	0.039	0.928	0.013	0.926	0.036	0.915	0.031	0.925	0.042	0.930
Al	0.024	0.002	0.017	0.001	0.007	0.007	0.032	0.002	0.024	0.004	0.012	0.003
Cr	0.008	0.004	0.004	0.002	0.002	0.004	0.005	0.003	0.007	0.004	0.006	0.005
Fe3+	1.864	0.097	1.901	0.142	0.632	0.136	1.892	0.165	1.906	0.141	1.898	0.132
Fe2+	1.030	0.877	1.028	0.848	0.340	0.846	1.023	0.841	1.008	0.837	1.018	0.837
Mn	0.013	0.056	0.008	0.063	0.004	0.070	0.010	0.060	0.013	0.075	0.012	0.086
Mg	0.005	0.013	0.000	0.016	0.002	0.008	0.002	0.013	0.006	0.010	0.007	0.005

Sample	27C		28A		28B		28C		29A		29B	
	Mt	Il	Mt	Il	Mt	Il	Mt	Il	Mt	Il	Mt	Il
TiO2	1.82	48.2	1.92	46.9	1.20	48.42	1.30	47.7	1.99	47.5	1.61	48.4
Al2O3	0.34	0.11	0.31	0.14	0.47	0.13	0.36	0.14	0.44	0.12	0.46	0.10
Cr2O3	0.22	0.17	0.22	0.17	0.23	0.18	0.20	0.18	0.24	0.15	0.22	0.19
Fe2O3	66.1	7.32	63.7	6.54	67.52	6.95	67.6	8.11	66.15	9.44	67.27	6.69
FeO	32.6	39.3	31.7	37.3	32.3	38.9	33.3	37.8	33.0	38.6	32.8	39.6
MnO	0.39	3.40	0.39	4.24	0.36	3.96	0.39	4.00	0.37	3.42	0.37	3.25
MgO	0.12	0.23	0.09	0.28	0.11	0.30	0.13	0.33	0.09	0.26	0.12	0.23
TOTAL	101.7	98.9	98.5	95.6	102.3	98.9	102.4	98.6	102.5	99.6	102.9	98.6
Ti	0.052	0.926	0.056	0.093	0.034	0.930	0.037	0.918	0.056	0.907	0.045	0.932
Al	0.015	0.003	0.014	0.004	0.021	0.004	0.016	0.004	0.019	0.004	0.018	0.003
Cr	0.007	0.003	0.007	0.004	0.007	0.004	0.006	0.004	0.007	0.003	0.007	0.004
Fe3+	1.875	0.141	1.867	0.130	1.905	0.134	1.905	0.156	1.862	0.180	1.886	0.129
Fe2+	1.027	0.841	1.033	0.823	1.012	0.830	1.011	0.810	1.033	0.820	1.022	0.849
Mn	0.013	0.074	0.013	0.095	0.011	0.086	0.012	0.087	0.012	0.074	0.012	0.071
Mg	0.007	0.009	0.005	0.011	0.006	0.011	0.007	0.013	0.005	0.010	0.007	0.009

Sample	29C		30A		30B		30C		31		35A	
	Mt	Il	Mt	Il	Mt	Il	Mt	Il	Mt	Il	Mt	Il
TiO2	1.63	47.50	1.49	47.7	1.38	47.1	1.41	48.4	0.93	49.60	1.26	48.40
Al2O3	0.45	0.14	0.41	0.14	0.34	0.10	0.33	0.11	0.22	0.10	0.63	0.12
Cr2O3	0.21	0.20	0.19	0.20	0.20	0.19	0.19	0.17	0.20	0.16	0.26	0.19
Fe2O3	67.2	8.50	67.33	7.71	67.1	8.47	67.5	7.22	67.12	5.25	66.65	6.84
FeO	32.8	38.9	32.7	39.1	32.2	38.5	32.5	39.1	31.5	39.4	32.1	37.2
MnO	0.35	3.31	0.37	3.15	0.39	3.38	0.40	3.89	0.32	4.74	0.41	4.43
MgO	0.10	0.20	0.09	0.20	0.12	0.14	0.10	0.17	0.09	0.17	0.11	0.37
TOTAL	102.9	98.8	102.7	98.3	101.9	98.0	102.6	99.1	100.5	99.5	101.5	98.7
Ti	0.046	0.914	0.042	0.921	0.039	0.914	0.040	0.927	0.027	0.947	0.036	0.931
Al	0.019	0.004	0.018	0.004	0.015	0.003	0.015	0.003	0.010	0.003	0.028	0.004
Cr	0.006	0.004	0.006	0.004	0.006	0.004	0.006	0.003	0.006	0.003	0.008	0.004
Fe3+	1.884	0.164	1.893	0.149	1.991	0.165	1.901	0.139	1.931	0.100	1.893	0.132
Fe2+	1.024	0.831	1.021	0.842	1.014	0.832	1.016	0.834	1.008	0.836	1.012	0.796
Mn	0.011	0.071	0.012	0.069	0.012	0.074	0.013	0.084	0.010	0.102	0.013	0.118
Mg	0.006	0.008	0.005	0.008	0.007	0.005	0.006	0.007	0.005	0.006	0.006	0.014

Sample	35B		35C		37A		37B		38		43	
	Mt	Il	Mt	Il	Mt	Il	Mt	Il	Mt	Il	Mt	Il
TiO2	1.69	49.40	1.11	48.89	0.89	46.82	0.49	46.27	0.48	47.80	1.27	48.94
Al2O3	0.60	0.15	0.56	0.14	0.20	0.06	0.23	0.04	0.23	0.11	0.57	0.14
Cr2O3	0.28	0.20	0.25	0.22	0.15	0.10	0.15	0.12	0.17	0.16	0.38	0.24
Fe2O3	65.77	5.71	67.15	6.63	67.37	7.29	69.30	8.71	67.63	8.95	67.2	6.81
FeO	32.3	37.8	31.9	37.8	31.8	36.6	31.9	35.4	30.7	37.6	32.3	40.8
MnO	0.51	5.82	0.43	5.35	0.31	5.23	0.29	6.00	0.33	4.72	0.33	2.33
MgO	0.12	0.34	0.14	0.33	0.00	0.09	0.00	0.06	0.09	0.26	0.14	0.39
TOTAL	101.4	99.5	101.6	99.5	100.7	96.2	102.4	96.6	99.9	99.7	102.2	99.8
Ti	0.048	0.941	0.032	0.932	0.026	0.926	0.014	0.913	0.014	0.911	0.036	0.931
Al	0.027	0.005	0.025	0.004	0.009	0.002	0.010	0.001	0.010	0.003	0.025	0.004
Cr	0.008	0.004	0.007	0.004	0.005	0.002	0.005	0.003	0.005	0.003	0.008	0.005
Fe3+	1.869	0.109	1.905	0.127	1.935	0.144	1.958	0.172	1.957	0.171	1.895	0.130
Fe2+	1.019	0.801	1.005	0.802	1.014	0.804	1.003	0.776	0.988	0.797	1.012	0.863
Mn	0.016	0.125	0.014	0.115	0.010	0.117	0.009	0.133	0.011	0.101	0.011	0.050
Mg	0.007	0.013	0.008	0.013	0.000	0.004	0.000	0.002	0.005	0.010	0.008	0.015

Sample	45		45A		51		53A		53B		54A	
	Mt	Il	Mt	Il	Mt	Il	Mt	Il	Mt	Il	Mt	Il
TiO2	1.05	48.55	1.02	48.07	1.39	50.59	1.44	48.98	1.77	49.54	1.79	49.08
Al2O3	0.20	0.04	0.15	0.06	0.76	0.12	0.54	0.06	1.07	0.05	0.30	0.04
Cr2O3	0.25	0.20	0.23	0.21	0.36	0.29	0.27	0.21	0.28	0.24	0.27	0.24
Fe2O3	67.8	7.03	68.1	7.09	65.1	4.14	66.23	6.71	64.82	5.92	66.7	6.27
FeO	32.1	38.7	32.0	38.8	31.9	43.0	32.3	41.2	32.6	41.7	33.0	40.5
MnO	0.35	4.62	0.41	4.21	0.29	1.63	0.36	2.19	0.35	2.22	0.39	3.17
MgO	0.00	0.04	0.00	0.00	0.11	0.43	0.00	0.25	0.04	0.27	0.02	0.16
TOTAL	101.9	99.3	102.1	98.6	100.0	100.2	101.3	99.7	101.1	100.0	102.6	99.6
Ti	0.030	0.930	0.029	0.929	0.040	0.957	0.041	0.933	0.050	0.941	0.050	0.937
Al	0.009	0.001	0.007	0.002	0.034	0.004	0.024	0.002	0.048	0.002	0.013	0.001
Cr	0.008	0.004	0.007	0.004	0.012	0.004	0.008	0.004	0.008	0.005	0.008	0.005
Fe3+	1.924	0.135	1.929	0.137	1.874	0.078	1.886	0.128	1.843	0.112	1.878	0.120
Fe2+	1.012	0.823	1.009	0.833	1.020	0.904	1.023	0.873	1.031	0.880	1.031	0.860
Mn	0.011	0.100	0.013	0.092	0.009	0.035	0.012	0.047	0.011	0.048	0.012	0.068
Mg	0.000	0.002	0.000	0.000	0.006	0.016	0.000	0.009	0.002	0.010	0.001	0.006

Sample	54B		64A		64B		70A		70B		77A	
	Mt	Il	Mt	Il	Mt		Mt	Il	Mt	Il	Mt	Il
TiO2	1.40	48.68	1.24	48.73	1.01	48.99	1.33	48.88	1.55	46.69	1.69	49.12
Al2O3	0.16	0.05	0.13	0.06	0.30	0.06	2.48	0.80	3.88	2.49	1.08	0.09
Cr2O3	0.29	0.21	0.26	0.24	0.28	0.20	0.35	0.20	0.36	0.23	0.29	0.25
Fe2O3	66.6	7.31	67.37	7.02	68.1	6.40	64.32	6.43	61.46	6.64	65.27	6.64
FeO	32.2	39.9	32.1	38.2	32.2	38.7	32.2	40.9	32.4	38.2	32.7	40.9
MnO	0.35	3.53	0.37	5.28	0.38	5.02	0.37	1.92	0.41	2.92	0.33	2.09
MgO	0.00	0.10	0.00	0.03	0.01	0.05	0.26	0.53	0.21	0.35	0.07	0.54
TOTAL	101.2	99.9	101.7	99.7	102.3	99.6	101.5	99.8	100.4	97.7	101.5	99.8
Ti	0.040	0.927	0.035	0.930	0.029	0.936	0.037	0.925	0.046	0.896	0.048	0.933
Al	0.007	0.002	0.006	0.002	0.013	0.002	0.109	0.026	0.171	0.075	0.048	0.003
Cr	0.009	0.004	0.008	0.005	0.008	0.004	0.010	0.004	0.011	0.005	0.009	0.005
Fe3+	1.904	0.139	1.916	0.134	1.922	0.122	1.806	0.122	1.731	0.128	1.848	0.126
Fe2+	1.023	0.845	1.016	0.810	1.010	0.822	1.005	0.862	1.014	0.916	1.028	0.865
Mn	0.011	0.076	0.012	0.114	0.012	0.108	0.012	0.041	0.013	0.065	0.011	0.045
Mg	0.000	0.004	0.000	0.001	0.001	0.002	0.015	0.020	0.012	0.015	0.004	0.020

Sample	77B		78A		78B		81B		MR-5A		MR-5B	
	Mt	Il	Mt	Il	Mt	Il	Mt	Il	Mt	Il	Mt	Il
TiO2	1.54	49.52	1.57	48.48	1.00	47.83	1.42	48.48	0.84	47.42	0.87	43.47
Al2O3	0.77	0.07	0.69	0.06	0.66	0.29	0.41	0.07	0.13	0.04	0.13	0.03
Cr2O3	0.35	0.23	0.35	0.23	0.25	0.20	0.24	0.24	0.18	0.15	0.16	0.14
Fe2O3	66.3	6.83	65.9	7.14	67.62	8.42	67.7	8.06	69.3	7.72	67.9	13.33
FeO	32.6	40.9	32.3	40.1	32.1	39.0	32.8	40.0	32.5	38.0	32.1	34.5
MnO	0.32	1.80	0.37	1.60	0.34	1.84	0.41	3.06	0.25	4.32	0.31	4.29
MgO	0.10	0.79	0.12	0.98	0.09	1.11	0.03	0.17	0.01	0.11	0.00	0.08
TOTAL	102.1	100.0	101.5	98.7	102.2	98.8	103.2	100.2	103.2	97.8	101.7	95.9
Ti	0.045	0.932	0.045	0.928	0.028	0.913	0.040	0.920	0.024	0.923	0.028	0.865
Al	0.034	0.002	0.031	0.002	0.029	0.009	0.018	0.002	0.006	0.001	0.006	0.001
Cr	0.010	0.005	0.010	0.005	0.007	0.004	0.007	0.005	0.005	0.003	0.005	0.003
Fe3+	1.869	0.129	1.870	0.137	1.907	0.161	1.896	0.153	1.942	0.150	1.934	0.266
Fe2+	1.022	0.860	1.020	0.853	1.007	0.828	1.020	0.645	1.013	0.822	1.015	0.764
Mn	0.010	0.038	0.012	0.035	0.011	0.040	0.013	0.065	0.008	0.095	0.010	0.096
Mg	0.006	0.030	0.007	0.037	0.005	0.042	0.002	0.006	0.001	0.004	0.000	0.003

Sample	81A		201		205		208		209		302	
	Mt	Il	Mt	Il	Mt	Il	Mt	Il	Mt	Il	Mt	Il
TiO2	1.47	40.47	1.79	49.97	2.02	49.39	0.77	49.96	0.67	49.56	1.69	49.76
Al2O3	0.39	0.09	0.26	0.10	0.39	0.09	0.16	0.10	0.21	0.06	0.63	0.17
Cr2O3	0.23	0.23	0.29	0.15	0.25	0.16	0.21	0.18	0.23	0.19	0.24	0.16
Fe2O3	68.17	21.65	65.64	5.25	64.38	5.30	66.94	5.32	68.28	4.52	65.42	5.03
FeO	33.1	33.2	32.4	41.5	32.5	41.4	31.0	38.7	31.4	39.1	32.3	42.1
MnO	0.38	2.78	0.36	3.07	0.38	2.54	0.35	5.77	0.33	4.76	0.33	2.06
MgO	0.03	0.13	0.08	0.14	0.09	0.22	0.09	0.14	0.09	0.12	0.12	0.24
TOTAL	103.9	98.7	101.0	100.2	100.0	99.1	99.7	100.3	101.4	98.7	100.9	99.6
Ti	0.011	0.786	0.051	0.947	0.058	0.946	0.022	0.946	0.019	0.954	0.048	0.948
Al	0.017	0.003	0.012	0.003	0.018	0.003	0.007	0.003	0.009	0.002	0.028	0.005
Cr	0.007	0.005	0.009	0.003	0.008	0.003	0.006	0.004	0.007	0.004	0.007	0.003
Fe3+	1.895	0.421	1.877	0.100	1.858	0.102	1.942	0.101	1.946	0.087	1.868	0.096
Fe2+	1.021	0.716	1.031	0.874	1.041	0.881	1.000	0.082	0.993	0.837	1.026	0.892
Mn	0.012	0.061	0.012	0.066	0.012	0.055	0.011	0.123	0.011	0.103	0.011	0.044
Mg	0.002	0.005	0.005	0.005	0.005	0.008	0.005	0.005	0.005	0.005	0.007	0.009

Sample	303		304		307		402		404		407	
	Mt	Il	Mt	Il	Mt	Il	Mt	Il	Mt	Il	Mt	Il
TiO2	6.08	49.70	1.73	49.36	1.38	49.69	1.59	50.39	1.85	50.21	1.67	50.13
Al2O3	0.59	0.22	0.90	0.18	0.43	0.18	0.38	0.07	0.32	0.09	0.69	0.18
Cr2O3	0.21	0.21	0.25	0.17	0.22	0.18	0.26	0.19	0.18	0.17	0.31	0.17
Fe2O3	57.4	5.59	64.7	5.89	66.3	5.81	65.2	3.86	65.1	4.67	64.6	4.37
FeO	36.5	42.1	32.3	41.9	32.1	41.3	31.4	41.9	32.2	39.8	32.1	42.0
MnO	0.43	2.20	0.33	1.83	0.33	2.99	0.35	2.65	0.43	4.84	0.28	1.92
MgO	0.10	0.14	0.12	0.29	0.07	0.15	0.09	0.33	0.10	0.15	0.13	0.58
TOTAL	101.5	100.3	100.4	99.7	100.9	100.4	99.9	99.5	100.3	100.1	99.8	99.4
Ti	0.172	0.942	0.050	0.940	0.039	0.941	0.046	0.960	0.053	0.953	0.048	0.954
Al	0.026	0.007	0.040	0.005	0.019	0.005	0.017	0.002	0.014	0.003	0.031	0.005
Cr	0.006	0.004	0.008	0.003	0.007	0.004	0.008	0.004	0.005	0.003	0.009	0.003
Fe3+	1.624	0.106	1.853	0.112	1.895	0.110	1.883	0.074	1.874	0.089	1.863	0.083
Fe2+	1.146	0.887	1.028	0.887	1.020	0.868	1.025	0.889	1.028	0.841	1.028	0.888
Mn	0.014	0.047	0.011	0.039	0.011	0.064	0.011	0.057	0.014	0.103	0.009	0.041
Mg	0.006	0.005	0.007	0.011	0.004	0.006	0.005	0.013	0.006	0.006	0.007	0.022

Analyses of Biotites from Centert II gabbroic rocks

Sample No	138	308	414	414	420	590	592	593	607
SiO2	37.28	35.04	36.49	36.31	35.47	36.87	37.15	34.94	36.66
TiO2	2.57	1.98	5.71	3.39	5.41	0.74	1.99	4.23	4.15
Al2O3	15.62	15.93	14.06	14.85	14.46	16.89	15.97	15.38	15.34
FeO	13.10	16.50	14.82	17.47	16.16	12.02	8.75	19.27	15.31
MnO	0.12	0.16	0.10	0.15	0.12	0.15	0.08	0.24	0.18
MgO	17.05	14.42	14.65	13.94	13.01	18.79	20.00	12.00	14.82
Na2O	0.96	0.39	0.44	0.22	0.21	0.45	0.80	0.68	0.57
K2O	8.54	10.24	9.44	9.99	9.36	10.71	10.43	9.49	10.53
TOTAL	95.24	94.66	95.71	96.32	94.20	96.62	95.17	96.23	97.56
Structural formulae based on 22 oxygens									
Si	5.494	5.346	5.429	5.442	5.409	5.385	5.409	5.289	5.397
Ti	0.285	0.227	0.639	0.382	0.621	0.081	0.218	0.482	0.460
Al	2.715	2.866	2.467	2.625	2.600	2.909	2.742	2.745	2.663
Fe	1.616	2.107	1.845	2.191	2.062	1.469	1.066	2.441	1.886
Mn	0.015	0.021	0.013	0.019	0.016	0.019	0.010	0.031	0.023
Mg	3.748	3.282	3.251	3.117	2.960	4.094	4.344	2.710	3.255
Na	0.275	0.116	0.127	0.064	0.062	0.128	0.226	0.200	0.163
K	1.607	1.995	1.793	1.912	1.822	1.997	1.939	1.834	1.979
Mole percent end members									
Annite	30.04	38.95	36.12	41.14	40.95	26.33	19.68	47.12	36.54
Phlogopite	69.68	60.66	63.63	58.5	58.74	73.34	80.14	52.29	63.03
Mn-Phyl*	0.28	0.38	0.25	0.36	0.31	0.33	0.18	0.59	0.44

*Manganophyllite

Analyses of Biotites from Centert II

Sample No	607	608	907	1084	1084	1084	1498	1496
SiO2	35.45	38.22	34.80	33.68	34.29	34.46	39.60	39.09
TiO2	4.50	2.34	2.45	3.54	3.04	0.14	3.49	2.87
Al2O3	14.88	15.73	13.73	15.71	14.41	16.34	13.89	13.21
FeO	15.76	12.09	23.49	25.69	23.74	21.77	8.60	9.87
MnO	0.22	0.10	0.33	0.21	0.28	0.19	0.09	0.09
MgO	13.86	18.20	11.74	6.57	9.72	12.01	20.74	20.80
Na2O	0.57	0.56	0.52	0.51	0.43	0.63	1.04	1.56
K2O	9.60	9.74	7.06	8.70	9.21	8.76	8.44	8.75
TOTAL	94.84	96.98	94.12	94.61	95.12	94.30	95.89	96.24
Structural Formulae based on 22 oxygens								
Si	5.375	5.513	5.453	5.355	5.382	5.375	5.657	5.628
Ti	0.513	0.254	0.289	0.423	0.359	0.016	0.375	0.311
Al	2.660	2.676	2.537	2.945	2.667	3.005	2.340	2.243
Fe	2.000	1.459	3.080	3.418	3.118	2.841	1.028	1.189
Mn	0.028	0.012	0.044	0.028	0.037	0.025	0.011	0.011
Mg	3.135	3.917	2.744	1.558	2.276	2.794	4.420	4.468
Na	0.168	0.157	0.158	0.157	0.131	0.191	0.288	0.436
K	1.858	1.794	1.412	1.766	1.845	1.744	1.539	1.608
Annite	38.74	27.09	52.5	68.31	57.42	50.2	18.84	20.99
Phlogopite	60.71	72.68	46.76	31.13	41.89	49.35	80.96	78.82
Mn-Phyl*	0.55	0.23	0.75	0.57	0.69	0.44	0.2	0.19

*Manganophyllite

Analyses of Biotites from Centert II

Sample No	1498	1500	1500	1502	1502	1503	1503
SiO2	37.95	38.22	38.41	39.52	36.51	38.22	40.00
TiO2	5.47	0.40	1.36	1.50	0.86	4.62	0.34
Al2O3	13.21	15.97	14.64	13.49	17.03	13.79	13.83
FeO	9.46	7.99	9.13	7.13	13.40	5.52	5.25
MnO	0.08	0.14	0.15	0.04	0.40	0.06	0.00
MgO	18.95	21.74	20.43	23.48	17.15	21.74	24.82
Na2O	1.08	0.46	0.58	0.65	0.39	0.94	0.73
K2O	8.86	10.76	9.82	9.64	10.82	9.32	9.98
TOTAL	95.06	95.68	94.52	95.45	95.56	94.21	94.95
Structural Formulae based on 22 oxygens							
Si	5.512	5.513	5.610	5.659	5.369	5.510	5.723
Ti	0.598	0.043	0.149	0.162	0.095	0.501	0.037
Al	2.262	2.716	2.521	2.278	2.953	2.344	2.334
Fe	1.150	0.964	1.116	0.854	1.649	0.666	0.629
Mn	0.010	0.017	0.019	0.005	0.050	0.007	0.000
Mg	4.106	4.678	4.451	5.015	3.763	4.675	5.298
Na	0.305	0.129	0.164	0.181	0.111	0.263	0.203
K	1.643	1.982	1.831	1.762	2.032	1.715	1.823
Annite	21.84	17.05	19.98	14.55	30.2	12.45	10.61
Phlogopite	77.97	82.65	79.68	85.37	68.88	87.41	89.39
Mn-Phyl*	0.19	0.3	0.33	0.08	0.91	0.14	0

*Manganophyllite